JUSTUS-LIEBIG-
UNIVERSITÄT
GIESSEN

Visualization of parasite–host interactions using atmospheric-pressure MALDI mass spectrometry imaging

Cumulative Dissertation in order
to achieve the Degree
Doctor rerum naturalium
– Dr. rer. nat. –

Prepared at the
Institute of Inorganic and Analytical Chemistry
Justus Liebig University Gießen
by

Katja Rebecca Wiedemann

– July 2025 –

This thesis was accepted as a doctoral dissertation in fulfillment of the requirements for the degree of *Doctor rerum naturalium* by the Faculty of Biology and Chemistry, Justus Liebig University Giessen, Germany.

1. Referee: Prof. Dr. Bernhard Spengler
2. Referee: PD Dr. Simone Häberlein

“ Das wichtigste ist es, nie zu vergessen, dass Du es tust, weil Du es liebst. ”

Jan Frodeno

Contents

List of Abbreviations

3-APA 3-aminopicolinic acid

3-AQ 3-aminoquinoline

9AA 9-aminoacridine

ANOVA analysis of variance

AP atmospheric pressure

AP-SMALDI atmospheric-pressure scanning microprobe matrix-assisted laser desorption/ionization

ATT 6-aza-2-thiothymine

B. besnoiti *Besnoitia besnoiti*

B. glabrata *Biomphalaria glabrata*

BUVEC bovine umbilical vein endothelial cells

C. parvum *Cryptosporidium parvum*

CDC Centers for Disease Control and Prevention

CE cholesteryl ester

Cer ceramide

α-CHCA α-cyano-4-hydroxycinnamic acid

CL cardiolipin

DDA data-dependent acquisition

DESI desorption electrospray ionization

DG diacylglyceride

DHAP 2,6-dihydroxyacetophenone

DHB 2,5-dihydroxybenzoic acid

DIA data-independent acquisition

DMPE dimethylphosphatidylethanolamine

DNA deoxyribonucleic acid

ELISA enzyme-linked immunosorbent assay

ESI electrospray ionization

FA fatty acid

FASI fatty acid synthase type I

FASII fatty acid synthase type II

FFPE formaldehyde-fixed paraffin-embedded

FT-ICR Fourier-transform ion cyclotron resonance

FWHM full width at half maximum

GC gas chromatography

GC-MS gas chromatography–mass spectrometry

GlcCer glycosylceramide

GLS glycosphingolipid

H&E hematoxylin-and-eosin

HPA 3-hydroxypicolinic acid

HPLC high performance liquid chromatography

HPTLC high-performance thin-layer chromatography

IFAT indirect fluorescence antibody test

LC-MS liquid chromatography-mass spectrometry

LC-MS/MS liquid chromatography-tandem mass spectrometry

LDI laser desorption/ionization

LPC lysophosphatidylcholine

LPE lysophosphatidylethanolamine

LPS lysophosphatidylserine

m/z mass-to-charge-number ratio

MALDI matrix-assisted laser desorption/ionization

MANOVA multivariate analysis of variance

MS mass spectrometry

MS/MS tandem mass spectrometry

MSI mass spectrometry imaging

NA nicotinic acid

nano-HILIC MS/MS nanoscale hydrophilic interaction liquid chromatography tandem mass spectrometry

NPOE 2-nitrophenyl octyl ether

NTD neglected tropical disease

P. falciparum *Plasmodium falciparum*

PA phosphatidic acid

PC phosphatidylcholine

PCA principal component analysis

PCR polymerase chain reaction

PE phosphatidylethanolamine

PG phosphatidylglycerol

PI phosphatidylinositol

PL phospholipid

PS phosphatidylserine

PZQ praziquantel

RP-HPLC reversed-phase high performance liquid chromatography

RT retention time

S. mansoni *Schistosoma mansoni*

SA sinapinic acid

SEA soluble egg antigens

SIMS secondary ion mass spectrometry

SM sphingomyelin

T. gondii *Toxoplasma gondii*

TG triacylglyceride

TLC thin-layer chromatography

WHO world health organization

List of Figures

List of Publications

1. Wiedemann KR, Peter Ventura A, Gerbig S, Roderfeld M, Quack T, Grevelding CG, Roeb E, Spengler B. "Changes in the lipid profile of hamster liver after *Schistosoma mansoni* infection, characterized by mass spectrometry imaging and LC–MS/MS analysis", *Analytical and Bioanalytical Chemistry*, 2022, 414, 3653-3665, DOI: 10.1007/s00216-022-04006-6.

2. von Bülow V, Gindner S, Baier A, Hehr L, Buss N, Russ L, Wrobel S, Wirth V, Tabatabai K, Quack T, Haeberlein S, Kadesch P, Gerbig S, Wiedemann KR, Spengler S, Mehl A, Morlock G, Schramm G, Pons-Kühnemann J, Falcone FH, Wilson RA, Bankov K, Wild P, Grevelding CG, Roeb E, Roderfeld M. "Metabolic reprogramming of hepatocytes by *Schistosoma mansoni* eggs", *JHEP Reports*, 2022, DOI: 10.1016/j.jhepr.2022.100625.

3. Wiedemann KR, Gerbig S, Ghezellou P, Pilgram A, Hermosilla C, Taubert A, Silva LMR, Spengler B. "Mass spectrometry imaging of lipid and metabolite distributions in cysts of *Besnoitia besnoiti*-infected bovine skin", *Journal of the American Society for Mass Spectrometry*, 2025, 36, 1017-1026, DOI: 10.1021/jasms.4c00466.

This doctoral thesis is based on publication one and three.

Eidesstattliche Versicherung

„Ich erkläre: Ich habe die vorgelegte Dissertation selbstständig und ohne unerlaubte fremde Hilfe und nur mit den Hilfen angefertigt, die ich in der Dissertation angegeben habe. Alle Textstellen, die wörtlich oder sinngemäß aus veröffentlichten Schriften entnommen sind, und alle Angaben, die auf mündlichen Auskünften beruhen, sind als solche kenntlich gemacht. Ich stimme einer evtl. Überprüfung meiner Dissertation durch eine Antiplagiat-Software zu. Bei den von mir durchgeführten und in der Dissertation erwähnten Untersuchungen habe ich die Grundsätze guter wissenschaftlicher Praxis, wie sie in der „Satzung der Justus-Liebig-Universität Gießen zur Sicherung guter wissenschaftlicher Praxis“ niedergelegt sind, eingehalten.“

Angaben zu auf künstlicher Intelligenz (KI) basierender Hilfen wie ChatGPT oder SchulKI von OpenAI oder Gemini von Google zur Erstellung meiner Dissertation (Zutreffendes angekreuzt):

☐ Ich habe bei der Erstellung dieses Textes kein KI-Tool verwendet.

☐ Ich habe ein KI-Tool in den folgenden Bereichen eingesetzt (Mehrfachnennungen möglich):

- ☐ Ideen finden, meine Kreativität anregen
- ☐ Verstehen von Konzepten, Recherche von Fakten und Definitionen
- ☐ Optimierung eines von mir verfassten Textes
- ☐ Erstellen ganzer Textpassagen nach meinen Vorgaben

Folgende KI-Tools habe ich verwendet, damit aufgeführte Teile meines Textes von dem Tool wie folgt profitiert haben:

Datum: _____ Unterschrift: _____

Abstract

Endoparasites completely rely on the host organism to survive, once they entered their host. Though, hosts do not capitulate but try to protect themselves against potential damage induced by the parasite. Taking these two effects together, leads to measurable changes in the composition and lateral distribution of metabolites in host tissue (upon infection). In order to find novel drug targets, further knowledge on such changes is crucial. Using mass spectrometry imaging to investigate host-parasite interactions *in vivo* in an untargeted fashion whilst maintaining the lateral information of metabolites is a powerful approach. Therefore, two distinct models were studied: *Schistosoma-mansoni*-egg-containing liver samples of hamsters infected with the blood flukes, and bovine skin tissue, showing cysts formed by the apicomplexan parasite *Besnoitia besnoiti*.

For both parasite-host systems, characteristic infection markers were found with significant changes in signal intensities.

Additionally, by benefiting from the fact that lateral information is kept during mass spectrometry imaging analysis, the lateral distribution of infection markers was revealed. For some of them, co-localized biological structures were observed in optical images of the analyzed tissues.

During schistosomiasis, *Schistosoma mansoni* eggs are deposited in the hamster liver, leading to granuloma formation around the eggs. The high lateral resolution of the AP-SMALDI5 AF ion source enabled the unambiguous visualization of both, eggs (100 µm to 200 µm in diameter) and local abundance changes of lipids in granulomatous tissue compared to healthy hepatic tissue. Guided by results obtained with liquid chromatography-tandem mass spectrometry, we observed a substructure in formed granulomas by applying mass spectrometry imaging. For example, ether-phosphatidylethanolamines were mainly found in the outer part of the granulomas. In total, 372 substances were found to be significantly changed due to infection.

In the skin of *Besnoitia besnoiti*-infected cattle, MS images showed both, enrichment and depletion of several lipid species inside parasite-formed cysts. Due to the high lateral resolution at 2 µm pixel size, some of them were even found to be characteristic for the thin cyst walls. Applying multiple MSI methodologies, cysts were further characterized by on-tissue tandem mass spectrometry as well as 3-dimensional imaging. Overall, 552 ions were found to be altered due to infection.

Overall, gained insights into parasite-host interactions can now be used as starting points for further metabolism studies and also serve as potential drug targets.

Zusammenfassung

Nach Eindringen in ihren Wirt sind Endoparasiten vollständig von diesen abhängig. Doch der Wirt wehrt sich und versuchst sich so gut möglich gegen potentiellen, durch den Parasit hervorgerufenen Schaden zu schützen. Diese beiden Effekte führen zu messbaren Unterschieden, sowohl in der Lipid- und Metabolitzusammensetzung, als auch -verteilung im Wirtsgewebe. Um neue, potentielle Angriffspunkte für Arzneimittel zu finden, ist die Kenntnis dieser Unterschiede entscheidend. Die Verwendung bildgebender Massenspektrometrie zur Untersuchung von Parasit-Wirt-Wechselwirkungen *in vivo* bietet hierbei zwei Vorteile: Einerseits die parallele Detektion hunderter Metabolite. Zudem wird gleichzeitig die laterale Verteilung der Metabolite erhalten und kann später bildlich dargestellt werden. Zwei verschiedene Modellsysteme wurden untersucht: Einerseits Eier-enthaltende Leber von mit *Schistosoma mansoni* infizierten Hamstern, andererseits Zysten-enthaltende Rinderhaut, hervorgerufen durch den Parasit *Besnoitia besnoiti*.

Für beide Parasit-Wirt-Systeme wurden charakteristische Infektionsmarker mit signifikanten Unterschieden bezüglich der Signalintensität gefunden.

Da die laterale Verteilung von Metaboliten bei der Analyse mittels bildgebender Massenspektrometrie erhalten wird, konnte außerdem die Signalintensität der Infektionsmarker bildlich dargestellt werden. Für einige passte diese zu biologischen Strukturen, die in optischen Bildern der untersuchten Gewebe erkannt wurden.

Im Verlauf der Schistosomiasis lagern sich einige *Schistosoma mansoni*-Eier in den Lebern der infizierten Hamster ein und rufen dort die Bildung von Granulomen hervor. Die hohe Auflösung der AP-SMALDI5 AF-Ionenquelle ermöglicht die gleichzeitige Darstellung sowohl der Eier (mit lediglich einem Durchmesser von 100 µm bis 200 µm), als auch des umliegenden Gewebes. Hierbei konnten Intensitätsunterschiede verschiedener Signale im Vergleich zu gesundem Lebergewebe festgestellt werden. Nach Erstellung einer Lipiddatenbank durch LC-MS/MS-Experimente konnten mittels bildgebender Massenspektrometrie Signale gefunden werden, die eine Substruktur in den gebildeten Granulomen abbilden. Beispielsweise wurden Ether-Phosphatidylethanolamine hauptsächlich im äußeren Rand der Granulome detektiert. In Summe wurden 372 *m/z*-Signale mit durch Infektion hervorgerufenen Intensitätsunterschieden gefunden.

In Hautproben von mit *Besnoitia besnoiti*-infizierten Rindern konnte in den massenspektrometrischen Bildern sowohl die An- als auch Abreicherung ausgewählter Lipide in den Parasiten-induzierten Zysten dargestellt werden. Dank der ultrahohen Auflösung (2 µm Pixelgröße) konnten sogar einige Lipide ausgemacht werden, die charakteristisch für die dünne Zystenwand sind. Durch Anwendung verschiedener, bildgebender massenspektrometrischer Techniken konnten die Zysten weiter charakterisiert werden. So ermöglichte auf Gewebe durchgeführte Tandemmassenspektrometrie die Iden-

tifizierung einiger annotierter Lipide. Unter Verwendung massenspektrometrischer Daten konnten die Zysten außerdem dreidimensional rekonstruiert werden. Insgesamt wurden 552 Ionensignale gefunden, die unterschiedliche Signalintensitäten in infizierten und gesunden Hautproben zeigten.

Alles in allem können die gewonnenen Erkenntnisse zu Parasit-Wirt-Wechselwirkungen nun als Ausgangspunkt für weitere Metabolismusstudien verwendet werden. Des Weiteren können sie als mögliche Anhaltspunkte bei der Suche nach neuen Wirkstoffen gegen die entsprechenden Krankheiten dienen.

1 Synopsis

1.1 Mass spectrometry

The simplified idea of mass spectrometry (MS) is the weighing of molecules or, to be correct, the mass determination of molecular ions. The output is a mass spectrum, where the signal intensity is plotted against the mass-to-charge-number ratio (m/z). There are several different analyzing techniques. They all have in common the need of charged molecules because they rely on electric/magnetic forces which cannot be applied to uncharged molecules. Therefore, prior to analysis, molecules must be ionized. Most prominent techniques are electrospray ionization (ESI), desorption electrospray ionization (DESI), secondary ion mass spectrometry (SIMS), matrix-assisted laser desorption/ionization (MALDI) and laser desorption/ionization (LDI). Because of several advantages, MALDI was the method of choice for the present scientific study.

1.1.1 MALDI MS

MALDI was first described by Karas, Bachmann and Hillenkamp in 1985.[1] In their initial experiments they used LDI for the analysis of amino acids. The threshold irradiance for detection of ion signals of pure alanine was up to tenfold higher than when this nonabsorbing amino acid was mixed with the absorbing amino acid tryptophan. The authors assumed that "[t]ryptophan thus must be regarded as an absorbing matrix resulting in molecular ion formation of the nonabsorbing alanine"[1] and called the process "matrix-assisted laser desorption".[1] Organic matrices mostly used today because of their high versatility and sensitivity compared to inorganic ones or nanoparticles.[2,3]

In distinction to LDI, the matrix is applied to the sample for several reasons: First, matrix molecules dilute and separate analyte molecules by co-crystallisation.[2,4,5] Second, the matrix segregates analyte molecules from contaminations and therefore purifies the sample. Hence, MALDI tolerates relatively high contaminant concentrations of up to 5 %.[2,6] Third, matrix molecules contain light absorbing systems, enabling the absorption of the laser energy and transfer to the analyte molecules.[1,4,7,8] Even analyte molecules containing their own light absorbing systems (so-called chromophores) show better ionization yields when analyzed after addition of a matrix. Sometimes, even chromophores cannot be analyzed without matrix at all. For instance, this was shown by Karas *et al.* for vitamin B12.[7] By adding this step (energy uptake by matrix, followed by energy transfer to the analyte molecule) to the ionization procedure, MALDI becomes softer than LDI because the matrix prevents analyte molecules from thermal decomposition. Therefore, analyte molecules stay intact and do not get fragmented.[7,9] Fourth, the matrix aids in votalization and evaporation of analyte molecules and ions.[1,2,7] Fifth, the matrix supports ion formation.[1,7,9] Depending on the circumstances, different mechanisms of ionization apply in varying proportions. One

model assumes preformed ions in the matrix crystals, either during crystallization or as chemical ionization, that are transferred to the gas phase, as it was suggested by Karas *et al.* For instance, they suggested a reaction between nicotinic acid (NA) matrix molecules in the excited-state (*) and analyte molecules (M):[7]

$$NA^* + M \longrightarrow [NA - H]^- + [M + H]^+$$

Furthermore, they suggested a proton-transfer reaction if a matrix radical was formed after irradiation, here in case of 2-nitrophenyl octyl ether (NPOE) as matrix:[7]

$$NPOE^{+\bullet} + M \longrightarrow [NPOE - H]^{\bullet} + [M + H]^+$$

Alternatively, ions can be formed in the gas phase.[10] The second approach is preferred for low molecular weight neutral species.[11] For larger molecules, such as peptides, proteins or oligosaccharides, preformed ions are the preferred mechanistic route.[5]

With the help of laser optics, the laser beam is focused onto the sample surface. The matrix absorbs the laser energy and the analytes are vaporized and ionized. Both, UV- (mostly N_2 or Nd:YAG), as well as IR-lasers (mostly Er:YAG) can be used.[12]

In general, MALDI-spectra nearly exclusively contain singly charged ions. This facilitates spectra interpretation because conclusions about the mass can be directly drawn from m/z:

$$m/z = m \quad \text{if } z = 1. \tag{1}$$

An explanation for the singly charged ion formation is the so-called "lucky-survivor model". According to this model, there are recombinations of cationic and anionic plasma compartments in the gas phase. These neutralization reactions occur slower for singly charged ions than for multiply charged ones, so that singly charged ions stay more often in the gas phase.[5] Despite all theoretical considerations, the interaction between matrix and analyte and therefore the suitability of a matrix for a particular biological sample can often not be predicted and has to be tested in experiments.[13]

For the analysis of oligonucleotides and deoxyribonucleic acid (DNA), commonly used matrices are 6-aza-2-thiothymine (ATT),[14] picolinic acid,[15] 3-hydroxypicolinic acid (HPA),[16] and 3-aminopicolinic acid (3-APA).[17] For oligosaccharides, gentisic acid (2,5-dihydroxybenzoic acid (DHB))[18] and 3-aminoquinoline (3-AQ)[19] are frequently used. Peptide and protein analysis can be carried out by applying sinapinic acid (SA),[20] α-cyano-4-hydroxycinnamic acid (α-CHCA)[21] or 2,6-dihydroxyacetophenone (DHAP).[22] Also, DHB works fine for proteins,[23] but also for lipids.[24] Additionally, 9-aminoacridine (9AA)[25] was established for lipid analysis. Furthermore, rather exotic molecules such as C_{60}-fullerene were applied for the analysis of biomolecules such as insuline, cytochrome c and bovine albumine,[26] but also inorganic molecules like phosphotungstic acid.[9]

1.1.2 MALDI MS imaging

If not only the mass spectra, but also the localization of the sample spots are recorded, then the generation of mass spectra-related images is possible, the so-called mass spectrometry imaging (MSI). The most prominent MSI methods are MALDI, SIMS, and DESI, all of which have their own advantages and disadvantages. MALDI MSI fits perfectly to our analytical question and was therefore employed for this study.

A big advantage of MALDI is that only minimal sample preparation is needed. In contrast to DESI, matrix coating is necessary,[27] but analytes do not have to be brought into liquid phase as it is the case of ESI. This allows direct ionization from the native biological sample. Hence, the spatial distribution of the analytes is preserved, enabling MSI, which was first presented by Spengler *et al.* in 1994.[28] Samples are scanned and the spatial information is matched to mass spectrometric information. Picking one *m/z* ratio and showing its intensities in grey scale results in a reproduction of the analyte distribution on the sample surface. Each measuring spot corresponds to a pixel, the collectivity results in an image. Using different colors or color scales, different *m/z* ratios can be shown in one image to visualize for example different compartments of biological tissue. However, to keep the image well-arranged, only a few *m/z* ratios should be shown in one image. Therefore, it can be necessary to show several images of different *m/z* ratios of the same data set to reproduce its full information content. Nonetheless, the displayed information is easy to comprehend without further knowledge of the used techniques. By overlaying MS images with optical images of the analyzed tissue, the localization of concentration gradients is possible.[29]

In order to achieve high lateral resolution, matrix application is a critical step.[13] It has been shown that analytes are not distributed equally within a matrix crystal and that crystallization time is a crucial parameter regarding crystal size and analyte distribution within the crystal.[30] Matrix application is commonly done by a pneumatic sprayer.[31] Alternatively, the matrix can be spotted on the sample, mostly done by a robot.[32] Otherwise, in case of solvent-free sample preparation, the matrix can also be sublimated onto the sample.[33] The overall goal is to get small pixels for high lateral resolution, at a sufficient analytical sensitivity. Therefore, fine matrix crystals are needed. Currently, resolutions of 5 µm to 10 µm are routinely used,[34] but even pixel sizes of 1.4 µm have been realized.[35]

With lower pixel sizes and therefore higher spatial resolutions, even MSI analyses of single cells are possible.[36] However, highly sensitive methods are needed to detect even small amounts of analytes. Smaller pixel sizes result in smaller ablation areas and thus lower numbers of generated ions. Consequently, only the abundant analytes can be detected. This often leads to the preferential detection of metabolites and lipids because they are present in relatively high concentrations in biological samples and are easily ionized.

The introduction of atmospheric pressure (AP) MALDI in 2000 made the analy-

sis of volatile compounds and the usage of volatile matrices possible.[37] This led to further development of so-called atmospheric-pressure scanning microprobe matrix-assisted laser desorption/ionization (AP-SMALDI),[38,39] combining analysis at atmospheric pressure and high lateral resolution of up to 1.4 µm.[35]

1.1.3 Orbital trapping mass spectrometer

Following ionization in the MALDI source, ions are analyzed with an orbital trapping mass spectrometer. Both, inventing the working principle and giving proof of the principle, was done by Alexander Makarov in 2000.[40] The instrument was introduced under the name "Orbitrap" in 2005.[41] Similar to a Fourier-transform ion cyclotron resonance (FT-ICR) instrument, it has a high mass resolving power (up to 1 000 000 full width at half maximum (FWHM) at *m/z* 200) and accuracy (< 1 ppm).[42] Since the orbitrap works without a magnetic field, it can be built in much smaller instruments and magnet cooling is avoided, leading to lower costs of acquisition and maintenance.[41]

The orbitrap is based on the Kingdon trap, which was invented in 1923 by Kingdon and further improved by Knight.[43,44] Inside the trap, ions circulate around a spindle-formed electrode. The electrostatic attraction of the central electrode is compensated by the centrifugal force, so that the ions are on stable orbits. The centrifugal force is a result of the tangential velocity that the ions have at their entrance into the trap.[45] The injection of ions is not perpendicular to the axis of the central electrode, but slightly offset to it. This results in an additional movement along this axis. Around the inner electrode, there is a second, barrel-shaped one which is split in two parts. Its electrostatic field catches the ions in their orbit. Altogether, there is a superposition of three different movements: ions circulate in orbits around the inner electrode, oscillate in their orbital radius and oscillate along the axis of this electrode in a periodic way.[40] These moving charges induce an electric image current in the outer electrode that can be detected. Its frequency ω_z, that can be determined using Fourier transformation, depends only on the *m/z* ratio of the ions with the following equation:

$$\omega_z = \sqrt{k\left(\frac{z}{m}\right)} \tag{2}$$

ω_z : frequency of the oscillation along the axis of the inner electrode (z-direction),

k : force constant, can be determined by calibration,

z : charge number of the ions,

m : mass of the ions.

Especially in higher *m/z* regions, neighbouring signals can easily overlap. For ex-

ample, this can be the case in biological samples that contain many lipids with similar mass. In order to disambiguate these signals, high mass resolution is crucial. Additionally, this allows the annotation of detected signals with the help of databases. High mass resolution also simplifies tandem mass spectrometry (MS/MS) experiments because precursor ions can be separated more efficiently prior to fragmentation. This leads to less fragments, thereby facilitating the identification of analyzed substances. For the biological samples in our studies, high mass resolution was crucial to analyze the complex analyte mixtures appropriately.

1.1.4 LC-MS/MS

When using an orbital trapping mass spectrometer, high mass accuracy is achieved. Using the accurate *m/z* values and database research, ion signals can be annotated with substances. However, no structural information is gained to prove an annotation and structural isomers cannot be separated. Therefore, additional information is needed.

The use of liquid chromatography-tandem mass spectrometry (LC-MS/MS) adds two new dimensions of information. On the one hand, prior to MS analysis, analytes are separated by high performance liquid chromatography (HPLC) according to their polarity. This provides a new parameter, retention time (RT), that can conversely be used to acquire information about the polarity of the analytes. Potential interactions between molecules can be bypassed by separating the molecules followed by stepwise analysis. Further, matrix effects and ion suppression are reduced because of the chromatographic separation. Depending on the column used, isobaric molecules (might) also be separated before they are ionized and analyzed, allowing for a higher resolution.[46] In order to couple HPLC and MS/MS, so-called reversed-phase high performance liquid chromatography (RP-HPLC) must be performed. The use of reversed-phase instead of normal-phase HPLC is crucial for the successful separation of polar biomolecules, such as peptides. In liquid chromatography-mass spectrometry (LC-MS), an ESI source is most commonly used.[47] Following ionization, molecules are measured in the mass spectrometer and their accurate mass is determined. The ions with the highest signal intensity are isolated and fragmented. Those fragments are then used to evaluate the molecular structures and distinguish between different isomeric forms.[46] Combined information of RT, accurate mass and fragmentation leads to not only annotation, but also identification (characterization) of analytes.

During the first step of method development, LC-MS/MS was used. It is the gold standard for the identification of analytes such as lipids.

In our case, samples were analyzed in data-dependent acquisition (DDA) manner: full MS scans were followed by fragmentation of the 15 most intense ions. The resulting fragment ions were then monitored by another MS scan.[46] In contrast, in data-independent acquisition (DIA) mode, all ions are fragmented in a set of *m/z* windows, leading to spectra that are more complicated to interpret.

1.1.5 On-tissue MS/MS

In the second study, on-tissue MS/MS experiments were performed to further reduce the sample preparation process while maintaining the same level of identification. Due to matrix effects, signal intensities are often lower in on-tissue experiments. This complicates MS/MS analyses. However, on-tissue MS/MS has already been succesfully applied to analyze proteins (after tryptic digestion),[48] lipids,[49] and glycolipids.[50]

1.2 Parasites, hosts, and their interactions

1.2.1 Parasites

According to the Centers for Disease Control and Prevention (CDC), the national public health agency of the United States of America, "a parasite is an organism that lives on or in a host organism and gets its food from or at the expense of its host."[51] Therefore, it is mostly dependent on its host in order to survive. In contrast to a symbiotic coexistence, the parasite harms its host, e.g. by scavenging nutrients.

The development of the parasites often results in the death of the host, in particular in the case of endoparasites. Many hosts developed methods to fight parasites, like building barriers and encapsulating the parasites. In general, the entering of a parasite into a host organism leaves marks that can be used to detect parasite infestation.

1.2.2 Hosts

Hosts can be categorized into different groups.

Intermediate hosts harbor intermediate life stages of the parasite. Intermediate hosts are needed for further (sexual) development of the parasite.

In contrast, through definitive hosts, parasites reach maturity and start to reproduce. Depending on the parasite, the parasite stays alive (inside the host) after reproduction or kills the host. However, it is usually not the intent of the parasite to kill the host since it depends on its host.

Another host type are accidental hosts. They are neither needed for the development of the parasite nor for its reproduction. Instead, no full development is possible. However, the host can still suffer from heavy diseases.

A reservoir host does not show any symptoms of infection, but can carry and maintain the parasite. Therefore, they are often transmitters of the infection without any notice.[52]

1.2.3 Parasite–host interactions

In order to find new strategies to fight parasites but not the host, knowledge about the interaction between the parasite and its host is crucial. Additionally, finding metabolic pathways that only occur in the parasite may lead to new drug targets.

Parasite–host interactions can have various aspects. The most prominent one is the scavenging of nutrients from the host by the parasite, such as blood in case of mosquitos and ticks. However, the interactions start even before blood sucking. In order to find a suitable host, ticks have the so-called Haller's organ to detect possible hosts via chemoreceptors.[53]

Additionally, parasites can induce behavioral changes in their host. A prominent example is *Toxoplasma gondii* (*T. gondii*), which infects rats as intermediate hosts.[54] Berdoy *et al.* showed that infected rats do not only lose their fear of cats but even trigger incautious behavior, such as more frequent visits to cat-smelling places.[55] Also, male rats infected by *T. gondii* were seen to be more appealing for females than healthy ones, promoting further sexual transmission.[56] This effect is caused by higher excretion of α2u-globulins in the urine of infected males.[57]

However, parasite–host relationships do not need to be exclusively negative. For example, patients infected with *Schistosoma mansoni* (*S. mansoni*) showed less positive skin prick tests for aeroallergens.[58] Another example is the usage of medicinal leeches, which were already used in ancient medicine for various implications.[59] Nowadays we know that their saliva contains anticoagulants as well as anesthetically-acting, anti-inflammatory substances.[60] For this reason, leeches are still in medical use today, for example to improve wound healing after transplanting surgeries.[59,61] However, to prevent transmission of parasites and diseases from patient to patient, each leech is only used a single time.[59]

1.3 *Schistosoma mansoni*

S. mansoni is a blood fluke infecting humans as their main host and inducing a disease called Schistosomiasis or Bilharzia.[62] According to the world health organization (WHO), nearly 240 million people suffer from the disease, and several million people have to live with serious health impairments as a consequence.[63] Therefore, it is classified as a neglected tropical disease (NTD).[64] Besides humans, it was found to also infect rodents, such as rats,[65] water rats,[66] African grass rats,[67] and Hubert's multimammate mice,[68] and primates, such as vervet monkeys[69] and baboons.[70,71]

Schistosomes belong to the group of trematodes and they have developed into two different sexes. *S. mansoni* can mostly be found in Africa and South America, but also in the Arabian region.[62] The spread of the parasite depends mostly on the spread of the intermediate host.[72,73] *S. mansoni* need fresh water snails of the genus *Biomphalaria* as intermediate hosts for further development.[74]

Beside *S. mansoni*, several other schistosomes are known to infect humans.

Infected definitive hosts excrete schistosome eggs, which can survive up to seven days. When they get in contact with water, miracidia hatch into the water. There, they enter their intermediate host. Inside the snails, miracidia multiply asexually. After four to six weeks, they develop to cercariae which can already be distinguished by

sex. One miracidium infecting a single snail can lead to several thousand cercariae. Cercariae are released into the water and stay infective for up to three days. They enter their definite host through the skin and migrate into the blood vessels, where they further develop into juvenile worms, the so-called schistosomulae. After another four to six weeks, schistosomulae mature to adult worms. They mate in the portal vein of the liver and move to the mesenteric veins of the gut, where they typically stay for three to five years, but they can live up to 30 years. After pairing, female *S. mansoni* worms live in a groove inside the male's body. Typically, the paired worms stay embraced. Here, the female worms fully mature and start to produce several hundred eggs per day. Eggs migrate into the intestine and are finally excreted, starting a new lifecycle.[62]

Directly after infection, irritated skin, so-called "swimmer's itch" can occur where cercariae entered the hosts body.[62] Four to nine weeks after infection, symptoms of acute schistosomiasis start to occur when the worms start to produce eggs. Symptoms are rather unspecific, such as fever, weakness, weight loss, headache, anorexia, diarrhea, or dry cough. Mostly, symptoms last for up to three months before improving mostly without medical treatment.[75] In rare cases, also more severe symptoms, like bloody diarrhea, mental dullness, or bronchospasm can arise. During the acute phase, schistosomiasis therapy is mainly directed against the symptoms, not the cause of the disease.[76]

After roughly 12 weeks, the infection shifts from the acute to its chronic stage. While the acute phase is characterized by reactions of the host immune system to migrating schisosomulae, the chronic stage is dominated by tissue damage induced by eggs, not from the worm itself.[76,77] The reason for this is that not all eggs migrate into the gut and are secreted with the feces. Around 50 % to 70 % stay in the organism of the host.[77] With the hosts blood stream, they move from the veins to different organs where they get trapped. Most of these misled eggs can be found in the liver. In the tissue, the eggs cause inflammatory reactions leading to granuloma formation. This process does also occur in the intestinal wall and is crucial for further transportation of the eggs to the gut lumen. However, in other tissues the eggs are not released, but stay trapped, and granulomas become fibrotic.[77]

During the chronic phase of the disease, the severity is mostly dependent on the total infection time, often correlating with the age of the patient. While teenagers mostly suffer from bleeding, ulceration and polyposis, elderly people are more affected by liver fibrosis and hydronephrosis. Ulceration is caused by inflammation, which is a reaction of the host tissue to misled eggs. Throughout further maturation of granulomas formed around the eggs, scar tissue is responsible for more severe issues, such as liver fibrosis. However, not all chronically infected humans show symptoms. Especially patients who already had contact to the parasite early in their life only have milder or do not show any symptoms.[76]

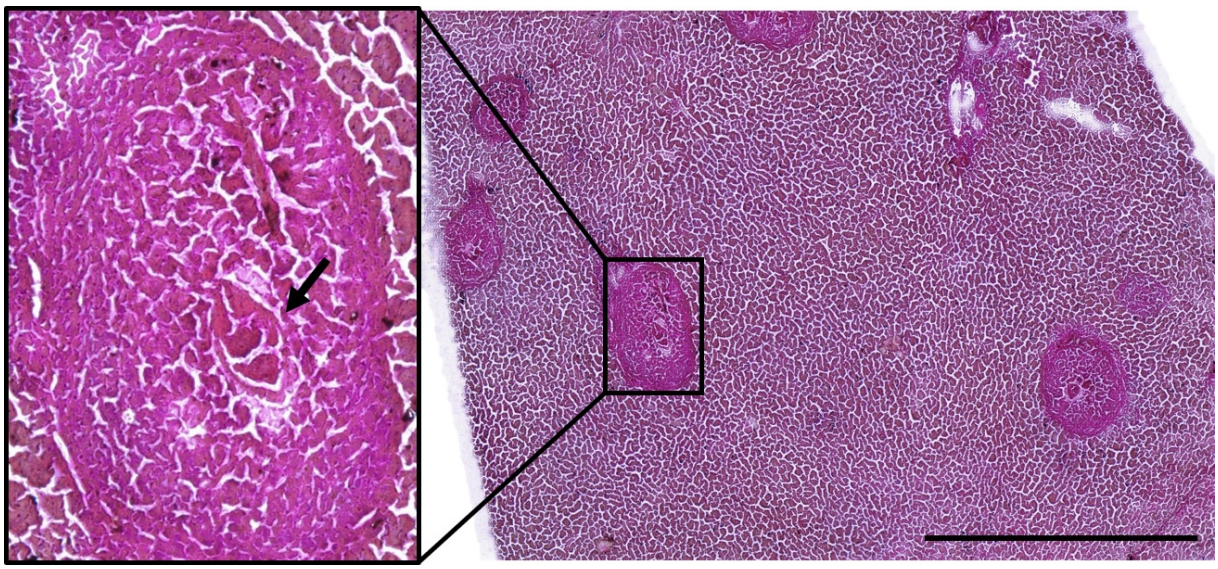

Figure 1: *S. mansoni* eggs induced granulomas in infected, H&E-stained tissue section. The section was prepared from fresh frozen hamster liver tissue and stained after MALDI MSI measurements. On the left-hand side, a zoom-in into the granulomatous region is shown. An arrow points at the *S. mansoni* egg. Scale bar is 1 mm.

Granulomas formed in hamster liver after infection with *S. mansoni* eggs can be seen in figure 1. After MALDI MSI measurements, matrix crystals were carefully washed away using ethanol, and the section was hematoxylin-and-eosin (H&E) stained. When zooming into a granuloma, even the eggs are still visible, as it can be seen on the left-hand side in figure 1. While the eggs are cone-shaped with a length of 100 µm to 200 µm,[78] granulomas are rounder and their cross section commonly has a size of 100 000 μm^2, leading to a diameter of approximately 350 µm when assuming a circular shape.[79]

Though, granulomas do not only harm the host and benefit the parasite. By enabling egg excretion of the living host, they protect the host from being killed to complete the parasites life cycle. Additionally, they are a physical barrier, separating egg and host tissue. Also, granulomas isolate antigenic substances segregated by the eggs, soluble egg antigens (SEA), protecting host tissue from further damage.[80] As the interface between the mammalian host and the parasitic egg, granulomas are of high interest when studying parasite–host interactions in *S. mansoni* infections.

1.4 *Besnoitia besnoiti*

Besnoitia besnoiti (*B. besnoiti*) is an apicomplexan parasite within the family of the *sarcocystidae* causing the so called Besnoitiosis. It is related to *T. gondii* (causing Toxoplasmosis), *Plasmodium falciparum* (*P. falciparum*) (causing malaria), and *Cryptosporidium parvum* (*C. parvum*) (causing Cryptosporidiosis).[81–83]

During its lifecycle, it is assumed that *B. besnoiti* infects different hosts.[84] Its definitive host is unknown, but it is known for infecting cattle as intermediate host.[85,86] Fe-

line species are suspected to be the definitive host,[87] but this could not be proven.[88] However, the final host is supposed to be a carnivore species.[86] There are other related parasites in the genus *Besnoitia* with different (intermediate) hosts. Infections to humans are not known.[85]

In addition to suspected vertical transmission (from definitive host to intermediate host), there is horizontal transmission (from intermediate to intermediate host) of *B. besnoiti*.[86] Sharif *et al.* demonstrated that transmission of *B. besnoiti* from chronically infected cattle to rabbits through stable flies is possible.[89] Due to climate changes, blood sucking insects are extending their habitats, which may lead to further spread of *B. besnoiti*.[90] However, the lifetime of *B. besnoiti* in insects is limited. According to Bigalke, *B. besnoiti* survives 1 h in stable flies, up to 3 h in tsetse flies, and up to 24 h in horse flies.[91] Therefore, it is unlikely that transmission occurs over longer distances via biting insects.[86] Gollnick *et al.* showed, that transmission cannot occur over distances longer than 20 m.[92]

Cattle infected with *B. besnoiti* develop a disease called Besnoitiosis.[85] Symptoms of the disease were described for the first time from Cadéac in 1884. He reported infected animals in the south of France.[93] In 1912, Besnoit *et al.* reported another case from the Pyrenees and described the parasite for the first time.[94] In honor of Besnoit the parasite was following called *Besnoitia besnoiti*.[95,96]

In Europe, the disease was only spread in the southwest (Portugal, France) at first,[86] but since the 1990s, it has also occurred in other parts of Europe.[85] Also in Spain,[97] Italy,[98,99] Germany,[87,100] Greece,[101] Swiss,[102] Hungary,[103] Belgium,[104] and Ireland[105] infected cattle were reported and parasites isolated and identified. Outside of Europe, *B. besnoiti* was also found in Simbabwe,[106] South Africa[107] and Israel.[108]

Besnoitiosis occurs in two stages with different symptoms. Up to two weeks after infection, bovines enter the acute stage. This stage is characterized by parasites in the tachyzoite stage, which replicate quickly, mostly in endothelial cells.[109] Roughly two weeks later, the disease progresses through the subacute stage, ending in the chronic stage around 70 days after infection. The chronic stage is characterized by parasites in the bradyzoite stage, which replicate slowly and are stored in mature tissue cysts. These cysts are mainly formed in skin and mucous membranes,[85,109] and they are the most important criterion to distinguish between the different stages of Besnoitiosis. Cysts have a characteristic shape and are easily identified, as it can be seen in figure 2 on the following page. There are no cysts during the acute stage, as they start to develop during the subacute stage. After entering the chronic phase, the cysts are fully developed.[110] The development of cysts is irreversible.[111]

In general, the symptoms of besnoitiosis are unspecific and can also be caused by other diseases such as scabies, fungal infection, and others.[112] During the acute stage, infected cattle can show fever, respiratory problems, loss of appetite and therefore loss of weight, swollen lymph nodes as well as hyperemia and edema of skin. In addition,

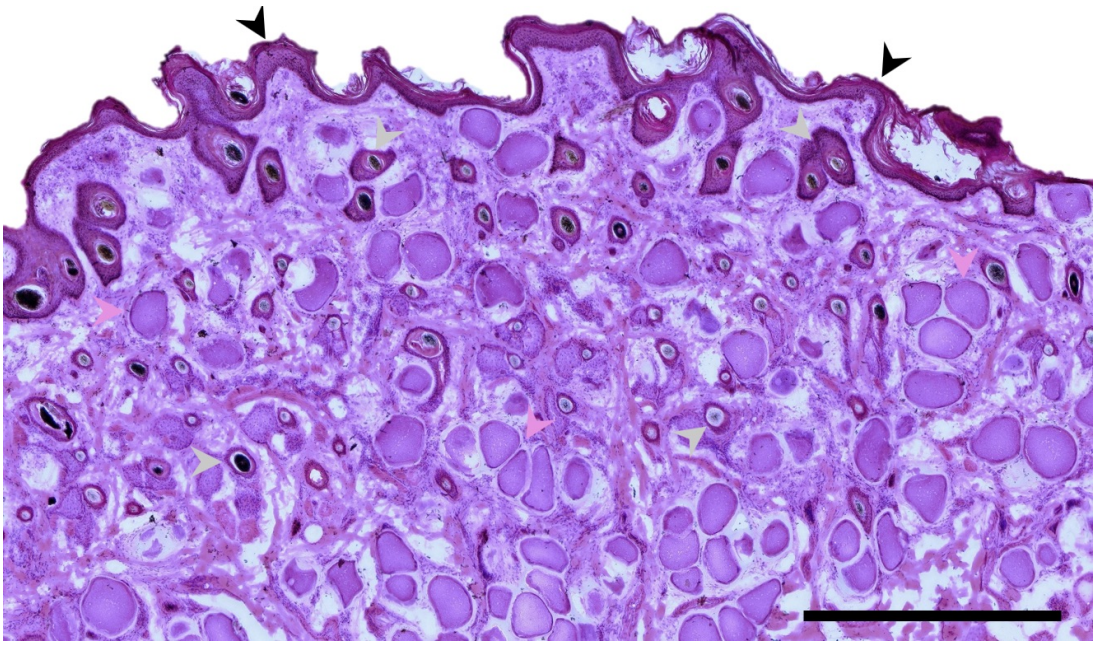

Figure 2: Skin cysts (rose-colored arrow heads) in *B. besnoiti*-infected, H&E-stained tissue section. The section was prepared from fresh frozen bovine skin tissue. Additionally, hair follicles (grey arrow heads) and epidermis (black arrow heads) are clearly recognizable. Scale bar is 1 mm.

bulls show inflamed testis, cows a decrease in milk production. In the chronic phase, edema decrease while typical symptoms such as thickening and hardening of skin, hair loss and sometimes still swollen limbs remain.[107,112] Bulls can even get permanently infertile. Many infected individuals do not show any or only very mild clinical symptoms and only have skin cysts, so that the disease is not easily diagnosed after recovery from a mild course of disease. Presumably, such animals are the main propagator of parasites.[85,107]

Confirmation of infection, and especially recognition of subclinical cases, is done serologically by detection of antibodies in the serum of (presumed to be) infected animals. This can be done either with indirect fluorescence antibody tests (IFATs),[113] western blots,[114] enzyme-linked immunosorbent assays (ELISAs),[114] smear tests,[115] or polymerase chain reaction (PCR).[112] Additionally, histological proof of parasites in skin and isolation of tachyzoites in cell culture should be performed.[112]

In rare cases (roughly 10 %),[116] Besnoitiosis directly causes the death of infected animals. Slaughter of affected cattle to prevent further spread in the herd is the common practice. Even when the course of disease is considered mild, it causes economic losses. Affected cattle produce less milk and have more miscarriages. Additionally, loss of weight and potential infertility of bulls can be observed. Also, the skin is less suitable for the production of leather due to the symptoms.[86]

Usually, only older animals are affected, but even a chronically infected calf, aged less than six months, was described in Spain in 2017.[117] Until today, there are neither effective drugs nor vaccines.[85] There are studies of live vaccines in South Africa[118] which are also used in Israel, but they are not licensed in Europe.[86] The scarce knowl-

edge of the chain of infection and primary way of infection in cattle makes it difficult to develop a safe immunization method.[112]

In order to find new treatments, it is crucial to know the influence of *B. besnoiti* on the metabolism of infected animals. In 2016, Taubert *et al.* found higher conversion rates of glucose, lactate, glutamine, glutamate, pyruvate, alanine and serine in *B. besnoiti*-infected bovine umbilical vein endothelial cells (BUVEC), leading to the assumption that the degradation of glucose, glutamine, and serine are upregulated. These metabolism processes are the major suppliers of energy for cell reproduction. Additionally, involved intermediates as well as the products themselves are important resources during cell proliferation. Both effects are needed for fast replicating parasites and might be a starting point for further drug research.[81]

Studying the parasite *in vivo* instead of *in vitro* can give further insights into metabolic changes induced by the parasite and therefore set the path for new therapeutics.

1.5 Statistical methods

In order to find changes between infected and non-infected samples, the following statistical methods were applied.

1.5.1 ANOVA

In general, the so-called one-way analysis of variance (ANOVA) is used to test if there is an influence in varying one factor $x_1, x_2, \ldots, x_k$ on the response variable y. In our case, the infection state was the varying factor (parasite tissue, infected-host tissue and non-infected host tissue), and the lipid content the response variable. When the test is performed to see if there are two varying factors with an influence (for example, infection state and sex of the host), the procedure is called two-way ANOVA. For more than two factors, it is called multivariate analysis of variance (MANOVA).[119]

ANOVA compares two different variances: the variance within one group from sample to sample and the variance between the groups. The null hypothesis H_0 is that there is no difference between the groups.[119]

By putting the inter-group variance in relation to the intra-group variance, a so-called F-score is calculated. If the calculated F-score is larger than the respective tabulated value, H_0 can be refused with a level of significance α. This means that there is a significant difference between at least one pair of probed groups. However, the test does not indicate between which groups the difference occurs. Therefore, post-hoc tests are needed.[119]

1.5.2 Tukey's post-hoc test

In order to perform Tukey's post-hoc test, it is required that the groups and samples have the same size. This was the case in our situation. In general, the test compares

the means of groups in a pairwise manner. If the difference between two groups is larger than a cut-off value, the groups are concerned to be significantly different. The cut-off depends on the number of groups and the desired level of significance and can be found tabulated.[120,121]

1.5.3 PCA

Beside searching for significantly different groups in a large data set, another statistical tool is the so-called principal component analysis (PCA). It allows the reduction of a complex data matrix to a simpler one without losing information. This is achieved by removing information that is redundant. Therefore, a data matrix with M dimensions is transformed to a new matrix with a lower number of dimensions.[122]

The axes of coordinates of this new matrix are the so-called principal components. By definition, the first principal component contains the most information about the input data. Subsequent principal components contain less information. By plotting the data points against the first two (or three) principal components, a 2- (or 3-) dimensional plot is obtained.[120] If the input data differ between the different sample groups, the samples within one group will cluster. By this, the different groups will be separated from each other. In our studies, this already provides first hints of a change in the lipid profile during infection.

1.6 Current state of research

1.6.1 Usage of MSI for parasite–host interaction studies

Only few studies used MALDI MSI for the analysis of parasite–host interactions. In 2017, Dopstadt *et al.* used MALDI MSI for the localization of alkaloids in rye after infection with *Claviceps purpurea*. They were able to visualize the distribution of mycotoxins and metabolites in infected grains. In this way, they demonstrated the promising usage of MALDI MSI for the analysis of parasite–host interactions. However, their lateral resolution with a pixel size of 35 µm was rather low.[123]

Negrao *et al.* analyzed footpads from mice infected with two different strains of *Leishmania* at different time points post infection with MALDI MSI. With a pixel size of 150 µm, they detected some peptides in the range of m/z 2000 to 10 000, being significantly altered during disease progression.[124]

Not only parasite–host interactions, but also symbiotic relationships can be studied by MALDI MSI. For instance, Gemperline *et al.* and Schoenian *et al.* used MALDI MSI to analyze the distribution and composition of bacteria-derived compounds on the bodies of leaf-cutter ants. The ants are growing fungi as a food source. The authors found that the bacteria living on the exoskeleton of the ants help them by protecting the fungi from other harmful bacteria.[125,126] Similar work was carried out by Kroiss

et al. by analyzing antibiotic substances formed by bacteria in the cocoon of beewolf digger wasp larvae with the help of LDI MSI.[127]

1.6.2 Lipidome and metabolome of *Schistosoma mansoni*

Different stages of *S. mansoni* have different requirements on their metabolism due to varying environments during development.[128] While free-living stages such as eggs, miracidia and cercariae have to survive on their own until they enter the next host, parasitic stages can rely on their host organism. However, also different hosts provide different environments: While miracidia develop to cercariae in water snails, these cercariae further grow inside their definitive mammalian host. Another striking difference beside the availability of substrates between free-living and parasitic stages is the presence of oxygen, which is needed for energy gaining reactions. Therefore, different substrates might be used as well.

S. mansoni was an object of research in several studies. Different methods, such as thin-layer chromatography (TLC), HPLC, high-performance thin-layer chromatography (HPTLC), gas chromatography (GC), gas chromatography–mass spectrometry (GC-MS), ESI MS, LC-MS/MS, as well as radioactivity-based assays were used to examine the lipid composition of different life stages. Additionally, the intermediate host *Biomphalaria glabrata* (*B. glabrata*) was included in some studies. The main lipid groups found were phospholipids (PLs), including phosphatidic acids (PAs), phosphatidylcholines (PCs), lysophosphatidylcholines (LPCs), phosphatidylethanolamines (PEs), lysophosphatidylethanolamines (LPEs), phosphatidylinositols (PIs), phosphatidylglycerols (PGs), phosphatidylserines (PSs), lysophosphatidylserines (LPSs), but also cardiolipins (CLs), ceramides (Cers), sphingomyelins (SMs), fatty acids (FAs), triacylglycerides (TGs), diacylglycerides (DGs), cholesterol and cholesteryl esters (CEs) were detected. An overview can be found in table 1 on page 20.

In conclusion, many different PLs were found to play an important role in the composition of all *S. mansoni* life-stages. Most of the presented studies used chromatography-based methods like, e.g., TLC or LC-MS/MS to analyze the lipid contents of different schistosome stages. These are excellent methods to gain a general overview of the lipid contents, but the lateral information about the origin of the lipids is lost during sample preparation. MSI is the perfect method to overcome this limitation.

1.6.3 MSI studies on *Schistosoma mansoni*

In a first study, Ferreira *et al.* analyzed male, female and paired *S. mansoni* worms from two different strains using MALDI MSI in 2014. Without further sample processing, they directly mounted the whole worms on targets and coated them with matrix. The authors were able to distinguish male and female worms as well as the two strains from each other based on the fingerprints of the obtained mass spectra. This was also

confirmed by PCA. Even with a relatively low lateral resolution (pixel size of 50 µm) and low mass resolution they were able to differentiate different biological structures within a single worm on the PL-, DG- and TG-level.[129]

Kadesch *et al.* also studied *S. mansoni* worms with MALDI MSI. The sample preparation in particular was a critical step because *S. mansoni* worms are only 7 mm to 20 mm long,[62] and 400 µm thick.[130] Unlike Ferreira *et al.*, Kadesch *et al.* prepared cryosections. This enabled the analysis of internal organs. *S. mansoni* were fixed with glutaraldehyde, placed directly on a miniaturized sample holder, covered with aqueous gelatin solution, and then were immediately frozen. This made the preparation of "artifact-free, longitudinal cryosections"[130] possible, which were required for further MALDI MSI analyses.[130]

Based on their first study, Kadesch *et al.* analyzed the lipidome of different schistosome compartments with a combination of MALDI MSI and LC-MS/MS and found characteristic differences between worm surface and inner tissue as well as between male and female worms. For instance, PCs and PEs showed higher intensities in the inner compartment of the worms and SMs were more found on the surface. Additionally, females seemed to contain TGs with shorter fatty acyl chain lengths, while fatty acids in TGs of male origin were less saturated.[131]

There is only one drug, praziquantel (PZQ), against *S. mansoni* available and a decrease in susceptibility to the drug is observed. This may be a hint that resistances start to occur.[132] Consequently, there is urgent need to find new drugs. Therefore, MALDI MSI experiments were performed on drug-treated *S. mansoni* worms.

Mokosch *et al.* investigated the drug uptake and metabolism of imatinib in schistosomes using MALDI MSI.[133] Imatinib is a potential new drug that is already used to cure cancer[134] and that showed promising results against schistosomes *in vitro*.[135] Mokosch *et al.* could show that imatinib seems to be mainly taken up via an oral route.[133]

Earlier, Ferreira *et al.* performed MALDI MSI experiments on *S. mansoni* worms treated *in vivo* with PZQ. Both male and female worms had altered lipid compositions after therapy, but the response was different.[136]

However, all experiments were conducted on whole worms outside their host, so the interaction between *S. mansoni* and its host could not be studied. Additionally, mislead eggs are more likely to be responsible for harmful effects of schistosoma infection than the worms themselves.[77] Therefore, we aimed to visualize the effects of *S. mansoni* eggs trapped inside the hosts liver, leading to granulomatous reactions.

Table 1: Literature overview of studies performed on *S. mansoni*.

year	parasite component	analytical methods	findings	authors	reference
1969	worms	TLC, GC-MS	chain length of FAs in TGs and PLs ranged between 12 to 24 carbon atoms, in rare cases also 13 to 23	Smith *et al.*	137
1970	worms	TLC, GC, radioactivity-based assays	no *de novo* FA and sterol synthesis, FA chain elongation, but no desaturation, TG and cholesterol main neutral lipids, PC and PE main PLs, also PG, CL, PS, PI found, FA chain length 16 to 20 carbon atoms	Meyer *et al.*	138
1982	worms	TLC	content: PC>PE>PS>PG	Young *et al.*	139
1986	tegument	TLC	PC main PL in the outer bilayer, PE main PL in the plasma membrane	Young *et al.*	140
1987	cercariae, worms, tegument	TLC, GC	SM, PC, PS, PE in all sample groups, high SM content and cholesterol/PL ratio in tegument, FA(20:1) essential in PLs of tegument	Allan *et al.*	141
1988	cercariae, schistosomula, adult worms	GC, HPLC	only cholesterol in adults, in cercariae and schistosomula also desmosterol, and phytosterols, which were also present in *B. glabrata*, PI, PS, PE, PC in all stages, SM and LPC in adults	Furlong *et al.*	142
2002	cercariae	HPTLC	most PLs PC and PE, also free FAs and sterols	Schariter *et al.*	143
1997	adults	TLC, HPLC, radioactivity-based assays	conversion FA(18:1) to FA(20:1), TGs no reservoir of FAs for PL synthesis, high FA turnover in PLs, low in TGs, quick assembly of FAs to PCs, slow to TGs	Brouwers *et al.*	144
2008	worms	LC-MS/MS	contain PCs, PEs, PSs, PIs	Retra *et al.*	145
2015	tegument	LC-MS/MS	LPE(20:1) and LPS(20:1) enriched	Retra *et al.*	146
2014	eggs, miracidia, cercariae	ESI MS	eggs: PC, TG, PA, PE, DG, glycosylated Cer, also different between different strains of *S. mansoni*	Ferreira *et al.*	147
2018	eggs, cercariae, worms	LC-MS/MS, GC-MS	CE, PE, LPE, DG, FA, PC, LPC, SM, TG in all stages, PC(34:1), PC(36:1) and PC(36:2) prevalent in all stages, eggs: mostly CE, LPC, PC, TG, worms: higher amounts of FAs than eggs, SM nearly exclusively, only few LPC	Giera *et al.*	148
2014	male, female, paired worms	MALDI MSI	distinguish male and female based on fingerprint MS, differentiate biol. structures based on PL, DG and TG distributions	Ferreira *et al.*	129
2020	worms	MALDI MSI, LC-MS/MS	differentiate surface and inner components, differentiate male and female worms, PC and PE higher in inner parts, more SM on surface, females: shorter FA chain in TGs, males: FA chains in TGs less saturated	Kadesch *et al.*	131
2021	worms treated with imatinib	MALDI MSI	imatinib uptake via oral route	Mokosch *et al.*	133
2015	worms treated with PZQ	MALDI MSI	altered lipid composition after treatment	Ferreira *et al.*	136

1.6.4 Studies on *Besnoitia besnoiti*

Not much research has been done on *B. besnoiti* and there are even less mass spectrometric studies of *B. besnoiti*.

In 2013 and 2014, there were three publications from a research group in Spain applying MS on *B. besnoiti*, but all of them focused on the proteome.[149–151]

Regarding the lipidome, there is only one MS study from 2020. Kadesch *et al.* analyzed pure *B. besnoiti* tachyzoites and found markers for infection with tachyzoites in BUVEC cell cultures. These markers were mainly PLs of the groups PA, PC, PE, PG, and PI, but also DG content was found to be changed.[152]

Apicomplexan parasites seem to be unable to synthesize cholesterol and therefore need to scavenge it from their host.[153,154] To have access to sufficient amounts of cholesterol, there are two different ways: Either taking it up from the blood stream of the host or upregulating the host cell's *de novo* cholesterol synthesis. By performing fluorescence experiments and quantitative PCR, Silva *et al.* showed that both occur in *B. besnoiti*-infected BUVEC.[155]

However, all these results were obtained in cell cultures. Currently neither lipid analysis nor mass spectrometry imaging studies have been carried out *in vivo*.

1.7 Study outline

Two different parasite–host systems were chosen. The first parasite was *S. mansoni*. Here, LC-MS/MS was combined with MALDI MSI. To further optimize the method, *B. besnoiti* was then studied by using only MALDI MSI. Additionally, ultra-high-resolution MSI experiments as well as a three-dimensional reconstruction based on MSI data were performed. Also, the statistical data evaluation was slightly modified to further simplify data analysis.

The two different parasite–host systems showed different manifestations of parasitic infection in the host tissue. One system, *S. mansoni*, showed visible host reaction: the manifestation of granulomas. The other system, *B. besnoiti*, showed especially the parasite's action: building of cysts, containing the "storage form" of the parasite. By combining different mass spectrometric approaches, manifold infection-induced changes in the lipid profile were found for both cases. In several cases they could also be aligned with infection-induced structural changes, giving insights into metabolic modifications due to infection. These variations now can be hints for potential drug targets.

1.7.1 Hamster liver containing *Schistosoma mansoni* eggs

In our first study, we wanted to examine the changes in the lipid composition of hamster liver due to infection of the hamster with *S. mansoni*.[156] We used a combination

of LC-MS/MS and MALDI MSI in order to not only annotate and localize, but also identify characteristic lipids and metabolites.

Three different sample groups were analyzed:

- **Bisex-infected samples**: Livers of hamsters infected with both male and female *S. mansoni* cercariae. These samples contained trapped eggs in the liver and, as a reaction, granulomas were formed around the eggs.
- **Singlesex-infected samples**: Livers of hamsters being infected only with one sex of *S. mansoni* cercariae either male or female. Therefore, they did not contain eggs and granulomas but their lipid composition in general was changed due to a systemic infection.
- **Non-infected samples**: Livers of hamsters being neither infected with male nor female *S. mansoni* cercariae.

1.7.1.1 Database generation

For all groups, three biological replicates (n=3) were used. All samples were received as fresh frozen tissue as well as under cryo-conditions prepared homogenates. Homogenates were used for lipid extraction[157] and were then subjected to LC-MS/MS analysis. Lipids were identified using Lipid Match Flow 3.1.[158] In total, 1450 ions of lipids and metabolites were identified in healthy as well as *S. mansoni* eggs-containing hamster liver tissue.

1.7.1.2 Statistically significant changes

Following database generation, statistical analyses were performed using the Perseus software package[159] according to Kadesch *et al.*[131] Of all ions found in hamster liver, 372 were significantly changed in signal intensities when comparing peak areas for infected and control samples ("infection markers"). These markers mainly belonged to the lipid classes of PCs, PEs, and TGs. Previously, Giera *et al.* mainly detected PCs and TGs in *S. mansoni* eggs, cercariae and worms.[148] Also the observation of other significantly altered lipids (such as CEs) is in good accordance with the previous study. However, we also found DGs, what might be a consequence of studying not only parasite material, but parasite and host tissue together. Most of the markers were found when comparing bisex-infected samples with single-sex as well as with non-infected samples. That leads to the assumption, that the effects of the eggs in the liver were more severe than the effects of the systemic infection. This matches to findings in literature were it is assumed that the misled eggs, trapped in organs such as the liver, do have more severe effects on the host than the actual worm infection.[77]

Regarding the lipid profile, we also found more significantly altered ions by comparison of bisex-infected samples and controls than by comparing singlesex-infected

samples to controls. While 80 % of all significantly enriched ions were found in comparison of bisex-infected to control samples, even 95 % of significantly depleted ions were found for the same constellation (see figure 3).

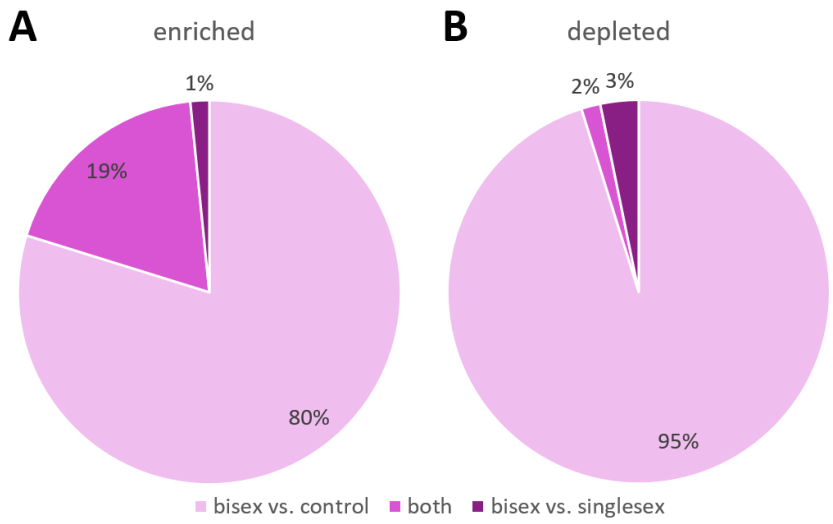

Figure 3: Percentage of infection markers found enriched (A) or depleted (B) when comparing bisex-infected samples to controls or to singlesex-infected ones. In both cases, many more markers were found when comparing bisex-infected samples to controls than to singlesex-infected samples. This can be a hint, that the influence of the eggs to the lipid profile of infected tissue is much higher than the systemic influece of the worms to the whole organism.

1.7.1.3 Visualization of infection-induced changes

Applying MALDI MSI gave us the opportunity to locate some of the infection-induced lipidomic changes to specific biological structures. By visual inspection of MS images and comparison to optical images that were obtained prior to MALDI measurements, lateral distributions of infection markers were assigned to specific infection-driven structures. Various examples of different distributions found in positive- as well as in negative-ion mode are shown in figure 4 on the next page. Observed biological structures were

- *S. mansoni* eggs (figure 4 C),
- granulomas around the eggs (figure 4 E, F, I, J, K, and L),
- unaffected liver tissue (figure 4 D, and H), and
- the whole liver tissue, containing unaffected tissue, granuloma regions and eggs (figure 4 B).

While some lipids were found exclusively in the designated regions, others were present in the whole tissue section, but in higher intensities in the granuloma regions, such as LPE(20:4) (figure 4 E), PC(41:4) (figure 4 J), or PC(O-16:1_18:0) (figure 4 K).

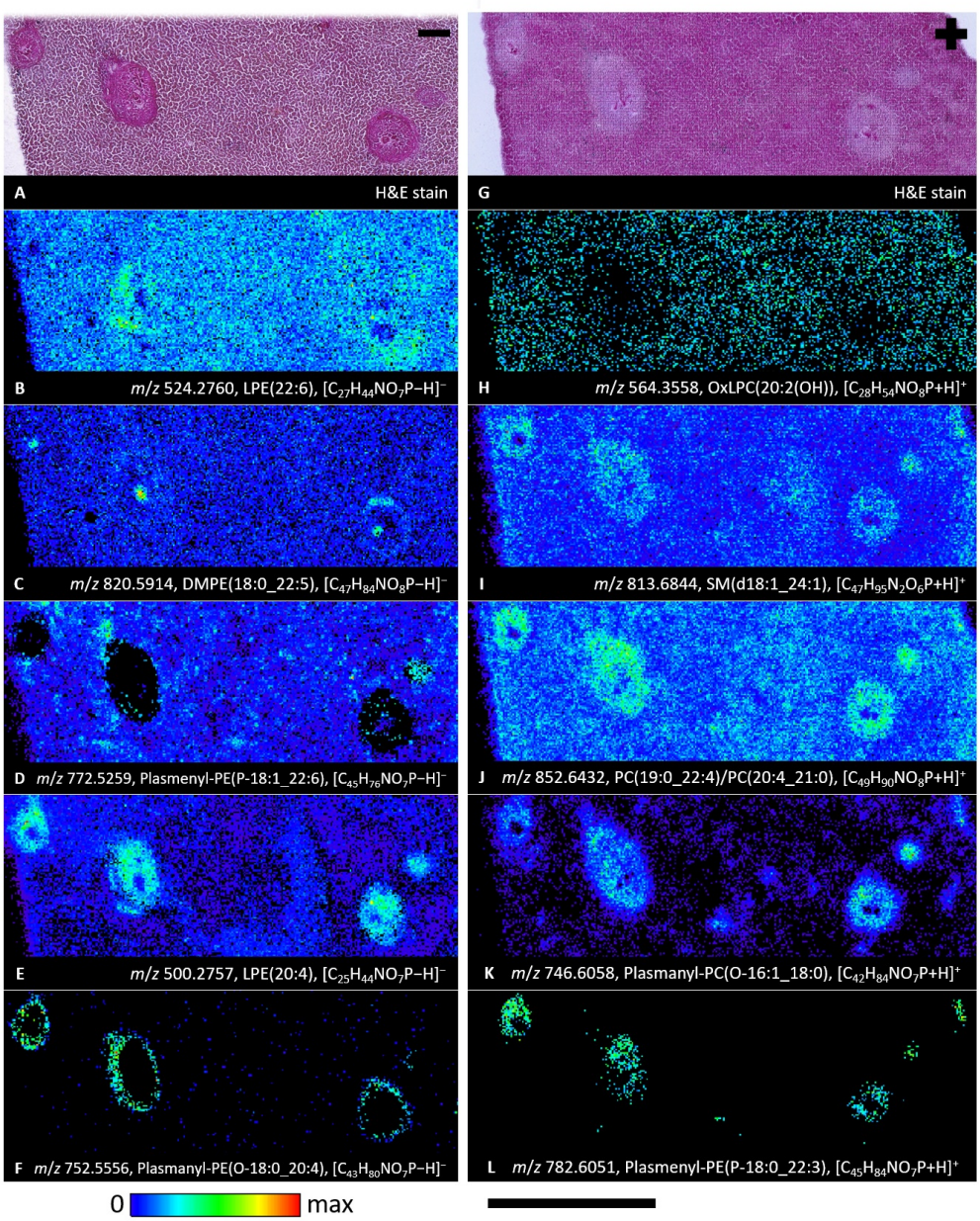

Figure 4: MS images of *S. mansoni* eggs-containing hamster liver tissue, reflecting different biological structures, and light microscopic images of the corresponding H&E-stained tissue sections. Scale bar applies for all images and is 1 mm. A: H&E-stained hamster liver tissue section after MSI measurement in negative-ion mode. Three large granulomas containing *S. mansoni* eggs and additionally the end of a granuloma without parts of the egg visible on the far-right side are recognizable. B: LPE(22:6), being found mainly evenly distributed in the whole tissue. C: DMPE(18:0_22:5), being found evenly distributed in the whole tissue, but enriched in the *S. mansoni* eggs. D: Plasmenyl-PE(P-18:1_22:6), being found evenly distributed in the whole tissue, but not in the granuloma regions. E: LPE(20:4), being found evenly distributed in the whole tissue, but with higher intensities in the granuloma regions (but not in the eggs). F: Plasmanyl-PE(O-18:0_20:4), being slightly found in the whole tissue, but mainly in the outer part of the granulomas. G: Consecutive H&E-stained hamster liver tissue section after MSI measurement in positive-ion mode. As in A, three large granulomas containing *S. mansoni* eggs and additionally the end of a granuloma without parts of the egg visible on the far-right side are recognizable. H: OxLPC(20:2(OH)), being found mainly evenly distributed in the whole tissue with slightly lower abundances in the granuloma regions. I: SM(d18:1_24:1), being found evenly distributed in the whole tissue, but slightly enriched in the granuloma regions. J: PC(41:4), being found evenly distributed in the whole tissue, but strongly enriched in the granuloma regions. K: Plasmanyl-PC(O-16:1_18:0), being slightly found in the whole tissue, but with higher intensities in the granulomas (without the eggs). L: Plasmenyl-PE(P-18:0_22:3), being only found in the granulomas.

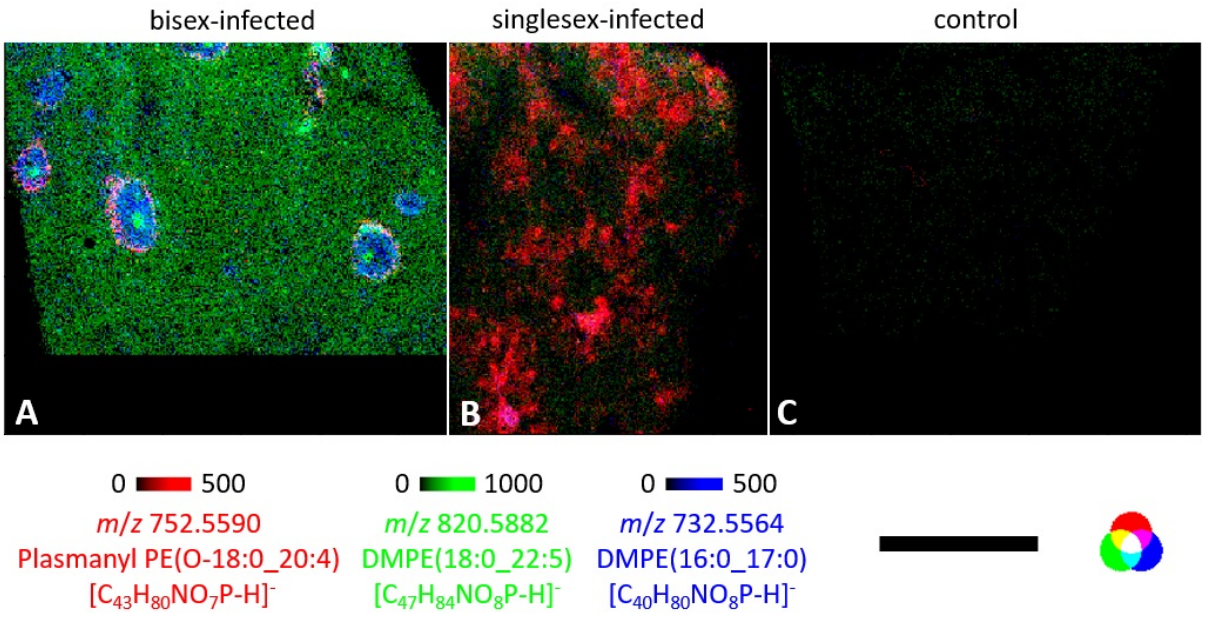

Figure 5: Overlaid MS images visualizing eggs in liver tissue of hamster infected with *S. mansoni* of both sexes and granulomas formed in the surrounding (A) in comparison to control samples of singlesex-infected (B) and healthy (C) hamsters. The same ion channels were used for all three subfigures and they were all adjusted to the same intensity levels. Scale bar is 1 mm.

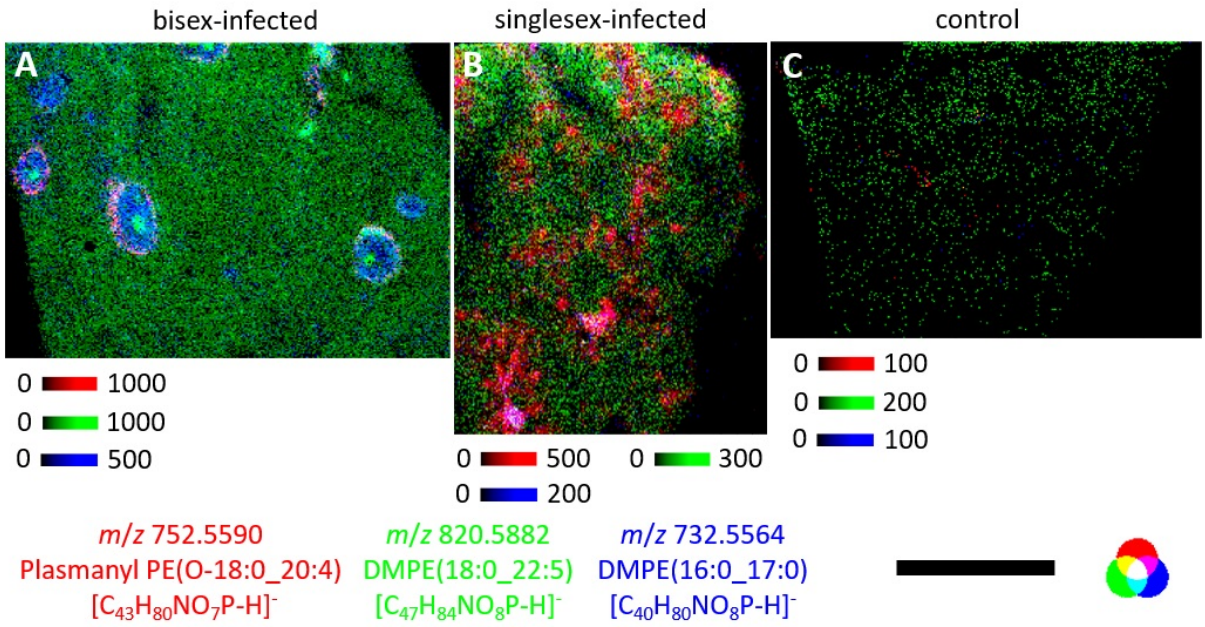

Figure 6: Overlaid MS images visualizing eggs in liver tissue of hamster infected with *S. mansoni* of both sexes and granulomas formed in the surrounding (A) in comparison to control samples of singlesex-infected (B) and healthy (C) hamsters. The same ion channels were used for all three subfigures. In contrast to figure 5, signal intensities were not adjusted globally, but for each measurement individually. Scale bar applies for all images and is 1 mm.

Not all infection markers matched to one of these groups but in total we were able to allocate 23 % of markers to the structures mentioned above.

Interestingly, structurally related lipids seemed to be accumulated in completely different lateral distributions. For example, PE(P-18:1_22:6) (see figure 4 D) was found evenly distributed in the unaffected tissue, but not in the granuloma regions. However, LPE(22:6) (figure 4 B) was found evenly distributed in the whole tissue, with slight enrichment in the granulomas. Inverse distributions were observed for PE(O-18:0_20:4) and LPE(20:4): While PE (figure 4F) was only detected in the outer parts of the granulomas, its lyso form (figure 4 E) was found in the whole tissue with strong enrichment in the granulomas. Nevertheless, it has to be kept in mind, that the lyso forms do not necessarily originate from the PEs mentioned. To verify a connection between the two forms, further studies, for example after feeding with isotope-labeled substances, could aid in clarification.

When overlaying the single-ion images, the biological structures nicely interdigitate, as figure 5 on the preceding page shows. Dimethylphosphatidylethanolamine (DMPE) (16:0_17:0), mostly found in the granulomas as shown in blue, fits perfectly into the "hole" formed by DMPE (18:0_22:5) represented in green. Also, the overlay verifies, that the plasmanyl-PE shown in red is an accumulation in the outer part of the granulomas and not a ring formed around the granulomas. This effect will be further discussed in section 1.7.1.4.

Additionally, the already described effect has become obvious in figure 5, that "significant changes" not necessarily means presence only in the bisex-infected samples. More often, signals were detected in both or even all three groups, but with varied intensities (figure 3 on page 23). This is nicely reflected by the MS images: ions shown in red and green are also present in the singlesex-infected sample in figure 5. When zooming in, also the blue ion channel becomes visible and even in the control sample some pixels in red, green and blue appeared. When not scaling the intensity levels globally, as it was done for figure 5, but instead for each sample individually, as it was done for figure 6, it can be clearly recognized, that the ions were also detected in the singlesex-infected and especially also in the control sample, but with much lower intensities.

1.7.1.4 Granulomatous substructures

Granulomas appeared not to be uniform, instead there was a substructure. This was not the case for all altered ions, but some examples are shown in figure 7 on the following page. Especially in the overlay figure 7 D (showing figure 7 A to C), three different layers of the granulomas can be recognized. All of the displayed ions are ether PLs. In contrast to normal PLs, ether PLs do not contain two fatty acids esterified to the glycerol backbone, but instead only one fatty acid. The other *sn* position is linked to a (vinyl-) ether. Plasmanyl-PLs (e. g. PC(O-36:4)) contain an aliphatic ether, plasmenyl-PLs (e. g. PE(P-36:3)), also called plasmalogens, contain a vinyl ether.[160] Finding ether lipids in the contact area between host and parasite (the granulomas) matches well to

the literature. Brouwers *et al.* detected plasmalogens in *S. mansoni* worms and found them enriched in the outer tegumental membranes.[161]

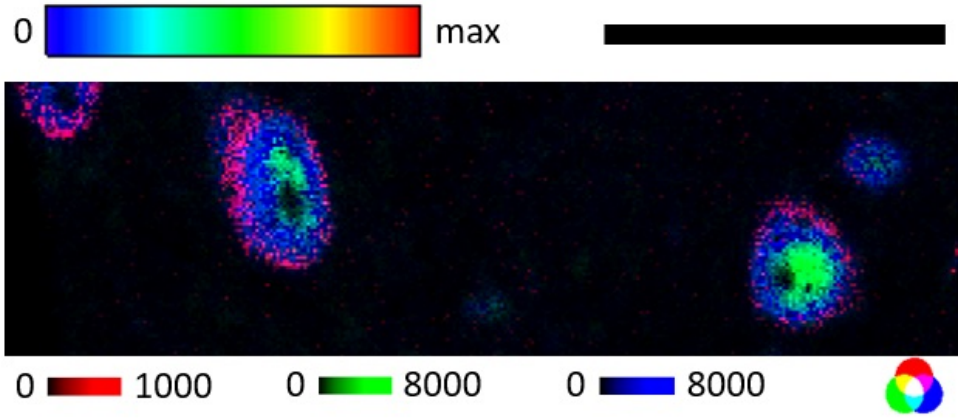

Figure 7: Substructure in granulomas formed around *S. mansoni* eggs in hamster liver visualized by MALDI MSI. Scale bar is 1 mm. Green: *m/z* 724.5309, identified as Plasmenyl-PE(P-16:0_20:3) as well as Plasmanyl-PE(O-16:0_20:4), $[C_{41}H_{76}NO_7P-H]^-$, being mainly found in the inner part of the granulomas. Blue: *m/z* 746.5141, identified as Plasmenyl-PE(P-16:0_22:6), $[C_{43}H_{74}NO_7P-H]^-$, being detected in the whole tissue sections, but with higher intensities in the granulomas and even more in the middle part of the granulomas, between egg and surrounding liver tissue. Red: *m/z* 752.5556, identified as Plasmanyl-PE(O-18:0_20:4), $[C_{43}H_{80}NO_7P-H]^-$, being only found in the outer part of the granulomas in the contact region between granulomas and surrounding tissue.

1.7.1.5 Conclusion first publication

We gained deeper insights into the interactions between the parasitic schistosome egg and the hosting hamster liver tissue. Due to infection, 372 compounds were significantly changed in signal intensity, most of them lipids. For roughly one quarter of them, characteristic lateral distributions were observed, matching to biological structures. For example, some lipids, e.g. Plasmenyl-PE(P-18:1_22:6) or MMPE(16:0_22:6), were found to be depleted around the egg. Lipids are important energy sources and building blocks, and the eggs cannot produce them on their own, so they need to scavenge them from their host. Also, ether lipids were found enriched in the granuloma region. Ether lipids are known to build a barrier against harm by soluble egg antigens. The presented study nicely fits into literature and adds lateral information by using MALDI MSI and therefore providing further knowledge about lipid concentrations and distributions upon infection.

1.7.2 Bovine skin containing *Besnoitia besnoiti* tissue cysts

For the second study we had two goals: First, we wanted to simplify our method and second, we wanted to apply it to a second, completely different parasite–host system to test its broad applicability. In this case, bovine skin of animals infected with the apicomplexan parasite *B. besnoiti* was used. Due to chronic infection, the skin contained parasite-filled cysts that were already visible with the naked eye. To streamline the

analytical method, we only performed MALDI MSI experiments without verification of our annotations with LC-MS/MS. Instead, we performed on-tissue MS/MS to identify part of the ions. Additionally, statistical analysis was done with MetaboAnalyst.[162]

In a previous experiment, formaldehyde-fixed paraffin-embedded (FFPE) tissue sections were tested for MALDI MSI analysis. In contrast to fresh-frozen tissue samples, they can be stored at room temperature for a long period of time without major degradation. Also, FFPE tissue samples can be cut thinner than fresh frozen ones, enabling better histological assessment. Therefore, they are the gold standard in histology, and huge tissue biorepositories exist. Being able to analyze FFPE tissue samples with MALDI MSI would open the door to huge sample collections, especially in cases, where sample material is rare, as is the case for *B. besnoiti*-infected bovine skin.

To perform MALDI MSI experiments, the paraffin needs to be removed prior to matrix coating, otherwise the paraffin would disturb the MS measurements. However, the washing steps with xylene also remove or at least relocate endogenous lipids and, depending on the chemical structure, also metabolites. To evaluate this effect, we analyzed an FFPE tissue section in comparison to a fresh frozen one, see figure 8 on the next page.

As it can be seen, lipid signals were either absent in the tissue section or are randomly distributed, not reflecting any biological structures in the FFPE slide. In contrast, lipid signals nicely reflect parasite-induced structures in the fresh frozen tissue section. Furthermore, detected lipids had significantly lower signal intensities: In the MS image from a fresh frozen sample (D), signal intensities of both ions were normalized to a level of 10 000. In case of the analysis of FFPE tissue (B), signal intensities were only normalized to a level of 100. Another aspect is the thickness of the sections. The FFPE sections were cut with a thickness of 7 µm, the fresh frozen cryosections with a thickness of 20 µm. Nonetheless, this effect is presumably not as important as the others, as both sections were easily H&E stained after the MALDI MSI measurements and as the optical images (figure 8 A and C) show, the structure of the tissue is nicely conserved and little material was ablated during the MSI experiment.

The disadvantage of using fresh samples is that only one infected animal with naturally acquired besnoitiosis and two control animals from the local slaughterhouse were available. Nevertheless, we had skin samples from three different parts of the diseased animal, originating from shoulder, neck, and elbow region. PCA analysis nicely reflected that the infected samples came from the same animal, while the controls originated from two different individuals (see figure 9 on page 30). The PCA was based on signal intensities in the MALDI MSI experiments of all signals. Therefore, the PCA plot already gives a hint about the different compositions of the infected and control samples regarding lipid and metabolite content.

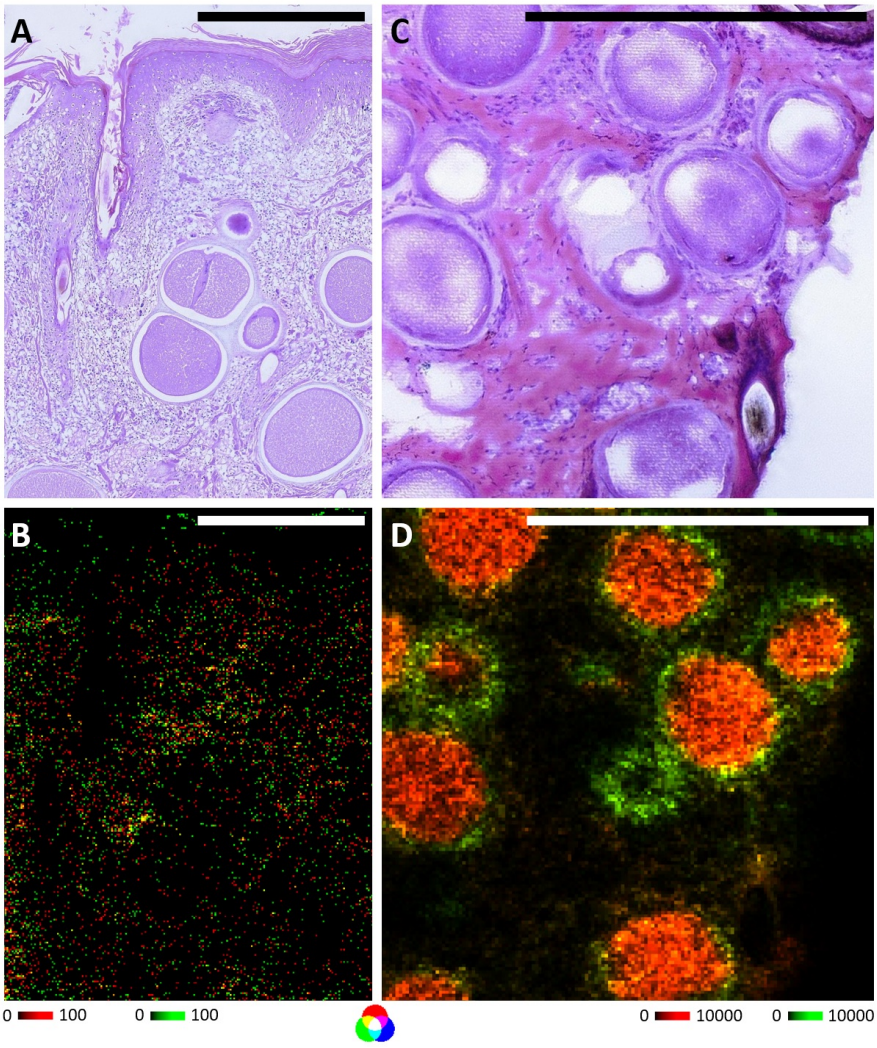

Figure 8: Comparison of MALDI MSI measurements of FFPE (A and B) and fresh frozen (C and D) bovine skin tissue infected with *B. besnoiti*. After MALDI MSI analysis, matrix was washed off with ethanol and sections were H&E stained (A and C). While generating the MS images (B and D), the same ions for both samples were used. However, signal intensities were adjusted differently, as the intensity scales show. The red ion channel represents *m/z* 786.6007, identified as PC(36:2), $[C_{44}H_{84}NO_8P + H]^+$; the green ion channel shows *m/z* 760.5850, identified as PC(34:1), $[C_{42}H_{82}NO_8P + H]^+$. Signal intensities are not only much lower in FFPE tissue (B) than in the fresh frozen one (D), the ions are also evenly spread over the whole tissue section in the measurement of an FFPE section, while they nicely reflect the parasite-induced cyst structures in the MS image of the fresh frozen sample. Scale bars are 1 mm.

In addition to PCA, all annotated lipids and metabolites of these two groups were compared in terms of signal intensity using t-tests. The received list of "marker" signals was then used to generate MS images, and the distribution patterns were inspected manually as it was previously done in the *S. mansoni* project.

In total, 552 ions were found to be influenced by *B. besnoiti* infection. However, they do not belong to 552 different molecular species. Some compounds were detected in multiple adduct forms ($+H^+$, $+Na^+$, and $+K^+$) or also in both ionization modes (as $+H^+$ as well as $-H^+$). Overall, 467 unique compounds were found to be affected by infection. Most of them were (phospho-)lipids, such as PAs, PSs, PCs, PEs, TGs, PIs, and PGs.

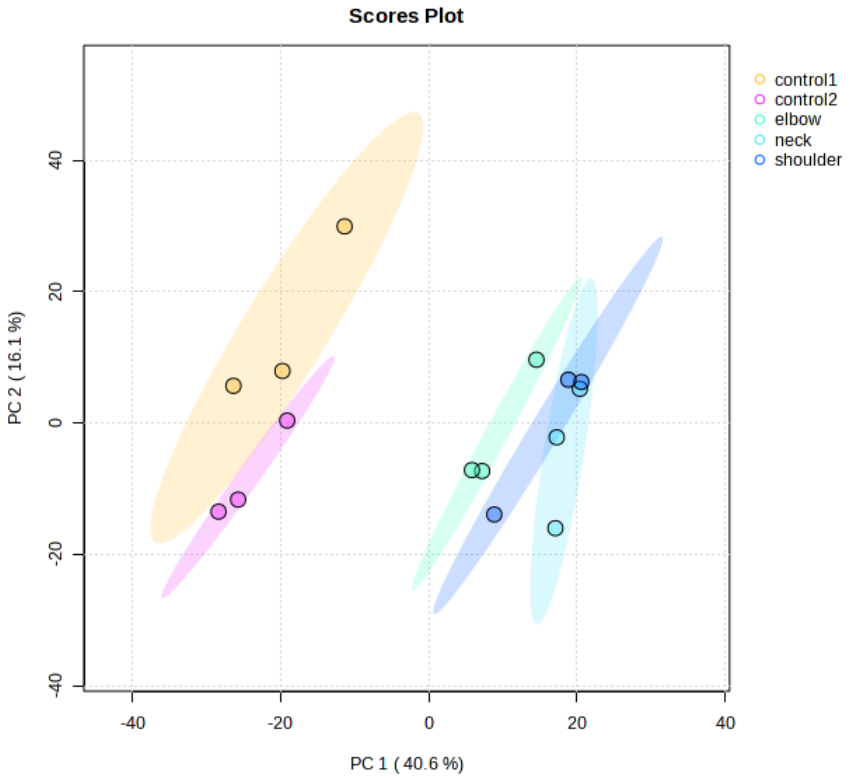

Figure 9: PCA plot of *B. besnoiti*-infected and control bovine skin samples based on signal intensities of all ions detected in MALDI MSI measurements. Control 1 and 2 originated from two different individuals. Elbow, shoulder and neck samples derived from the same, chronically *B. besnoiti*-infected animal. Control and infected samples are nicely grouped together but separated by group.

1.7.2.1 Visualization of infection-induced changes

MSI measurement of tissue sections with 5 µm pixel size enables discrimination of different skin cyst compartments. While the *S. mansoni* egg-induced granulomas were found with higher distance between each other, the *B. besnoiti* skin cysts were closer to each other. Higher lateral resolution always comes with the price of longer analysis time: By dividing the length of a pixel into halves, the analysis time of the same area increases by a factor of four.

As it was already observed in the first study, some of the significantly changed lipids and metabolites showed distribution patterns matching with biological structures. Examples can be found in figure 10 on page 32 and also in figure 3 of the second publication. These structures include

- *B. besnoiti* skin cysts (figure 10 B),
- walls of the *B. besnoiti*-containing cysts (figure 10 H),
- unaffected skin tissue (figure 10 G),
- hair follicles (figure 10 I), and

- the whole skin tissue, containing unaffected tissue and skin cysts (figure 10 C and D).

In total, 61 % of all significantly altered ions due to infection showed a reasonable lateral distribution pattern. The fact, that this is much more than in the first project is most probably a consequence of the modified workflow. In the first study, different ionization methods were used for compound identification and localization (LC-MS/MS vs. MALDI MSI with on-tissue MS/MS). Different ionization methods have different ionization efficiencies for different lipid groups, explaining the poor overlap. According to literature, the overlap between ESI-based and MALDI analysis is roughly 25 %.[163] In the second study, annotation was in a first step based on Metaspace, followed by identification of some ions with on-tissue MS/MS. Both were based on MALDI data, so only one ionization method was applied. Additionally, with Metaspace, only ions with a reasonable lateral distribution get annotated[164] (avoiding annotations of noise signals), resulting in a higher number of ions with biological-structure matches.

Interestingly, structurally related molecules showed different lateral distributions, like the two FAs FA(18:1) and FA(18:3), with the same chain length, but varying in the number of double bonds. While FA(18:1) was detected everywhere in the tissue, with slight enrichments in the cyst walls (figure 10E), FA(18:3) was only found in the dermis and around hair follicles (figure 10F). Another example is shown in figure 11 on page 33. All ions were annotated as FAs with 20 carbon atoms, but different unsaturations. While the higher unsaturated FA(20:4) and FA(20:3) were only detected in the unaffected tissue for infected samples and everywhere in control samples, the lower unsaturated FA(20:2) and FA(20:1) seemed to accumulate in the cyst walls of infected samples and were only found in lower intensities in the control samples. All four FAs showed significant differences in intensities when infected samples were compared to controls. Apicomplexa are able to synthesize FAs *de novo* but also scavenge lipids and FAs from their host.[165,166] In the Apicoplast, the name-giving organelle all Apicomplexa have in common, FA synthesis takes place via the fatty acid synthase type II (FASII). This pathway mainly produces unsaturated short chain FAs up to chain lengths of 18 carbon atoms.[167] In bradyzoites, the fatty acid synthase type I (FASI) pathway could be of higher relevance.[166] Both, depletion in the parasite-containing regions as well as accumulation around the parasite-formed cysts, can be a hint that the parasites scavenge these FAs to further incorporate them in TGs, which are then used for energy storage and prevent lipotoxicity.[166]

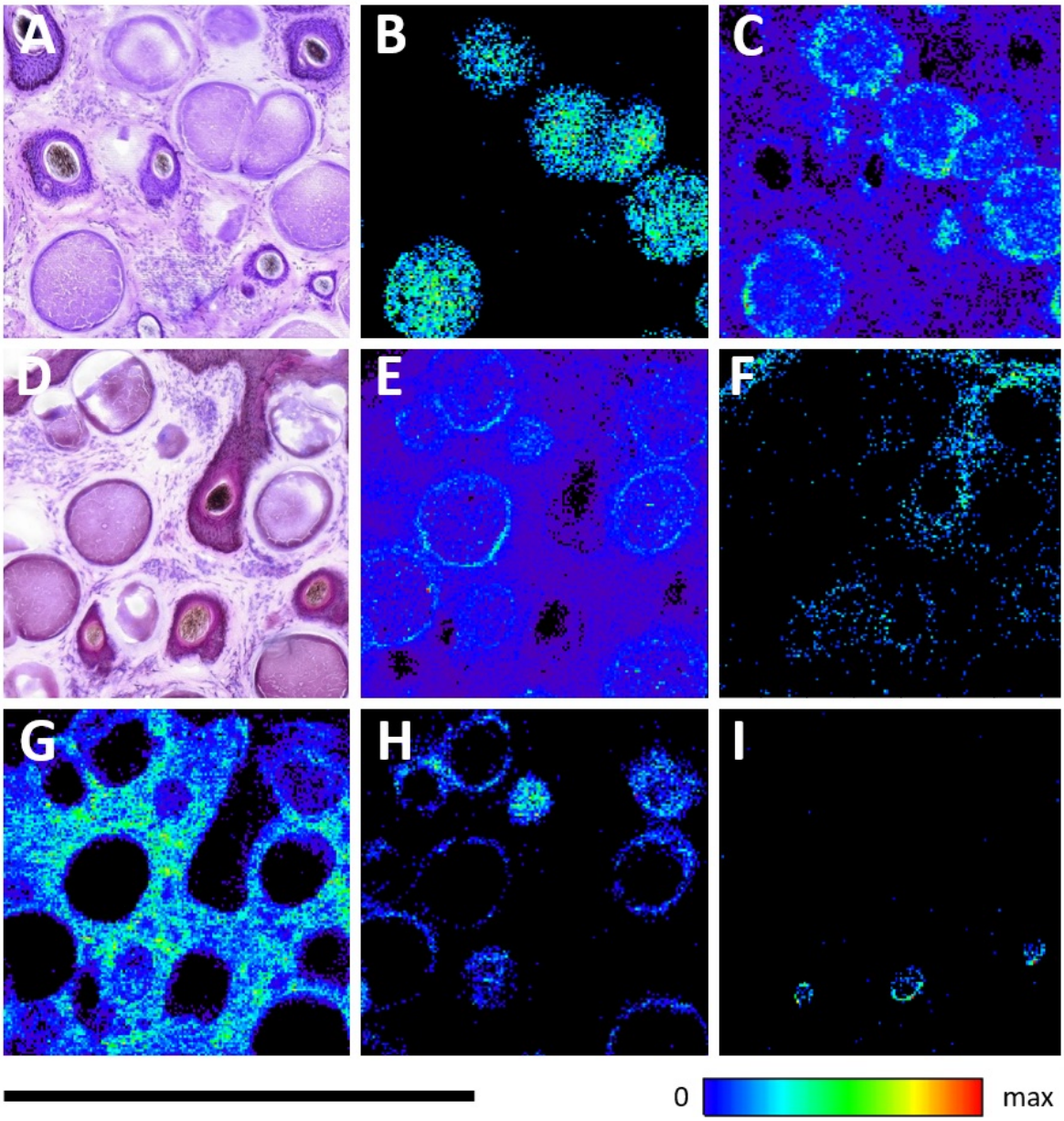

Figure 10: MS images of *B. besnoiti* cysts in bovine skin tissue, reflecting different biological structures, and light microscopic images of the corresponding H&E-stained tissue sections. Scale bar applies for all images and is 1 mm. A: H&E-stained bovine skin tissue section after MSI measurement in positive-ion mode. Several *B. besnoiti* bradyzoites containing cysts as well as hair follicles are recognizable. B: *m/z* 605.4541, annotated as DG(32:1), $[C_{35}H_{66}O_5 + K]^+$, being found only inside the cysts. C: *m/z* 760.5847, identified as PC(34:1), $[C_{42}H_{82}NO_8P + H]^+$, being found evenly distributed in the whole tissue, but enriched in the *B. besnoiti* cysts. D: H&E-stained bovine skin tissue section after MSI measurement in negative-ion mode. As in A, various *B. besnoiti* bradyzoites containing cysts as well as hair follicles, but also small parts of the dermis are recognizable. E: *m/z* 281.2486, annotated as FA(18:1), $[C_{18}H_{34}O_2 - H]^-$, being found mainly evenly distributed in the whole tissue with slightly higher abundances in the cyst wall regions. F: *m/z* 277.2173, annotated as FA(18:3), $[C_{18}H_{30}O_2 - H]^-$, being mainly found in the dermis and around the hair follicles. G: *m/z* 788.5441, identified as PS(18:1_18:0), $[C_{42}H_{80}NO_{10}P - H]^-$, being found evenly distributed in the unaffected tissue. H: *m/z* 915.5946, annotated as PI(40:3), $[C_{49}H_{89}O_{13}P - H]^-$, being only found in the cyst walls. I: *m/z* 372.2755, annotated as 3-hydroxytridecanoyl carnitine, $[C_{20}H_{39}NO_5 - H]^-$, being only found inside the hair follicles.

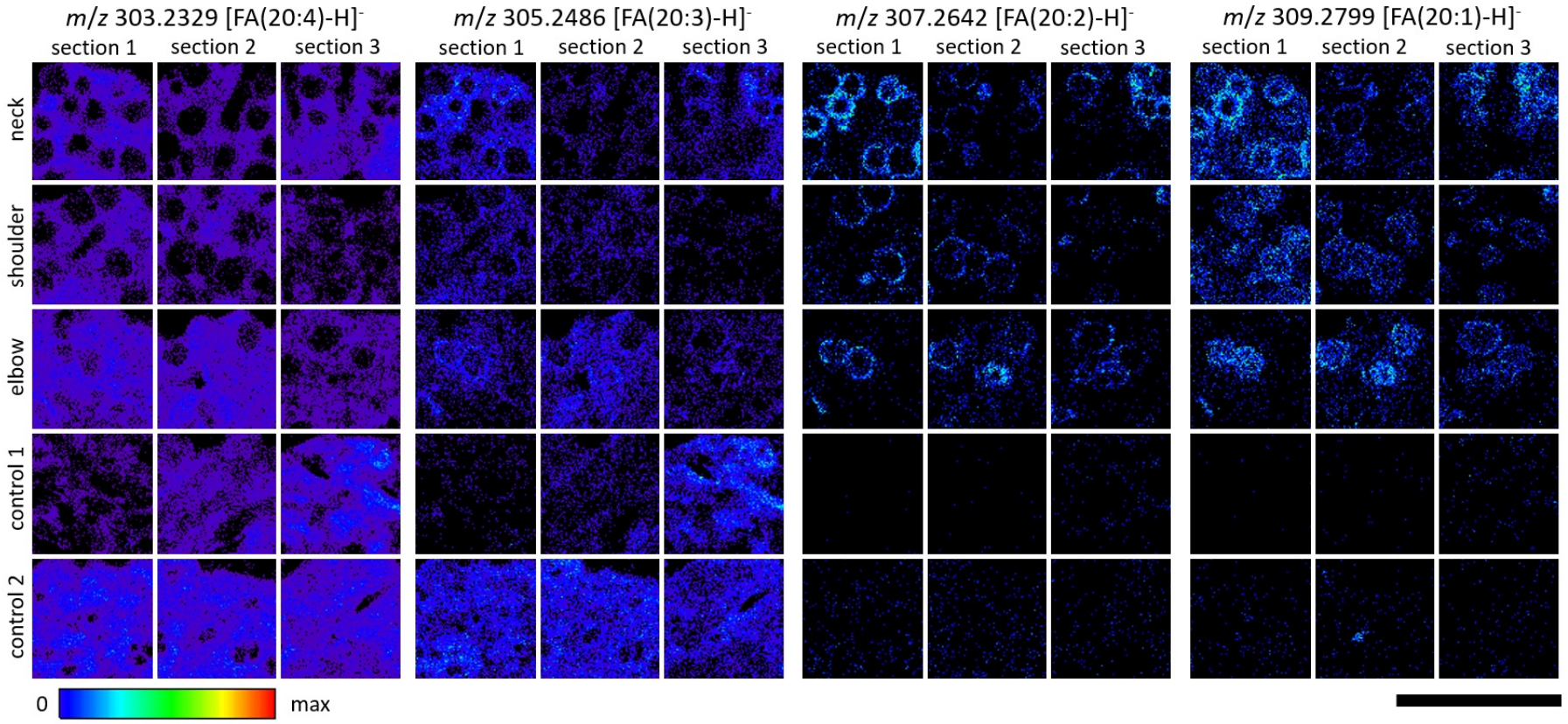

Figure 11: MS images of fatty acids with 20 carbon atoms but different numbers of unsaturations, showing different lateral distributions in *B. besnoiti*-infected and control bovine skin. Scale bar is 1 mm. Displayed are MS images for all five samples (neck, shoulder, elbow, control 1, and control 2) in technical triplicates, belonging to the two groups "infected" or "control". Within one group, the distribution of the FA is coherent, but since parasite-induced structures are represented by the distributions, they vary between infected and control samples. FA(20:4) and FA(20:3) were only found in the unaffected tissue, but FA(20:2) and FA(20:1) mainly around the skin cysts, which are only present in *B. besnoiti*-infected samples. In the controls, the corresponding ions were rarely found.

1.7.2.2 Ultra-high-resolution MSI experiments

By using a prototype AP-SMALDI ion source, we also performed MSI experiments at 2 µm pixel size. The intention was to enable further discrimination of different cyst wall compartments. Most probably due to a loss in signal intensities when minimizing the ablation spot size from 25 µm^2 to 4 µm^2, this was not successful. Nevertheless, 30 % of infection markers with reasonable lateral distributions found for the 5 µm-measurements were also observed in the ultra-high resolution 2 µm-measurements, examples can be seen in figure 12 on the next page. The potassium adducts of the two PCs PC(34:1) and PC(36:2) were chosen because their lateral distribution was of interest. Both lipids were found in the whole tissue section, but in higher intensities in the cyst areas. While PC(34:1) seems to accumulate in the cyst wall, PC(36:2) was found to be enriched in the whole cysts. However, minor differences in signal intensities were observed, especially for PC(36:3) (figure 12 C): While most pixels inside the cyst content are green (medium intensity), some were blue (lower intensity) and few yellow or even red (high intensity). In the higher-resolved image (figure 12 F), signal intensities in general were lower, resulting in artifacts inside the cysts. With a length of roughly 8 µm,[168] single bradyzoites are too small to be resolved with fine structures individually. Nevertheless, intensity gradients inside the cysts were better visible, giving a hint about possible aggregations of parasites.

Additionally, higher lateral resolution enables better discrimination between ions originating from the cyst walls and the cyst content. An example is shown in figure 13 on page 36. Both lateral resolutions are able to differentiate cyst wall (green ion-channel, representing the glycosylceramide (GlcCer) GlcCer(41:6)) and cyst content (red ion-channel, representing PC(36:2)) tissue. However, zooming into the contact area between walls and content reveals many yellow pixels between the red and the green ones in the measurement taken with 5 µm pixel size (figure 13 C), but only few yellow pixels in the 2 µm resolution analysis (figure 13 D). Yellow pixels are the result of overlaying red and green pixels, meaning that both ions, the one shown in red as well as the one shown in green, were detected in the same ablation area when using 5 µm pixel size, while they are separated when using 2 µm pixel size.

Unfortunately, due to the lower signal intensities, ultra-high-resolution measurements were only possible in positive-ion mode.

1.7.2.3 3-dimensional MSI reconstruction

Furthermore, we made use of a relatively new approach, the so-called three-dimensional MSI. Therefore, 16 consecutive sections were measured and the resulting ion images were stitched afterwards. In order to achieve consistent quality of the cryosections, the sample preparation procedure was slightly modified. Instead of directly mounting the skin tissue on top of a cryosectioning plate, the tissue was embedded in

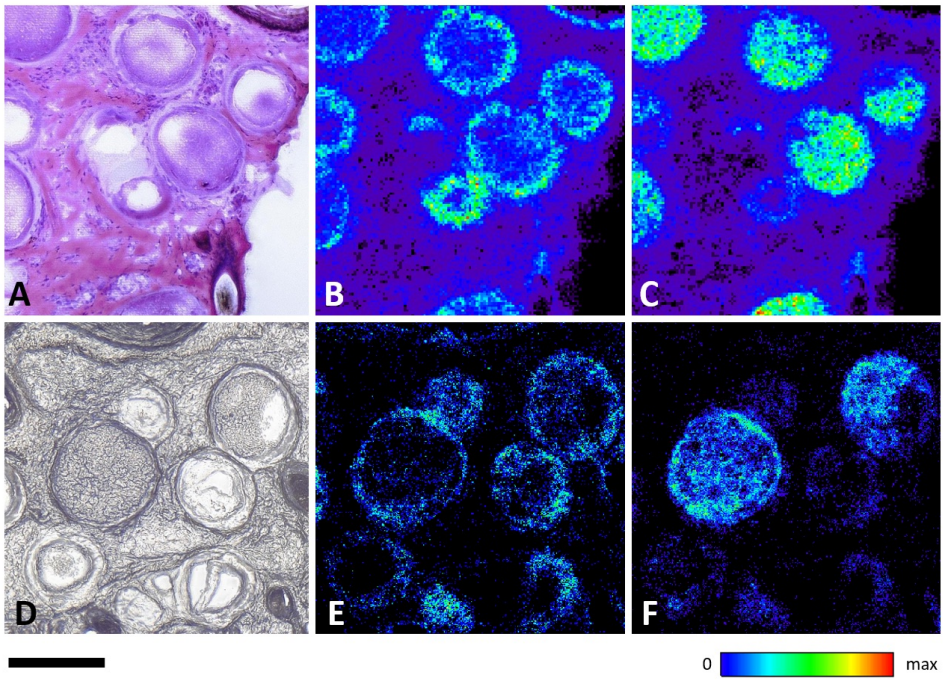

Figure 12: Comparison of MALDI MS images of *B. besnoiti*-infected bovine skin with either 5 µm (upper line) or 2 µm (lower line) pixel size. Scale bar applies for all images and is 200 µm. A and D show the corresponding light microscopic images, in the case of A after MSI measurement and H&E-staining. D is the optical image taken prior to the measurement. During matrix wash-off and staining, too much, especially parasitic, tissue was washed away, therefore the unstained image is shown. B and E represent *m/z* 798.5407, identified as PC(34:1), $[C_{42}H_{82}NO_8P + K]^+$, either with 5 µm (B) or 2 µm (E) pixel size. C and F visualize *m/z* 824.5563, identified as PC(36:2), $[C_{44}H_{84}NO_8P + K]^+$, either with 5 µm (C) or 2 µm (F) pixel size. As expected, image quality improved with smaller pixel sizes and intensity gradients are finer granulated.

gelatin first. Experiments showed that it was of great importance to keep a relatively large gelatin framework around the tissue to achieve proper consecutive cryosections in a replicable quality. Finally, cryosections with a thickness of 14 µm were obtained in a repeatable manner. This limited the pixel size of the following MALDI MSI measurements also to 14 µm because the goal was to obtain cubic and not rectangular cuboid-shaped voxels. After conversion of obtained mass spectra into the imzML-format, they were further processed using the M2aia-software package.[169] With this software tool, images of chosen *m/z* were stacked and finally visualized in a three-dimensional way. Screenshots of the reconstructions can be found in figure 14 on page 37, videos in the supplementary information of the second publication.[170] These screenshots reflect two different ions, showing the stack from top and down view. A and B represent *m/z* 798.5, identified as PC(34:1), $[C_{42}H_{82}NO_8P + K]^+$; C and D visualize *m/z* 824.5, identified as PC(36:2), $[C_{44}H_{84}NO_8P + K]^+$. As it can be seen in figure 12, both lipids were found in the whole tissue section, but in higher intensity in the *B. besnoiti*-cyst area, what is also nicely reflected in the 3-dimensional reconstructions. These reconstructions helped to get a better understanding of the cyst orientation as well as the distribution of lipids and metabolites between the cysts.

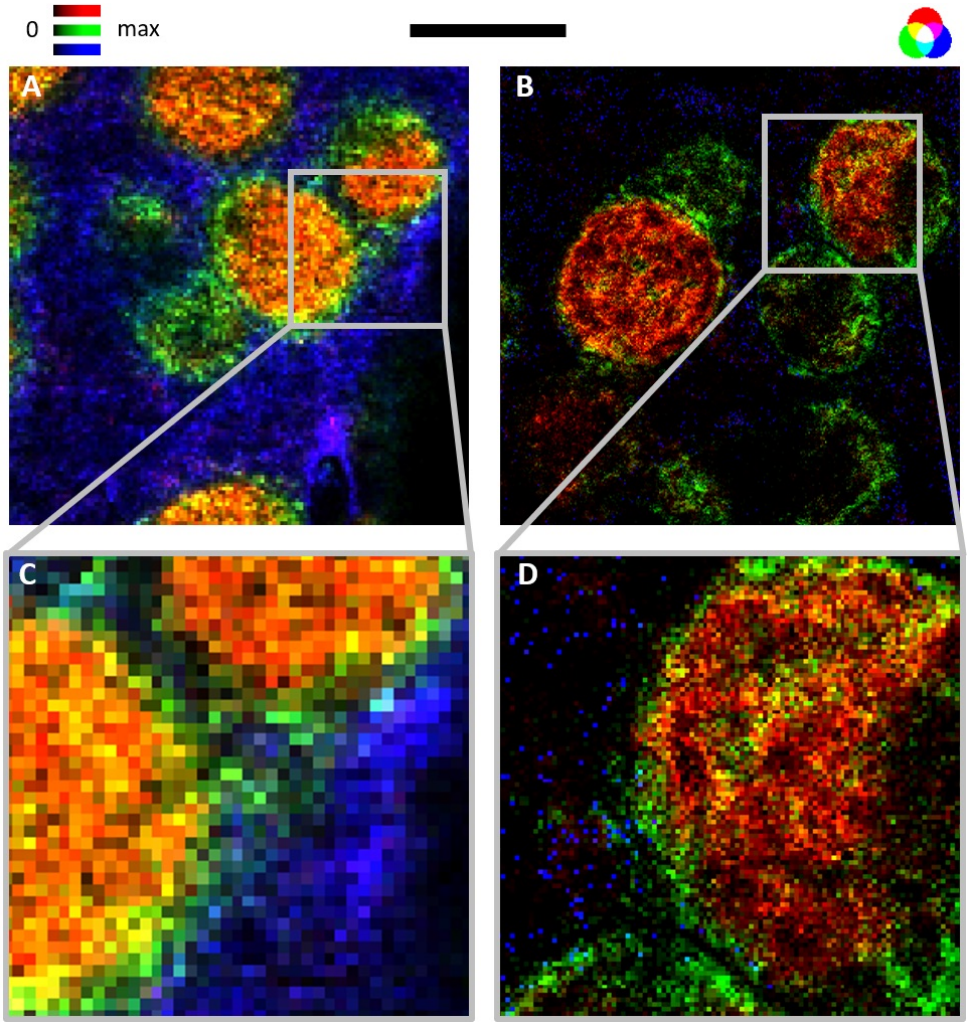

Figure 13: Comparison of MALDI MS images of *B. besnoiti*-infected bovine skin with either 5 µm (A and C) or 2 µm (B and D) pixel size. C and D are roughly three times magnified regions of A and B, respectively. Scale bar applies for sub-images A and B and is 200 µm. The same ion channels and color-coding were used for all images. Red: *m/z* 786.6005, identified as PC(36:2), $[C_{44}H_{84}NO_8P + H]^+$; green: *m/z* 842.5540, annotated as GlcCer(41:6), $[C_{47}H_{81}NO_9 + K]^+$; blue: *m/z* 725.5566, annotated as SM(34:1), $[C_{39}H_{79}N_2O_6P + Na]^+$.

However, these static reconstructions cannot be used to conclude potentially occurring exchange between the cysts. Therefore, additional experiments using for example isotope-labeled metabolites and nutrients are needed to follow the path of these compounds inside and potential interactions between the cysts.

1.7.2.4 Conclusion second publication

Using this multiplex MSI approach, we gained deeper insights into the composition of parasitic tissue cysts following chronic *B. besnoiti* infection. Also, we observed metabolic changes in the direct environment of the cyst, as a possible indication of underlying metabolic pathways affected. In total, 552 signals were changed in intensity when comparing infected with healthy tissue. Regarding the group of infected samples, there was no significant difference between the three sampling areas, despite the

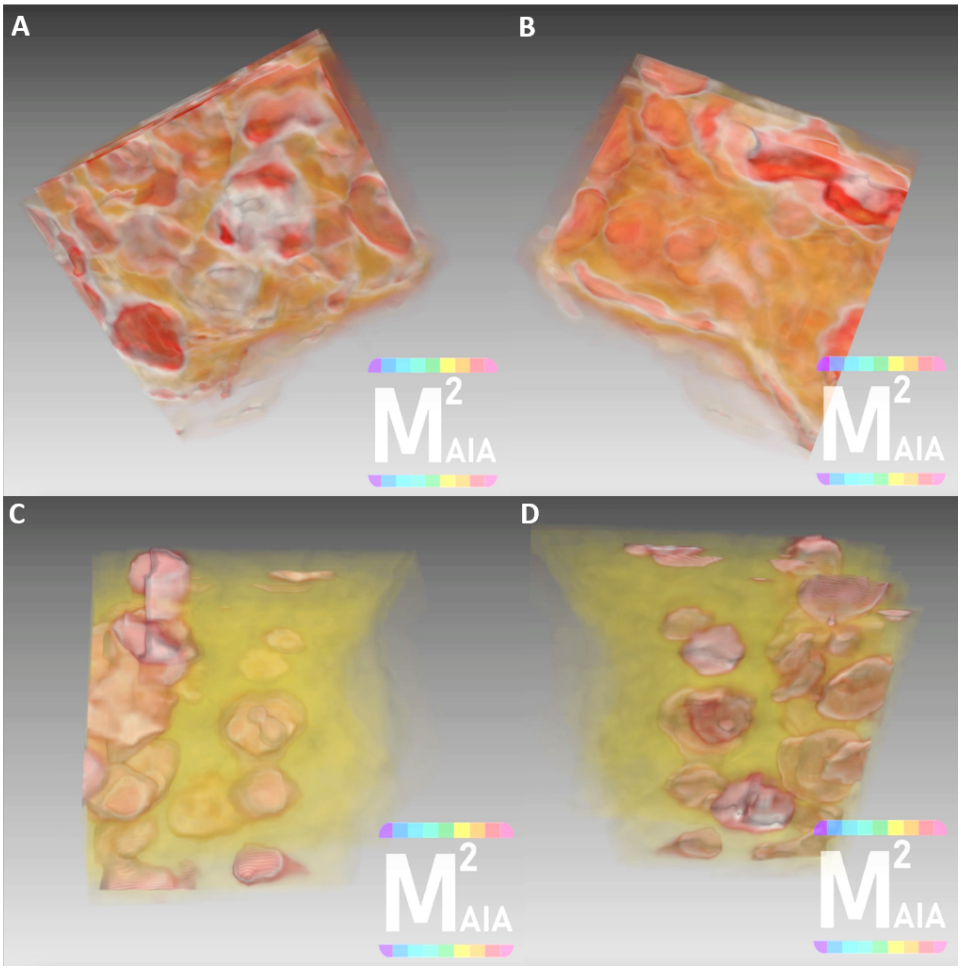

Figure 14: 3-dimensional MSI reconstructions of *B. besnoiti*-infected bovine skin. Reconstructions were obtained by stitching measurements of 16 consecutive tissue sections. The cryosections had a thickness of 14 µm, pixel size was also 14 µm. Displayed here are screenshots of two different ions, showing the stack from top and down view. A and B represent *m/z* 798.5, identified as PC(34:1), $[C_{42}H_{82}NO_8P + K]^+$; C and D visualize *m/z* 824.5, identified as PC(36:2), $[C_{44}H_{84}NO_8P + K]^+$. As it can be seen in figure 12, both lipids were found in the whole tissue section, but in higher intensities in the *B. besnoiti*-cyst area, what is also nicely reflected in the 3-dimensional reconstructions. Videos, better reflecting the 3-dimensional proportions, can be found in the supplementary information of the second publication.[170]

fact that the elbow samples contained less parasite-formed cysts than neck and shoulder samples. However, it has to be kept in mind that infected tissues all originated from one animal and results might be slightly different when expanding the study to a larger cohort. Nevertheless, the detected alterations in the lipid profile can serve as starting points for further metabolism studies.

1.8 Conclusion and Outlook

Combining MS/MS and (ultra-)high resolution AP-SMALDI MSI enabled the investigation of parasite–host interactions in two different model systems.

Regarding the schistosomiasis model, three different infection stages of hamster liver were studied: Bisex-infected animals, where the liver contained eggs and, as a reaction, formed granulomas; singlesex-infected animals, which were only infected with female cercariae and therefore no eggs were found in the liver; and non-infected animals. For each group, three individual samples were analyzed. By comparing these three sample groups, 372 infection markers were found using LC-MS/MS and MALDI MSI. Hamster liver tissue containing *S. mansoni* eggs showed significant differences in the lipid profile and lipid distribution when compared to control tissue. The lateral distribution of some of these infection markers was successfully correlated with biological structures such as eggs, granulomas or non-affected tissue. Observed substructures inside the granulomas, which are formed around the eggs as an inflammatory response to infection, can be a potential starting point for further drug target research.

Concerning besnoitiosis, the chronic stage of the disease was compared to control samples. 552 significantly altered ions were determined using MALDI MSI. Further confirmation of lipid annotation was performed by on-tissue MS/MS. Differences in the lateral distribution, matching biological structures, were observed. Ultra-high-resolution MALDI MSI enabled further characterization of parasite-containing cysts in bovine skin. Additionally, findings were compared to previous results on pure parasites, showing that most of the lipids found in the acute stage of the parasite (tachyzoites) are still present in the chronic stage (bradyzoites).

Recent studies used our established method to obtain further knowledge about the effects of especially SEA on the host liver tissue. Buelow *et al.* "[found indications] that *S. mansoni* eggs completely reprogram lipid and carbohydrate metabolism via soluble factors, which results in oxidative stress-induced cell damage in the host parenchyma."[171] Regarding MALDI MSI, TGs were found to be depleted in the unaffected tissue, but accumulated in the granulomatous regions and especially of higher intensity inside the eggs, as it can be seen in figure 15 on the next page.

Based on our study of the lipidome of *S. mansoni*-infected hamster liver tissue, Luh *et al.* investigated infection-induced changes in the glycosphingolipid (GLS) content of hamster livers containing *S. mansoni* eggs. Using a combined approach of nanoscale hydrophilic interaction liquid chromatography tandem mass spectrometry (nano-HILIC MS/MS) and AP-SMALDI MSI, 50 GLSs were found to be significantly upregulated in bisex-infected samples when compared to controls. Additionally, the lateral distribution of 44 GLSs reflected biological structures induced by infection. In total, GLSs seem to be important during granuloma formation. Also, smaller pixel sizes (3 µm) enabled deeper insights into the egg composition. As such, HexCer(20:0;O3/16:0) was only found on the egg shell.[172]

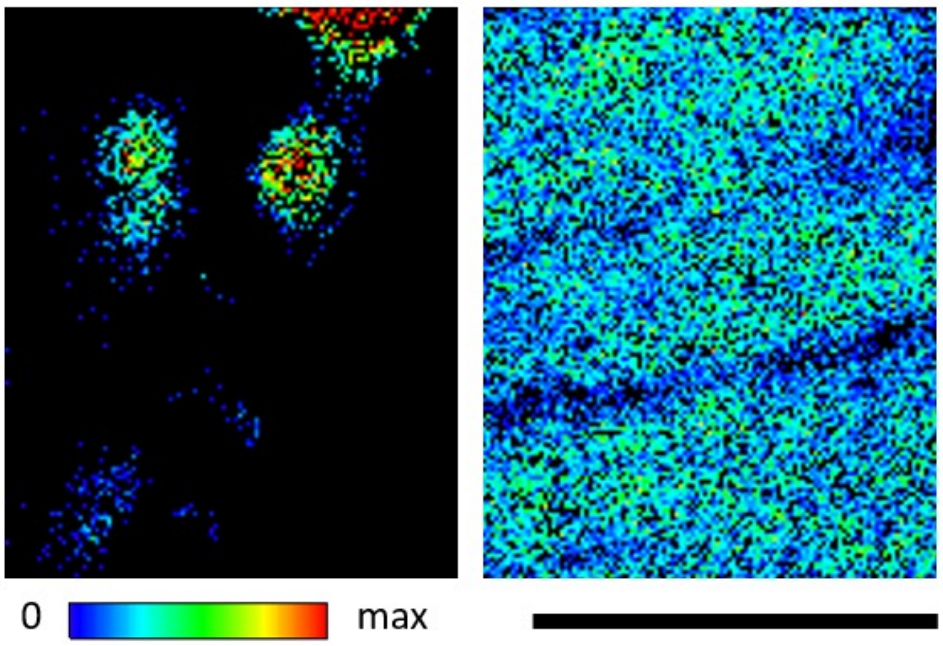

Figure 15: MALDI MS images of *m/z* 895.7149, identified as TG(16:0_18:1_18:2), $[C_{55}H_{100}O_6 + K]^+$. The left-hand side shows a bisex-infected sample and the right-hand side a control sample. Both images were scaled to the same intensity levels. Scale bar applies for both images and is 1 mm.

Also, Ghezellou *et al.* examined livers of hamsters infected with *S. mansoni*. They validated our results and extended them to the proteomic level. The authors further differentiated between male and female hamsters and found host-sex-specific alterations. For the altered proteins, mostly down-regulated proteins were part of metabolic pathways while up-regulated ones are crucial in immune reaction to *S. mansoni* infection.[173]

A previous study on *B. besnoiti* has shown that glycolysis is upregulated due to *B. besnoiti* infection.[81] First experiments found altered lateral distributions of glycolysis intermediates, as it can be seen in figure 16 on the following page. Intermediates seem to accumulate inside the cysts, proving the previous findings. Further method optimization is needed to enable the detection of all intermediates from the whole metabolic pathway.

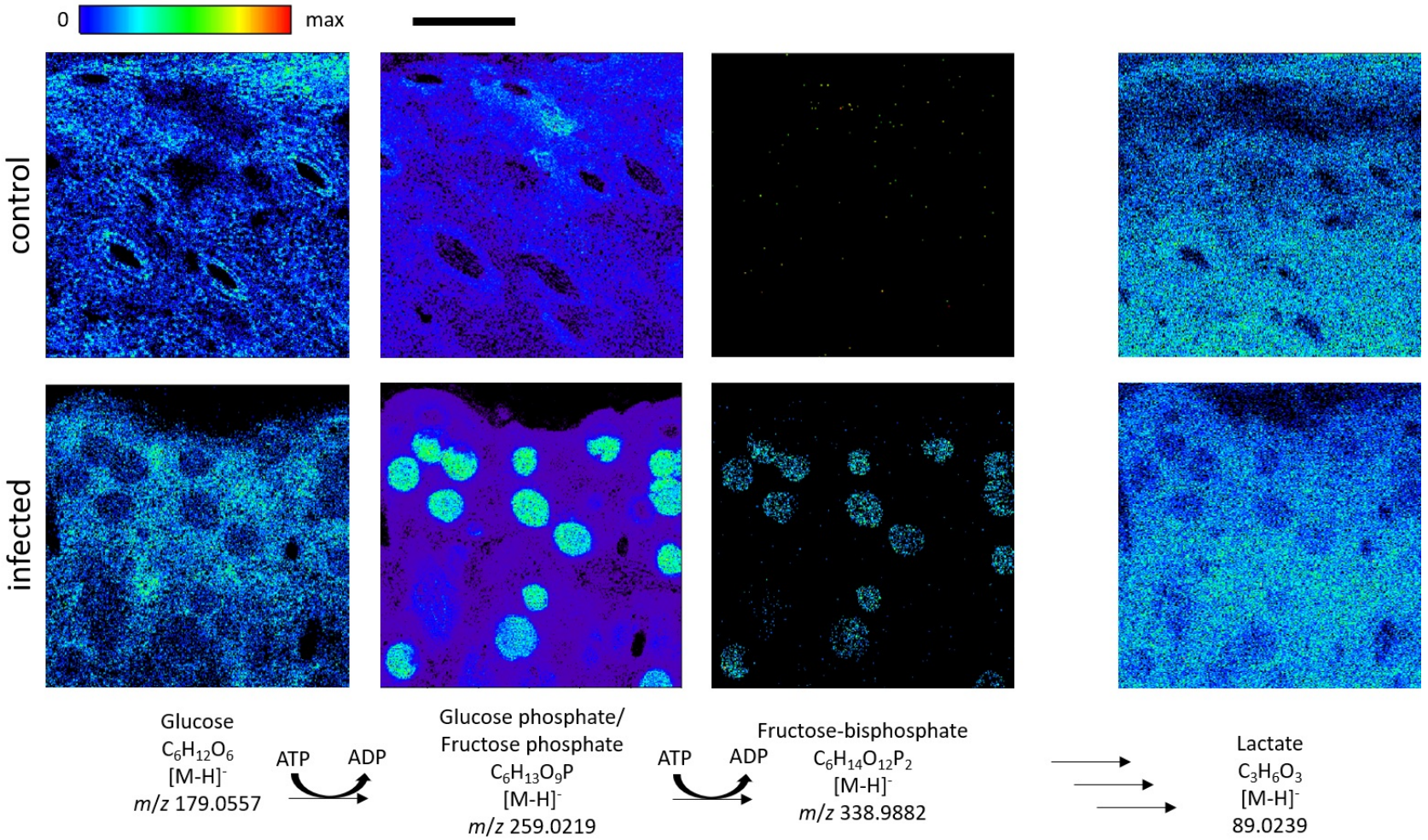

Figure 16: MALDI MS images tracking the glycolysis pathway in a *B. besnoiti*-infected and a control bovine skin sample. Missing intermediates were not detected. Scale bar applies for all images and is 1 mm.

1.9 References

(1) M. Karas, D. Bachmann and F. Hillenkamp, *Analytical Chemistry*, 1985, **57**, 2935–2939.

(2) M. Karas, U. Bahr and U. Gießmann, *Mass Spectrometry Reviews*, 1991, **10**, 335–357.

(3) C. D. Calvano, A. Monopoli, T. R. I. Cataldi and F. Palmisano, *Analytical and Bioanalytical Chemistry*, 2018, **410**, 4015–4038.

(4) M. Karas, U. Bahr, A. Ingendoh, E. Nordhoff, B. Stahl, K. Strupat and F. Hillenkamp, *Analytica Chimica Acta*, 1990, **241**, 175–185.

(5) M. Karas, M. Glückmann and J. Schäfer, *Journal of Mass Spectrometry*, 2000, **35**, 1–12.

(6) R. C. Beavis and B. T. Chait, *Proceedings of the National Academy of Sciences*, 1990, **87**, 6873–6877.

(7) M. Karas, D. Bachmann, U. Bahr and F. Hillenkamp, *International Journal of Mass Spectrometry and Ion Processes*, 1987, **78**, 53–68.

(8) P. Juhasz, C. E. Costello and K. Biemann, *Journal of the American Society for Mass Spectrometry*, 1993, **4**, 399–409.

(9) F. G. Hopwood, L. Michalak, D. S. Alderdice, K. J. Fisher and G. D. Willett, *Rapid Communications in Mass Spectrometry*, 1994, **8**, 881–885.

(10) M. Glückmann, A. Pfenninger, R. Krüger, M. Thierolf, M. Karasa, V. Horneffer, F. Hillenkamp and K. Strupat, *International Journal of Mass Spectrometry*, 2001, **210-211**, 121–132.

(11) M. Karas, U. Bahr, I. Fournier, M. Glückmann and A. Pfenninger, *International Journal of Mass Spectrometry*, 2003, **226**, 239–248.

(12) E. Nordhoff, A. Ingendoh, R. Cramer, A. Overberg, B. Stahl, M. Karas, F. Hillenkamp and P. F. Crain, *Rapid communications in mass spectrometry*, 1992, **6**, 771–776.

(13) I. S. Gilmore, S. Heiles and C. L. Pieterse, *Annual Review of Analytical Chemistry*, 2019, **12**, 201–224.

(14) P. Lecchi, H. M. T. Le and L. K. Pannell, *Nucleic Acids Research*, 1995, **23**, 1276–1277.

(15) K. Tang, N. I. Taranenko, S. L. Allman, C. H. Chen, L. Y. Chang and K. B. Jacobson, *Rapid Communications in Mass Spectrometry*, 1994, **8**, 673–677.

(16) K. J. Wu, A. Steding and C. H. Becker, *Rapid Communications in Mass Spectrometry*, 1993, **7**, 142–146.

(17) N. I. Taranenko, K. Tang, S. L. Allman, L. Y. Chang and C. H. Chen, *Rapid Communications in Mass Spectrometry*, 1994, **8**, 1001–1006.

(18) F. Hillenkamp, M. Karas, R. C. Beavis and B. T. Chait, *Analytical Chemistry*, 1991, **63**, 1193 A–1202 A.

(19) M. Rohmer, B. Meyer, M. Mank, B. Stahl, U. Bahr and M. Karas, *Analytical Chemistry*, 2010, **82**, 3719–3726.

(20) R. C. Beavis and B. T. Chait, *Rapid Communications in Mass Spectrometry*, 1989, **3**, 432–435.

(21) R. C. Beavis, T. Chaudhary and B. T. Chait, *Organic Mass Spectrometry*, 1992, **27**, 156–158.

(22) J. J. Gorman, B. L. Ferguson and T. B. Nguyen, *Rapid Communications in Mass Spectrometry*, 1996, **10**, 529–536.

(23) K. Strupat, M. Karas and F. Hillenkamp, *International Journal of Mass Spectrometry and Ion Processes*, 1991, **111**, 89–102.

(24) B. Spengler, *Analytical Chemistry*, 2015, **87**, 64–82.

(25) T. J. A. Dekker, E. A. Jones, W. E. Corver, R. J. M. van Zeijl, A. M. Deelder, R. A. E. M. Tollenaar, W. E. Mesker, H. Morreau and L. A. McDonnell, *Analytical and Bioanalytical Chemistry*, 2015, **407**, 2167–2176.

(26) L. Michalak, K. J. Fisher, D. S. Alderdice, D. R. Jardine and G. D. Willett, *Organic Mass Spectrometry*, 1994, **29**, 512–515.

(27) P. J. Todd, T. G. Schaaff, P. Chaurand and R. M. Caprioli, *Journal of Mass Spectrometry*, 2001, **36**, 355–369.

(28) B. Spengler, M. Hubert and R. Kaufmann, *Proceedings of the 42nd ASMS Conference On Mass Spectrometry*, 1994, 1041.

(29) J. H. Gross, *Massenspektrometrie - Ein Lehrbuch*, 2013.

(30) W. Bouschen and B. Spengler, *International Journal of Mass Spectrometry*, 2007, **266**, 129–137.

(31) Y. Sugiura, S. Shimma and M. Setou, *Matrix*, 2006, **78**, 8227–8235.

(32) D. S. Cornett, M. L. Reyzer, P. Chaurand and R. M. Caprioli, *Nature Methods*, 2007, **4**, 828–833.

(33) J. A. Hankin, R. M. Barkley and R. C. Murphy, *Journal of the American Society for Mass Spectrometry*, 2007, **18**, 1646–1652.

(34) S. Guenther, A. Römpp, W. Kummer and B. Spengler, *International Journal of Mass Spectrometry*, 2011, **305**, 228–237.

(35) M. Kompauer, S. Heiles and B. Spengler, *Nature Methods*, 2016, **14**, 90–96.

(36) M. J. Taylor, J. K. Lukowski and C. R. Anderton, *Journal of the American Society for Mass Spectrometry*, 2021, **32**, 872–894.

(37) V. V. Laiko, M. A. Baldwin and A. L. Burlingame, *Analytical Chemistry*, 2000, **72**, 652–657.

(38) B. Spengler and M. Hubert, *Journal of the American Society for Mass Spectrometry*, 2002, **13**, 735–748.

(39) M. Koestler, D. Kirsch, A. Hester, A. Leisner, S. Guenther and B. Spengler, *Rapid Communications in Mass Spectrometry*, 2008, **22**, 3275–3285.

(40) A. Makarov, *Analytical Chemistry*, 2000, **72**, 1156–1162.

(41) Q. Hu, R. J. Noll, H. Li, A. Makarov, M. Hardman and R. G. Cooks, *Journal of Mass Spectrometry*, 2005, **40**, 430–443.

(42) Thermo Fisher Scientific, *Key benefits of Orbitrap mass spectrometry*, https://www.thermofisher.com/de/de/home/industrial/mass-spectrometry/liquid-chromatography-mass-spectrometry-lc-ms/lc-ms-systems/orbitrap-lc-ms.html#benefits (visited on 11/27/2023).

(43) K. H. Kingdon, *Physical Review*, 1923, **21**, 408–418.

(44) R. D. Knight, *Applied Physics Letters*, 1981, **38**, 221–223.

(45) M. Scigelova and A. Makarov, *Practical Proteomics*, 2006, **6**, 16–21.

(46) J. F. Xiao, B. Zhou and H. W. Ressom, *Trends in Analytical Chemistry*, 2012, **32**, 1–14.

(47) B. P. Bowen and T. R. Northen, *Journal of the American Society for Mass Spectrometry*, 2010, **21**, 1471–1476.

(48) T. Nakanishi, M. Ito, T. Nirasawa, M. Tsuji and T. Takubo, *Clinical Biochemistry*, 2013, **46**, 1595–1600.

(49) C. A. Mitchell, H. Long, M. Donaldson, S. Francese and M. R. Clench, *Lipids in Health and Disease*, 2015, **14**, 84.

(50) A. Harris, A. Roseborough, R. Mor, K. K.-C. Yeung and S. N. Whitehead, *Journal of the American Society for Mass Spectrometry*, 2020, **31**, 479–487.

(51) Centers for Disease Control and Prevention, *About Parasites*, https://www.cdc.gov/parasites/about.html (visited on 01/17/2023).

(52) D. Haydon, S. Cleaveland, L. Taylor and M. Laurenson, *Emerging Infectious Diseases*, 2002, **8**, 1468–1473.

(53) A. L. Carr, R. D. Mitchell, A. Dhammi, B. W. Bissinger, D. E. Sonenshine and R. M. Roe, *International Journal of Molecular Sciences*, 2017, **18**, 1563.

(54) A. Vyas, *PLoS Pathogens*, 2015, **11**, e1004935.

(55) M. Berdoy, J. P. Webster and D. W. Macdonald, *Proceedings of the Royal Society B - Biological Sciences*, 2000, **267**, 1591–1594.

(56) S. A. H. Dass, A. Vasudevan, D. Dutta, L. J. T. Soh, R. M. Sapolsky and A. Vyas, *PLoS One*, 2011, **6**, e27229.

(57) A. Vasudevan, V. Kumar, Y. N. Chiang, J. Y. Yew, S. Cheemadan and A. Vyas, *The ISME Journal*, 2015, **9**, 2112–2115.

(58) M. I. Araujo and E. M. de Carvalho, in *Parasites and Allergy*, ed. M. Capron and F. Trottein, S.Karger AG, 2006.

(59) A. M. Abdualkader, A. M. Ghawi, M. Alaama, M. Awang and A. Merzouk, *Indian Journal of Pharmaceutical Sciences*, 2013, **75**, 127–137.

(60) A. P. Singh, *Complementary Therapies in Clinical Practice*, 2010, **16**, 213–215.

(61) K. d. C. Figueiredo Bordon, C. T. Cologna, E. C. Fornari-Baldo, E. L. Pinheiro-Junior, F. A. Cerni, F. G. Amorim, F. A. Pino Anjolette, F. A. Cordeiro, G. A. Wiezel, I. G. Cardoso, Iara Aime and, I. S. de Oliveira, J. Boldrini-Franca, M. B. Pucca, M. A. Baldo and E. C. Arantes, *Frontiers in Pharmacology*, 2020, **11**, 1132.

(62) B. Gryseels, K. Polman, J. Clerinx and L. Kes, *Lancet*, 2006, **368**, 1106–1118.

(63) World Health Organization, *Schistosomiasis (Bilharzia)*, `https://www.who.int/health-topics/schistosomiasis` (visited on 02/09/2024).

(64) World Health Organization, *Schistosomiasis fact sheet*, `https://www.who.int/news-room/fact-sheets/detail/schistosomiasis` (visited on 01/04/2024).

(65) B. de Noya, J. Pointer, C. Colmenares, A. Théron, C. Balzan, I. Cesari, S. González and O. Noya, *Acta Tropica*, 1997, **68**, 11–21.

(66) P. S. D'Andrea, L. S. Maroja, R. Gentile, R. Cerqueira, A. Maldonado Júnior and L. Rey, *Parasitology*, 2000, **120**, 573–582.

(67) J. M. Duplantier and M. Sène, *Journal of helminthology*, 2000, **74**, 129–135.

(68) S. Catalano, A. Symeou, K. J. Marsh, A. Borlase, E. Léger, C. B. Fall, M. Sène, N. D. Diouf, D. Ianniello, G. Cringoli, L. Rinaldi, K. Bâ and J. P. Webster, *Parasites & Vectors*, 2019, **12**, 439.

(69) S. M. Muriuki, R. K. Murugu, E. Munene, G. M. Karere and D. C. Chai, *Acta Tropica*, 1998, **71**.

(70) A. Ghandour, N. Zahid, A. Banaja, K. Kamal and A. Bouq, *Journal of Tropical Medicine and Hygiene*, 1995, **98**, 431–439.

(71) C. Müller-Graf, D. Collins, C. Packer and M. Woolhouse, *Parasitology*, 1997, **115**, 621–627.

(72) D. G. Colley, A. L. Bustinduy, W. E. Secor and C. H. King, *Lancet*, 2014, **383**, 2253–2264.

(73) R. J. DeJong, J. A. T. Morgan, W. L. Paraense, J.-P. Pointier, M. Amarista, P. F. K. Ayeh-Kumi, A. Babiker, C. S. Barbosa, P. Brémond, A. Pedro Canese, C. P. de Souza, C. Dominguez, S. File, A. Gutierrez, R. N. Incani, T. Kawano, F. Kazibwe, J. Kpikpi, N. J. S. Lwambo, R. Mimpfoundi, F. Njiokou, J. Noël Poda, M. Sene, L. E. Velásquez, M. Yong, C. M. Adema, B. V. Hofkin, G. M. Mkoji and E. S. Loker, *Molecular Biology and Evolution*, 2001, **18**, 2225–2239.

(74) J. A. Morgan, R. J. Dejong, S. D. Snyder, G. M. Mkoji and E. S. Loker, *Parasitology*, 2001, **123**, S211–28.

(75) L. J. R, *Revista do Instituto de Medicina Tropical de Sao Paulo*, 1993, **35**, 399–404.

(76) C. H. King, *Hospital Practice*, 1991, **26**, 117–130.

(77) C. Schwartz and P. G. Fallon, *Frontiers in Immunology*, 2018, **9**, 2492.

(78) Y.-Z. Xu and M. H. Dresden, *The Journal of Parasitology*, 1989, **75**, 481–483.

(79) W. K. Anyan, T. Seki, T. Kumagai, K. Obata-Ninomiya, R. Furushima-Shimogawara, B. Kwansa-Bentum, N. Akao, K. M. Bosompem, D. A. Boakye, M. D. Wilson, H. Karasuyama and N. Ohta, *Parasitology International*, 2013, **62**, 508–513.

(80) E. Hams, G. Aviello and P. G. Fallon, *Frontiers in Immunology*, 2013, **4**, 89.

(81) A. Taubert, C. R. Hermosilla, L. M. R. Silva, A. Wieck, K. Failing and S. Mazurek, *Parasitology Research*, 2016, **115**, 2023–2034.

(82) J. T. Ellis, O. J. M. Holmdahl, C. Ryce, J. M. Njenga, P. A. Harper and D. A. Morrison, *Protist*, 2000, **151**, 329–336.

(83) H. J. Vial, P. Eldin, A. G. M. Tielens and J. J. van Hellemond, *Molecular and Biochemical Parasitology*, 2003, **126**, 143–154.

(84) P. Olias, B. Schade and H. Mehlhorn, *Infection, Genetics and Evolution*, 2011, **11**, 1564–1576.

(85) EFSA, *EFSA Journal*, 2010, **8**, 1499–1514.

(86) G. Álvarez-García, C. F. Frey, L. M. O. Mora and G. Schares, *Trends in Parasitology*, 2013, **29**, 407–415.

(87) H. Mehlhorn, S. Klimpel, E. Schein, A. O. Heydorn, S. Al-Quraishy and J. Selmair, *Parasitology Research*, 2009, **104**, 861–868.

(88) L. Diesing, A. O. Heydorn, F. R. Matuschka, C. Bauer, E. Pipano, D. T. de Waal and F. T. Potgieter, *Parasitology Research*, 1988, **75**, 114–117.

(89) S. Sharif, P. Jacquiet, F. Prevot, C. Grisez, I. Raymond-Letron, M. O. Semin, A. Geffré, C. Trumel, M. Franc, Bouhsira and E. Liénard, *Medical and Veterinary Entomology*, 2019, **33**, 247–255.

(90) P. Jacquiet, E. Liénard and M. Franc, *Veterinary Parasitology*, 2010, **174**, 30–36.

(91) R. D. Bigalke, *Onderstepoort Journal of Veterinary Research*, 1968, **35**, 3–137.

(92) N. S. Gollnick, J. C. Scharr, G. Schares and M. C. Langenmayer, *BMC Veterinary Research*, 2015, **11**, 1–16.

(93) C. Cadéac, *Revue vétérinaire*, 1884, **521**, 521–540.

(94) C. Besnoit and V. Robin, *Revue vétérinaire*, 1912, **37**, 649–663.

(95) M. Marotel, *Bull. et Mem. de la Société des Sciences Vetétérinaires de Lyon et de la Société de Médecine Vetétérinaire de Lyon et du Sud-Est*, 1912, **15**, 196–217.

(96) W. L. Jellison, *Annals of the New York Academy of Sciences-Series*, 1956, **64**, 268–270.

(97) A. Fernández-García, V. Risco-Castillo, S. Pedraza-Díaz, A. Aguado-Martínez, G. Álvarez-García, M. Gómez-Bautista, E. Collantes-Fernández and L. M. Ortega-Mora, *Journal of Parasitology*, 2009, **95**, 474–476.

(98) N. S. Gollnick, A. Gentile and G. Schares, *Veterinary Record*, 2010, **166**, 599.

(99) A. Gentile, G. Militerno, G. Schares, A. Nanni, S. Testoni, P. Bassi and N. S. Gollnick, *Veterinary Parasitology*, 2012, **184**, 108–115.

(100) G. Schares, W. Basso, M. Majzoub, H. C. Cortes, A. Rostaher, J. Selmair, W. Hermanns, F. J. Conraths and N. S. Gollnick, *Veterinary Parasitology*, 2009, **163**, 315–322.

(101) E. Papadopoulos, G. Arsenos, S. Ptochos, P. Katsoulos, G. Oikonomou, M. A. Karatzia and K. H., *Journal of the Hellenic Veterinary Medical Society*, 2014, **65**, 115–120.

(102) M. Lesser, U. Braun, P. Deplazes, B. Gottstein, M. Hilbe and W. Basso, *Schweizer Archiv fur Tierheilkunde*, 2012, **154**, 469–474.

(103) S. Hornok, A. Fedak, F. Baska, R. Hofmann-Lehmann and W. Basso, *Parasites & Vectors*, 2014, **7**, 20.

(104) A. Vanhoudt, B. Pardon, P. De Schutter, T. Bosseler, C. Sarre, J. Vercruysse and P. Deprez, *Vlaams Diergeneeskundig Tijdschrift*, 2015, **84**, 205–211.

(105) E. G. Ryan, A. Lee, C. Carty, J. O'Shaughnessy, P. Kelly, J. P. Cassidy, M. Sheehan, A. Johnson and T. de Waal, *Veterinary Record*, 2016, **178**.

(106) P. Chatikobo, T. Choga, C. Ncube and J. Mutambara, *Preventive Veterinary Medicine*, 2013, **109**, 327–333.

(107) K. C. A. Schulz, *Journal of the South African Veterinary Association*, 1960, **31**, 21–36.

(108) M. Goldman and E. Pipano, *Tropical Animal Health and Production*, 1983, **15**, 32–38.

(109) P. A. Basson, R. M. McCully and R. D. Bigalke, *Onderstepoort Journal of Veterinary Research*, 1970, **37**, 105–126.

(110) M. C. Langenmayer, N. S. Gollnick, M. Majzoub-Altweck, J. C. Scharr, G. Schares and W. Hermanns, *Veterinary Pathology*, 2015, **52**, 476–488.

(111) H. C. E. Cortes, Y. Reis, H. Waap, R. Vidal, H. Soares, I. Marques, I. Pereira da Fonseca, I. Fazendeiro, M. L. Ferreira, V. Caeiro, V. Shkap, A. Hemphill and A. Leitão, *Veterinary Parasitology*, 2006, **141**, 226–233.

(112) H. Cortes, A. Leitão, B. Gottstein and A. Hemphill, *Parasitology*, 2014, **141**, 1406–1417.

(113) V. Shkap, A. Reske, E. Pipano, L. Fish and T. Baszler, *Veterinary parasitology*, 2002, **106**, 35–43.

(114) H. C. Cortes, S. Nunes, Y. Reis, D. Staubli, R. Vidal, H. Sager, A. Leitão and B. Gottstein, *Veterinary Parasitology*, 2006, **141**, 216–225.

(115) A. Sannusi, *Veterinary Parasitology*, 1991, **39**, 185–188.

(116) J. W. Pols, *Onderstepoort Journal of Veterinary Research*, 1960, **28**, 265–356.

(117) C. Diezma-Díaz, A. Jiménez-Meléndez, M. Fernández, D. Gutiérrez-Expósito, P. García-Lunar, L. M. Ortega-Mora, J. A. Pérez-Salas, J. Blanco-Murcia, I. Ferre and G. Álvarez-García, *Veterinary Parasitology*, 2017, **247**, 10–18.

(118) R. D. Bigalke, J. H. Schoeman and R. M. McCully, *Onderstepoort Journal of Veterinary Research*, 1974, **41**, 1–5.

(119) H.-J. Mittag, *Statistik : Eine Einführung mit interaktiven Elementen*, Springer Berlin Heidelberg, Berlin, Heidelberg, 4 th ed., 2016.

(120) K. Backhaus, B. Erichson, S. Gensler, R. Weiber and T. Weiber, *Multivariate Analysemethoden: Eine anwendungsorientierte Einführung*, Springer Fachmedien Wiesbaden, Wiesbaden, 17 th ed., 2023.

(121) B. Rasch, M. Friese, W. Hofmann and E. Naumann, *Quantitative Methoden 2: Einführung in die Statistik für Psychologie, Sozial- & Erziehungswissenschaften*, Springer, Berlin, Heidelberg, 5th ed., 2021.

(122) M. Schneider, *Datenanalyse für Naturwissenschaftler, Mediziner und Ingenieure*, Springer Berlin Heidelberg, Berlin, Heidelberg, 1st ed., 2020.

(123) J. Dopstadt, S. Vens-Cappell, L. Neubauer, P. Tudzynski, B. Cramer, K. Dreisewerd and H.-U. Humpf, *Analytical and Bioanalytical Chemistry*, 2017, **409**, 1221–1230.

(124) F. Negrao, D. F. d. O. Rocha, C. F. Jaeeger, F. J. S. Rocha, M. N. Eberlin and S. Giorgio, *Molecular Biosystems*, 2017, **13**, 2036–2043.

(125) E. Gemperline, H. A. Horn, K. DeLaney, C. R. Currie and L. Li, *ACS Chemical Biology*, 2017, **12**, 1980–1985.

(126) I. Schoenian, M. Spiteller, M. Ghaste, R. Wirth, H. Herz and D. Spiteller, *Proceedings of the National Academy of Sciences of the United States of America*, 2011, **108**, 1955–1960.

(127) J. Kroiss, M. Kaltenpoth, B. Schneider, M.-G. Schwinger, C. Hertweck, R. K. Maddula, E. Strohm and A. Svatos, *Nature Chemical Biology*, 2010, **6**, 261–263.

(128) J. F. H. M. Brouwers, J. J. VanHellemond and A. G. M. Tielens, *Netherlands Journal of Zoology*, 1996, **46**, 206–215.

(129) M. S. Ferreira, D. N. de Oliveira, R. N. de Oliveira, S. M. Allegretti, A. E. Vercesi and R. R. Catharino, *Journal of Mass Spectrometry*, 2014, **49**, 86–92.

(130) P. Kadesch, T. Quack, S. Gerbig, C. G. Grevelding and B. Spengler, *Analytical Chemistry*, 2019, **91**, 4520–4528.

(131) P. Kadesch, T. Quack, S. Gerbig, C. G. Grevelding and B. Spengler, *PLoS Neglected Tropical Diseases*, 2020, **14**.

(132) W. Wang, L. Wang and Y.-S. Liang, *Parasitology Research*, 2012, **111**, 1871–1877.

(133) A. S. Mokosch, S. Gerbig, C. G. Grevelding, S. Haeberlein and B. Spengler, *Analytical and Bioanalytical Chemistry*, 2021, **413**, 2755–2766.

(134) C. F. Waller, in *Small Molecules in Hematology*, ed. U. M. Martens, Springer International Publishing, Cham, 2018, pp. 1–27.

(135) S. Beckmann and C. G. Grevelding, *International Journal for Parasitology*, 2010, **40**, 521–526.

(136) M. S. Ferreira, R. N. de Oliveira, D. N. de Oliveira, C. Z. Esteves, S. M. Allegretti and R. R. Catharino, *International Journal for Parasitology*, 2015, **45**, 385–391.

(137) T. M. Smith, T. J. Brooks and H. B. White, *Lipids*, 1969, **4**, 31–36.

(138) F. Meyer, H. Meyer and E. Bueding, *Biochimica et Biophysica Acta (BBA) - Lipids and Lipid Metabolism*, 1970, **210**, 257–266.

(139) B. W. Young and R. B. Podesta, *Molecular and Biochemical Parasitology*, 1982, **5**, 165–172.

(140) B. W. Young and R. B. Podesta, *The Journal of Parasitology*, 1986, **72**, 802–803.

(141) D. Allan, G. Payares and W. H. Evans, *Molecular and Biochemical Parasitology*, 1987, **23**, 123–128.

(142) S. T. Furlong and J. P. Caulfield, *Experimental Parasitology*, 1988, **65**, 222–231.

(143) J. Schariter, J. Pachuski, B. Fried and J. Sherma, *Journal of Liquid Chromatography & Related Technologies*, 2002, **25**, 1615–1622.

(144) J. F. Brouwers, I. M. Smeenk, L. M. van Golde and A. G. Tielens, *Molecular and Biochemical Parasitology*, 1997, **88**, 175–185.

(145) K. Retra, O. B. Bleijerveld, R. A. van Gesteil, A. G. M. Tielens, J. J. van Hellemond and J. F. Brouwers, *Rapid Communications ins Mass Spectrometry*, 2008, **22**, 1853–1862.

(146) K. Retra, S. deWalick, M. Schmitz, M. Yazdanbakhsh, A. G. M. Tielens, J. F. H. M. Brouwers and J. J. van Hellemond, *International Journal for Parasitology*, 2015, **45**, 629–636.

(147) M. S. Ferreira, D. N. de Oliveira, R. N. de Oliveira, S. M. Allegretti and R. R. Catharino, *Analytica Chimica Acta*, 2014, **845**, 62–69.

(148) M. Giera, M. M. M. Kaisar, R. J. E. Derks, E. Steenvoorden, Y. C. M. Kruize, C. H. Hokke, M. Yazdanbakhsh and B. Everts, *Analytica Chimica Acta*, 2018, **1037**, 107–118.

(149) A. Fernández-García, G. Alvarez-García, V. Marugán-Hernández, P. García-Lunar, A. Aguado-Martínez, V. Risco-Castillo and L. M. Ortega-Mora, *Parasitology*, 2013, **140**, 999–1008.

(150) P. García-Lunar, J. Regidor-Cerrillo, L. Ortega-Mora, D. Gutiérrez-Expósito and G. Álvarez-García, *Veterinary Parasitology*, 2014, **205**, 434–443.

(151) P. García-Lunar, J. Regidor-Cerrillo, D. Gutiérrez-Expósito, L. Ortega-Mora and G. Alvarez-García, *Veterinary Parasitology*, 2013, **195**, 24–34.

(152) P. Kadesch, T. Hollubarsch, S. Gerbig, L. Schneider, L. M. R. Silva, C. R. Hermosilla, A. Taubert and B. Spengler, *Journal of the American Society for Mass Spectrometry*, 2020, **31**, 1815–1824.

(153) S. T. Furlong, *Experimental Parasitology*, 1989, **68**, 482–485.

(154) D. Bansal, H. S. Bhatti and R. Sehgal, *Lipids in Health and Disease*, 2005, **4**, 10.

(155) L. M. R. Silva, D. Lütjohann, P. Hamid, Z. D. Velasquez, K. Kerner, C. Larrazabal, K. Failing, C. Hermosilla and A. Taubert, *Scientific Reports*, 2019, **9**, 6650.

(156) K. R. Wiedemann, A. Peter Ventura, S. Gerbig, M. Roderfeld, T. Quack, C. G. Grevelding, E. Roeb and B. Spengler, *Analytical and Bioanalytical Chemistry*, 2022, **414**, 3653–3665.

(157) S. B. Breitkopf, M. D. O. Taveira, M. Yuan, G. M. Wulf and J. M. Asara, *Scientific Reports*, 2017, **7**, 14503.

(158) J. P. Koelmel, N. M. Kroeger, C. Z. Ulmer, J. A. Bowden, R. E. Patterson, J. A. Cochran, C. W. W. Beecher, T. J. Garrett and R. A. Yost, *BMC Bioinformatics*, 2017, **18**, 331.

(159) S. Tyanova, T. Temu, P. Sinitcyn, A. Carlson, M. Y. Hein, T. Geiger, M. Mann and J. Cox, *Nature Methods*, 2016, **13**, 731–740.

(160) J. P. Koelmel, C. Z. Ulmer, C. M. Jones, R. A. Yost and J. A. Bowden, *Biochimica et Biophysica Acta - Molecular and Cell Biology of Lipids*, 2017, **1862**, 766–770.

(161) J. F. Brouwers, J. J. Van Hellemond, L. M. van Golde and A. G. Tielens, *Molecular and Biochemical Parasitology*, 1998, **96**, 49–58.

(162) J. Chong, O. Soufan, C. Li, I. Caraus, S. Li, G. Bourque, D. S. Wishart and J. Xia, *Nucleic Acids Research*, 2018, **46**, W486–W494.

(163) L. J. Sparvero, A. A. Amoscato, C. E. Dixon, J. B. Long, P. M. Kochanek, B. R. Pitt, H. Bayir and V. E. Kagan, *Chemistry and Physics of Lipids*, 2012, **165**, 545–562.

(164) A. Palmer, P. Phapale, I. Chernyavsky, R. Lavigne, D. Fay, A. Tarasov, V. Kovalev, J. Fuchser, S. Nikolenko, C. Pineau, M. Becker and T. Alexandrov, *Nature Methods*, 2017, **14**, 57–60.

(165) P. Gornicki, *International Journal for Parasitology*, 2003, **33**, 885–896.

(166) S. Shunmugam, C.-S. Arnold, S. Dass, N. J. Katris and C. Y. Botté, *PLOS Pathogens*, 2022, **18**, 1–19.

(167) S. Ramakrishnan, M. D. Docampo, J. I. MacRae, F. M. Pujol, C. F. Brooks, G. G. van Dooren, J. K. Hiltunen, A. J. Kastaniotis, M. J. McConville and B. Striepen, *Journal of Biological Chemistry*, 2012, **287**, 4957–4971.

(168) J. P. Dubey, E. van Wilpe, D. J. C. Blignaut, G. Schares and J. H. Williams, *Journal of Parasitology*, 2013, **99**, 459–466.

(169) J. Cordes, T. Enzlein, C. Marsching, M. Hinze, S. Engelhardt, C. Hopf and I. Wolf, *GigaScience*, 2021, **10**, giab049.

(170) K. R. Wiedemann, S. Gerbig, P. Ghezellou, A. Pilgram, C. Hermosilla, A. Taubert, L. M. Silva and B. Spengler, *Journal of the American Society for Mass Spectrometry*, 2025, **36**, 1017–1026.

(171) V. von Buelow, S. Gindner, A. Baier, L. Hehr, N. Buss, L. Russ, S. Wrobel, V. Wirth, K. Tabatabai, T. Quack, S. Haeberlein, P. Kadesch, S. Gerbig, K. R. Wiedemann, B. Spengler, A. Mehl, G. Morlock, G. Schramm, J. Pons-Kuehnemann, F. H. Falcone, R. A. Wilson, K. Bankov, P. Wild, C. G. Grevelding, E. Roeb and M. Roderfeld, *JHEP Reports*, 2023, **5**, 100625.

(172) D. Luh, S. Heiles, M. Roderfeld, C. G. Grevelding, E. Roeb and B. Spengler, *Analytical Chemistry*, 2024, **96**, 6311–6320.

(173) P. Ghezellou, V. von Buelow, D. Luh, E. Badin, W. Albuquerque, M. Roderfeld, E. Roeb, C. G. Grevelding and B. Spengler, *PNAS Nexus*, 2024, **3**.

2 Hamster liver containing *Schistosoma mansoni* eggs

2.1 Changes in the lipid profile of hamster liver after *Schistosoma mansoni* infection, characterized by mass spectrometry imaging and LC–MS/MS analysis

Analytical and Bioanalytical Chemistry (2022) 414:3653–3665
https://doi.org/10.1007/s00216-022-04006-6

RESEARCH PAPER

Changes in the lipid profile of hamster liver after *Schistosoma mansoni* infection, characterized by mass spectrometry imaging and LC–MS/MS analysis

Katja R. Wiedemann[1] · Alejandra Peter Ventura[1] · Stefanie Gerbig[1] · Martin Roderfeld[2] · Thomas Quack[3] · Christoph G. Grevelding[3] · Elke Roeb[2] · Bernhard Spengler[1]

Received: 14 October 2021 / Revised: 18 January 2022 / Accepted: 3 March 2022 / Published online: 23 March 2022

Abstract
Schistosomiasis, caused by the human parasite *Schistosoma mansoni*, is one of the WHO-listed neglected tropical diseases (NTDs), and it has severe impact on morbidity and mortality, especially in Africa. Not only the adult worms but also their eggs are responsible for health problems. Up to 50% of the eggs produced by the female worms are not excreted with the feces but are trapped in the host tissue, such as the liver, where they provoke immune responses and a change in the lipid profile. We built up a database with 372 infection markers found in livers of *S. mansoni*-infected hamsters, using LC–MS/MS for identification, followed by statistical analysis. Most of them belong to the lipid classes of phosphatidylcholines (PCs), phosphatidylethanolamines (PEs), and triglycerides (TGs). We assigned some of these markers to specific anatomical structures by applying high-resolution MALDI MSI to cryosections of hamster liver and generating ion images based on the marker list from the LC–MS/MS experiments. Furthermore, enrichment and depletion of several markers were visualized.

Keywords Schistosomiasis · AP-SMALDI · Mass spectrometry imaging · Infection · Host-parasite interaction · Granuloma · Parasites · *Schistosoma mansoni*

Abbreviations

AA, 20:4	Arachidonic acid
CL	Cardiolipin
CE	Cholesterol ester
DAN	1,5-Diaminonaphthalene
DG	Diglyceride
DHB	2,5-Dihydroxybenzoic acid
DMPE	Dimethylphosphatidylethanolamine
DHA, 22:6	Docosahexaennoic acid
ECN	Equivalent carbon number
FDR	False discovery rate
LC–MS/MS	Liquid chromatography tandem mass spectrometry
LDL	Low-density lipoprotein
LPE	Lysophosphatidylethanolamine
MALDI MSI	Matrix-assisted laser desorption/ionization mass spectrometry imaging
MMPE	Monomethylphosphatidylethanolamine
NTDs	Neglected tropical diseases
PC	Phosphatidylcholine
PE	Phosphatidylethanolamine
PS	Phosphatidylserine
PZQ	Praziquantel
PCA	Principal component analysis
So	Sphingosine
TG	Triglyceride

✉ Bernhard Spengler
bernhard.spengler@anorg.chemie.uni-giessen.de

[1] Institute of Inorganic and Analytical Chemistry, Justus Liebig University Giessen, Giessen, Germany

[2] Gastroenterology, Justus Liebig University Giessen, Giessen, Germany

[3] Institute for Parasitology, Justus Liebig University Giessen, Giessen, Germany

Introduction

Infection with the blood fluke *Schistosoma mansoni* leads to severe health issues. The resulting disease schistosomiasis can occur in two different stages, an acute and a chronic form. During acute infection, patients typically suffer from non-specific symptoms such as fever, fatigue, malaise, and cough. When the worms start to migrate, abdominal

symptoms can occur [1]. Main symptoms of chronic infection are abdominal pain, diarrhea or bloody stool, and inflammation of inner organs such as the liver, spleen, and gut [2].

Humans infected with *S. mansoni* excrete parasite eggs with their feces. When the eggs enter fresh water, the first larval stage, miracidia hatch and infect their intermediate host, a snail of the genus *Biomphalaria*. Inside the snails, the parasite multiplies asexually and develops after 4 to 6 weeks to male and female cercariae, which are then released into water. Cercariae penetrate the skin of their vertebrate host and migrate to the blood vessels. During this phase, cercariae transform into schistosomula and subsequently to adult schistosomes. In the portal vein of the liver, male and female worms mate and migrate as couples to the mesenteric veins of the gut, where they can live for up to 30 years. A unique feature of schistosome biology is that the sexual maturation of the female is only achieved upon a constant pairing contact with the male. Following pairing, the female reproductive organs fully differentiate; the female starts the production of several hundred eggs per day, which reach the gut lumen and are excreted by the host [1, 2].

Schistosomiasis is classified as an endemic disease being prevalent in tropical and subtropical regions worldwide. According to the WHO, schistosomiasis belongs to the NTDs and is mainly spread in Africa, Asia, the Middle East, the Caribbean, and parts of South America [2, 3].

Improving both hygienic conditions as well as developing chemotherapeutics plays an important role in combating schistosomiasis and preventing the further spread of the disease [1]. Since 1977, praziquantel (PZQ) is the main drug against schistosomiasis [4]. PZQ is effectively targeting all schistosome species, but due to the risk of upcoming resistances against PZQ, new drugs are urgently needed. Additionally, PZQ affects adult but not juvenile worms [5].

In case of *S. mansoni*, about 50% of the eggs are excreted with the feces, the other 50% are mostly trapped in the liver and intestine of the host and secrete antigens and other factors, which can affect the host [6, 7]. Trapped eggs are the primary reason for the pathological consequences of schistosomiasis. While the host's immune response is mainly directed towards antigens produced by the schistosome worms during the first weeks of infection, the immune response shifts after 5 to 6 weeks. After pairing, female schistosomes start to produce eggs, which then provoke the type 2 response of the host's immune system [7, 8]. This immune response is essential for the egg's movement through the intestinal wall to reach the gut lumen [7]. Due to the reaction of the tissue, granuloma formation occurs around the eggs within a few days [1]. Granuloma have a dual function as they appear to be important for the survival of the host by protecting hepatocytes from toxins released by the eggs. In addition, granuloma results from inflammatory processes that finally lead to liver fibrosis [7]. Granuloma in general mainly consists of macrophages which mass together [9]. However, liver granulomas are more heterogenic in cell types and contain also T and B lymphocytes as well as eosinophils and mast cells [10]. Furthermore, it appears that granuloma formation differs in naturally infected hosts from those observed under laboratory conditions [11]. It is known that *S. mansoni* infection in general leads to lower cholesterol, low-density lipoprotein (LDL), and TG levels in host blood streams [12, 13]. Another study revealed that lipid uptake in hepatic stellate cells was provoked around trapped eggs [14]. Stanley et al. showed that lower cholesterol blood levels were caused by factors secreted by the schistosome eggs. Additionally, they observed agglomeration of cells with higher lipid contents in the outer parts of the granuloma [15]. The described processes in livers of infected animals and humans underline the importance of research regarding infection-induced metabolic changes.

Investigating lipids has become a highly active research area in the last years including instrumental advances, the detection of lipid biomarkers for various conditions, unraveling of double-bond positions in fatty acids, and the characterization of the lipidome of biological samples [16–19]. Although literature is available on the lipid composition of trematodes, the interaction of parasite and host has not been studied on the lipid level yet [20, 21]. Mostly, enzymes related to lipid metabolism have been investigated to speculate about their impact on lipid composition of worms and the host [22].

The parallel use of matrix-assisted laser desorption/ionization mass spectrometry imaging (MALDI MSI) and liquid chromatography tandem mass spectrometry (LC–MS/MS) is a widely used technique to investigate lipidomic profiles of samples while keeping the lateral information of the analytes. Commonly, lateral resolutions of about 10 µm are used [23]. This setup has already been applied to the analysis of *S. mansoni* worms [20, 24] and has now been optimized for egg-infected hamster liver tissue.

The combination of MALDI MSI and LC–MS/MS is the key to get a deeper understanding of the interactions between trapped eggs and the surrounding tissue. Analyzing infected tissue that still contains the parasites is beneficial to get an overview of the metabolic changes in both, the host tissue and the eggs. Due to the small size of the *S. mansoni* eggs of about 60–200 µm [25], a high lateral resolution of the applied MSI technique was essential. To the best of our knowledge, this is the first study of interactions of *S. mansoni* eggs (parasite) with the host liver tissue using MALDI MSI.

Materials and methods

Chemicals

A list of chemicals and suppliers is found in Table S1 in the Supplementary Information.

Tissue samples

To keep the *S. mansoni* life cycle, *Biomphalaria glabrata* snails served as intermediate hosts and Syrian hamsters (*Mesocricetus auratus*) as final hosts [26]. The hamster model has been established because it is more permissive for schistosome infection compared to the mouse model, which requires more animals (reduction principle of the 3Rs). Both snails and hamsters were bred in-house (Biomedical Research Center Seltersberg, Giessen, Germany). All animal experiments were approved by the Regierungspraesidium Giessen (V54-19 c 20/15 h 02 GI 18/10 No. A 14/2017) and performed in accordance with the European Convention for the Protection of Vertebrate Animals used for experimental and other scientific purposes (ETS No. 123; revised Appendix A). For this study, liver samples of female hamsters were used. Three different groups of hamster livers were examined: non-infected hamsters were used as controls, hamsters infected with only one sex of *S. mansoni* cercariae (monosex-infected), and hamsters infected with both sexes of cercariae (bisex-infected) [26–28]. Each group consisted of three biological replicates. Bisex infections were carried out according to established protocols and were performed for 46 days, while monosex infections persisted up to 67 days [29] to ensure a sufficient quality of the worms. This especially applies for female schistosomes that need longer to grow and develop in hamsters without male partner. Non-infected controls were age-matched with bisex-infected hamsters. Liver samples were shock frosted in liquid nitrogen immediately after perfusion and subsequently stored at − 80 °C. Optical images of all measured samples can be found in Figure S14.

OilRed staining

Neutral lipids were stained as described before [30]. Briefly, 8- to 10-µm cut-frozen sections were air-dried on glass slides, subsequently 10 min fixed in 10% formalin, briefly washed with running tap water 1–10 min, and afterwards rinsed for 2 s with 60% *iso*-propanol before staining with freshly prepared Oil Red O working solution (0.2% in 50% *iso*-propanol) for 15 min. After staining, slides were rinsed for 2 s with 60% *iso*-propanol, lightly stained with alum hematoxylin (5 dips), and rinsed with distilled water before mounting in aqueous mountant or glycerin jelly.

MALDI MSI sample preparation

Fresh frozen liver samples were kept at − 80 °C prior to sample preparation. Cryosections of 20 µm thickness without any further fixation were prepared at − 25 °C using a Cryostat Microm HM 525 (Epredia, MI, USA). After cutting, sections were thaw-mounted onto common glass slides. Microscopic images were taken using a digital microscope (VHX-5000, Keyence, Neu-Isenburg, Germany). Sections were kept at − 80 °C until measurement.

For MS imaging analysis, samples were thawed in a desiccator for 30 min. For positive-ion mode, 2,5-dihydroxybenzoic acid (DHB) and for negative-ion mode, 1,5-diaminonaphthalene (DAN) were applied. 30 mg/mL of DHB was dissolved in acetone/H_2O/trifluoroacetic acid (49.95:49.95:0.1, *v*:*v*:*v*). DAN was prepared at a concentration of 3.3 mg/mL in H_2O/methanol (1:9, *v*:*v*). Matrix was applied using an ultrafine pneumatic sprayer (SMALDIPrep, TransMIT GmbH, Giessen, Germany) as described elsewhere [31]. In brief, 100 µL DHB and 400 µL DAN solution were applied with a flow rate of 10 µL/min and 30 µL/min, respectively. Nitrogen pressure was adjusted to 1 bar.

MALDI MSI analysis

For MSI analysis, a high-resolution atmospheric-pressure MALDI imaging ion source (AP-SMALDI5 AF, TransMIT GmbH), coupled to an orbital trapping mass spectrometer (Q Exactive HF, Thermo Fisher Scientific (Bremen) GmbH, Bremen, Germany), was employed. Instrumental settings are listed in Table S2.

Mass accuracy of ± 1 ppm was maintained by internal calibration to a matrix cluster ion (*m*/*z* 716.12461 [5 DHB − 4 $H_2O + NH_4]^+$).

H&E staining

After MSI measurements, matrix was washed off with ethanol. Afterwards, sections were stained the following way:

At first, sections were rehydrated using 100%, 70%, and 40% ethanol and deionized water, 2 min each. Afterwards, samples were kept in hematoxylin solution for 12 min, followed by 10 min in tap water and 5 min in deionized water. After 1 min in eosin y solution, samples were dehydrated using deionized water, 40%, 70%, and 100% ethanol and xylene for 2 min each. Finally, samples were covered with Eukitt and a cover slip.

LC–MS/MS sample preparation

For LC–MS/MS experiments, lipid extraction was performed according to Breitkopf et al. [32] with minor changes. In brief, 10 mg liver homogenate, 100 µL PBS buffer, and 350 µL methanol were vortexed for 1 min at 1500 rpm. Afterwards, 1 mL MTBE was added, and the mixture was shaken for 1 h at 20 °C and 1000 rpm. For better phase separation, 300 µL H_2O was added, mixed for 1 min at 1000 rpm, and centrifuged for 8 min at 13,000 rpm. 1 mL of the organic upper phase was separated and dried under nitrogen flow. Dried samples were stored at − 80 °C until measurement. Prior to analysis, samples were reconstituted with 100 µL acetonitrile/*iso*-propanol/H_2O (65:30:5, *v*:*v*:*v*). The whole extraction procedure was done additionally with 100 µL PBS as extraction blank; reconstitution buffer was used as blank. Samples obtained from different animals were used for LC–MS/MS analysis and for imaging experiments.

LC–MS/MS analysis

Separation was performed on a UHPLC system (Ultimate 3000 UHPLC, Thermo Fisher Scientific) equipped with a reversed-phase 1.8 µm column (100 X 2.1 mm) (ACQUITY UPLC HSS T3, Waters GmbH, Eschborn, Germany). Mobile phase A consisted of H_2O/acetonitrile (40:60, *v*:*v*), mobile phase B of *iso*-propanol/acetonitrile (90:10, *v*:*v*), both with 10 mM ammonium formate and 0.1 vol-% formic acid, as previously published [33]. Column gradient parameters for reversed-phase liquid chromatography separation are listed in Table S3. Flow rate was kept constant at 0.25 mL/min, injection volume was 10 µL. All samples of one group were measured consecutively. After each group, blanks were injected to clean the column. The gradient was used for both positive- and negative-ion mode.

After separation, tandem mass spectra were recorded using an orbital trapping mass spectrometer (Q Exactive HF-X, Thermo Fisher Scientific) for all samples. Heated electrospray ionization parameters are listed in Table S4, MS/MS parameters are listed in Table S5.

For quality control, pooled samples, containing 10 µL of all individual samples were added at the beginning, the middle and the end of the run. LC–MS/MS data were analyzed using LipidMatch Flow 3.1 [34]. To maximize the identification output, all samples were used as targets and ddMS2. Additionally, the equivalent carbon numbers (EQN) were calculated as EQN = CN − 2•DB, with CN: carbon number of the fatty acids and DB: double bonds.

Statistical analysis and MS image generation

Statistical analyses were performed using Perseus [35] and MetaboAnalyst [36] as described elsewhere [20]. For principal component analysis (PCA), data were not filtered, but row-wise normalized to constant sum. Afterwards, data were transformed by log10 normalization. For marker search, lipids found in bisex-infected samples were compared to monosex-infected and control samples, respectively. Therefore, measurements were grouped according to their biological sample group (control, monosex, bisex). For normalization, all signal intensities, expressed as peak areas, were divided by the total ion count of one sample. Values were standardized using *z*-scores. Afterwards, ANOVA tests with a permutation-based false discovery rate (FDR) of up to 5% were performed. Significant values were filtered and Tukey's post hoc test was performed. The results were hierarchically clustered, leading to a list of significant "infection markers".

These lists (for positive- and negative-ion mode) were used to generate MS images with Mirion [37]. Prior to image generation, no normalization or any other data processing was performed. Images were assessed manually for interesting distributions and overlaid according to their patterns. Identifications in the imaging data are only tentative. They were identified according to their exact mass by comparison with the list of markers identified by LC–MS/MS. Due to insufficient signal intensities, no MS/MS analyses were performed during the MSI measurements.

Results and discussion

Granuloma around eggs in liver tissue of infected animals exhibits an accumulation of lipids

It is well known that schistosome infection leads to granuloma formation around eggs deposited in tissues such as the liver [7]. Granuloma mainly consist of macrophages and other immune cells [9, 10], which are assumed among others to play important roles in providing nutrients in form of lipids for the eggs [11]. On the other hand, they shield other hepatocytes from injury [38]. Granulomas are readily visible in the microscopic images of prepared liver sections as shown in Fig. 1A. Staining with oil red revealed an accumulation of neutral lipids in the granuloma as shown in Fig. 1B.

To distinguish between effects of the eggs and systemic effects of worm infection, bisex-infected samples were compared to monosex-infected samples, which are expected to produce no eggs. In rare cases, however, non-fertilized egg-like structures appear in hamsters infected with clonal female cercariae (monosex-infected), which can be accompanied by other types of host reactions [39]. For our studies, only monosex-infected samples without eggs were included. Non-infected samples were defined as controls to differentiate between healthy (no eggs) and infected (eggs) samples. Microscopic images of the three different sample types

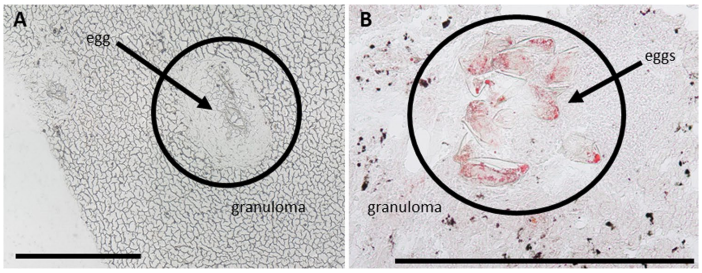

Fig. 1 Microscopic images of eggs with granuloma in livers of bisex-infected hamsters. (**A**) Light microscopic image of unstained tissue. (**B**) Tissue stained with oil red. Lipid accumulation in granuloma is clearly visible. Scale bars are 500 µm

used in this study are shown in Figure S1 in the supplementary file. While a detailed histological investigation of the involved cell types in the immune response of the hamster is not the scope of this study, further information on the topic will be found in the literature [von Bülow et al. 2022, in preparation]. Granulomas were formed due to trapped eggs in the bisex-infected (C) samples. The *S. mansoni* eggs are clearly visible within the granulomatous area in the zoomed-in image (D) of the bisex-infected samples. Tissue areas that were subsequently subjected to MS imaging experiments were selected based on microscopic images to ensure granuloma inclusion in case of bisex samples.

During further analysis, microscopic images were used to allocate identified markers to infection-specific morphological structures, such as eggs and granuloma. While overlaying optical and MS images, marker localization was confirmed. Due to the high thickness of tissue sections used for MALDI (≈ 20 µm), histological investigation is hindered. Moreover, tissue sections can only be stained after the MSI experiment, and cellular structures are affected and partly destroyed by the laser irradiation.

An exemplary microscopic image of an H&E-stained section after MSI analysis can be found in Figure S2.

LC–MS/MS analysis detected infection markers

In order to identify markers for *S. mansoni* infection and to determine their distributions in the tissue, we combined different mass spectrometric techniques. Experiments were performed with three sample groups (non-infected, monosex-infected, and bisex-infected), comprising three biological replicates of each group. An overview of the workflow is given in Fig. 2. The top right part shows a piece of hamster liver that was used for analysis. Following the figure counterclockwise, parts of liver samples were homogenized followed by lipid extraction. Applying LC–MS/MS, 372 significantly occurring markers were found in the extracts after lipid identification in positive- and negative-ion mode with LipidMatch Flow and statistical analysis of the data with Perseus. An exemplary LC–MS/MS spectrum can be found in Figure S3. All lipid identifications are based on head group and fatty acid fragments with one exception that was only confirmed by class. Using MetaboAnalyst, PCA was performed. As the scores plot in Figure S5 shows, the three sample groups were well separated based on LC–MS/MS data, already suggesting that the lipid profiles vary significantly. Additionally, the PCA shows all three technical replicates of the pool samples arranged in very close vicinity, indicating that the LC measurements were acquired with stable performance.

In parallel, cryosections of the liver samples were prepared and analyzed in positive- as well as in negative-ion mode with MALDI MSI, as shown in Fig. 2. For some of the infection markers, distribution patterns matching with optical images were found by annotating MSI data using the marker list from LC–MS/MS experiments in Mirion. The three native color channels (red, green, and blue) were used to overlay the three selected MS images (D), showing significantly different spatial distributions for the three markers. Comparison with the microscopic image revealed their connection to different compartments of the inflammation. All identified markers and their predominant localization (if applicable) are listed in an additional excel sheet (see supplemental information, "infection marker list").

The overlap between the detected *m*/*z* data sets of LC–MS/MS and MALDI MSI was not perfect. Most of the detected *m*/*z* values were found with only one method. This effect is due to the different ionization mechanisms of ESI and MALDI that favor ionization of different lipid classes as well as the formation of different adduct species. While the solvent in LC–MS/MS experiments contained ammonium formate, and predominantly $[M+NH_4]^+$ ions were formed, for example, for triglycerides, the same lipid species were detected as alkali metal adducts with MALDI MSI. To enhance the overlap of the two data sets, the *m*/*z* values of the identified lipids in LC–MS/MS were re-calculated. In case of triglycerides, *m*/*z* values for $[M+H]^+$, $[M+Na]^+$, and $[M+K]^+$ ions were calculated and were used to create images. An example can be found in Figure S6 and is discussed later in the MSI part. Another aspect that has to be

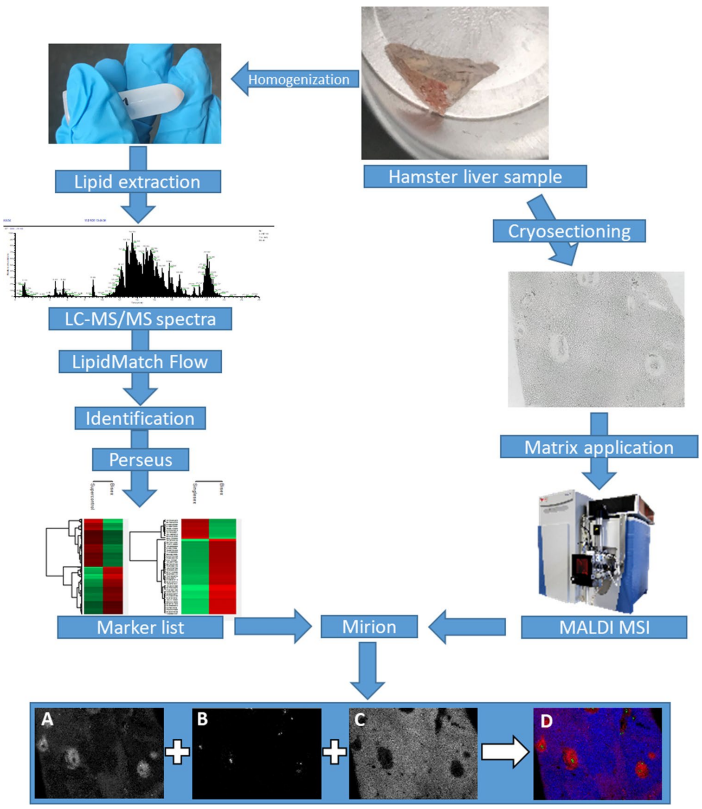

Fig. 2 Hamster liver samples were either homogenized or cryosectioned. After homogenization, lipids were extracted, and samples were analyzed using LC–MS/MS. With the help of LipidMatch Flow and Perseus, identified signals were annotated and markers were identified that occurred with statistically determined significance. After cryosectioning, matrix was applied, and samples were measured using MALDI MSI. Using the software Mirion and the marker list from LC–MS/MS experiments, MS images were generated: (**A**) m/z 500.275684, LPE(20:4), $[M-H]^-$; (**B**) m/z 866.592639, PS(42:4), $[M-H]^-$; (**C**) m/z 776.526946, MMPE(16:0_22:6), $[M-H]^-$; (**D**) RGB overlay of MS images A, B, C

kept in mind is the difference in sample preparation. While samples for LC were homogenized and lipid extraction was performed, whole tissue sections were used for MSI experiments. Therefore, matrix effects might play an important role regarding comparability of MSI data to LC–MS/MS data. Matrix effects are present also for LC measurements but should be smaller compared to MSI. Furthermore, some markers detected in MSI measurements might be absent in LC data due to low solubility.

More markers distinguish between bisex-infected and control samples than between bisex- and monosex-infected samples, as seen in Fig. 3. Markers found for monosex-infected samples were mostly those also found for bisex-infected samples (35 "enriched" markers in Fig. 3). The effects of *S. mansoni* infection on the lipid composition of the host liver tissue are manifold. Although infection with monosex cercariae does not result in egg deposition and granuloma formation, the unpaired parasites still provoke the host organism and the cercarium develops into an adult worm that resides in different organs of the host. In a previous study, up to 85% of the unpaired female worms and 65% of male worms were found in mouse liver after 8 weeks. The female worm induced an accumulation of inflammatory cells in blood vessels and the surrounding liver tissue [40–42]. These effects also play a role when paired worms from a bisex-infection are present, but morbidity-inducing liver damage is ultimately caused by the deposited eggs. Altogether, the hepatic lipid composition of bisex-infection shows more similarities to a monosex-infection than to the control which might reflect the common changes due to worm presence in both infection states.

Changes in lipid composition were mostly found in the groups of PCs, PEs, and TG (Fig. 4). All subgroups of one major phospholipid class were summed in the same group. As an example, all PEs, lyso-PEs, oxidized PEs and oxidized lyso-PEs were summed up and shown in the PE bar (for full

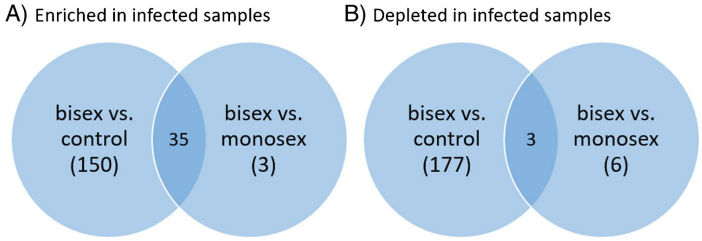

Fig. 3 Venn diagram showing the numbers of infection markers found. Many more infection markers were found to be enriched when comparing bisex-infected with control samples than with monosex-infected samples (**A**). The same holds for depleted infection markers (**B**). The terms "enriched" and "depleted" have to be used carefully since further biological analysis is needed to verify that the eggs actually take up and metabolize the lipids. Here, the terms are meant to describe changes in signal intensities found in LC–MS/MS measurements

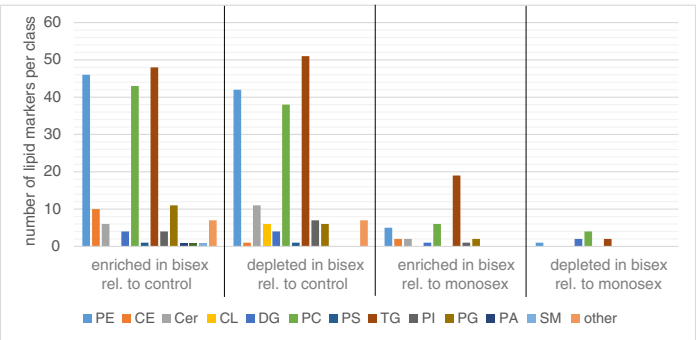

Fig. 4 Enrichment and depletion of lipids of several lipid classes in bisex-infected hamster liver, relative to non-infected controls or monosex-infected hamsters. Significantly more enriched/depleted markers were observed relative to controls than to monosex-infected samples. Markers were found by comparing the groups of bisex-infected samples to monosex-infected or control samples. No individual comparison between the three samples of one sample group was performed. Lipids with a FDR of up to 5% were assumed as infection markers

information on the lipid species detected, please refer to the "Infection marker" table in the Supplementary information). Interesting lateral distributions of such subgroups are discussed in more detail below in the MS imaging part. Both enrichment and depletion were found due to egg deposition. The terms "enriched" and "depleted" have to be used carefully here, since further biological analyses are needed to verify that the eggs take up and metabolize the depleted lipids. Until then, the terms are meant to describe changes in signal intensity during LC–MS/MS measurements with no information about depletion or enrichment location.

The majority of markers belong to the TGs, followed by PEs and PCs. These lipid classes are known for their good detectability in LC–MS measurements. We calculated the average number of carbon atoms and double bonds in the detected PC, PE, and TG markers for comparison between the sample groups. While no striking difference was found for PC and PE markers, triglycerides revealed a varying number of double bonds in the fatty acid chains. The 48 TG markers that were found enriched in bisex-infected samples compared to control had an average number of double bonds of $n = 8.4$ while the 51 TG markers depleted in bisex-infected samples compared to control samples had an average double bond number of $n = 3.1$. The carbon number differed only in the range of the standard deviation. By examining the "Infection marker" table in the Supplementary information, one can find no arachidonic acid (AA, 20:4) or docosahexaennoic acid (DHA, 22:6) in the markers of the control samples, but one or both of these fatty acids appear in 52% of TGs enriched in bisex-infected samples. It was shown previously that AA treatment of hamsters infected with *S. mansoni* reduced worm burden

and the number of eggs [41], so the presence of AA in bisex-infected samples might be a protective response of the immune system. The treatment with DHA also resulted in reduced worm burden and lower egg count, but the effect was not as clear as for AA.

Enrichment was found in LC–MS/MS measurements for all cholesterol ester markers (CE), while none of the CE signals was found to be depleted relative to control samples. Cardiolipin markers (CL), on the other hand, were found depleted, while no detected CL was enriched relative to control samples. No characteristic distribution patterns were found for these species (CE and CL) in MALDI MSI measurements, which is either due to a missing lateral specificity or an insufficient signal-to-noise ratio in MALDI for these compounds at small spot sizes (high lateral resolution).

Lipid distributions revealed by MALDI MSI

In Fig. 5A and C, lateral distributions of selected markers defined in our LC–MS/MS experiments are shown. For all images, MMPE(16:0_22:6) (monomethylphosphatidyl ethanolamine) was chosen to visualize the liver tissue in blue. This signal was only observed in the non-affected tissue surrounding the granuloma. The corresponding ion was found as a marker that is enriched in bisex samples compared to control samples. Inside the granuloma, lysolipid metabolites of PE were found (red). Images B and D, obtained from non-infected samples, do not show any localized enrichment of these markers that can be attributed to tissue structures. This suggests that the eggs might accumulate certain lipid species, for example, the tentatively identified PS(42:4) (Fig. 5). On the other hand, they appear to consume and

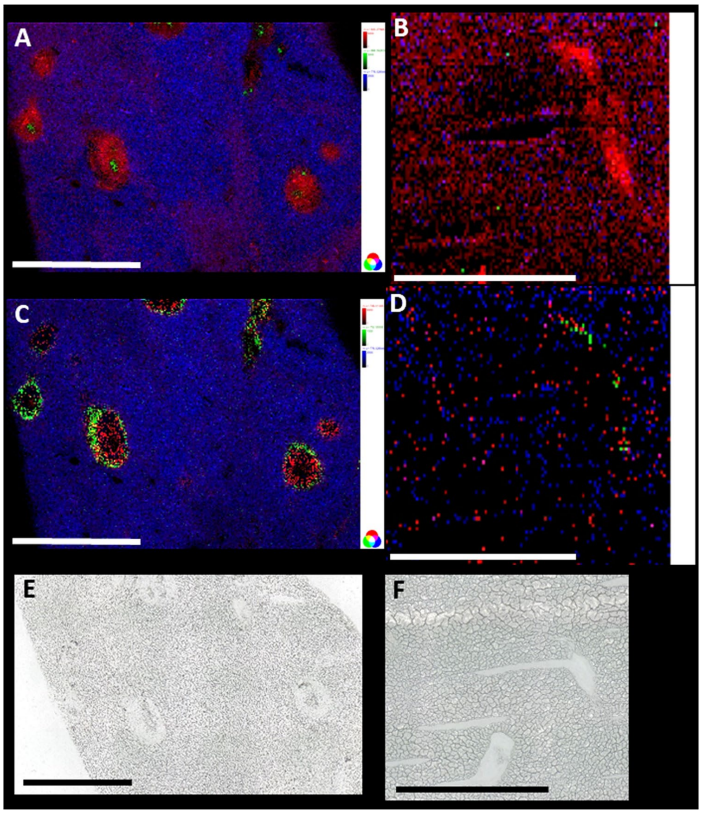

Fig. 5 Comparison between liver sections of a bisex-infected hamster (**A, C**) and a healthy control sample (**B, D**). For A, m/z 500.275684, LPE(20:4), $[M-H]^-$ (red) was found to be a marker for granuloma; m/z 776.526946, MMPE(16:0_22:6), $[M-H]^-$ (blue) a marker for surrounding tissue; and m/z 866.592639, PS(42:4), $[M-H]^-$ (green) a marker for schistosome eggs. For the non-infected sample, B shows the same ions in the same colors, but no characteristic distribution was found. This underlines that statistical markers found by LC–MS/MS also show recognizable and allocatable distributions in the imaging measurements. In image C, m/z 746.511353, plasmenyl-PE(P-16:0/22:6), $[M-H]^-$ (red) as a marker for granuloma and m/z 752.555581, plasmanyl-PE(O-18:0/20:4), $[M-H]^-$ (green) as a marker for granuloma borders were selected for creating the RGB image. Again, m/z 776.526946 was taken as a marker for non-affected tissue (blue). The same coding as in C was chosen for image D of a non-infected (control) sample, and again, we found no characteristic distribution. Scale bars are 1 mm. Single-ion images are shown in Figure S7 and Figure S8. **E** and **F** are the corresponding optical images of the samples

thus downgrade the contents of certain lipids in the close vicinity of granulomas in bisex samples, as, for example, for MMPE (see single-ion images and optical images in Figure S7, S8, and S14). Taking a look at the single-ion images, "holes" in the distribution of granuloma-specific ions were observed. The microscopic images show that this is not due to missing tissue but schistosome eggs are found at these positions. This is a further hint that the eggs take up these lipids and metabolize them. However, as no labelled tracer studies were carried out, this is only a hint and not a clear proof. A deeper look into lipid uptake of schistosome eggs is described in a recent study of von Bülow et al. [in preparation]. Of special interest are the two lipids shown in the green color channel in Fig. 5A and C, which were found in distinct areas of the granuloma only. The compound at *m/z* 752.555581 was identified by LC–MS/MS as a PE lipid (plasmanyl-PE(O-18:0/20:4), $[M-H]^-$); the other compound at *m/z* 866.592639 was tentatively assigned as PS(42:4), $[M-H]^-$. Other examples can be found in Figure S9. While some marker lipids were found within or in direct contact to the eggs, others were located mostly in the outer regions of the granuloma (shown in the green color channel). Eggs have to take up nutrients from their host tissue to survive [43] and our MS image data seem to substantiate this assumption. The enrichment or depletion of specific lipids might be related to the presence of cells forming the granuloma and therefore displacing the hepatocytes. We found no clear correlation between localization and an entire lipid class but only with individual lipid species.

Additionally, the distribution pattern based on different adducts for the same lipid was investigated. This can be exemplarily seen in Figure S6. Here, the distribution of PC(O-34:1) is shown as proton, sodium, and potassium adducts. In general, this lipid was mainly found in the granuloma around but not in the eggs. However, on closer examination, signal intensities and localization outside the granuloma region vary slightly. This can be due to different distributions of the alkali metals in the tissue. In general, signal intensities of some lipid classes (e.g., TGs) were not that high. After dividing low abundance of one compound to three different adduct signals, intensities might be too low for detection. Therefore, not all adducts were found for each lipid.

We have chosen the lipid class of PCs to take a deeper look at the distributions of several lipid species. Interestingly, different distribution patterns were found. For example, PC(16:0_20:5), observed at *m/z* 802.535727 as $[M+Na]^+$, was found to be evenly distributed in the whole sample except in the granulomatous areas in liver samples of bisex-infected hamsters, where it was depleted (Figure S10). In contrast, PC(19:0_20:2), detected at *m/z* 850.629627 as $[M+Na]^+$, was found to be enriched in granulomas (Figure S11). PC(16:0_18:0), detected at *m/z* 800.556617 as $[M+K]^+$, was found only in the granulomas and just rarely in the surrounding tissue or in not-infected samples (Figure S12). The according mass spectrum and extracted ion chromatogram are shown in Figure S4. PC(20:0_20:3), detected at *m/z* 862.630305 as $[M+Na]^+$, showed some enrichment in and directly around the eggs, but not in the rest of the sample (Figure S13). These observations provide first hints about possible metabolic changes in the tissue due to infection.

Another example is shown in Fig. 6. Here, the lateral distribution of TG(50:2), detected as $[M+K]^+$ ion at *m/z* 869.69869, is shown. This lipid was detected at *m/z* 848.771097 as $[M+NH_4]^+$ in LC–MS/MS experiments and also found in eggs before by Giera et al. [21]. Our statistical LC–MS/MS analysis revealed that this TG was depleted in tissue of bisex-infected hamsters. MSI data revealed distribution changes due to infection. While the lipid was found to be evenly distributed in the three control samples, it was only found in the granuloma of the bisex-infection group. All images shown in Fig. 6 were adjusted to the same signal intensity. Therefore, pixel brightness in all sub-images corresponds to the same signal intensity scale. Bisex samples on the left-hand side show negligible signal intensities of TG(50:2) except from the granulomatous areas, where signal intensities peaked to $NL = 8*10^3$. In the control samples, the lipid was found ubiquitously and signal intensities were in the range of $NL = 1*10^3$ to $NL = 2.2*10^3$. In control sample 1, signal intensities were lower compared to the other control samples, but the signal was still evenly distributed throughout the whole tissue section.

This tendency was also observed for eight other triglycerides. Due to low signal intensities, however, the effect was not as obvious in some cases. For the triglycerides with the lowest signal intensities, accumulation of the respective lipid was observed in the granuloma of the bisex-infection group, whereas detection in control samples was limited to only a few pixels per sample. Interestingly, we have not observed the opposite trend of a depletion in granuloma for any triglyceride in our MSI data. These data provide new insights into the localization and accumulation of triglycerides in livers of *Schistosoma*-infected hamsters at the level of individual lipid species.

We also compared infection markers found in our study with those found in schistosome eggs by Giera et al. [21]. Tentative markers that we specifically found in eggs (DMPE(18:0_22:5) and PS(42:4)) were not detected by Giera et al. or Kadesch et al., neither in eggs nor in schistosome worms. Infection markers of the lipid classes CE, LPC, PC, and TG were in good accordance with previous data [20, 21], suggesting that the eggs might take up the respective lipids, perhaps as nutrients. Other markers, such as PEs, CLs, dimethylphosphatidylethanolamines (DMPEs), and

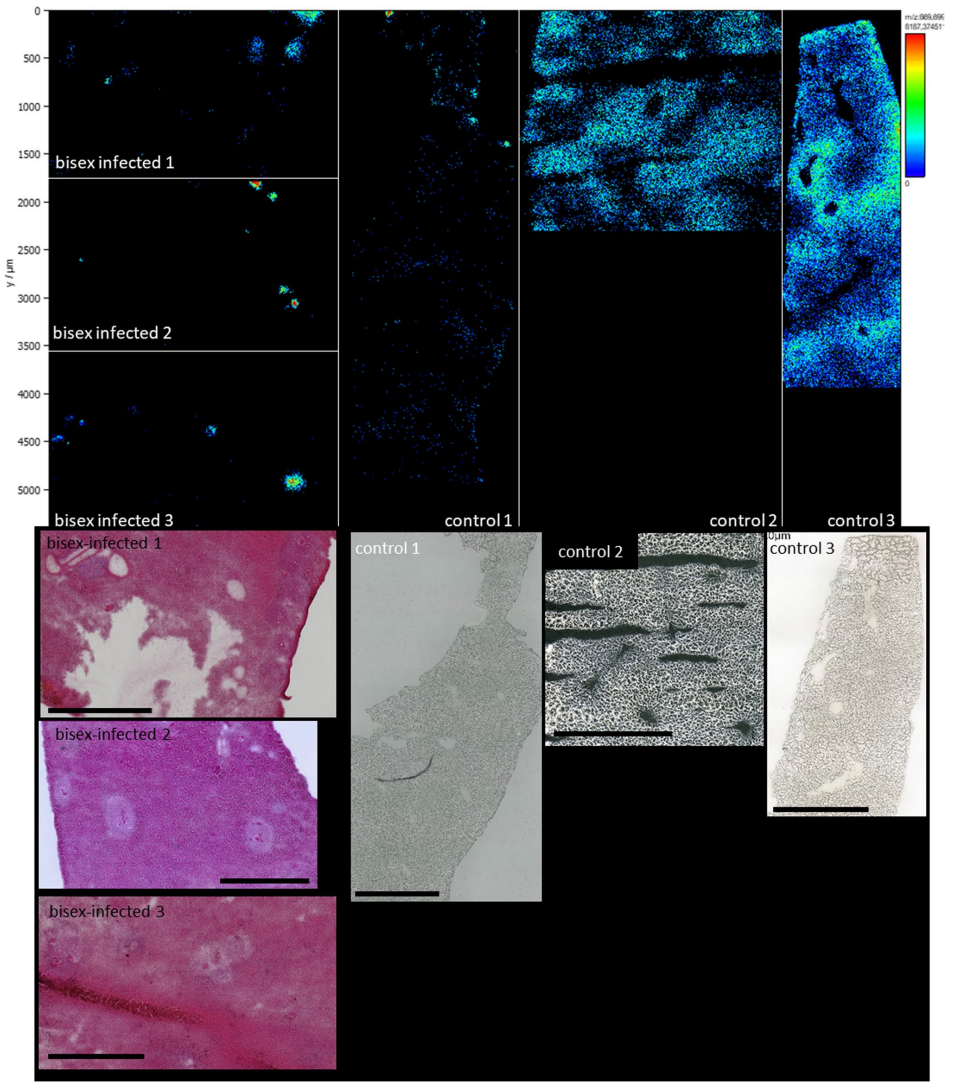

Fig. 6 Upper part: Distribution comparison of m/z 869.698690 TG(16:0_16:1_18:1) $[M+K]^+$. Liver samples of bisex-infected hamsters are shown on the left side; control samples are grouped on the right side. While the lipid is evenly distributed in the control samples, accumulation in the eggs and the surrounding granuloma area of the bisex sample group is clearly visible. Overall, this triglyceride was found enriched in control samples by LC–MS/MS. Lower part: Corresponding optical images of the samples. Scale bars are 1 mm

diglycerides (DGs), seemed to be characteristic for the host tissue since they were not detected in eggs by Giera et al.

Additional investigations are needed to get a better understanding of the underlying mechanisms of lipid localization, presumptive uptake mechanisms, and accumulation. These might be related to lipid consumption by the eggs or to reactions of the host's immune system. Other studies have shown that granuloma protects the host from enzymes secreted by the eggs [7, 44], and the identified lipids in the outer regions of the granuloma might be part of this defense mechanism. Stanley et al. reported about lipid-enriched cells in the outer part of the granuloma and suggested that immune cells, such as macrophages, might play an important role in the changes of the lipid profile of the host's liver [15]. According to our findings, only plasmanyl- and plasmenyl-PEs (plasmalogens) seemed to accumulate at the borders of granuloma (see Fig. 5). Plasmalogens were mainly found in the outer tegumental membranes of adult worms [45]. This membrane is the contact region between host and parasite and plays an important role in defending the parasite against the host's immune system [46, 47].

The results of our study provide first insights into the alteration of lipid profiles in hamster livers after infection with *S. mansoni* and egg deposition. Especially the detailed information on lipid species level that was achieved by LC–MS/MS analysis in connection with lateral information gained through MALDI MSI will open novel perspectives to unravel the roles of individual lipid species and lipid classes in the context of the egg-induced pathological changes in the host liver tissue.

Conclusion

With the help of mass spectrometric techniques, we characterized morphological changes, such as granuloma formation in the liver tissue of *S. mansoni*-infected hamsters at a molecular level. Alterations in the lipid profile were examined by LC–MS/MS of homogenized samples, and for the first time, we identified markers specific for infection. These markers were additionally analyzed by MALDI MSI, exhibiting their distribution in tissue sections. The established protocol allowed not only to visualize and analyze entire granulomas based on selected markers but also to indicate substructures inside the granulomas. Furthermore, we provided evidence for a specific distribution of individual lipid species and their enrichment or absence in tissue sections containing parasite eggs. It is tempting to speculate about a parasitic role also for the egg stage of *S. mansoni*, which might acquire lipid resources from its host tissue environment. Further studies will address presumptive uptake mechanisms and the role of these lipids in the host-parasite interaction of *S. mansoni*.

Supplementary Information The online version contains supplementary material available at https://doi.org/10.1007/s00216-022-04006-6.

Acknowledgements We thank TransMIT GmbH, Giessen, Germany, for technical support. We kindly thank Vannuruswamy Garikapati and David Lüke for their help with the LC-MS/MS experiments as well as Christina Scheld and Georgette Stovall for excellent technical assistance in maintaining the parasite cycle.

Funding Open Access funding enabled and organized by Projekt DEAL. This work received financial support from the Hessian Ministry of Science, Higher Education and Art (HMWK), LOEWE Center DRUID, and from Deutsche Forschungsgemeinschaft DFG (Sp314/13–1, INST 162/500–1 FUGG, and RO3714/4–1).

Declarations

Ethics approval, source of biological material, and statement on animal welfare To keep the *S. mansoni* life cycle, *Biomphalaria glabrata* snails served as intermediate hosts and Syrian hamsters (*Mesocricetus auratus*) as final hosts. The hamster model has been established because it is more permissive for schistosome infection compared to the mouse model, which requires more animals (reduction principle of the 3Rs). Both snails and hamsters were bred in-house (Biomedical Research Center Seltersberg, Giessen, Germany). All animal experiments were conducted in accordance with the European Convention for the Protection of Vertebrate Animals Used for Experimental and Other Scientific Purposes (ETS No 123; revised Appendix A), and they were additionally approved by the Regional Council (Regierungspraesidium) Giessen (V54-19 c 20/15 c GI 18/10).

Conflict of interest B.S. and C.G.G. are consultants of TransMIT GmbH, Giessen, Germany. The other authors declare to have no conflicts of interest.

References

1. Gryseels B, Polman K, Clerinx J, Kestens L. Human schistosomiasis. Lancet. 2006;368(9541):1106–18.
2. World Health Organization. Integrating neglected tropical diseases into global health and development: fourth WHO report on neglected tropical diseases. 2017.
3. World Health Organization. Prevention and control of schistosomiasis and soil-transmitted helminthiasis. 2002.

4. Vale N, Gouveia MJ, Rinaldi G, Brindley PJ, Gartner F, da Costa JMC. Praziquantel for schistosomiasis: single-drug metabolism revisited, mode of action, and resistance. Antimicrob Agents Ch. 2017;61(5):16.
5. Caffrey CR. Chemotherapy of schistosomiasis: present and future. Curr Opin Chem Biol. 2007;11(4):433–9.
6. Schramm G, Hamilton JV, Balog CIA, Wuhrer M, Gronow A, Beckmann S, Wippersteg V, Grevelding CG, Goldmann T, Weber E, Brattig NW, Deelder AM, Dunne DW, Hokke CH, Haas H, Doenhoff MJ. Molecular characterisation of kappa-5, a major antigenic glycoprotein from Schistosoma mansoni eggs. Mol Biochem Parasit. 2009;166(1):4–14.
7. Hams E, Aviello G, Fallon PG. The Schistosoma granuloma: friend or foe? Front Immunol. 2013;4:8.
8. Vella AT, Hulsebosch MD, Pearce EJ. Schistosoma-mansoni eggs induce antigen-responsive CD44-HI T-helper 2-cells and IL-4-secreting CD44-LO cells – Potential for T-helper 2 subset differentiation is evident at the precursor level. J Immunol. 1992;149(5):1714–22.
9. Adams DO. Granulomatous inflammatory response. Am J Pathol. 1976;84(1):164–91.
10. Weinstock JV, Boros DL. Organ-dependent differences in composition and function observed in hepatic and intenstinal granulomas isolated from mice with schistosomiasis mansoni. J Immunol. 1983;130(1):418–22.
11. Wilson JL, Mayr HK, Weichhart T. Metabolic programming of macrophages: implications in the pathogenesis of granulomatous disease. Front Immunol. 2019;10:22.
12. Doenhoff MJ, Stanley RG, Griffiths K, Jackson CL. An anti-atherogenic effect of Schistosoma mansoni infections in mice associated with a parasite-induced lowering of blood total cholesterol. Parasitology. 2002;125:415–21.
13. Da Silva FL, Del-Rei RP, Fraga DBM, Leony LM, de Souza A, Santos FLN. Alterations in the lipid profiles and circulating liver enzymes in individuals infected by Schistosoma mansoni. Rev Soc Bras Med. 2018;51(6):795–801.
14. Anthony B, Mathieson W, de Castro-Borges W, Allen J. Schistosoma mansoni: egg-induced downregulation of hepatic stellate cell activation and fibrogenesis. Exp Parasitol. 2010;124(4):409–20.
15. Stanley RG, Jackson CL, Griffiths K, Doenhoff MJ. Effects of Schistosoma mansoni worms and eggs on circulating cholesterol and liver lipids in mice. Atherosclerosis. 2009;207(1):131–8.
16. Rustam YH, Reid GE. Analytical challenges and recent advances in mass spectrometry based lipidomics. Anal Chem. 2018;90(1):374–97.
17. Li F, Qin XZ, Chen HQ, Qiu L, Guo YM, Liu H, Chen G, Song G, Wang X, Li F, Guo S, Wang B, Li Z. Lipid profiling for early diagnosis and progression of colorectal cancer using direct-infusion electrospray ionization Fourier transform ion cyclotron resonance mass spectrometry. Rapid Commun Mass Spectrom. 2013;27(1):24–34.
18. Waldchen F, Mohr F, Wagner AH, Heiles S. Multifunctional reactive MALDI matrix enabling high-lateral resolution dual polarity ms imaging and lipid C=C position-resolved MS2 imaging. Anal Chem. 2020;92(20):14130–8.
19. Surma MA, Herzog R, Vasilj A, Klose C, Christinat N, Morin-Rivron D, Simons K, Masoodi M, Sampaio JL. An automated shotgun lipidomics platform for high throughput, comprehensive, and quantitative analysis of blood plasma intact lipids. Eur J Lipid Sci Tech. 2015;117(10):1540–9.
20. Kadesch P, Quack T, Gerbig S, Grevelding CG, Spengler B. Tissue- and sex-specific lipidomic analysis of Schistosoma mansoni using high-resolution atmospheric pressure scanning microprobe matrix-assisted laser desorption/ionization mass spectrometry imaging. Plos Neglect Trop D. 2020;14(5):17.
21. Giera M, Kaisar MMM, Derks RJE, Steenvoorden E, Kruize YCM, Hokke CH, Yazdanbakhsh M, Evert B. The Schistosoma mansoni lipidome: leads for immunomodulation. Anal Chim Acta. 2018;1037:107–18.
22. Yang XY, Ding WM, Qian XY, Jiang PF, Chen QQ, Zhang X, Lu Y, Wu J, Sun F, Pan Z, Li X, Pan W. Schistosoma japonicum infection leads to the reprogramming of glucose and lipid metabolism in the colon of mice. Front Vet Sci. 2021;8:10.
23. Koestler M, Kirsch D, Hester A, Leisner A, Guenther S, Spengler B. A high-resolution scanning microprobe matrix-assisted laser desorption/ionization ion source for imaging analysis on an ion trap/Fourier transform ion cyclotron resonance mass spectrometer. Rapid Commun Mass Sp. 2008;22(20):3275–85.
24. Mokosch AS, Gerbig S, Grevelding CG, Haeberlein S, Spengler B. High-resolution AP-SMALDI MSI as a tool for drug imaging in Schistosoma mansoni. Anal Bioanal Chem. 2021;413(10):2755–66.
25. Xu YZ, Dresden MH. Schistosoma mansoni – Egg morphology and hatchability. J Parasitol. 1989;75(3):481–3.
26. Grevelding CG. Genomic instability in Schistosoma mansoni. Mol Biochem Parasit. 1999;101(1–2):207–16.
27. Roderfeld M, Padem S, Lichtenberger J, Quack T, Weiskirchen R, Longerich T, Schramm G, Churin Y, Irungbam K, Tschuschner A, Windhorst A, Grevelding CG, Roeb E. Schistosoma mansoniEgg-Secreted Antigens Activate Hepatocellular Carcinoma-Associated Transcription Factors c-Jun and STAT3 in Hamster and Human Hepatocytes. Hepatology. 2020;72(2):626–41.
28. Weglage J, Wolters F, Hehr L, Lichtenberger J, Wulz C, Hempel F, Baier A, Quack T, Köhler K, Longerich T, Schramm G, Irungbam K, Mueller H, von Buelow V, TschuschnerA, Odenthal M, Drebber U, el Arousy M, Ramalho LNZ, Bankov K, Wild P, Pons-Kühnemann J, Tschammer J, Grevelding CG, Roeb E, Roderfeld M. Schistosoma mansoni eggs induce Wnt/beta-catenin signaling and activate the protooncogene c-Jun in human and hamster colon. Sci Rep. 2020;10(1):14.
29. Lu ZG, Sessler F, Holroyd N, Hahnel S, Quack T, Berriman M, Grevelding CG. Schistosome sex matters: a deep view into gonad-specific and pairing-dependent transcriptomes reveals a complex gender interplay. Sci Rep. 2016;6:14.
30. Lillie RD, Ashburn LL. Supersaturated solutions of fat stains in dilute isopropanol for demonstration of acute fatty degeneration not shown by Herxheimer's technique. Arch Pathol. 1943;36:432–40.
31. Bouschen W, Schulz O, Eikel D, Spengler B. Matrix vapor deposition/recrystallization and dedicated spray preparation for high-resolution scanning microprobe matrix-assisted laser desorption/ionization imaging mass spectrometry (SMALDI-MS) of tissue and single cells. Rapid Commun Mass Spectrom. 2010;24(3):355–64.
32. Breitkopf SB, Taveira MD, Yuan M, Wuif GM, Asara JM. Serial-omics of P53-/-, Brca1-/- mouse breast tumor and normal mammary gland. Sci Rep. 2017;7:17.
33. Garikapati V, Colasante C, Baumgart-Vogt E, Spengler B. Sequential lipidomic, metabolomic and proteomic analyses of serum, liver and heart tissue specimens from peroxisomal biogenesis factor 11α knockout mice. Anal Bioanal Chem. 2022;414:2235–50.
34. Koelmel JP, Kroeger NM, Ulmer CZ, Bowden JA, Patterson RE, Cochran JA, Beecher CWW, Garrett TJ, Yost RA. LipidMatch: an automated workflow for rule-based lipid identification using untargeted high-resolution tandem mass spectrometry data. BMC Bioinformatics. 2017;18:11.
35. Tyanova S, Temu T, Sinitcyn P, Carlson A, Hein MY, Geiger T, Mann M, Cox J. The Perseus computational platform for comprehensive analysis of (prote)omics data. Nat Meth. 2016;13(9):731–40.
36. Chong J, Soufan O, Li C, Caraus I, Li SZ, Bourque G, Wishart DS, Xia J. MetaboAnalyst 4.0: towards more transparent

and integrative metabolomics analysis. Nucleic Acids Res. 2018;46(W1):W486-W94.
37. Paschke C, Leisner A, Hester A, Maass K, Guenther S, Bouschen W, Spengler B. Mirion-A Software Package for Automatic Processing of Mass Spectrometric Images. J Am Soc Mass Spectr. 2013;24(8):1296–306.
38. Girgis NM, Gundra UM, Ward LN, Cabrera M, Frevert U, Loke P. Ly6C(high) monocytes become alternatively activated macrophages in schistosome granulomas with help from CD4+ cells. Plos Pathog. 2014;10(6):13.
39. Shaw MK. Schistosoma-mansonii – Vitelline gland development in females from single sex infections. J Helminthol. 1987;61(3):253–9.
40. Mone H, Boissier J. Sexual biology of schistosomes. Adv Parasit. 2004;57(57):89–189.
41. El Ridi R, Tallima H, Salah M, Aboueldahab M, Fahmy OM, Al-Halbosiy MF, Mahmoud SS. Efficacy and mechanism of action of arachidonic acid in the treatment of hamsters infected with Schistosoma mansoni or Schistosoma haematobium. Int J Antimicrob Ag. 2012;39(3):232–9.
42. Standen OD. The relationship of sex in Schistosoma-mansoni to migration within the hepatic portal system of experimentally infected mice. Ann Trop Med Parasit. 1953;47(2):139–45.
43. Bexkens ML, Mebius MM, Houweling M, Brouwers JF, Tielens AGM, van Hellemond JJ. Schistosoma mansoni does not and cannot oxidise fatty acids, but these are used for biosynthetic purposes instead. Int J Parasitol. 2019;49(8):647–56.
44. Colley DG, Bustinduy AL, Secor E, King CH. Human schistosomiasis. Lancet. 2014;383(9936):2253–64.
45. Brouwers J, Van Hellemond JJ, van Golde LMG, Tielens AGM. Ether lipids and their possible physiological function in adult Schistosoma mansoni. Mol Biochem Parasit. 1998;96(1–2):49–58.
46. Jokiranta TS, Jokipii L, Meri S. Complement resistance of parasites. Scand J Immunol. 1995;42(1):9–20.
47. Fishelson Z. Novel mechanisms of immune evasion by schistosoma-mansoni. Mem I Oswaldo Cruz. 1995;90(2):289–92.

2.2 Supplementary information

Supplementary information

Changes in the lipid profile of hamster liver after *Schistosoma mansoni* infection, characterized by mass spectrometry imaging and LC-MS/MS analysis

Katja R. Wiedemann[1], Alejandra Peter Ventura[1], Stefanie Gerbig[1], Martin Roderfeld[2], Thomas Quack[3], Christoph G. Grevelding[3], Elke Roeb[2], Bernhard Spengler[1#]

[1]*Institute of Inorganic and Analytical Chemistry, Justus Liebig University Giessen, Giessen, Germany*
[2]*Gastroenterology, Justus Liebig University Giessen, Giessen, Germany*
[3]*Institute for Parasitology, Justus Liebig University Giessen, Giessen, Germany*

Author to whom correspondence should be addressed
e-Mail address: bernhard.spengler@anorg.chemie.uni-giessen.de

Chemicals

Table S1: Used chemicals and their specifications.

Chemical name	Quality grade	manufacturer
1,5-diaminonapthalene (DAN)	97%	Acros Organics, Geel, Belgium
2,5-dihydroxy benzoic acid (DHB)	for synthesis	Merck, Darmstadt, Germany
2-propanol	for HPLC	Chemsolute, Renningen, Germany
acetone	HiPerSolv	VWR International, Fontenay-sous-Bois, France
ammonium formate	99.995%	Sigma-Aldrich, Steinheim, Germany
acetonitrile	HiPerSolv	VWR International, Fontenay-sous-Bois, France
Eosin Y solution		Sigma-Aldrich, Steinheim, Germany
ethanol	Uvasol	Merck, Darmstadt, Germany
Eukitt quick hardening medium		Sigma-Aldrich, Steinheim, Germany
formic acid	for mass spectrometry	Honeywell, Morris Plains, NJ, USA
Mayer's hematoxylin solution		Sigma-Aldrich, Steinheim, Germany
methanol	LiChroSolv	Merck, Darmstadt, Germany
Methyl-tert-butylether (MTBE)	for HPLC	Sigma-Aldrich, Steinheim, Germany
Oil Red		Sigma-Aldrich, Steinheim, Germany
paraformaldehyde		Roth, Karlsruhe, Germany
phosphate buffered saline (PBS)		Gibco, Carlsbad, CA, USA
trifluoro acetic acid	Uvasol	Merck, Darmstadt, Germany
water	HiPerSolv	VWR International, Fontenay-sous-Bois, France
xylene	for analysis	Merck, Darmstadt, Germany

MALDI MSI measurements

Table S2: Settings used for data acquisition with MALDI MSI.

Parameter	Setting
m/z	250-1000
Ion mode	Positive and negative
Resolution	240,000 at *m/z* 200
Ion injection time	500 ms
Scan rate	1 / s
Spray voltage	3 kV
Capillary temperature	250°C
Lock mass	*m/z* 716.12461 [5 DHB − 4 H_2O + NH_4]$^+$, none for DAN
Pixel size	10 µm

Mode	2D pixel mode
20% filter	On
Attenuator	15-20°

LC-MS/MS measurements

Table S3: LC gradient.

Time / min	Mobile phase A / %	Mobile phase B / %
0	70	30
2	57	43
2.1	45	55
12	35	65
18	15	85
20	0	100
25	0	100
25.1	70	30
28	70	30

Table S4: Source parameters for LC-MS measurements.

Parameter	Positive-ion mode	Negative-ion mode
Sheath gas / a.u.	40	45
Auxiliary gas / a.u.	15	12
Sweep gas / a.u.	2	1
Spray voltage / kV	3.5	3.5
Capillary temperature / °C	300	320
S-lens RF	50	55
Auxiliary heater temperature / °C	300	320

Table S5: MS parameters for LC-MS measurements, in () for MS/MS.

Parameters	Positive-ion mode	Negative-ion mode
Run time / min	28	28
Internal lock mass	391.28421	-
Charge state	1	1
Exclusion list [47]	On	-
Resolution	70k (35k)	70k (35k)
AGC target	10^6 (10^5)	10^6 (10^5)
Maximum injection time / ms	250 (75)	250 (75)
Scan range	200-1800	200-1800
Top N	15	15
Isolation window / *m/z*	1	1
Stepped NCE	25, 30	20, 30, 40
Underfilll ration / %	0.6	0.6
Intensity threshold	$8{\cdot}10^3$	$8{\cdot}10^3$
Exclude isotopes	On	On
Dynamic exclusion / s	8	8

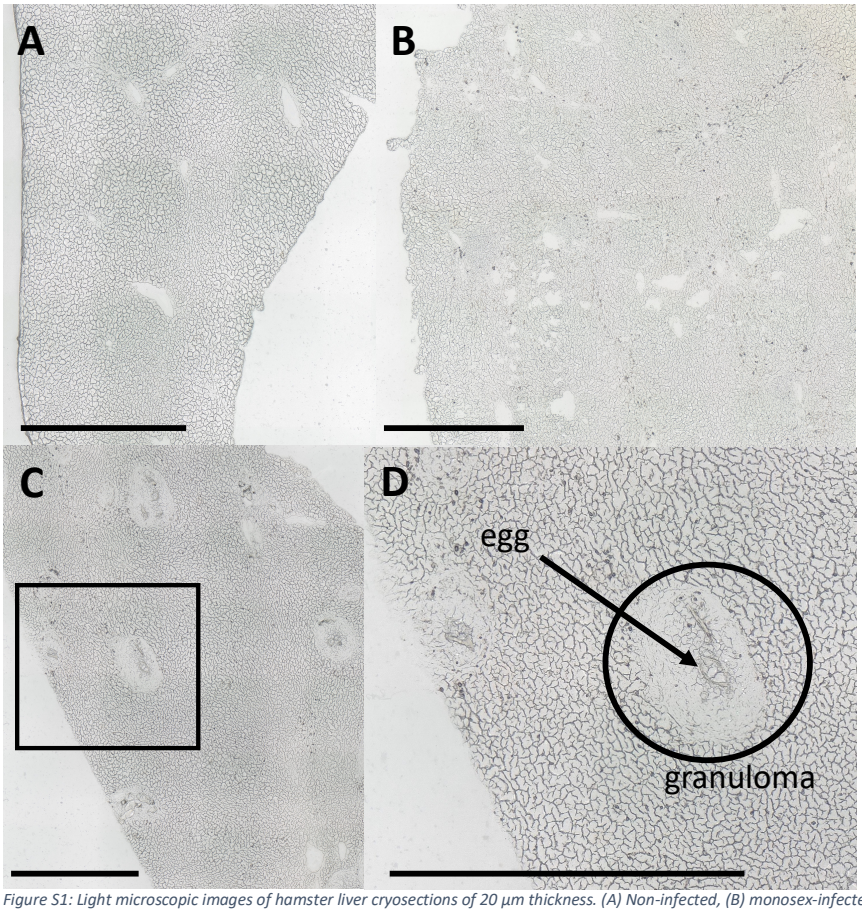

Figure S1: Light microscopic images of hamster liver cryosections of 20 µm thickness. (A) Non-infected, (B) monosex-infected, (C) bisex-infected, (D) zoomed area of (C), showing a nested egg and inflammation area around egg; scale bars are 1 mm.

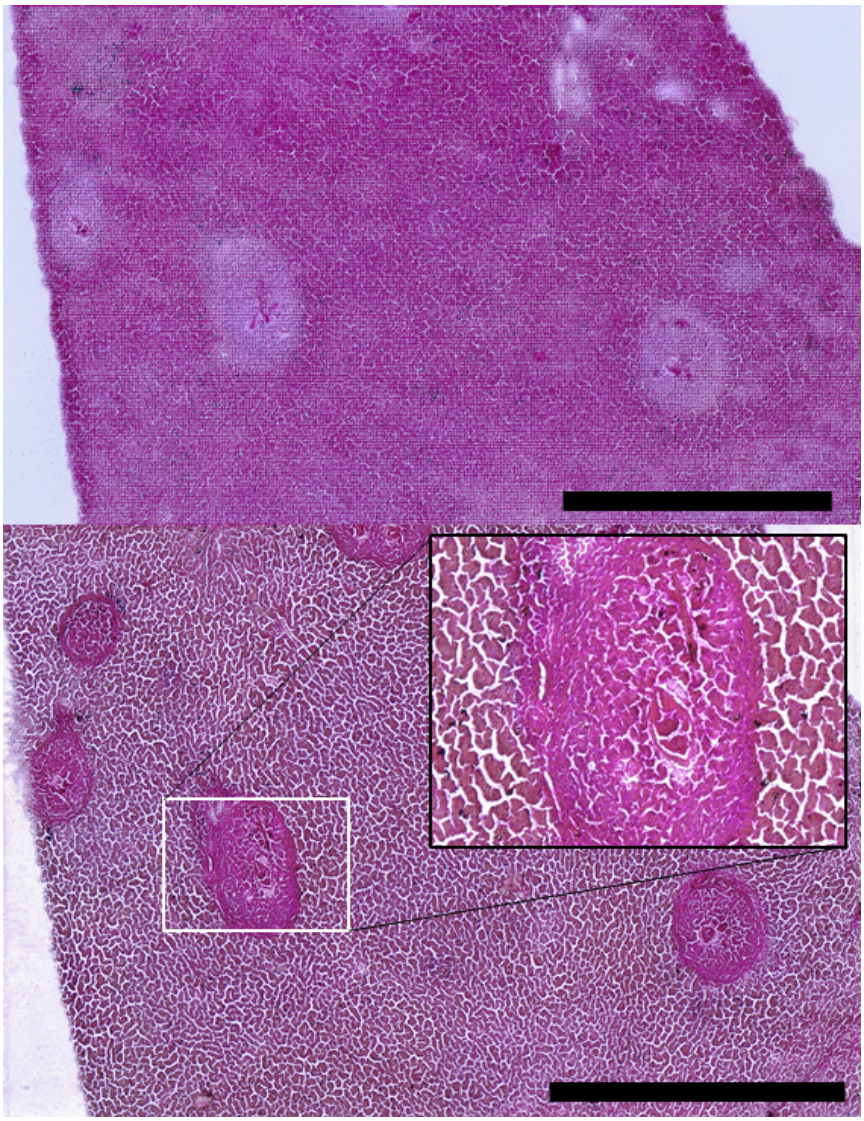

Figure S2: H&E stained sections of bisex-infected sample 2. Staining was performed after MSI measurements, therefore laser ablation spots are clearly visible. However, granuloma can still be identified around the eggs.

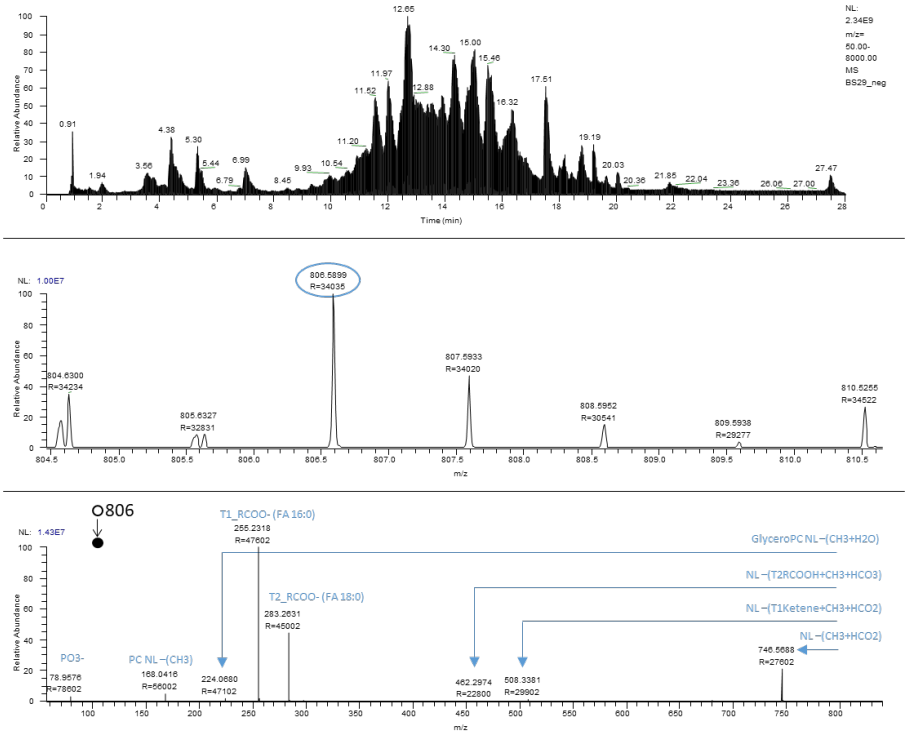

Figure S3: Exemplary LC-MS/MS spectra. In the upper part, the chromatogram of the LC separation is shown. In the middle, a zoom of the full MS spectra can be found. The peak of interest is marked with a blue circle. The lower part shows the MS/MS spectra of the peak of interest. Fragment ions and losses are stated in blue.

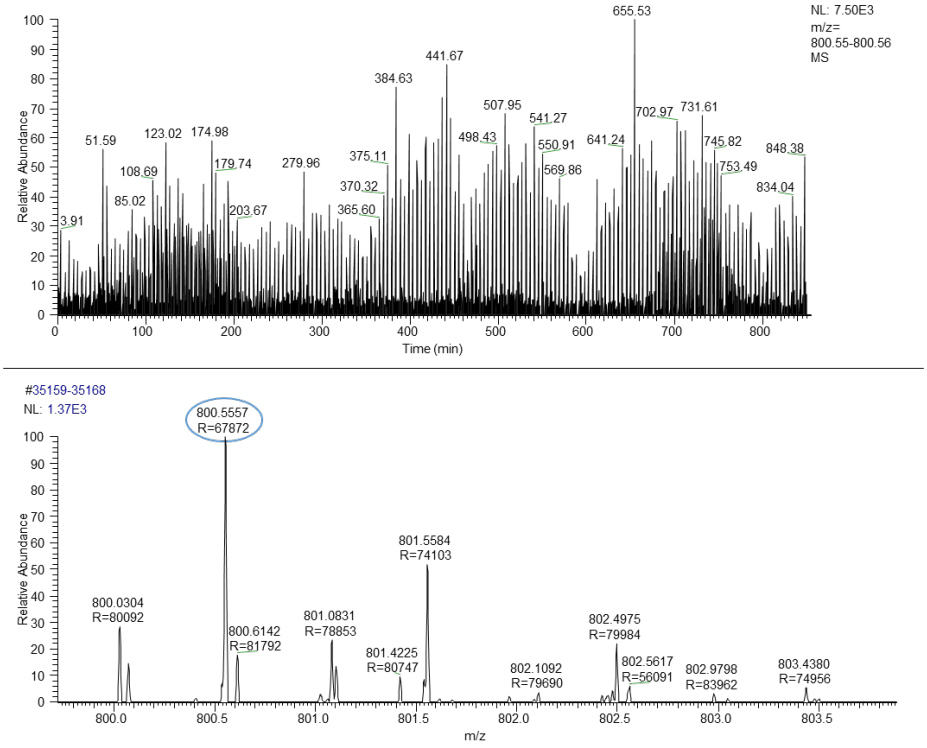

Figure S4: Exemplary MALDI spectrum. In the upper part, the extracted ion chromatogram of m/z 800.5557 is shown. The lower part shows the summed spectrum. The ion of interest is marked with a blue circle. According to the LC-MS/MS data, this peak belongs to PC(16:0_18:0) $[M+K]^+$.

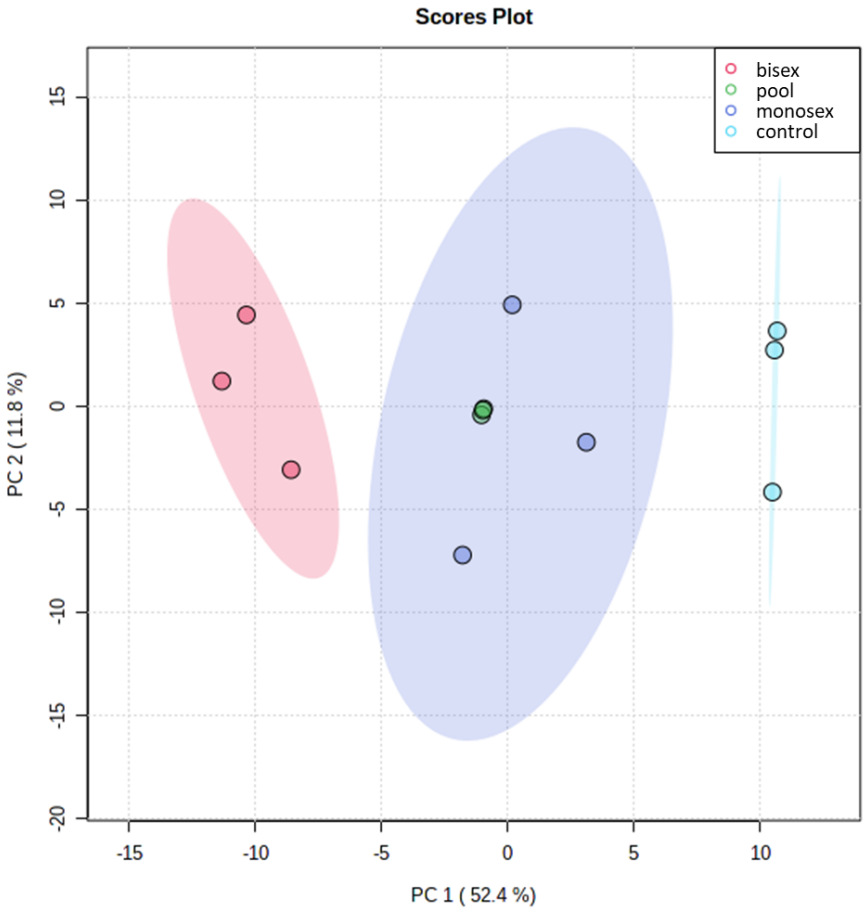

Figure S5: PCA scores plot from MetaboAnalyst[36]*, showing that the three sample groups are clearly distinguishable. The pool samples group nicely on nearly the same point, what is reasonable since they are only technical replicates.*

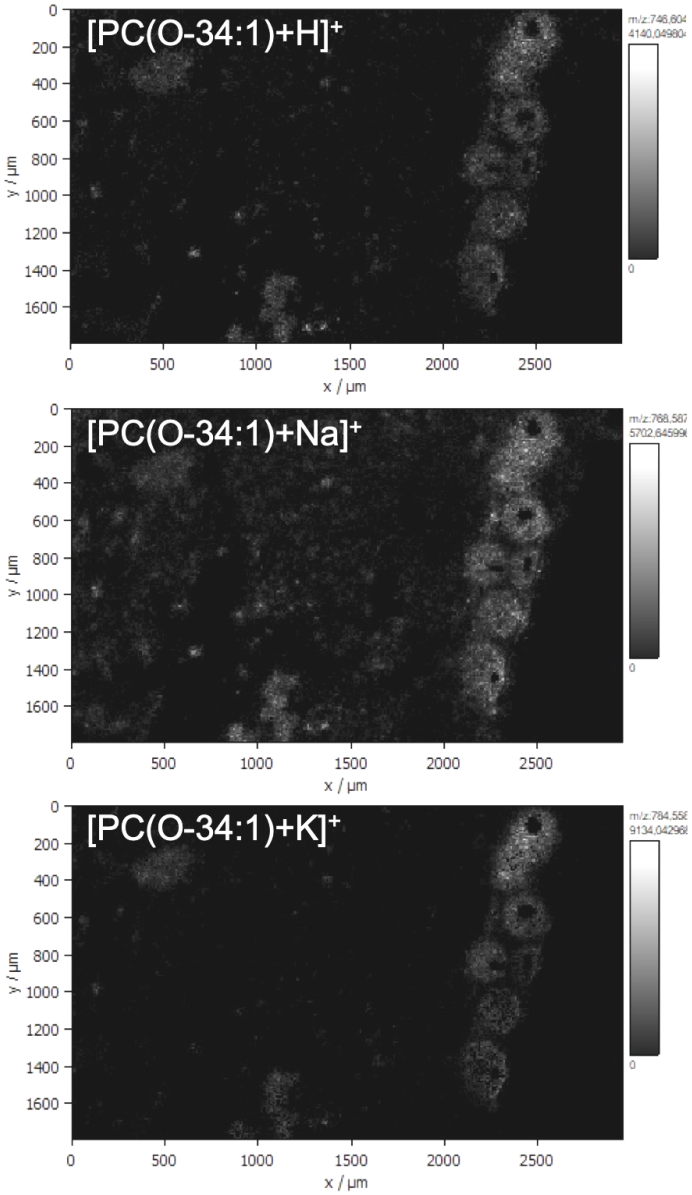

Figure S6: Comparison of different adducts for one lipid. Nearly the same distribution patterns were found. However, for most of the lipids, not all adducts were observed.

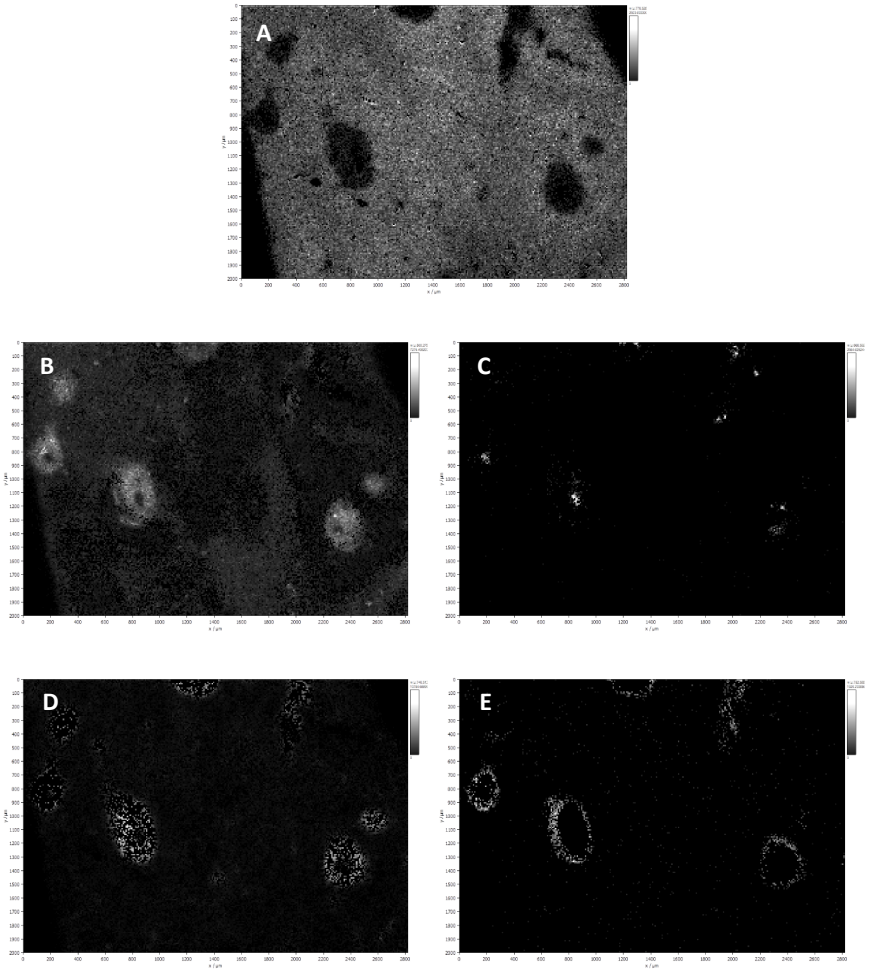

Figure S7: Single-ion images that were used for overlays of a bisex-infected sample as shown in Figure 5. A: m/z 776.526946, MMPE(16:0_22:6), $[M-H]^-$, B: m/z 500.275684, LPE(20:4), $[M-H]^-$, C: m/z 866.592639, PS(42:4), $[M-H]^-$, D: m/z 746.511353, plasmenyl-PE(P-16:0/22:6), $[M-H]^-$, E: m/z 752.555581, plasmanyl-PE(O-18:0/20:4), $[M-H]^-$.

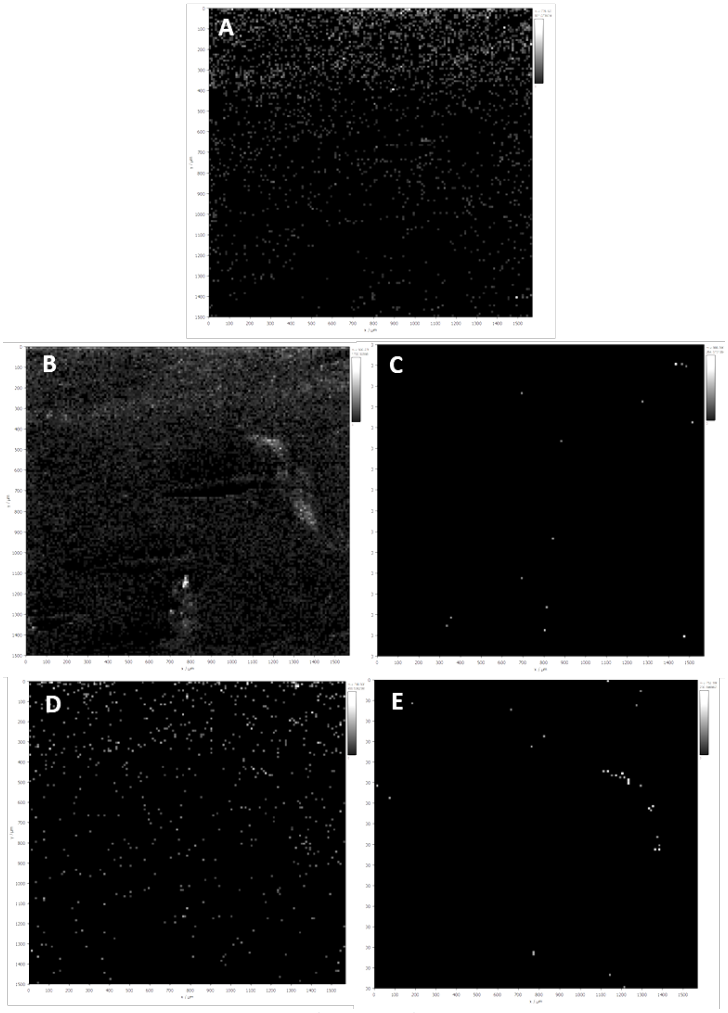

Figure S8: Single-ion images that were used for overlays of a control sample as shown in Figure 5. A: m/z 776.526946, MMPE(16:0_22:6), $[M-H]^-$, B: m/z 500.275684, LPE(20:4), $[M-H]^-$, C: m/z 866.592639, PS(42:4), $[M-H]^-$, D: m/z 746.511353, plasmenyl-PE(P-16:0/22:6), $[M-H]^-$, E: m/z 752.555581, plasmanyl-PE(O-18:0/20:4), $[M-H]^-$.

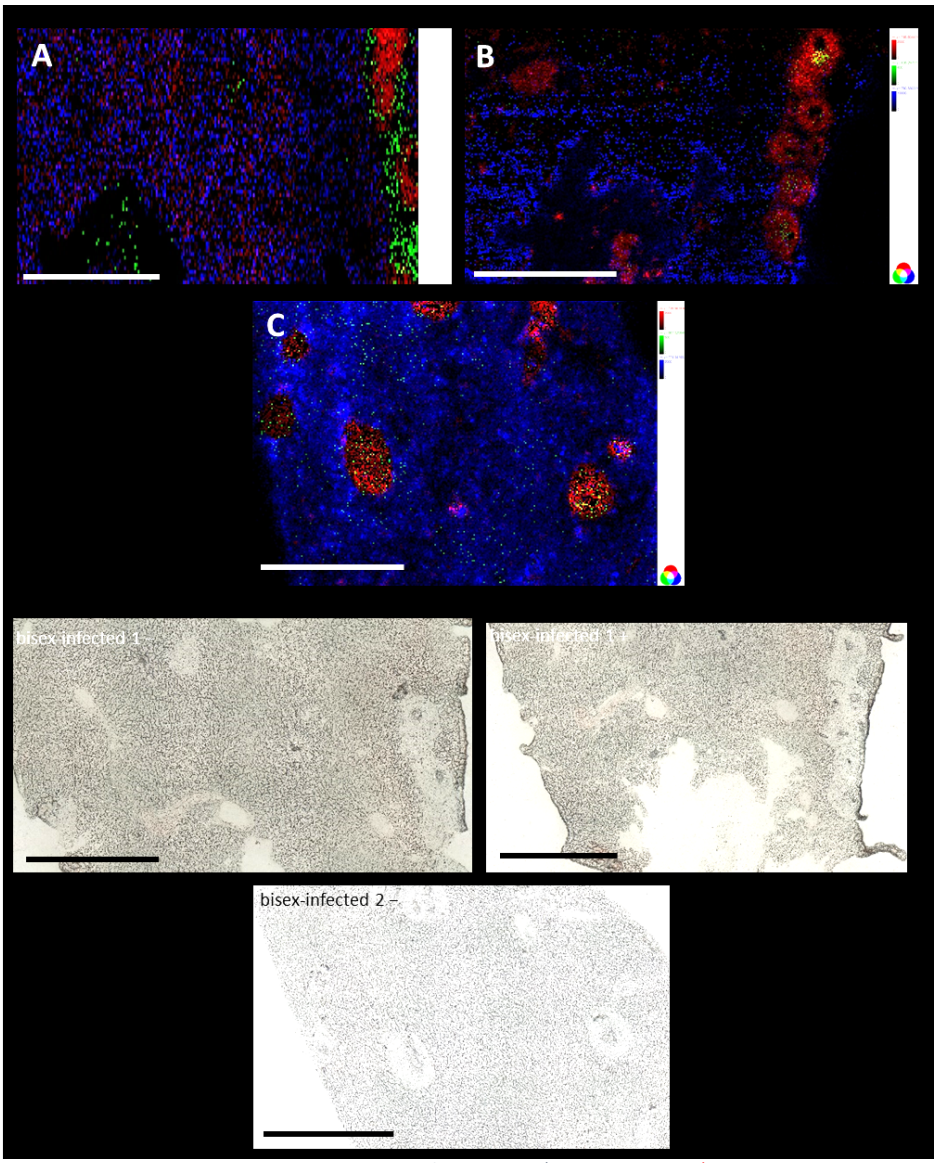

Figure S9: Upper part: Overlay MS images based on markers found by LC-MS/MS analysis. For A, m/z 836.545472, tentatively assigned to PS(40:5), $[M-H]^-$ was found to be a marker for granuloma, m/z 788.529391, DMPE(18:3_20:4), $[M-H]^-$ a marker for surrounding tissue and m/z 752.557091, plasmanyl-PE (O-18:0_20:4), $[M-H]^-$ a marker for the outer part of the granuloma. For B, m/z 746.604414, plasmanyl-PC(O-16:1_18:0), $[M+H]^+$ was found to be a marker for granuloma, m/z 780.550319, PE(17:0_22:5), $[M+H]^+$ a marker for surrounding tissue and m/z 438.297017, plasmenyl-LPE (P-16:0), $[M+H]^+$ as a marker for an enrichment inside the granuloma. For C, m/z 728.561836, plasmenyl-PE(P-18:0_18:1) or plasmanyl-PE(O-18:0_18:2), $[M-H]^-$ as a marker for granuloma and m/z 867.520849, PG(22:5_22:6), $[M-H]^-$ as a marker for an enrichment inside the granuloma. m/z 774.541653, plasmenyl-PE(P-18:0_22:6), $[M-H]^-$ was taken as a marker for surrounding tissue. Lower part: Corresponding microscopically images. Scale bars are 1 mm.

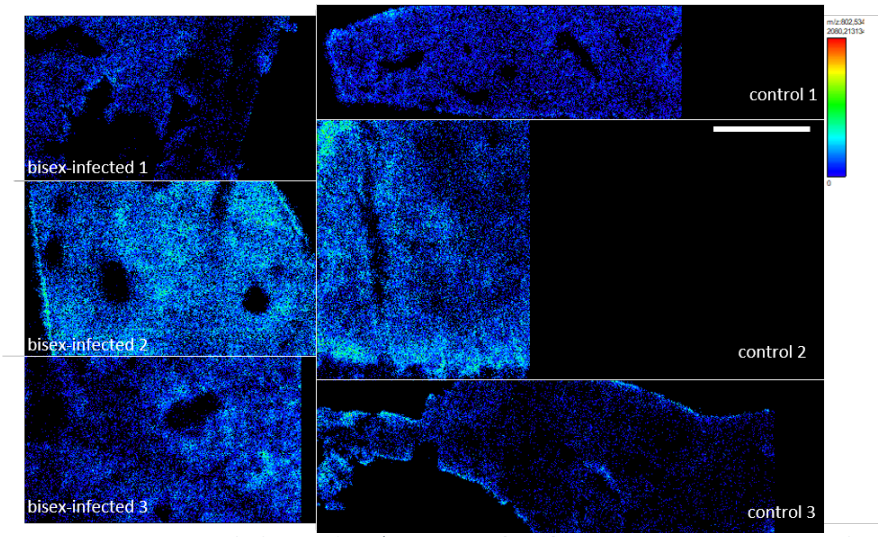

Figure S10: Lateral distribution of PC(16:0_20:5) at m/z 802.535727 as $[M+Na]^+$. While the lipid is depleted in the area of granulomas of liver samples of bisex-infected hamsters (left), it is evenly distributed in the control samples (right). Scale bars are 1 mm.

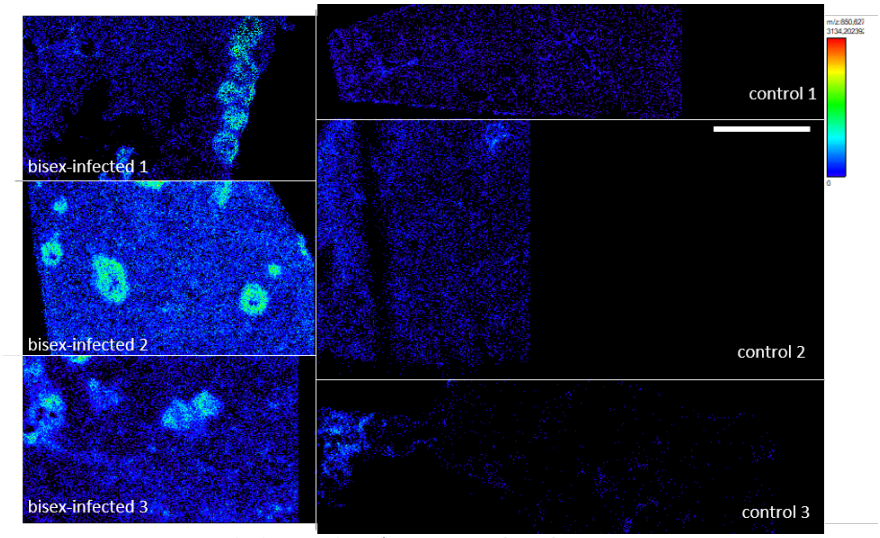

Figure S11: Lateral distribution of PC(19:0_20:2) at m/z 850.629627 as $[M+Na]^+$. While the lipid is evenly distributed in the control samples (right), enrichment in the granulomas is recognizable in liver samples of bisex-infected hamsters (left). However, the lipid is still detectable in the non-affected parts of the tissue. Scale bars are 1 mm.

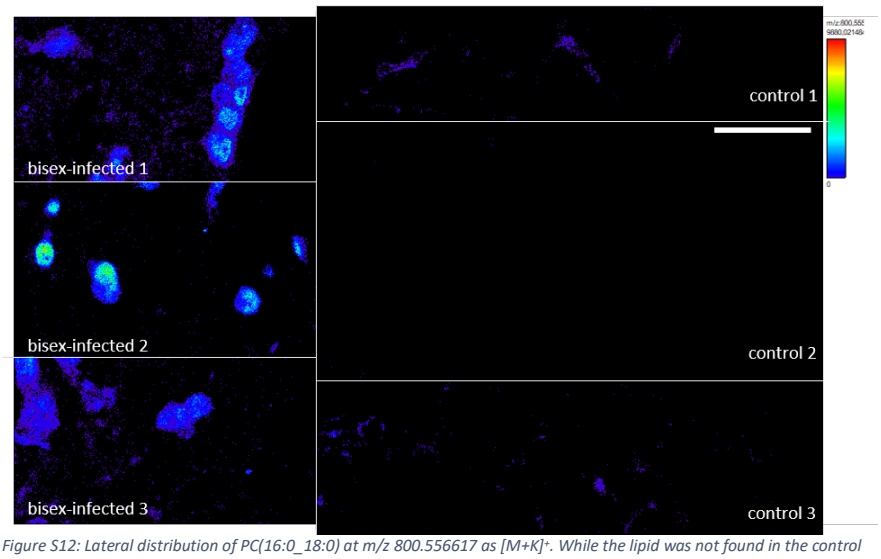

Figure S12: Lateral distribution of PC(16:0_18:0) at m/z 800.556617 as $[M+K]^+$. While the lipid was not found in the control samples (right), strong enrichment in the granulomas is recognizable in liver samples of bisex-infected hamsters (left). The lipid species was found accumulated especially in direct contact around the eggs. Scale bars are 1 mm.

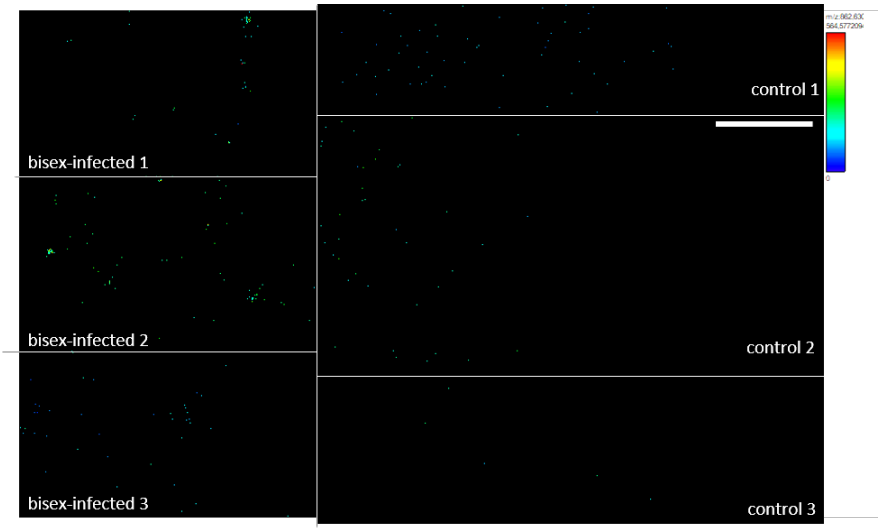

Figure S13: Lateral distribution of PC(20:0_20:3) at m/z 862.630305 as $[M+Na]^+$. The lipid was neither found in the control samples, nor in the non-affected tissue of liver samples of bisex-infected hamsters but was only found in and directly around the eggs. Scale bars are 1 mm.

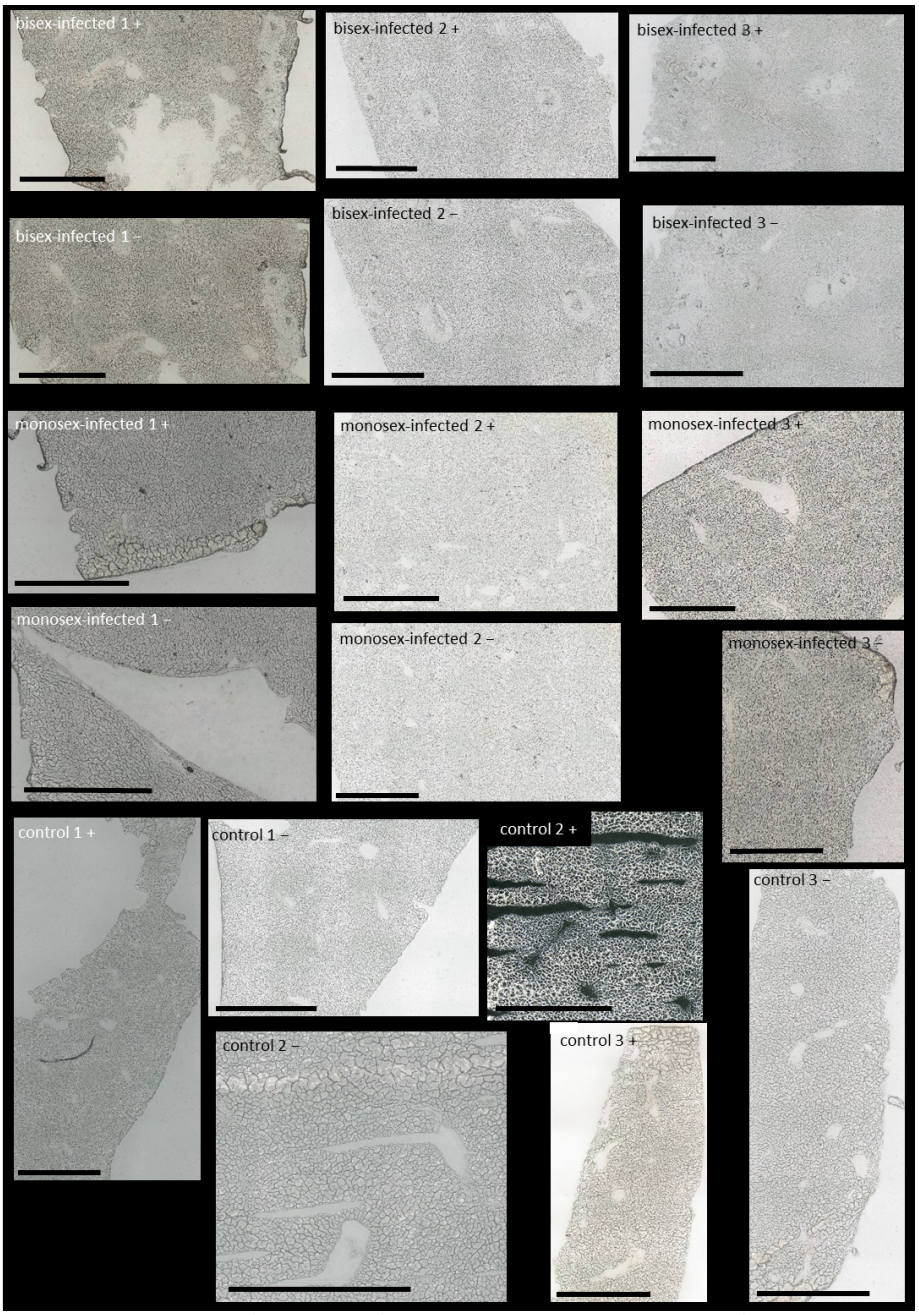

Figure S14: Microscopical images of all samples used for MALDI MSI experiments. Pictures were taken before matrix application and measurement. Scale bars are 1 mm.

2.3 Infection markers

CN	DB	ECN	retention time / min	m/z detected	substance class	ion	substance	significant pair	sum formula	monoisotopic mass	m/z theoretical	D / ppm	also found for	lateral distribution	average peak area bisex-infected	average peak area control	average peak area monosex-infected	bisex/ control	monosex/ control
34	3	28	9.98	762.529879	BMP	[M+NH4]+	BMP(16:1_18:2)	Supercontrol_Bisex	C40H73PO10	744.494137	762.527962	2.51			2574071.32	2766879.81	2898994.35	0.93	1.05
36	5	26	9.09	786.530124	BMP	[M+NH4]+	BMP(18:2_18:3)	Supercontrol_Bisex	C42H73PO10	768.494137	786.527962	2.75			8717193.41	11836605.42	9792217.65	0.74	0.83
38	4	30	10.32	816.572494	BMP	[M+NH4]+	BMP(18:1_20:3)	Supercontrol_Bisex	C44H79PO10	798.541087	816.574913	-2.96			5882394.11	15569013.50	12805423.66	0.38	0.82
38	4	30	8.72	816.574966	BMP	[M+NH4]+	BMP(18:0_20:4)	Supercontrol_Bisex	C44H79PO10	798.541087	816.574913	0.06			16023863.65	25521854.11	19615933.40	0.63	0.77
42	10	22	9.60	860.545214	BMP	[M+NH4]+	BMP(20:4_22:6)	Bisex_Supercontrol	C48H75PO10	842.509787	860.543613	1.86			23185287.77	1917276.94	8492770.50	12.09	4.43
42	8	26	11.58	864.577382	BMP	[M+NH4]+	BMP(20:4_22:4)	Bisex_Supercontrol	C48H79PO10	846.541087	864.574913	2.86			18831493.98	3194461.36	2357874.55	5.90	0.74
44	10	24	11.41	888.575784	BMP	[M+NH4]+	BMP(22:5_22:5)	Bisex_Supercontrol	C50H79PO10	870.541087	888.574913	0.98		granuloma	20390169.89	1308348.30	29641271.53	15.58	22.66
16	0	16	22.68	642.619574	CE	[M+NH4]+	CE(16:0)	Bisex_Supercontrol	C43H76O2	624.584532	642.618357	1.89			51811918.32	27283286.87	45734388.51	1.90	1.68
18	0	18	22.94	670.650349	CE	[M+NH4]+	CE(18:0)	Bisex_Supercontrol	C45H80O2	652.615832	670.649657	1.03			44941609.91	6241467.46	26827811.16	7.20	4.30
20	4	12	22.30	690.619448	CE	[M+NH4]+	CE(20:4)	Bisex_Supercontrol	C47H76O2	672.584532	690.618357	1.58			532583926.19	103265957.33	266902844.14	5.16	2.58
20	3	14	22.47	692.634736	CE	[M+NH4]+	CE(20:3)	Bisex_Supercontrol	C47H78O2	674.600182	692.634007	1.05			286038883.56	43685145.77	107721260.99	6.55	2.47
20	2	16	22.69	694.650683	CE	[M+NH4]+	CE(20:2)	Bisex_Supercontrol	C47H80O2	676.615832	694.649657	1.48			294732726.39	32414380.85	87216372.36	9.09	2.69
20	1	18	22.62	696.665862	CE	[M+NH4]+	CE(20:1)	Supercontrol_Bisex	C47H82O2	678.631482	696.665307	0.80			35034189.77	51479208.71	63675167.35	0.68	1.24
21	0	21	22.94	712.697213	CE	[M+NH4]+	CE(21:0)	Bisex_Supercontrol	C48H86O2	694.662782	712.696608	0.85			76074434.21	16764288.63	49074748.44	4.54	2.93
22	5	12	22.38	716.634647	CE	[M+NH4]+	CE(22:5)	Bisex_Supercontrol	C49H78O2	698.600182	716.634007	0.89			563751132.70	27911361.93	232128939.90	20.20	8.32
22	4	14	22.52	718.650682	CE	[M+NH4]+	CE(22:4)	Bisex_Singlesex	C49H80O2	700.615832	718.649657	1.43	Bisex_ Supercontrol		1020014397.86	24951967.34	119447953.46	40.88	4.79
22	2	18	22.92	722.682109	CE	[M+NH4]+	CE(22:2)	Bisex_Supercontrol	C49H84O2	704.647132	722.680957	1.59			76341684.44	2136114.13	11280404.77	35.74	5.28
24	1	22	23.39	752.728792	CE	[M+NH4]+	CE(24:1)	Bisex_Singlesex	C51H90O2	734.694082	752.727908	1.18	Bisex_ Supercontrol		27802598.77	0.00	2419325.05	#DIV/0!	#DIV/0!
34	0	34	15.59	584.524400	Cer-NDS	[M+HCO2]-	Cer-NDS(d18:0/16:0)	Bisex_Singlesex	C34H69NO3	539.527745	584.525948	-2.65	Bisex_ Supercontrol		67618549.24	17465663.06	25741863.49	3.87	1.47
42	1	40	19.54	694.634251	Cer-NDS	[M+HCO2]-	Cer-NDS(d18:0/24:1)	Bisex_Singlesex	C42H83NO3	649.637296	694.635498	-1.80			105881833.15	49367809.61	28993807.30	2.14	0.59
42	0	42	20.19	696.649656	Cer-NDS	[M+HCO2]-	Cer-NDS(d18:0/24:0)	Bisex_Supercontrol	C42H85NO3	651.652946	696.651148	-2.14			16795966.46	8090750.48	9550306.85	2.08	1.18
36	3	30	19.11	562.520705	Cer-NS	[M+H]+	Cer-NS(d18:1/18:2)	Supercontrol_Bisex	C36H67NO3	561.512095	562.519371	2.37			38265797.81	41602757.98	44365497.49	0.92	1.07
33	1	31	13.46	568.493091	Cer-NS	[M+HCO2]-	Cer-NS(d17:1/16:0)	Supercontrol_Bisex	C33H65NO3	523.496445	568.494648	-2.74			1325093.11	3069510.63	2752295.62	0.43	0.90
37	3	31	18.76	576.536242	Cer-NS	[M+H]+	Cer-NS(d17:1/20:2)	Supercontrol_Bisex	C37H69NO3	575.527745	576.535022	2.12			696180686.97	1464126849.67	1594678230.64	0.48	1.09
38	4	30	19.08	588.536391	Cer-NS	[M+H]+	Cer-NS(d18:2/20:2)	Bisex_Supercontrol	C38H69NO3	587.527745	588.535022	2.33			132126962.15	48095231.59	111796254.98	2.75	2.32
39	3	33	19.70	604.568052	Cer-NS	[M+H]+	Cer-NS(d17:1/22:2)	Supercontrol_Bisex	C39H73NO3	603.559045	604.566322	2.86			5574516.99	3373800.03	29282887.30	0.17	0.87
38	1	36	18.02	638.571578	Cer-NS	[M+HCO2]-	Cer-NS(d18:1/20:0)	Bisex_Supercontrol	C38H75NO3	593.574695	638.572898	-2.07			92411487.03	21803086.90	60523034.05	4.24	2.78
43	4	35	20.48	658.613650	Cer-NS	[M+H]+	Cer-NS(d19:2/24:2)	Supercontrol_Bisex	C43H79NO3	657.605995	658.613272	0.57			3025218.04	11363034.30	8275637.88	0.27	0.73
41	3	35	18.08	676.587175	Cer-NS	[M+HCO2]-	Cer-NS(d18:3/23:0)	Supercontrol_Bisex	C41H77NO4	631.590345	676.588548	-2.03			1826880.26	7287151.15	4478170.85	0.25	0.61
41	1	39	19.51	680.619864	Cer-NS	[M+HCO2]-	Cer-NS(d18:1/23:0)	Supercontrol_Bisex	C41H81NO5	635.621645	680.619848	0.02			373162899.88	774698497.46	728244778.64	0.48	0.94
43	3	37	18.77	704.618752	Cer-NS	[M+HCO2]-	Cer-NS(d18:2/25:1)	Supercontrol_Bisex	C43H81NO5	659.621645	704.619848	-1.56			5493009.20	7946900.76	7482419.56	0.69	0.94
43	1	41	20.28	708.651754	Cer-NS	[M+HCO2]-	Cer-NS(d18:1/25:0)	Supercontrol_Bisex	C43H85NO5	663.652946	708.651148	0.85			52413901.11	93109296.04	66811356.01	0.56	0.72
72	8	56	21.85	723.478017	CL	[M-2H]2-	CL(18:1_18:2_18:2_18:3)	Supercontrol_Bisex	C81H142O17P2	1448.972226	723.478837	-1.13			9618358.87	18594325.89	14004071.66	0.52	0.75
78	7	64	13.93	766.532332	CL	[M-2H]2-	CL(18:1_20:2_20:2_20:2)	Supercontrol_Bisex	C87H156O17P2	1535.081780	766.533614	-1.67			191016910.71	347764118.06	279769697.25	0.55	0.80
82	13	56	12.02	788.519304	CL	[M-2H]2-	CL(20:2_20:2_20:4_22:5)	Supercontrol_Bisex	C91H152O17P2	1579.050480	788.517964	1.70			2742970.49	21201707.89	7857498.39	0.13	0.37
82	9	64	15.18	792.551682	CL	[M-2H]2-	CL(20:1_20:1_20:1_22:6)	Supercontrol_Bisex	C91H160O17P2	1587.113080	792.549264	3.05			1809207.47	295416174.42	112313263.83	0.01	0.38
82	8	66	15.74	793.556196	CL	[M-2H]2-	CL(20:1_20:1_20:1_22:5)	Supercontrol_Bisex	C91H162O17P2	1589.128731	793.557089	-1.13			159832143.14	578124069.19	343452631.16	0.28	0.59
		0	19.99	744.592519	CoQ	[M+NH4]+	Co(Q8)	Supercontrol_Bisex	C49H74O4	726.558711	744.592536	-0.02		granuloma	3940681.29	12843740.96	15160905.13	0.31	1.18
26	2	22	9.50	498.416380	DG	[M+NH4]+	DG(8:0_18:2)	Singlesex_Bisex	C29H52O5	480.381475	498.415300	2.17			310774.13	2888503.26	5317662.94	0.11	1.84
33	1	31	17.82	598.541738	DG	[M+NH4]+	DG(15:0_18:1)	Singlesex_Bisex	C36H68O5	580.506675	598.540501	2.07			10704759.63	34235013.83	42920567.05	0.31	1.25
38	6	26	17.03	658.541512	DG	[M+NH4]+	DG(16:0_22:6)	Bisex_Supercontrol	C41H68O5	640.506675	658.540501	1.54			1522959151.88	293328011.61	780112981.01	5.19	2.66
38	5	28	17.67	660.557328	DG	[M+NH4]+	DG(16:0_22:5)	Bisex_Supercontrol	C41H70O5	642.522325	660.556151	1.78			649984057.37	216394561.12	320732811.95	3.00	1.48
38	4	30	18.02	662.572714	DG	[M+NH4]+	DG(18:1_20:3)	Supercontrol_Bisex	C41H72O5	644.537975	662.571801	1.38			80268449.19	139157410.44	174794407.65	0.58	1.26
40	5	30	18.94	688.588925	DG	[M+NH4]+	DG(18:0_22:5)	Bisex_Supercontrol	C43H74O5	670.553625	688.587451	2.14			197362761.86	78618256.10	105258113.55	2.51	1.34
40	4	32	18.02	690.604526	DG	[M+NH4]+	DG(18:1_22:3)	Supercontrol_Bisex	C43H76O5	672.569276	690.603101	2.06			10713168.84	38528966.74	26650990.97	0.28	0.69
40	4	32	19.24	690.604590	DG	[M+NH4]+	DG(18:0_22:4)	Bisex_Singlesex	C43H76O5	672.569276	690.603101	2.16	Bisex_ Supercontrol		106370356.16	42795002.77	58140230.34	2.49	1.36
40	3	34	19.64	692.620106	DG	[M+NH4]+	DG(18:2_22:1)	Supercontrol_Bisex	C43H78O5	674.584926	692.618751	1.96			11244653.14	13393309.41	10935316.20	0.84	0.82
40	2	36	19.44	694.634942	DG	[M+NH4]+	DG(18:1_22:1)	Supercontrol_Bisex	C43H80O5	676.600576	694.634401	0.78			5294944.71	32913251.30	18900253.88	0.16	0.57
32	1	30	11.82	716.521576	DMPE	[M-H]-	DMPE(16:0_16:1)	Supercontrol_Bisex	C39H76NO8P	717.530857	716.523580	-2.80		granuloma	31173969.69	204125033.87	111839046.59	0.15	0.55
32	0	32	13.63	718.536806	DMPE	[M-H]-	DMPE(16:0_16:0)	Bisex_Supercontrol	C39H78NO8P	719.546507	718.539230	-3.37			495148896.00	146166094.23	365092249.63	3.39	2.50
33	2	29	11.23	728.522203	DMPE	[M-H]-	DMPE(15:0_18:2)	Supercontrol_Bisex	C40H76NO8P	729.530857	728.523580	-1.89		not affected tissue	1465723.93	38729618.31	30860742.76	0.04	0.80
33	1	31	12.80	730.537066	DMPE	[M-H]-	DMPE(15:0_18:1)	Supercontrol_Bisex	C40H78NO8P	731.546507	730.539230	-2.96		granuloma	1376622.93	20561155.33	12405851.68	0.07	0.60
33	0	33	14.73	732.554323	DMPE	[M-H]-	DMPE(16:0_17:0)	Bisex_Supercontrol	C40H80NO8P	733.562157	732.554880	-0.76		granuloma	9249157.44	1890487.76	5504775.63	4.89	2.91
34	3	28	11.27	740.521752	DMPE	[M-H]-	DMPE(16:0_18:3)	Bisex_Supercontrol	C41H76NO8P	741.530857	740.523580	-2.47			108398138.63	30139350.88	72588302.70	3.60	2.41
34	0	34	15.88	746.568449	DMPE	[M-H]-	DMPE(16:0_18:0)	Bisex_Supercontrol	C41H82NO8P	747.577807	746.570531	-2.79		granuloma	81413322.22	12821093.61	37170886.18	6.35	2.90
35	3	29	11.67	754.537649	DMPE	[M-H]-	DMPE(17:1_18:2)	Supercontrol_Bisex	C42H78NO8P	755.546507	754.539230	-2.10			4184421.03	11417308.84	9992388.92	0.37	0.88
35	2	31	13.21	756.552830	DMPE	[M-H]-	DMPE(17:0_18:2)	Supercontrol_Bisex	C42H80NO8P	757.562157	756.554880	-2.71			25873853.15	143115325.25	94482833.97	0.18	0.66

* only identified by head group fragments

CN	DB	ECN	retention time / min	m/z detected	substance class	ion	substance	significant pair	sum formula	monoisotopic mass	m/z theoretical	D / ppm	also found for	lateral distribution	average peak area bisex-infected	average peak area control	average peak area monosex-infected	bisex/ control	monosex/ control
36	2	32	14.62	770.568586	DMPE	[M-H]-	DMPE(18:0_18:2)	Supercontrol_Bisex	C43H82NO8P	771.577807	770.570531	-2.52			848927977.64	1944390796.70	1495533344.57	0.44	0.77
37	4	29	13.39	780.552889	DMPE	[M-H]-	DMPE(17:0_20:4)	Bisex_Supercontrol	C44H80NO8P	781.562157	780.554880	-2.55			29073467.92	3713949.07	19660524.57	7.83	5.29
37	2	33	15.42	784.584098	DMPE	[M-H]-	DMPE(18:2_19:0)	Supercontrol_Bisex	C44H84NO8P	785.593457	784.586181	-2.65			24534508.36	124792167.36	84745303.87	0.20	0.68
37	1	35	16.62	786.600308	DMPE	[M-H]-	DMPE(18:1_19:0)	Supercontrol_Bisex	C44H86NO8P	787.609107	786.601831	-1.94			18921091.10	50631187.40	35086498.41	0.37	0.69
38	7	24	9.69	788.524908	DMPE	[M-H]-	DMPE(18:3_20:4)	Supercontrol_Bisex	C45H76NO8P	789.530857	788.523580	1.68		not affected tissue	3057281.28	9576839.41	9826942.21	0.32	1.03
38	6	26	11.70	790.537195	DMPE	[M-H]-	DMPE(16:0_22:6)	Bisex_Supercontrol	C45H78NO8P	791.546507	790.539230	-2.58		granuloma	926420257.01	367673530.21	838456254.21	2.52	2.28
38	2	34	16.39	798.600426	DMPE	[M-H]-	DMPE(18:0_20:2)	Supercontrol_Bisex	C45H86NO8P	799.609107	798.601831	-1.76		granuloma	32067998.71	91154622.71	87133252.04	0.35	0.96
39	4	31	15.22	808.585228	DMPE	[M-H]-	DMPE(19:0_20:4)	Supercontrol_Bisex	C46H84NO8P	809.593457	808.586181	-1.18			2792852.52	18427856.06	18516900.95	0.15	1.00
39	3	33	15.95	810.599885	DMPE	[M-H]-	DMPE(19:0_20:3)	Supercontrol_Bisex	C46H86NO8P	811.609107	810.601831	-2.40			5595732.92	7528010.39	9088252.40	0.74	1.21
39	2	35	16.90	812.615760	DMPE	[M-H]-	DMPE(19:0_20:2)	Supercontrol_Bisex	C46H88NO8P	813.624757	812.617481	-2.12			377173.75	3971171.14	2490326.64	0.09	0.63
40	5	30	15.49	820.587334	DMPE	[M-H]-	DMPE(18:0_22:5)	Bisex_Supercontrol	C47H84NO8P	821.593457	820.586181	1.41		eggs	55687565.58	9105020.32	33984365.03	6.12	3.73
40	4	32	17.47	822.599310	DMPE	[M-H]-	DMPE(18:0_22:4)	Bisex_Supercontrol	C47H86NO8P	823.609107	822.601831	-3.06		granuloma	45143797.11	15969704.71	14761474.36	2.83	0.92
16	0	16	5.09	438.298865	ether-LPE	[M+H]+	Plasmenyl-LPE(P-16:0)	Bisex_Supercontrol	C21H44NO6P	437.290625	438.297901	2.20		inner part of granuloma	91069682.62	2046013.41	29090777.52	44.51	14.22
18	0	18	6.20	468.346862	ether-LPE	[M+H]+	Plasmanyl-LPE(O-18:0)	Bisex_Supercontrol	C23H50NO6P	467.337575	468.344851	4.29			10903963.38	366538.48	7053257.03	29.75	19.24
32	1	30	13.47	762.564358	ether-PC	[M+HCO2]-	Plasmanyl-PC(O-16:1/16:0)	Bisex_Supercontrol	C40H80NO7P	717.567241	762.565443	-1.42			32338317.98	2022184.42	18065895.17	15.99	8.93
32	0	32	15.10	764.579767	ether-PC	[M+HCO2]-	Plasmanyl-PC(O-16:0/16:0)	Bisex_Supercontrol	C40H82NO7P	719.582891	764.581093	-1.73			332340768.27	34253938.00	253051961.98	9.70	7.39
34	2	30	13.82	788.580048	ether-PC	[M+HCO2]-	Plasmanyl-PC(O-16:0/18:2)	Bisex_Supercontrol	C42H82NO7P	743.582891	788.581093	-1.33			157820286.10	9806168.58	86906857.01	16.09	8.86
34	1	32	15.43	790.594959	ether-PC	[M+HCO2]-	Plasmanyl-PC(O-18:1/16:0)	Bisex_Singlesex	C42H84NO7P	745.598541	790.596744	-2.26	Bisex_ Supercontrol		742015424.99	26518777.18	205915324.47	27.98	7.76
34	0	34	16.95	792.612551	ether-PC	[M+HCO2]-	Plasmanyl-PC(O-18:0/16:0)	Bisex_Supercontrol	C42H86NO7P	747.614191	792.612394	0.20			106160854.72	6125724.47	60950559.68	17.33	9.95
38	4	30	16.22	794.606773	ether-PC	[M+H]+	Plasmenyl-PC(P-18:0/20:4)	Bisex_Supercontrol	C46H84NO7P	793.598541	794.605817	1.20		granuloma	321649947.27	47752418.47	157830562.71	6.74	3.31
36	5	26	13.27	810.563448	ether-PC	[M+HCO2]-	Plasmanyl-PC(O-16:1/20:4)	Bisex_Singlesex	C44H80NO7P	765.567241	810.565443	-2.46	Bisex_ Supercontrol		62056767.91	8547298.92	26050754.02	7.26	3.05
36	3	30	13.99	814.594325	ether-PC	[M+HCO2]-	Plasmanyl-PC(O-18:1/18:2)	Bisex_Supercontrol	C44H84NO7P	769.598541	814.596744	-2.97			126248777.93	12763648.39	65484046.04	9.89	5.13
36	2	32	15.90	816.611277	ether-PC	[M+HCO2]-	Plasmanyl-PC(O-18:1/18:1)	Bisex_Singlesex	C44H86NO7P	771.614191	816.612394	-1.37	Bisex_ Supercontrol		154235391.26	17584348.29	61965711.96	8.77	3.52
36	2	32	16.07	816.612056	ether-PC	[M+HCO2]-	Plasmanyl-PC(O-18:0/18:2)	Bisex_Supercontrol	C44H86NO7P	771.614191	816.612394	-0.41			97214593.59	8264440.19	39158811.80	11.76	4.74
36	1	34	17.19	818.626320	ether-PC	[M+HCO2]-	Plasmanyl-PC(O-18:1/18:0)	Bisex_Supercontrol	C44H88NO7P	773.629841	818.628044	-2.11			68597087.07	5984521.31	28295904.27	11.46	4.73
36	1	34	17.89	818.628314	ether-PC	[M+HCO2]-	Plasmanyl-PC(O-18:0/18:1)	Bisex_Supercontrol	C44H88NO7P	773.629841	818.628044	0.33			32916872.12	1617341.91	13237570.50	20.35	8.18
40	3	34	17.23	824.654000	ether-PC	[M+H]+	Plasmenyl-PC(P-24:2/16:1)	Bisex_Supercontrol	C48H90NO7P	823.645491	824.652767	1.49		granuloma	869091050.60	96579246.24	394235816.33	9.00	4.08
38	6	26	13.14	836.578801	ether-PC	[M+HCO2]-	Plasmanyl-PC(O-16:0/22:6)	Bisex_Supercontrol	C46H82NO7P	791.582891	836.581093	-2.74			67981752.74	4030525.74	20714746.03	16.87	5.14
38	5	28	13.84	838.594925	ether-PC	[M+HCO2]-	Plasmanyl-PC(O-18:1/20:4)	Bisex_Supercontrol	C46H84NO7P	793.598541	838.596744	-2.17			726194284.34	89473940.87	417431889.22	8.12	4.67
38	4	30	15.82	840.610457	ether-PC	[M+HCO2]-	Plasmanyl-PC(O-18:0/20:4)	Bisex_Supercontrol	C46H86NO7P	795.614191	840.612394	-2.30			282002280.77	53207852.08	169650742.56	5.30	3.19
38	3	32	16.59	842.627934	ether-PC	[M+HCO2]-	Plasmanyl-PC(O-18:0/20:3)	Bisex_Supercontrol	C46H88NO7P	797.629841	842.628044	-0.13			18140392.08	3354532.32	11504935.32	5.41	3.43
40	6	28	15.17	864.610071	ether-PC	[M+HCO2]-	Plasmanyl-PC(O-18:1/22:5)	Bisex_Supercontrol	C48H86NO7P	819.614191	864.612394	-2.69			18463423.03	1040087.04	7029325.54	17.75	6.76
40	5	30	15.59	866.626148	ether-PC	[M+HCO2]-	Plasmanyl-PC(O-18:1/22:4)	Bisex_Supercontrol	C48H88NO7P	821.629841	866.628044	-2.19			64195813.68	6645293.46	21197576.01	9.66	3.19
40	5	30	16.52	866.626344	ether-PC	[M+HCO2]-	Plasmanyl-PC(O-18:0/22:5)	Bisex_Supercontrol	C48H88NO7P	821.629841	866.628044	-1.96			21703393.12	1907901.19	8711358.99	11.38	4.57
40	4	32	16.91	868.643851	ether-PC	[M+HCO2]-	Plasmanyl-PC(O-18:0/22:4)	Bisex_Singlesex	C48H90NO7P	823.645491	868.643694	0.18	Bisex_ Supercontrol		52020884.35	7321624.56	20850131.05	7.11	2.85
42	5	32	17.06	894.657190	ether-PC	[M+HCO2]-	Plasmanyl-PC(O-20:1/22:4)	Bisex_Singlesex	C50H92NO7P	849.661141	894.659344	-2.41			15121666.74	3641981.60	3220748.43	4.15	0.88
34	1	32	15.88	700.527105	ether-PE	[M-H]-	Plasmenyl-PE(P-16:0/18:1)	Bisex_Supercontrol	C39H76NO7P	701.535940	700.528664	-2.23		outter part of granuloma	319682618.81	28842060.44	130310775.49	11.08	4.52
34	0	34	16.04	702.542136	ether-PE	[M-H]-	Plasmenyl-PE(P-18:0/16:0)	Bisex_Supercontrol	C39H78NO7P	703.551590	702.544314	-3.10		granuloma	69409637.49	4941116.43	30511230.05	14.05	6.17
34	1	32	16.66	702.543162	ether-PE	[M+H]+	Plasmenyl-PE(P-18:1/16:0)	Bisex_Supercontrol	C39H76NO7P	701.535940	702.543217	-0.08		granuloma	607995795.30	22316510.60	79830878.21	27.24	3.58
34	0	34	15.14	704.558962	ether-PE	[M-H]-	Plasmanyl-PE(O-18:0/16:0)	Bisex_Supercontrol	C39H80NO7P	705.567241	704.559964	-1.42		granuloma	46355093.54	1606594.17	26519707.75	28.85	16.51
34	1	32	14.10	722.511072	ether-PE	[M-H]-	Plasmenyl-PE(P-16:0/20:4)	Bisex_Supercontrol	C41H74NO7P	723.520290	722.513014	-2.69		outter part of granuloma	1302727397.04	361609616.07	910287044.28	3.60	2.52
36	3	30	15.10	724.526411	ether-PE	[M-H]-	Plasmenyl-PE(P-16:0/20:3)	Bisex_Supercontrol	C41H76NO7P	725.535940	724.528664	-3.11		granuloma	44221731.30	9325525.74	19563736.38	4.74	2.10
36	4	28	14.62	724.526998	ether-PE	[M-H]-	Plasmanyl-PE(O-16:0/20:4)	Bisex_Supercontrol	C41H76NO7P	725.535940	724.528664	-2.30		granuloma	146752374.69	31584545.61	76679623.13	4.65	2.43
36	2	32	16.47	728.557575	ether-PE	[M-H]-	Plasmanyl-PE(O-18:0/18:2)	Bisex_Supercontrol	C41H80NO7P	729.567241	728.559964	-3.28		outter part of granuloma/full	48994453.47	23645206.86	40767473.69	2.07	1.72
36	1	34	17.41	728.558778	ether-PE	[M-H]-	Plasmenyl-PE(P-18:0/18:1)	Bisex_Singlesex	C41H80NO7P	729.567241	728.559964	-1.63	Bisex_ Supercontrol	outter part of granuloma/full	120795821.19	24680959.43	56331045.53	4.89	2.28
36	0	36	15.40	730.573647	ether-PE	[M-H]-	Plasmenyl-PE(P-20:0/16:0)	Bisex_Supercontrol	C41H82NO7P	731.582891	730.575614	-2.69		outter part of granuloma/full	82849555.32	3846517.27	34730534.71	21.54	9.03
36	1	34	17.59	730.574286	ether-PE	[M-H]-	Plasmanyl-PE(O-18:0/18:1)	Bisex_Supercontrol	C41H82NO7P	731.582891	730.575614	-1.82		outter part of granuloma/full	24714919.01	3163340.26	11798495.34	7.81	3.73
36	0	36	16.98	732.590350	ether-PE	[M-H]-	Plasmanyl-PE(O-20:0/16:0)	Bisex_Singlesex	C41H84NO7P	733.598541	732.591264	-1.25	Bisex_ Supercontrol		12554299.22	447036.04	5524879.40	28.08	12.36
36	1	34	18.09	732.590562	ether-PE	[M+H]+	Plasmanyl-PE(36:1)	Bisex_Supercontrol	C41H82NO7P	731.582891	732.590167	0.54		granuloma	37881093.30	4901725.24	14168077.04	7.73	2.89

* only identified by head group fragments

CN	DB	ECN	retention time / min	m/z detected	substance class	ion	substance	significant pair	sum formula	monoisotopic mass	m/z theoretical	D / ppm	also found for	lateral distribution	average peak area bisex-infected	average peak area control	average peak area monosex-infected	bisex/ control	monosex/ control
38	6	26	13.55	746.510712	ether-PE	[M-H]-	Plasmenyl-PE(P-16:0/22:6)	Bisex_Supercontrol	C43H74NO7P	747.520290	746.513014	-3.08		granuloma	408300508.90	24305130.79	163571193.56	16.80	6.73
38	5	28	14.39	748.527177	ether-PE	[M-H]-	Plasmenyl-PE(P-18:1/20:4)	Bisex_Supercontrol	C43H76NO7P	749.535940	748.528664	-1.99		not affected tissue	791004666.22	170927456.10	429439215.78	4.63	2.51
38	5	28	15.04	748.527490	ether-PE	[M-H]-	Plasmenyl-PE(P-16:0/22:5)	Bisex_Supercontrol	C43H76NO7P	749.535940	748.528664	-1.57		not affected tissue	242455064.96	22398364.69	107975496.12	10.82	4.82
38	4	30	16.16	750.542925	ether-PE	[M-H]-	Plasmenyl-PE(P-18:0/20:4)	Bisex_Supercontrol	C43H78NO7P	751.551590	750.544314	-1.85			1565323280.03	418400899.96	861815728.01	3.74	2.06
38	4	30	16.45	752.557824	ether-PE	[M-H]-	Plasmanyl-PE(O-18:0/20:4)	Bisex_Supercontrol	C43H80NO7P	753.567241	752.559964	-2.84		outer part of granuloma	345509687.62	43161375.74	241118792.43	8.01	5.59
40	7	26	13.95	772.527015	ether-PE	[M-H]-	Plasmenyl-PE(P-18:1/22:6)	Bisex_Singlesex	C45H76O7NP	773.535940	772.528664	-2.13	Bisex_ Supercontrol	not affected tissue	181306553.75	7142255.01	48593677.84	25.39	6.80
40	6	28	15.80	774.542366	ether-PE	[M-H]-	Plasmenyl-PE(P-18:0/22:6)	Bisex_Singlesex	C45H78NO7P	775.551590	774.544314	-2.52	Bisex_ Supercontrol	not affected tissue	328978492.68	10174578.46	73239073.92	32.33	7.20
40	6	28	16.03	776.558183	ether-PE	[M-H]-	Plasmanyl-PE(O-18:0/22:6)	Bisex_Supercontrol	C45H80NO7P	777.567241	776.559964	-2.29			276213534.68	65351011.54	146698595.32	4.23	2.24
40	5	30	16.22	776.558196	ether-PE	[M-H]-	Plasmenyl-PE(P-18:1/22:4)	Bisex_Supercontrol	C45H80NO7P	777.567241	776.559964	-2.28			248918940.63	42985598.35	113827723.34	5.79	2.65
40	5	30	16.34	776.558358	ether-PE	[M-H]-	Plasmenyl-PE(P-18:0/22:5)	Bisex_Supercontrol	C45H80NO7P	777.567241	776.559964	-2.07			193190876.84	40035741.38	83821510.75	4.83	2.09
40	4	32	17.72	778.573837	ether-PE	[M-H]-	Plasmenyl-PE(P-20:0/20:4)	Bisex_Supercontrol	C45H82NO7P	779.582891	778.575614	-2.28			54680344.00	8508906.56	22313804.38	6.43	2.62
40	4	32	17.26	778.574584	ether-PE	[M-H]-	Plasmenyl-PE(P-18:0/22:4)	Bisex_Singlesex	C45H82NO7P	779.582891	778.575614	-1.32	Bisex_ Supercontrol		366755690.35	95431643.82	194684720.45	3.84	2.04
40	4	32	17.76	780.589214	ether-PE	[M-H]-	Plasmanyl-PE(O-20:0/20:4)	Bisex_Supercontrol	C45H84NO7P	781.598541	780.591264	-2.63		outter part of granuloma	26248455.08	9605991.78	17650306.25	2.73	1.84
40	4	32	17.50	780.589512	ether-PE	[M-H]-	Plasmanyl-PE(O-18:0/22:4)	Bisex_Supercontrol	C45H84NO7P	781.598541	780.591264	-2.24		outter part of granuloma	76173216.08	18515955.47	54169136.94	4.11	2.93
40	3	34	18.25	782.606414	ether-PE	[M+H]+	Plasmenyl-PE(P-18:0/22:3)	Bisex_Supercontrol	C45H84NO7P	781.598541	782.605817	0.76		granuloma	66923864.21	21262110.46	36398147.37	3.15	1.71
42	6	30	17.91	804.589375	ether-PE	[M+H]+	Plasmenyl-PE(P-20:0/22:6)	Bisex_Supercontrol	C47H82NO7P	803.582891	804.590167	-0.98		granuloma	40018628.44	3680217.57	17367014.36	10.87	4.72
41	0	41	17.85	844.643444	ether-PS	[M-H]-	Plasmenyl-PS(P-18:0/23:0)	Bisex_Supercontrol	C47H92NO9P	845.650970	844.643694	-0.30			48902939.09	8669101.15	40492187.70	5.64	4.67
42	4	34	16.53	850.595589	ether-PS	[M-H]-	Plasmenyl-PS(P-20:0/22:4)	Supercontrol_Bisex	C48H86NO9P	851.604020	850.596744	-1.36			3936209.91	3673352.27	6530298.37	1.07	1.78
52	2	48	22.48	862.824305	ether-TG	[M+NH4]+	plasmanyl-TG(O-18:1_16:0_18:1)	Bisex_Supercontrol	C55H104O5	844.788376	862.822202	2.44			296883718.21	133193636.87	146187924.01	2.23	1.10
58	8	42	22.22	934.823355	ether-TG	[M+NH4]	plasmanyl-TG(O-16:0_20:4_22:4)	Bisex_Singlesex	C61H104O5	916.788376	934.822202	1.23	Bisex_ Supercontrol		53015471.88	10325020.27	7972284.57	5.13	0.77
58	7	44	22.36	936.839619	ether-TG	[M+NH4]	plasmanyl-TG(O-20:1_18:2_20:4)	Bisex_Supercontrol	C61H106O5	918.804026	936.837852	1.89			92212650.03	31738799.71	32984255.02	2.91	1.04
60	8	44	22.38	962.854339	ether-TG	[M+NH4]	plasmanyl-TG(O-18:0_20:4_22:4)	Bisex_Supercontrol	C63H108O5	944.819677	962.853502	0.87			48533569.71	3238027.38	9555163.63	14.99	2.95
34	4	26	10.53	763.500246	GlcADG	[M-H]-	GlcADG(16:1_18:3)	Supercontrol_Bisex	C43H72O11	764.507463	763.500187	0.08			363910.38	8131489.18	4436345.68	0.04	0.55
38	0	38	14.93	827.626506	GlcADG	[M-H]-	GlcADG(19:0_19:0)	Supercontrol_Bisex	C47H88O11	828.632664	827.625387	1.35			0.00	1554636.73	1006275.13	0.00	0.65
52	4	44	19.10	1007.730767	HBMP	[M-H]-	HBMP(16:1_18:1_18:2)	Supercontrol_Bisex	C58H105PO11	1008.739453	1007.732176	-1.40			3259038.47	4433162.85	3589521.94	0.74	0.81
52	3	46	19.57	1009.746990	HBMP	[M-H]-	HBMP(16:0_18:1_18:2)	Supercontrol_Bisex	C58H107PO11	1010.755103	1009.747826	-0.83			6066933.80	11411620.69	7005405.32	0.53	0.61
52	2	48	20.04	1011.762289	HBMP	[M-H]-	HBMP(16:0_18:1_18:1)	Supercontrol_Bisex	C58H109PO11	1012.770753	1011.763476	-1.17			4826408.67	8908852.62	4298343.98	0.54	0.48
54	5	44	19.15	1033.746352	HBMP	[M-H]-	HBMP(18:1_18:2_18:2)	Supercontrol_Bisex	C60H107PO11	1034.755103	1033.747826	-1.43			5556038.73	16379146.64	7790046.76	0.34	0.48
54	4	46	19.66	1035.763040	HBMP	[M-H]-	HBMP(18:1_18:1_18:2)	Supercontrol_Bisex	C60H109PO11	1036.770753	1035.763476	-0.42			7964380.22	20271024.47	9059681.68	0.39	0.45
54	3	48	20.15	1037.779521	HBMP	[M-H]-	HBMP(18:0_18:2_18:1)	Supercontrol_Bisex	C60H111PO11	1038.786403	1037.779126	0.38			6452639.37	11476508.75	6085923.88	0.56	0.53
31	1	29	7.27	658.527224	HexCer-NS	[M+H]+	HexCer-NS(d18:1/13:0)	Supercontrol_Bisex	C37H71NO8	657.517968	658.525245	3.01			4177066.43	3253026.53	4369409.69	1.28	1.34
41	2	37	17.51	840.656046	HexCer-NS	[M+HCO2]-	HexCer-NS(d18:2/23:0)	Supercontrol_Bisex	C47H89NO8	795.658819	840.655925	0.14			5905401.25	10948882.34	13105422.25	0.54	1.20
42	2	38	17.88	854.671725	HexCer-NS	[M+HCO2]-	HexCer-NS(d18:1/24:1)	Bisex_Supercontrol	C48H91NO8	809.674469	854.671575	0.18			237852686.44	32308428.68	148674677.24	7.36	4.60
42	1	40	18.88	856.687298	HexCer-NS	[M+HCO2]-	HexCer-NS(d18:1/24:0)	Bisex_Supercontrol	C48H93NO8	811.690119	856.687225	0.09			151007977.08	55993934.62	93826808.21	2.70	1.68
17	2	13	5.07	506.325954	LPC	[M+H]+	LPC(17:2)	Supercontrol_Bisex	C25H48NO7P	505.316840	506.324116	3.63			5738837.59	7729331.25	9683719.39	0.74	1.25
18	1	16	4.52	566.345655	LPC	[M+HCO2]-	LPC(18:1)	Bisex_Supercontrol	C26H52NO7P	521.348140	566.346342	-1.21			483074198.61	164479235.27	284614846.87	2.94	1.73
19	0	19	5.53	582.377500	LPC	[M+HCO2]-	LPC(19:0)	Supercontrol_Bisex	C27H56NO7P	537.379440	582.377643	-0.25			24706417.44	116707312.72	118156057.95	0.21	1.01
16	1	14	3.50	450.262027	LPE	[M-H]-	LPE(16:1)	Supercontrol_Bisex	C21H42NO7P	451.269889	450.262613	-1.30		not affected tissue	9063879.23	15132934.96	18077538.56	0.60	1.19
18	2	14	3.68	476.277402	LPE	[M-H]-	LPE(18:2)	Supercontrol_Bisex	C23H44NO7P	477.285539	476.278263	-1.81		overall, little enrichment in	72396549.58	101107326.80	70449395.81	0.72	0.70
20	4	12	3.64	500.277549	LPE	[M-H]-	LPE(20:4)	Bisex_Supercontrol	C25H44NO7P	501.285539	500.278263	-1.43		granuloma without eggs	215987534.85	115622049.81	172201677.24	1.87	1.49
22	6	10	3.49	524.277645	LPE	[M-H]-	LPE(22:6)	Bisex_Supercontrol	C27H44NO7P	525.285539	524.278263	-1.18			127913003.57	55500047.37	77314146.66	2.30	1.39
20	4	12	3.25	619.288466	LPI	[M-H]-	LPI(20:4)	Bisex_Singlesex	C29H49O12P	620.296164	619.288887	-0.68	Bisex_ Supercontrol		33660401.12	15877097.17	17474092.48	2.12	1.10
35	1	33	14.13	744.552376	MMPE	[M-H]-	MMPE(17:1_18:0)	Bisex_Supercontrol	C41H80NO8P	745.562157	744.554880	-3.36		granuloma	1050779984.22	221359167.13	600723303.36	4.75	2.71
38	6	26	10.80	776.524927	MMPE	[M-H]-	MMPE(16:0_22:6)	Bisex_Supercontrol	C44H76NO8P	777.530857	776.523580	1.73		not affected tissue	18682796.63	1468830.47	12360935.89	12.72	8.42
76	11	54	11.42	780.478574	OxCL	[M-2H]2-	OxCL(16:0_20:3_20:4(OOH) _20:4(OOH))	Supercontrol_Bisex	C85H144O21P2	1562.967538	780.476493	2.67		granuloma	2718700.87	15262809.86	10658516.94	0.18	0.70
18	1	16	4.83	538.351587	OxLPC	[M+H]+	OxLPC(18:1(OH))	Bisex_Supercontrol	C26H52NO8P	537.343056	538.350332	2.33			166373561.34	60862491.95	133059572.57	2.73	2.19
20	3	14	4.34	562.351351	OxLPC	[M+H]+	OxLPC(20:3(OH))	Bisex_Supercontrol	C28H52NO8P	561.343056	562.350332	1.81			40224218.12	8439902.14	29870439.96	4.77	3.54

* only identified by head group fragments

CN	DB	ECN	retention time / min	m/z detected	substance class	ion	substance	significant pair	sum formula	monoisotopic mass	m/z theoretical	D / ppm	also found for	lateral distribution	average peak area bisex-infected	average peak area control	average peak area monosex-infected	bisex/ control	monosex/ control
20	2	16	4.95	564.367081	OxLPC	[M+H]+	OxLPC(20:2(OH))	Bisex_Supercontrol	C28H54NO8P	563.358706	564.365983	1.95			52942174.31	7412829.58	24661732.16	7.14	3.33
20	1	18	5.73	566.383189	OxLPC	[M+H]+	OxLPC(20:1(OH))	Bisex_Supercontrol	C28H56NO8P	565.374356	566.381633	2.75			47629343.49	18157445.81	32157353.54	2.62	1.77
20	3	14	4.96	578.346207	OxLPC	[M+H]+	OxLPC(20:3(OO))	Supercontrol_Bisex	C28H52NO9P	577.337971	578.345247	1.66			6076426.37	11877626.03	9762973.94	0.51	0.82
24	1	22	5.07	636.424312	OxLPC	[M+H]+	OxLPC(24:1(KeOH))	Supercontrol_Bisex	C32H62NO9P	635.416221	636.423497	1.28			23258124.44	40816898.50	29559037.59	0.57	0.72
24	1	22	4.92	638.439053	OxLPC	[M+H]+	OxLPC(24:1(OO))	Supercontrol_Bisex	C32H64NO9P	637.431871	638.439147	-0.15			4603411.63	16620929.55	7710232.18	0.28	0.46
22	3	16	4.87	564.330535	OxLPE	[M+H]+	OxLPE(22:3(OO))	Supercontrol_Bisex	C27H50NO9P	563.322321	564.329597	1.66			2872252.06	4908414.02	3749360.92	0.59	0.76
22	2	18	5.57	566.346943	OxLPE	[M+H]+	OxLPE(22:2(OO))	Supercontrol_Bisex	C27H52NO9P	565.337971	566.345247	2.99			1868153.11	4154511.45	3674355.29	0.45	0.88
34	3	28	7.97	816.540137	OxPC	[M+HCO2]-	OxPC(16:0_18:3(OH))	Supercontrol_Bisex	C42H78NO9P	771.541421	816.538527	1.97			510765.62	3067509.71	260370.75	0.17	0.08
34	3	28	7.66	816.540468	OxPC	[M+HCO2]-	OxPC(16:0_18:3(1O))	Supercontrol_Bisex	C42H78NO9P	771.541421	816.538527	2.38			3706466.42	4406970.21	5367159.66	0.84	1.22
34	2	30	7.57	818.556045	OxPC	[M+HCO2]-	OxPC(16:0_18:2(1O))	Singlesex_Bisex	C42H80NO9P	773.557072	818.554177	2.28			16995476.73	54743048.02	58760852.06	0.31	1.07
34	1	32	8.54	820.569586	OxPC	[M+HCO2]-	OxPC(16:0_18:1(1O))	Supercontrol_Bisex	C42H82NO9P	775.572722	820.569827	-0.29			7363651.58	16490002.54	10890888.60	0.45	0.66
34	2	30	6.85	832.534932	OxPC	[M+HCO2]-	OxPC(16:0_18:2(KeOH))	Supercontrol_Bisex	C42H78NO10P	787.536336	832.533442	1.79			2831411.31	4369501.05	6208135.19	0.65	1.42
34	3	28	6.60	832.535084	OxPC	[M+HCO2]-	OxPC(16:0_18:3(OO))	Supercontrol_Bisex	C42H78NO10P	787.536336	832.533442	1.97			1295397.05	4120140.71	3084805.82	0.31	0.75
34	2	30	6.40	834.551453	OxPC	[M+HCO2]-	OxPC(16:0_18:2(2O))	Supercontrol_Bisex	C42H80NO10P	789.551986	834.549092	2.83			7263016.40	16618792.06	13301915.13	0.44	0.80
36	5	26	6.93	840.539664	OxPC	[M+HCO2]-	OxPC(18:2_18:3(OH))	Supercontrol_Bisex	C44H78NO9P	795.541421	840.538527	1.35		not affected tissue	3866209.38	7108300.42	5831343.63	0.54	0.82
36	4	28	6.88	842.554819	OxPC	[M+HCO2]-	OxPC(18:2_18:2(OH))	Supercontrol_Bisex	C44H80NO9P	797.557072	842.554177	0.76			2936445.54	15137095.83	9450536.68	0.19	0.62
36	4	28	8.44	842.555762	OxPC	[M+HCO2]-	OxPC(16:0_20:4(1O))	Supercontrol_Bisex	C44H80NO9P	797.557072	842.554177	1.88			10001100.01	14679066.07	14340267.96	0.68	0.98
36	3	30	7.80	844.570615	OxPC	[M+HCO2]-	OxPC(18:1_18:2(1O))	Supercontrol_Bisex	C44H82NO9P	799.572722	844.569827	0.93			5542625.48	13199232.52	15177079.72	0.42	1.15
36	2	32	9.14	846.585842	OxPC	[M+HCO2]-	OxPC(18:0_18:2(1O))	Supercontrol_Bisex	C44H84NO9P	801.588372	846.585477	0.43			14261063.75	27544014.96	20180671.58	0.52	0.73
34	2	30	5.38	850.544850	OxPC	[M+HCO2]-	OxPC(16:0_18:2(OOO))	Supercontrol_Bisex	C42H80NO11P	805.546901	850.544006	0.99			2837355.34	9212693.95	7162091.97	0.31	0.78
34	1	32	5.28	852.559590	OxPC	[M+HCO2]-	OxPC(16:0_18:1(3O))	Supercontrol_Bisex	C42H82NO11P	807.562551	852.559657	-0.08			1768119.58	6794481.85	6143964.72	0.26	0.90
36	4	28	5.97	858.551626	OxPC	[M+HCO2]-	OxPC(18:2_18:2(OOH))	Supercontrol_Bisex	C44H80NO10P	813.551986	858.549092	2.95			2246889.50	4738475.88	5137783.00	0.47	1.08
37	2	33	9.81	860.601181	OxPC	[M+HCO2]-	OxPC(19:0_18:2(OH))	Supercontrol_Bisex	C45H86NO9P	815.604022	860.601127	0.06		granuloma	174994.21	2198540.62	1023670.54	0.08	0.47
36	2	32	7.56	862.581976	OxPC	[M+HCO2]-	OxPC(18:0_18:2(2O))	Supercontrol_Bisex	C44H84NO10P	817.583286	862.580392	1.84			3730786.91	8546380.04	7503682.50	0.44	0.88
28	0	28	4.78	664.419136	OxPE	[M-H]-	OxPE(16:0_12:0(COOH))	Supercontrol_Bisex	C33H64NO10P	665.426786	664.419509	-0.56			3345080.13	7746966.62	4092764.49	0.43	0.53
34	2	30	7.91	730.503478	OxPE	[M-H]-	OxPE(16:0_18:2(1O))	Supercontrol_Bisex	C39H74NO9P	731.510121	730.502845	0.87			2055067.82	8016643.97	5861996.70	0.26	0.73
34	1	32	9.85	732.517585	OxPE	[M-H]-	OxPE(16:0_18:1(1O))	Supercontrol_Bisex	C39H76NO9P	733.525771	732.518495	-1.24			119345.68	2003747.00	1045356.83	0.06	0.52
36	4	28	8.16	754.503174	OxPE	[M-H]-	OxPE(18:1_18:3(OH))	Supercontrol_Bisex	C41H74NO9P	755.510121	754.502845	0.44			4135484.19	11369843.89	8689595.40	0.36	0.76
36	3	30	9.60	756.517499	OxPE	[M-H]-	OxPE(18:0_18:3(OH))	Supercontrol_Bisex	C41H76NO9P	757.525771	756.518495	-1.32		not affected tissue	2816989.05	5817214.07	4291272.00	0.48	0.74
36	3	30	8.17	756.518471	OxPE	[M-H]-	OxPE(18:1_18:2(1O))	Supercontrol_Bisex	C41H76NO9P	757.525771	756.518495	-0.03		not affected tissue	5355887.51	15355287.37	12293438.88	0.35	0.80
36	2	32	9.46	758.533490	OxPE	[M-H]-	OxPE(18:0_18:2(1O))	Supercontrol_Bisex	C41H78NO9P	759.541421	758.534145	-0.86		not affected tissue	2950772.76	10346024.74	5975574.70	0.29	0.58
36	2	32	7.60	758.534466	OxPE	[M-H]-	OxPE(18:1_18:1(1O))	Supercontrol_Bisex	C41H78NO9P	759.541421	758.534145	0.42		not affected tissue	2003346.98	4733646.85	4564025.53	0.42	0.96
38	5	28	9.11	780.518675	OxPE	[M-H]-	OxPE(18:1_20:4(1O))	Supercontrol_Bisex	C43H76NO9P	781.525771	780.518495	0.23		not affected tissue	13179481.23	23582932.61	23467326.83	0.56	1.00
40	6	28	9.29	806.534840	OxPE	[M-H]-	OxPE(18:0_22:6(OH))	Supercontrol_Bisex	C45H78NO9P	807.541421	806.534145	0.86		not affected tissue	4954060.13	6915450.83	5277363.70	0.72	0.76
34	0	34	9.70	781.520690	OxPG	[M-H]-	OxPG(16:0_18:0(2O))	Supercontrol_Bisex	C40H79O12P	782.530916	781.523640	-3.77			3314961.17	6513004.05	4917132.51	0.51	0.75
38	4	30	8.81	901.545122	OxPI	[M-H]-	OxPI(18:0_20:4(1O))	Supercontrol_Bisex	C47H83O14P	902.552046	901.544769	0.39		not affected tissue	4908077.22	6918079.22	5137213.81	0.71	0.74
44	3	38	20.61	776.640970	OxTG	[M+NH4]+	OxTG(16:0_18:1_10:2(CHO))	Supercontrol_Bisex	C47H82O7	758.606055	776.640429	0.70			150354.79	7812114.13	794995.19	0.02	0.10
46	4	38	20.71	802.657098	OxTG	[M+NH4]+	OxTG(16:0_18:2_12:2(CHO))	Supercontrol_Bisex	C49H84O7	784.621705	802.656079	1.27			276618.24	6354836.97	742924.81	0.04	0.12
50	3	44	20.21	860.736202	OxTG	[M+NH4]+	OxTG(16:0_18:2_16:1(CHO))	Supercontrol_Bisex	C53H94O7	842.699955	860.734329	2.18			1964104.22	20625571.73	4166181.10	0.10	0.20
50	2	46	21.47	862.749213	OxTG	[M+NH4]+	OxTG(18:1_18:1_14:0(CHO))	Bisex_Supercontrol	C53H96O7	844.715605	862.749980	-0.89			40094254.27	1910778.90	2155441.98	20.98	1.13
50	2	46	20.77	862.750156	OxTG	[M+NH4]+	OxTG(16:0_18:1_16:1(CHO))	Supercontrol_Bisex	C53H96O7	844.715605	862.749980	0.21			8723378.97	46629136.56	30434801.86	0.19	0.65
50	3	44	20.64	862.750172	OxTG	[M+NH4]+	OxTG(16:0_16:1_18:2(OH))	Supercontrol_Bisex	C53H96O7	844.715605	862.749980	0.22			11037128.89	77693743.00	37303664.96	0.14	0.48
50	2	46	21.04	864.765417	OxTG	[M+NH4]+	OxTG(16:0_16:0_18:2(OH))	Supercontrol_Bisex	C53H98O7	846.731255	864.765630	-0.25			13532640.47	91116145.76	37017105.51	0.15	0.41
52	4	44	20.74	888.765998	OxTG	[M+NH4]+	OxTG(16:0_18:2_18:2(OH))	Supercontrol_Bisex	C55H98O7	870.731255	888.765630	0.41			68386939.59	342494074.23	176407285.71	0.20	0.52
52	4	44	20.94	888.766516	OxTG	[M+NH4]+	OxTG(16:0_18:1_18:3(OH))	Supercontrol_Bisex	C55H98O7	870.731255	888.765630	1.00			40789238.18	75248808.55	81787250.00	0.54	1.09
52	3	46	20.77	890.780225	OxTG	[M+NH4]+	OxTG(16:0_18:2_18:1(OH))	Supercontrol_Bisex	C55H100O7	872.746906	890.781280	-1.18			75446745.88	170038467.91	107007187.14	0.44	0.63
52	3	46	21.07	890.781469	OxTG	[M+NH4]+	OxTG(16:0_18:1_18:2(OH))	Supercontrol_Bisex	C55H100O7	872.746906	890.781280	0.21			115511395.75	494611211.17	245558001.16	0.23	0.50
52	2	48	21.16	892.794156	OxTG	[M+NH4]+	OxTG(16:0_18:1_18:1(OH))	Supercontrol_Bisex	C55H102O7	874.762556	892.796930	-3.11			33843219.83	137129963.60	54869612.46	0.25	0.40
54	6	42	20.40	912.767550	OxTG	[M+NH4]+	OxTG(18:2_18:2_18:2(OH))	Supercontrol_Bisex	C57H98O7	894.731255	912.765630	2.10	Singlesex_ Bisex		13097586.71	59056986.75	56579340.06	0.22	0.96
54	5	44	20.77	914.782073	OxTG	[M+NH4]+	OxTG(18:1_18:2_18:2(OH))	Supercontrol_Bisex	C57H100O7	896.746906	914.781280	0.87			40555981.35	166054860.38	87705433.13	0.24	0.53
54	5	44	20.32	914.782315	OxTG	[M+NH4]+	OxTG(18:2_18:2_18:1(OH))	Supercontrol_Bisex	C57H100O7	896.746906	914.781280	1.13			3621178.97	24887295.61	15243787.88	0.15	0.61
54	4	46	20.72	916.796929	OxTG	[M+NH4]+	OxTG(18:1_18:1_18:2(OH))	Supercontrol_Bisex	C57H102O7	898.762556	916.796930	0.00			53612222.25	159550527.13	105139030.03	0.34	0.66
54	4	46	21.10	916.796948	OxTG	[M+NH4]+	OxTG(18:1_18:2_18:1(OH))	Supercontrol_Bisex	C57H102O7	898.762556	916.796930	0.02			68232618.84	223859649.59	130728090.55	0.30	0.58

* only identified by head group fragments

CN	DB	ECN	retention time / min	m/z detected	substance class	ion	substance	significant pair	sum formula	monoisotopic mass	m/z theoretical	D / ppm	also found for	lateral distribution	average peak area bisex-infected	average peak area control	average peak area monosex-infected	bisex/ control	monosex/ control
54	3	48	21.01	918.811346	OxTG	[M+NH4]+	OxTG(18:1_18:1_18:1(OH))	Supercontrol_Bisex	C57H104O7	900.778206	918.812580	-1.34			56645461.69	141654573.95	81235824.86	0.40	0.57
56	4	48	21.32	944.827769	OxTG	[M+NH4]+	OxTG(18:1_18:1_20:2(OH))	Supercontrol_Bisex	C59H106O7	926.793856	944.828230	-0.49			4479340.23	12576373.12	6551907.81	0.36	0.52
38	2	34	15.72	727.526120	PA	[M-H]-	PA(18:0_20:2)	Bisex_Supercontrol	C41H77O8P	728.535606	727.528330	-3.04		granuloma	33956992.16	8836160.78	40994832.71	3.84	4.64
32	4	24	9.01	726.508070	PC	[M+H]+	PC(12:0_20:4)	Bisex_Supercontrol	C40H72NO8P	725.499555	726.506831	1.71			27838673.95	5500403.91	12429406.20	5.06	2.26
32	3	26	9.17	772.513016	PC	[M+HCO2]-	PC(14:0_18:3)	Supercontrol_Bisex	C40H74NO8P	727.515205	772.513408	-0.51			6647887.37	16269533.91	11776190.44	0.41	0.72
32	0	32	13.64	778.558961	PC	[M+HCO2]-	PC(16:0_16:0)	Bisex_Supercontrol	C40H80NO8P	733.562155	778.560358	-1.79			3864655844.37	680313931.86	2401753086.82	5.68	3.53
38	2	34	26.44	786.602397	PC	[M+H]+	PC(17:2_19:0)	Supercontrol_Bisex	C44H84NO8P	785.593455	786.600732	2.12			7764825.33	8878525.73	7370032.29	0.87	0.83
36	0	36	17.82	790.631254	PC	[M+H]+	PC(18:0_18:0)	Bisex_Supercontrol	C44H88NO8P	789.624755	790.632032	-0.98			870147623.43	246171503.53	509198958.44	3.53	2.07
33	0	33	14.29	792.576374	PC	[M+HCO2]-	PC(16:0_17:0)	Supercontrol_Bisex	C41H82NO8P	747.577805	792.576008	0.46			1092365.66	66046657.82	45775911.99	0.02	0.69
34	3	28	10.70	800.542965	PC	[M+HCO2]-	PC(16:1_18:2)	Supercontrol_Bisex	C42H78NO8P	755.546505	800.544708	-2.18			579867344.11	2090593852.70	1649131160.63	0.28	0.79
34	0	34	15.81	806.591009	PC	[M+HCO2]-	PC(16:0_18:0)	Bisex_Supercontrol	C42H84NO8P	761.593455	806.591658	-0.81			698528018.32	166666240.01	396224332.42	4.19	2.38
38	5	28	15.53	808.584442	PC	[M+H]+	PC(18:0_20:5)	Supercontrol_Bisex	C46H82NO8P	807.577805	808.585082	-0.79		not affected tissue	847478475.60	1373146735.05	1032223719.76	0.62	0.75
35	4	27	10.30	812.544074	PC	[M+HCO2]-	PC(17:2_18:2)	Supercontrol_Bisex	C43H78NO8P	767.546505	812.544708	-0.78			5481875.29	18376654.51	17025186.19	0.30	0.93
35	3	29	11.63	814.558648	PC	[M+HCO2]-	PC(17:1_18:2)	Singlesex_Bisex	C43H80NO8P	769.562155	814.560358	-2.10		granuloma	53443869.46	132457772.97	152589399.23	0.40	1.15
35	2	31	13.29	816.573832	PC	[M+HCO2]-	PC(17:0_18:2)	Supercontrol_Bisex	C43H82NO8P	771.577805	816.576008	-2.66			700914826.49	1367597635.45	902145768.53	0.51	0.66
36	6	24	8.77	822.529413	PC	[M+HCO2]-	PC(18:3_18:3)	Supercontrol_Bisex	C44H76NO8P	777.530855	822.529058	0.43			3712905.08	11313743.71	8826715.05	0.33	0.78
36	5	26	10.81	824.543151	PC	[M+HCO2]-	PC(16:0_20:5)	Bisex_Supercontrol	C44H78NO8P	779.546505	824.544708	-1.89			771835475.54	268074360.39	676112554.12	2.88	2.52
36	4	28	11.12	826.558257	PC	[M+HCO2]-	PC(18:2_18:2)	Supercontrol_Bisex	C44H80NO8P	781.562155	826.560358	-2.54			1234312029.76	5188177867.92	3081999423.25	0.24	0.59
37	6	25	10.83	836.543048	PC	[M+HCO2]-	PC(15:0_22:6)	Bisex_Supercontrol	C45H78NO8P	791.546505	836.544708	-1.98		granuloma	129591875.83	3592234.20	94286673.63	36.08	26.25
40	3	34	17.23	840.647797	PC	[M+H]+	PC(20:0_20:3)	Bisex_Supercontrol	C48H90NO8P	839.640405	840.647682	0.14		not affected tissue	1338639771.94	496868857.19	644272797.07	2.69	1.30
38	7	24	9.67	848.543364	PC	[M+HCO2]-	PC(18:3_20:4)	Supercontrol_Bisex	C46H78NO8P	803.546505	848.544708	-1.58		not affected tissue	15376684.10	118742440.96	92561087.23	0.13	0.78
38	5	28	13.08	852.573826	PC	[M+HCO2]-	PC(16:0_22:5)	Bisex_Supercontrol	C46H82NO8P	807.577805	852.576008	-2.56			2566020295.89	1059032020.75	2089537342.77	2.42	1.97
41	4	33	17.07	852.645554	PC	[M+H]+	PC(19:0_22:4)	Supercontrol_Bisex	C49H90NO8P	851.640405	852.647682	-2.50		granuloma	283939147.95	432793862.77	406991902.24	0.66	0.94
41	4	33	17.72	852.646465	PC	[M+H]+	PC(20:4_21:0)	Singlesex_Bisex	C49H90NO8P	851.640405	852.647682	-1.43		granuloma	54934847.33	50783186.74	91428601.25	1.08	1.80
38	2	34	16.37	858.621175	PC	[M+HCO2]-	PC(18:0_20:2)	Supercontrol_Bisex	C46H88NO8P	813.624755	858.622958	-2.08			297894521.55	763490282.68	615084171.45	0.39	0.81
39	6	27	12.75	864.573658	PC	[M+HCO2]-	PC(17:0_22:6)	Bisex_Supercontrol	C47H82NO8P	819.577806	864.576008	-2.72		granuloma	206303963.52	39033228.45	143913733.89	5.29	3.69
39	5	29	13.70	866.590067	PC	[M+HCO2]-	PC(17:0_22:5)	Supercontrol_Bisex	C47H84NO8P	821.593455	866.591658	-1.84		eggs	19799864.37	58164982.71	50408236.02	0.34	0.87
42	1	40	18.38	868.679313	PC	[M+H]+	PC(18:2_24:1)	Bisex_Supercontrol	C50H94NO8P	867.671706	868.678982	0.38			480328830.74	119998918.57	277039983.28	4.00	2.31
39	2	35	16.99	872.637377	PC	[M+HCO2]-	PC(19:0_20:2)	Supercontrol_Bisex	C47H90NO8P	827.640405	872.638608	-1.41			21207592.62	49435607.23	45389257.13	0.43	0.92
43	2	39	19.85	884.709625	PC	[M+H]+	PC(18:2_25:0)	Singlesex_Bisex	C51H98NO8P	883.703006	884.710282	-0.74	Supercontrol_ Bisex		14839708.70	19502626.47	25840573.01	0.76	1.32
40	1	38	18.62	888.668849	PC	[M+HCO2]-	PC(16:0_24:1)	Bisex_Supercontrol	C48H94NO8P	843.671706	888.669908	-1.19			27538840.84	4651397.83	10813379.35	5.92	2.32
42	9	24	11.22	900.574129	PC	[M+HCO2]-	PC(20:4_22:5)	Supercontrol_Bisex	C50H82NO8P	855.577805	900.576008	-2.09		not affected tissue	19106916.32	43992756.31	35271400.93	0.43	0.80
41	2	37	18.52	900.668797	PC	[M+HCO2]-	PC(18:2_23:0)	Supercontrol_Bisex	C49H94NO8P	855.671706	900.669908	-1.23			5498348.05	7360753.22	10557984.95	0.75	1.43
42	5	32	16.54	908.636995	PC	[M+HCO2]-	PC(20:4_22:1)	Bisex_Supercontrol	C50H90NO8P	863.640405	908.638608	-1.78		granuloma	54831357.98	15809695.51	25989186.84	3.47	1.64
44	5	34	17.82	936.667934	PC	[M+HCO2]-	PC(20:4_24:1)	Bisex_Singlesex	C52H94NO8P	891.671706	936.669908	-2.11	Bisex_ Supercontrol		18773864.79	1957951.02	7525697.91	9.59	3.84
34	3	28	11.31	712.490563	PE	[M-H]-	PE(16:0_18:3)	Supercontrol_Bisex	C39H72NO8P	713.499555	712.492278	-2.41		not affected tissue	124198715.28	631104817.05	386272172.06	0.20	0.61
34	3	28	11.98	714.507391	PE	[M+H]+	PE(16:1_18:2)	Supercontrol_Bisex	C39H72NO8P	713.499555	714.506831	0.78		not affected tissue	151741005.76	1868547979.68	1329999877.66	0.08	0.71
34	0	34	16.36	718.537063	PE	[M-H]-	PE(16:0_18:0)	Bisex_Supercontrol	C39H78NO8P	719.546505	718.539229	-3.01			12234248.13	3319306.58	6637290.36	3.69	2.00
36	6	24	9.23	734.476637	PE	[M-H]-	PE(18:3_18:3)	Supercontrol_Bisex	C41H70NO8P	735.483905	734.476628	0.01			804739.07	6377089.80	2904837.69	0.13	0.46
36	5	26	11.00	736.490332	PE	[M-H]-	PE(16:1_20:4)	Supercontrol_Bisex	C41H72NO8P	737.499555	736.492278	-2.64		not affected tissue	71917636.43	552133750.29	370632540.30	0.13	0.67
36	5	26	11.20	738.508113	PE	[M+H]+	PE(18:2_18:3)	Singlesex_Bisex	C41H72NO8P	737.499555	738.506831	1.74		not affected tissue	37277810.01	725466386.24	270167982.39	0.05	0.37
36	1	34	16.60	744.553482	PE	[M-H]-	PE(18:0_18:1)	Bisex_Supercontrol	C41H80NO8P	745.562155	744.554879	-1.88		granuloma	955870607.09	321395428.18	507643093.82	2.97	1.58
37	2	33	15.96	756.553126	PE	[M-H]-	PE(18:2_19:0)	Supercontrol_Bisex	C42H80NO8P	757.562155	756.554879	-2.32			47774836.16	506035100.18	252961539.40	0.09	0.50
38	7	24	10.15	760.490808	PE	[M-H]-	PE(18:3_20:4)	Supercontrol_Bisex	C43H72NO8P	761.499555	760.492278	-1.93			224921.33	67829470.36	23033024.23	0.00	0.34
38	8	22	10.24	760.492697	PE	[M+H]+	PE(38:8)	Supercontrol_Bisex	C43H70NO8P	759.483905	760.491181	1.99			2110912.13	9394515.01	10900557.01	0.22	1.16
38	6	26	11.57	762.505833	PE	[M-H]-	PE(18:2_20:4)	Supercontrol_Bisex	C43H74NO8P	763.515205	762.507929	-2.75			146574563.89	747982381.43	461285221.75	0.20	0.62
38	6	26	12.40	762.505901	PE	[M-H]-	PE(16:0_22:6)	Bisex_Supercontrol	C43H74NO8P	763.515205	762.507929	-2.66			5352312068.11	3398317627.16	4737702036.20	1.57	1.39
38	7	24	8.31	762.508628	PE	[M+H]+	PE(18:2_20:5)	Supercontrol_Bisex	C43H72NO8P	761.499555	762.506831	2.36		not affected tissue	7074961.01	7690693.27	10922135.68	0.92	1.42
39	4	31	15.86	780.553148	PE	[M-H]-	PE(19:0_20:4)	Supercontrol_Bisex	C44H80NO8P	781.562155	780.554879	-2.22			754682610.47	1649546504.12	1176622324.35	0.46	0.71
39	5	29	15.25	780.554041	PE	[M+H]+	PE(17:0_22:5)	Supercontrol_Bisex	C44H78NO8P	779.546505	780.553782	0.33		not affected tissue	45442999.10	207370232.41	181462071.13	0.22	0.88

* only identified by head group fragments

CN	DB	ECN	retention time / min	m/z detected	substance class	ion	substance	significant pair	sum formula	monoisotopic mass	m/z theoretical	D / ppm	also found for	lateral distribution	average peak area bisex-infected	average peak area control	average peak area monosex-infected	bisex/ control	monosex/ control
39	1	37	18.18	786.602420	PE	[M-H]-	PE(19:0_20:1)	Supercontrol_Bisex	C44H86NO8P	787.609105	786.601829	0.75			1612171.32	3607341.93	2467011.03	0.45	0.68
40	6	28	14.71	790.537181	PE	[M-H]-	PE(18:0_22:6)	Bisex_Supercontrol	C45H78NO8P	791.546505	790.539229	-2.59		granuloma	2600165401.71	1160200133.16	2089435528.54	2.24	1.80
40	6	28	13.88	790.537259	PE	[M-H]-	PE(18:1_22:5)	Supercontrol_Bisex	C45H78NO8P	791.546505	790.539229	-2.49		granuloma	110629170.27	702793171.97	399699868.46	0.16	0.57
40	4	32	16.47	794.569125	PE	[M-H]-	PE(18:0_22:4)	Bisex_Supercontrol	C45H82NO8P	795.577805	794.570529	-1.77			622134110.40	268891236.84	430455478.08	2.31	1.60
42	10	22	10.70	810.506274	PE	[M-H]-	PE(20:4_22:6)	Supercontrol_Bisex	C47H74NO8P	811.515205	810.507929	-2.04			387510.78	17116627.46	12651393.68	0.02	0.74
42	9	24	12.12	812.522029	PE	[M-H]-	PE(20:4_22:5)	Supercontrol_Bisex	C47H76NO8P	813.530855	812.523579	-1.91		not affected tissue	167746.90	1664930.15	1300514.41	0.10	0.78
32	2	28	8.80	717.471435	PG	[M-H]-	PG(16:1_16:1)	Supercontrol_Bisex	C38H71O10P	718.478485	717.471209	0.32			208542.82	1902907.79	775794.52	0.11	0.41
32	1	30	10.06	719.486202	PG	[M-H]-	PG(16:0_16:1)	Supercontrol_Bisex	C38H73O10P	720.494135	719.486859	-0.91		granuloma	940131.28	5165986.56	2655217.15	0.18	0.51
35	3	29	9.94	757.500679	PG	[M-H]-	PG(17:1_18:2)	Supercontrol_Bisex	C41H75O10P	758.509785	757.502509	-2.42			5101645.92	10691423.43	12153986.93	0.48	1.14
36	5	26	8.51	767.487296	PG	[M-H]-	PG(18:2_18:3)	Supercontrol_Bisex	C42H73O10P	768.494135	767.486859	0.57			25363323.91	48683052.20	40762019.76	0.52	0.84
38	5	28	10.38	795.516771	PG	[M-H]-	PG(18:1_20:4)	Supercontrol_Bisex	C44H77O10P	796.525435	795.518159	-1.74			71606174.44	156346784.49	158455863.88	0.46	1.01
38	4	30	12.12	797.532257	PG	[M-H]-	PG(18:1_20:3)	Bisex_Supercontrol	C44H79O10P	798.541085	797.533809	-1.95			18810050.96	3560035.53	9991726.83	5.28	2.81
38	2	34	15.86	801.563364	PG	[M-H]-	PG(18:0_20:2)	Bisex_Supercontrol	C44H83O10P	802.572385	801.565109	-2.18			16456294.38	5583260.62	8400148.11	2.95	1.50
40	9	22	8.23	815.487902	PG	[M-H]-	PG(18:3_22:6)	Bisex_Supercontrol	C46H73O10P	816.494135	815.486859	1.28			21040037.27	6275524.31	11724913.02	3.35	1.87
40	8	24	9.06	817.502379	PG	[M-H]-	PG(18:2_22:6)	Bisex_Supercontrol	C46H75O10P	818.509785	817.502509	-0.16		granuloma	376442839.21	85721535.45	190513499.41	4.39	2.22
40	7	26	10.27	819.516775	PG	[M-H]-	PG(18:1_22:6)	Bisex_Singlesex	C46H77O10P	820.525435	819.518159	-1.69	Bisex_ Supercontrol	overall, little enrichment in	1029279792.17	318420737.97	584233693.94	3.23	1.83
42	8	26	10.56	845.531710	PG	[M-H]-	PG(20:4_22:4)	Bisex_Supercontrol	C48H79O10P	846.541085	845.533809	-2.48			95212636.75	30102225.54	65422320.94	3.16	2.17
44	11	22	9.60	867.517124	PG	[M-H]-	PG(22:5_22:6)	Bisex_Singlesex	C50H77O10P	868.525435	867.518159	-1.19	Bisex_ Supercontrol	granuloma	313418939.04	27926079.20	91596452.72	11.22	3.28
44	10	24	10.71	869.532522	PG	[M-H]-	PG(22:4_22:6)	Bisex_Supercontrol	C50H79O10P	870.541085	869.533809	-1.48			160689365.74	75273700.23	124310255.81	2.13	1.65
44	10	24	10.87	869.532683	PG	[M-H]-	PG(22:5_22:5)	Bisex_Supercontrol	C50H79O10P	870.541085	869.533809	-1.29			135257772.07	21286973.12	64476442.95	6.35	3.03
44	9	26	11.42	871.547337	PG	[M-H]-	PG(22:4_22:5)	Bisex_Supercontrol	C50H81O10P	872.556735	871.549459	-2.43			56584790.54	6351563.16	31209403.30	8.91	4.91
44	12	20	9.26	884.545348	PG	[M+NH4]+	PG(22:6_22:6)	Bisex_Supercontrol	C50H75O10P	866.509785	884.543611	1.96			33288149.82	1131994.61	7614354.83	29.41	6.73
34	3	28	10.28	831.501304	PI	[M-H]-	PI(16:0_18:3)	Supercontrol_Bisex	C43H77O13P	832.510179	831.502903	-1.92			5458582.73	15911198.35	7086374.40	0.34	0.45
36	4	28	11.39	857.516513	PI	[M-H]-	PI(16:0_20:4)	Supercontrol_Bisex	C45H79O13P	858.525829	857.518553	-2.38			313414372.68	652635126.91	338140120.31	0.48	0.52
36	2	32	14.20	861.547833	PI	[M-H]-	PI(18:0_18:2)	Bisex_Supercontrol	C45H83O13P	862.557129	861.549853	-2.34			20334407.71	3473607.15	13848982.55	5.85	3.99
38	7	24	9.04	879.504509	PI	[M-H]-	PI(18:3_20:4)	Supercontrol_Bisex	C47H77O13P	880.510179	879.502903	1.83			492079.16	2943472.19	611904.17	0.17	0.21
38	5	28	11.55	883.533212	PI	[M-H]-	PI(18:1_20:4)	Supercontrol_Bisex	C47H81O13P	884.541479	883.534203	-1.12			83056876.60	151428633.28	90805741.74	0.55	0.60
38	2	34	15.61	889.579032	PI	[M-H]-	PI(18:0_20:2)	Supercontrol_Bisex	C47H87O13P	890.588429	889.581153	-2.38		not affected tissue	12413861.18	34735660.27	23375092.36	0.36	0.67
38	5	28	12.69	902.577612	PI	[M+NH4]+	PI(38:5)*	Bisex_Supercontrol	C47H81O13P	884.541479	902.575305	2.56			32694167.15	4671558.63	4747140.73	7.00	1.02
40	5	30	14.52	911.564141	PI	[M-H]-	PI(18:0_22:5)	Bisex_Supercontrol	C49H85O13P	912.572779	911.565503	-1.49		not affected tissue	20377602.15	5695420.49	12747115.20	3.58	2.24
40	4	32	15.00	913.580713	PI	[M-H]-	PI(18:0_22:4)	Supercontrol_Bisex	C49H87O13P	914.588429	913.581153	-0.48		granuloma	5807155.56	13465354.64	8509977.78	0.43	0.63
18	0	18	4.89	552.367035	Plasmanyl-LP(	[M+HCO2]-	Plasmanyl-LPC(O-18:0)	Bisex_Supercontrol	C26H54NO6P	507.368877	552.367080	-0.08			70635082.76	10596912.76	43430902.81	6.67	4.10
34	1	32	16.08	746.606605	Plasmanyl-PC	[M+H]+	Plasmanyl-PC(O-16:1/18:0)	Bisex_Supercontrol	C42H84NO7P	745.598541	746.605817	1.06		granuloma	1805690279.41	979417837.21	5749726887.38	18.44	5.87
38	5	28	15.67	794.606766	Plasmanyl-PC	[M+H]+	Plasmanyl-PC(O-16:0/22:5)	Bisex_Supercontrol	C46H84NO7P	793.598541	794.605817	1.19		granuloma	385795121.94	36955337.58	127677819.05	10.44	3.45
40	3	34	18.16	826.670277	Plasmanyl-PC	[M+H]+	Plasmanyl-PC(O-22:1/18:2)	Bisex_Supercontrol	C48H92NO7P	825.661141	826.668417	2.25			159745834.52	41018842.52	70837732.27	3.89	1.73
40	4	32	16.23	866.626477	Plasmenyl-PC	[M+HCO2]-	Plasmenyl-PC(P-20:0/20:4)	Bisex_Supercontrol	C48H88NO7P	821.629841	866.628044	-1.81			21845156.95	3644265.74	9747723.70	5.99	2.67
42	2	38	17.86	813.685505	SM	[M+H]+	SM(d18:1/24:1)	Bisex_Supercontrol	C47H95N2O6P	814.692775	813.685499	0.01		overall, little enrichment in granuloma	36732222545.46	############	22417289359.47	2.90	1.77
18	1	16	3.87	300.290207	So	[M+H]+	So(d18:1)	Bisex_Supercontrol	C18H37NO2	299.282429	300.289706	1.67			148699879.10	71480963.40	92957798.91	2.08	1.30
18	0	18	4.23	302.305933	So	[M+H]+	So(d18:0)	Bisex_Supercontrol	C18H39NO2	301.298079	302.305356	1.91			58857709.58	13745270.76	31104149.18	4.28	2.26
46	2	42	21.47	792.708435	TG	[M+NH4]+	TG(12:0_16:0_18:2)	Singlesex_Bisex	C49H90O6	774.673741	792.707566	1.10	Supercontrol_ Bisex		98265520.33	437434253.66	262766923.64	0.22	0.60
46	1	44	21.70	794.723472	TG	[M+NH4]+	TG(14:0_16:0_16:1)	Supercontrol_Bisex	C49H92O6	776.689391	794.723216	0.32			20248028.90	454059172.34	148881699.25	0.04	0.33
57	2	53	21.60	806.723562	TG	[M+NH4]+	TG(14:0_15:0_18:2)	Supercontrol_Bisex	C50H92O6	788.689391	806.723216	0.43			44755349.13	129692240.74	111754218.59	0.35	0.86
48	3	42	21.52	818.723930	TG	[M+NH4]+	TG(14:0_16:1_18:2)	Supercontrol_Bisex	C51H92O6	800.689391	818.723216	0.87			548079990.53	803358661.51	693494399.81	0.68	0.86
48	2	44	21.73	820.739674	TG	[M+NH4]+	TG(14:0_16:0_18:2)	Supercontrol_Bisex	C51H94O6	802.705041	820.738866	0.98			628433400.17	2279893938.37	1465614483.38	0.28	0.64
36	4	28	21.42	830.723900	TG	[M+NH4]+	TG(13:0_18:2_18:2)	Supercontrol_Bisex	C52H92O6	812.689391	830.723216	0.82			74648950.10	119123258.45	120720294.28	0.63	1.01
49	2	45	21.87	834.755125	TG	[M+NH4]+	TG(15:0_16:0_18:2)	Supercontrol_Bisex	C52H96O6	816.720691	834.754516	0.73			137001860.24	696890716.30	528813156.68	0.20	0.76
50	4	42	21.55	844.739692	TG	[M+NH4]+	TG(14:0_18:2_18:2)	Supercontrol_Bisex	C53H94O6	826.705041	844.738866	0.98			1640764349.67	3011175135.83	3278968929.69	0.54	1.09
50	3	44	21.76	846.755013	TG	[M+NH4]+	TG(16:0_16:1_18:2)	Supercontrol_Bisex	C53H96O6	828.720691	846.754516	0.59			3105546086.93	8289797295.89	5862893026.68	0.37	0.71
50	2	46	21.95	848.771097	TG	[M+NH4]+	TG(16:0_16:1_18:1)	Supercontrol_Bisex	C53H98O6	830.736341	848.770166	1.10			4275375498.77	############	7429247812.23	0.37	0.64
50	1	48	22.13	850.786677	TG	[M+NH4]+	TG(16:0_16:0_18:1)	Supercontrol_Bisex	C53H100O6	832.751991	850.785816	1.01			3676677189.95	9428700542.63	5693765482.04	0.39	0.60
51	5	41	21.50	856.740387	TG	[M+NH4]+	TG(15:0_18:2_18:3)	Supercontrol_Bisex	C54H94O6	838.705041	856.738866	1.77			193301638.38	486217924.73	539740323.07	0.40	1.11
51	4	43	21.70	858.755452	TG	[M+NH4]+	TG(15:1_18:1_18:2)	Supercontrol_Bisex	C54H96O6	840.720691	858.754516	1.09			409688172.22	1116836423.15	1587720551.80	0.37	1.42
51	3	45	21.90	860.770810	TG	[M+NH4]+	TG(15:0_18:1_18:2)	Supercontrol_Bisex	C54H98O6	842.736341	860.770166	0.75			826534182.04	2258134961.16	1877396862.38	0.37	0.83
51	2	47	22.07	862.785882	TG	[M+NH4]+	TG(16:0_17:1_18:1)	Supercontrol_Bisex	C54H100O6	844.751991	862.785816	0.08			932223452.88	2406074081.76	1652543385.11	0.39	0.69

* only identified by head group fragments

CN	DB	ECN	retention time / min	m/z detected	substance class	ion	substance	significant pair	sum formula	monoisotopic mass	m/z theoretical	D / ppm	also found for	lateral distribution	average peak area bisex-infected	average peak area control	average peak area monosex-infected	bisex/ control	monosex/ control
52	7	38	21.14	866.724609	TG	[M+NH4]+	TG(16:1_18:3_18:3)	Bisex_Supercontrol	C55H92O6	848.689391	866.723216	1.61			239386242.51	119858928.62	177530055.02	2.00	1.48
52	7	38	21.41	866.725240	TG	[M+NH4]+	TG(16:0_18:3_18:4)	Bisex_Singlesex	C55H92O6	848.689391	866.723216	2.33	Bisex_ Supercontrol		65169206.12	3622774.89	14499432.63	17.99	4.00
52	3	46	21.99	874.786968	TG	[M+NH4]+	TG(16:0_18:1_18:2)	Supercontrol_Bisex	C55H100O6	856.751991	874.785816	1.32			29318474013.27	############	33484322084.29	0.74	0.85
52	2	48	22.15	876.802096	TG	[M+NH4]+	TG(16:0_18:1_18:1)	Supercontrol_Bisex	C55H102O6	858.767641	876.801467	0.72			22624652535.66	############	27912810724.93	0.59	0.72
53	6	41	21.37	882.756842	TG	[M+NH4]+	TG(17:1_18:2_18:3)	Supercontrol_Bisex	C56H96O6	864.720691	882.754516	2.63			30780062.98	97175999.29	18803333.63	0.32	0.19
53	5	43	21.73	884.771308	TG	[M+NH4]+	TG(17:0_18:2_18:3)	Supercontrol_Bisex	C56H98O6	866.736341	884.770166	1.29			403686661.87	913278252.03	842002901.93	0.44	0.92
53	4	45	21.90	886.785962	TG	[M+NH4]+	TG(17:0_18:2_18:2)	Supercontrol_Bisex	C56H100O6	868.751991	886.785816	0.16			1147220607.28	2482973452.66	2041991676.17	0.46	0.82
53	3	47	22.09	888.801566	TG	[M+NH4]+	TG(17:0_18:1_18:2)	Supercontrol_Bisex	C56H102O6	870.767641	888.801467	0.11			1659051482.31	3614179081.92	2645211337.05	0.46	0.73
54	9	36	21.09	890.725399	TG	[M+NH4]+	TG(18:2_18:3_18:4)	Bisex_Supercontrol	C57H92O6	872.689391	890.723216	2.45			66740718.91	5623897.39	27520182.95	11.87	4.89
53	2	49	22.26	890.817864	TG	[M+NH4]+	TG(17:0_18:1_18:1)	Supercontrol_Bisex	C56H104O6	872.783291	890.817117	0.84			1630935605.16	3866496916.39	2692296545.38	0.42	0.70
54	8	38	21.34	892.740548	TG	[M+NH4]+	TG(18:1_18:3_18:4)	Bisex_Supercontrol	C57H94O6	874.705041	892.738866	1.88			258229600.17	54772871.04	121746794.54	4.71	2.22
53	1	51	22.41	892.832551	TG	[M+NH4]+	TG(16:0_18:1_19:0)	Supercontrol_Bisex	C56H106O6	874.798941	892.832767	-0.24			451811959.99	1373648187.46	616995675.36	0.33	0.45
55	8	39	21.54	906.755257	TG	[M+NH4]+	TG(15:0_18:2_22:6)	Bisex_Supercontrol	C58H96O6	888.720691	906.754516	0.82			51114650.39	7699937.74	41959563.85	6.64	5.45
54	1	52	22.50	906.847481	TG	[M+NH4]+	TG(16:0_18:1_20:0)	Supercontrol_Bisex	C57H108O6	888.814591	906.848417	-1.03			976540113.56	1962091892.41	999699695.54	0.50	0.51
55	7	41	21.75	908.771822	TG	[M+NH4]+	TG(15:0_18:1_22:6)	Bisex_Supercontrol	C58H98O6	890.736341	908.770166	1.82			76530491.64	9152817.35	42691499.96	8.36	4.66
56	10	36	21.14	916.741101	TG	[M+NH4]+	TG(16:1_20:4_20:5)	Bisex_Supercontrol	C59H94O6	898.705041	916.738866	2.44			69424194.31	17652671.65	41687581.78	3.93	2.36
56	9	38	21.44	918.755836	TG	[M+NH4]+	TG(16:0_18:3_22:6)	Bisex_Supercontrol	C59H96O6	900.720691	918.754516	1.44			869609016.28	199518745.89	512548335.68	4.36	2.57
55	2	51	22.80	918.848627	TG	[M+NH4]+	TG(18:0_18:2_19:0)	Supercontrol_Bisex	C58H108O6	900.814591	918.848417	0.23			225684079.05	702431576.53	377577515.05	0.32	0.54
55	2	51	23.47	918.849306	TG	[M+NH4]+	TG(17:0_18:1_20:1)	Supercontrol_Bisex	C58H108O6	900.814591	918.848417	0.97			67094262.73	125742605.32	42893548.55	0.53	0.34
55	1	53	22.58	920.862923	TG	[M+NH4]+	TG(16:0_18:1_21:0)	Supercontrol_Bisex	C58H110O6	902.830241	920.864067	-1.24			175650335.22	493400532.36	221390517.60	0.36	0.45
56	7	42	22.11	922.786097	TG	[M+NH4]+	TG(16:0_18:1_22:6)	Bisex_Supercontrol	C59H100O6	904.751991	922.785816	0.30			48138449.03	5577289.96	18024047.79	8.63	3.23
56	7	42	21.82	922.786208	TG	[M+NH4]+	TG(18:1_18:2_20:4)	Bisex_Supercontrol	C59H100O6	904.751991	922.785816	0.42			4007211390.64	1107317463.94	2687972945.01	3.62	2.43
56	6	44	22.21	924.801559	TG	[M+NH4]+	TG(18:0_18:1_20:5)	Bisex_Supercontrol	C59H102O6	906.767641	924.801467	0.10			220731836.59	68455257.86	119362261.30	3.22	1.74
56	6	44	21.93	924.801892	TG	[M+NH4]+	TG(16:0_18:2_22:4)	Bisex_Singlesex	C59H102O6	906.767641	924.801467	0.46	Bisex_ Supercontrol		5655507033.93	2876271469.38	3618432429.34	1.97	1.26
57	9	39	21.59	932.770910	TG	[M+NH4]+	TG(17:1_18:2_22:6)	Bisex_Singlesex	C60H98O6	914.736341	932.770166	0.80	Bisex_ Supercontrol		22621384.91	2751696.31	13965369.14	8.22	5.08
57	8	41	21.76	934.787552	TG	[M+NH4]+	TG(17:0_18:2_22:6)	Bisex_Singlesex	C60H100O6	916.751991	934.785816	1.86	Bisex_ Supercontrol		105634062.52	26206174.98	48571489.46	4.03	1.85
57	6	45	22.08	938.817295	TG	[M+NH4]+	TG(18:2_19:0_20:4)	Bisex_Supercontrol	C60H104O6	920.783291	938.817117	0.19			177234282.08	100016206.93	129952656.04	1.77	1.30
58	10	38	21.62	944.771708	TG	[M+NH4]+	TG(16:0_20:4_22:6)	Bisex_Supercontrol	C61H98O6	926.736341	944.770166	1.63			910849156.46	12747086.87	122081475.40	71.46	9.58
58	10	38	21.50	944.771981	TG	[M+NH4]+	TG(18:2_18:2_22:6)	Bisex_Supercontrol	C61H98O6	926.736341	944.770166	1.92			685363483.86	238646120.56	637969212.94	2.87	2.67
57	3	51	22.42	944.864974	TG	[M+NH4]+	TG(18:1_18:2_21:0)	Supercontrol_Bisex	C60H110O6	926.830241	944.864067	0.96			259542415.71	408839096.10	286647696.16	0.63	0.70
58	9	40	21.71	946.786917	TG	[M+NH4]+	TG(18:1_18:2_22:6)	Bisex_Singlesex	C61H100O6	928.751991	946.785816	1.16	Bisex_ Supercontrol		2137162749.50	467849026.81	899420553.25	4.57	1.92
58	8	42	21.90	948.803126	TG	[M+NH4]+	TG(18:1_18:2_22:5)	Bisex_Singlesex	C61H102O6	930.767641	948.801467	1.75	Bisex_ Supercontrol		2354112920.44	881417782.58	819275825.03	2.67	0.93
58	6	46	22.11	952.832925	TG	[M+NH4]+	TG(18:0_18:2_22:4)	Bisex_Singlesex	C61H106O6	934.798941	952.832767	0.17	Bisex_ Supercontrol		1953837090.30	1261659832.15	1130199924.43	1.55	0.90
59	10	39	21.74	958.788426	TG	[M+NH4]+	TG(17:0_20:5_22:5)	Bisex_Supercontrol	C62H100O6	940.751991	958.785816	2.72			29030364.49	1049864.90	3246832.68	27.65	3.09
59	7	45	22.13	964.833831	TG	[M+NH4]+	TG(18:2_19:0_22:5)	Bisex_Supercontrol	C62H106O6	946.798941	964.832767	1.10			42061256.87	1103315.01	21453952.61	38.12	19.44
60	13	34	21.18	966.757004	TG	[M+NH4]+	TG(18:3_20:4_22:6)	Bisex_Supercontrol	C63H96O6	948.720691	966.754516	2.57			21058026.05	465629.23	4772466.77	45.22	10.25
60	12	36	21.45	968.772162	TG	[M+NH4]+	TG(18:2_20:4_22:6)	Bisex_Supercontrol	C63H98O6	950.736341	968.770166	2.06			168615736.80	20694636.67	89150738.80	8.15	4.31
60	11	38	21.64	970.787738	TG	[M+NH4]+	TG(18:1_20:4_22:6)	Bisex_Supercontrol	C63H100O6	952.751991	970.785816	1.98			588085373.16	59872499.21	149390448.22	9.82	2.50
59	4	51	22.48	970.881286	TG	[M+NH4]+	TG(18:2_18:2_23:0)	Supercontrol_Bisex	C62H112O6	952.845891	970.879717	1.62			112474946.45	260764195.39	203714451.37	0.43	0.78
60	10	40	21.75	972.801855	TG	[M+NH4]+	TG(18:1_20:4_22:5)	Bisex_Singlesex	C63H102O6	954.767641	972.801467	0.40	Bisex_ Supercontrol		490453606.14	220117381.99	197079742.70	2.23	0.90
59	3	53	22.60	972.896961	TG	[M+NH4]+	TG(18:1_18:2_23:0)	Supercontrol_Bisex	C62H114O6	954.861541	972.895367	1.64			80803710.86	212034000.51	130477966.46	0.38	0.62
60	9	42	21.91	974.818364	TG	[M+NH4]+	TG(18:0_20:4_22:5)	Bisex_Singlesex	C63H104O6	956.783291	974.817117	1.28	Bisex_ Supercontrol		729489111.58	250979800.71	253035086.92	2.91	1.01
59	2	55	22.78	974.913129	TG	[M+NH4]+	TG(18:0_18:2_23:0)	Supercontrol_Bisex	C62H116O6	956.877191	974.911017	2.17			42563775.43	121653074.79	95395936.54	0.35	0.78
60	8	44	22.00	976.830457	TG	[M+NH4]+	TG(18:1_20:3_22:4)	Bisex_Singlesex	C63H106O6	958.798941	976.832767	-2.36			387810234.78	430707668.49	140652083.10	0.90	0.33
60	7	46	22.10	978.849050	TG	[M+NH4]+	TG(18:1_20:2_22:4)	Bisex_Singlesex	C63H108O6	960.814591	978.848417	0.65	Bisex_ Supercontrol		588000110.24	341527284.59	299102120.85	1.72	0.88
62	14	34	21.34	992.772366	TG	[M+NH4]+	TG(18:2_22:6_22:6)	Bisex_Supercontrol	C65H98O6	974.736341	992.770166	2.22			65362584.15	470809.65	9672507.25	138.83	20.54
62	13	36	21.54	994.786478	TG	[M+NH4]+	TG(18:2_22:5_22:6)	Bisex_Supercontrol	C65H100O6	976.751991	994.785816	0.67			109537266.07	689791.80	14733596.47	158.80	21.36
62	12	38	21.70	996.803158	TG	[M+NH4]+	TG(18:2_22:4_22:6)	Bisex_Supercontrol	C65H102O6	978.767641	996.801467	1.70			193027425.84	7490236.37	24654656.22	25.77	3.29
61	5	51	22.52	996.897036	TG	[M+NH4]+	TG(18:2_18:3_25:0)	Supercontrol_Bisex	C64H114O6	978.861541	996.895367	1.67			60416044.08	66986191.25	48976493.58	0.90	0.73
62	11	40	21.76	998.816461	TG	[M+NH4]+	TG(18:1_22:4_22:6)	Bisex_Singlesex	C65H104O6	980.783291	998.817117	-0.66	Bisex_ Supercontrol		92952999.17	47641696.65	30216179.85	1.95	0.63

* only identified by head group fragments

CN	DB	ECN	retention time / min	m/z detected	substance class	ion	substance	significant pair	sum formula	monoisotopic mass	m/z theoretical	D / ppm	also found for	lateral distribution	average peak area bisex-infected	average peak area control	average peak area monosex-infected	bisex/ control	monosex/ control
62	10	42	21.92	1000.833394	TG	[M+NH4]+	TG(18:1_22:4_22:5)	Bisex_Singlesex	C65H106O6	982.798941	1000.832767	0.63	Bisex_ Supercontrol		217063994.77	69277960.98	73881952.20	3.13	1.07
62	8	46	22.24	1004.864049	TG	[M+NH4]+	TG(18:0_22:4_22:4)	Bisex_Singlesex	C65H110O6	986.830241	1004.864067	-0.02	Bisex_ Supercontrol		253544936.81	87368375.93	100486840.21	2.90	1.15
62	7	48	22.31	1006.880459	TG	[M+NH4]+	TG(18:1_22:2_22:4)	Bisex_Supercontrol	C65H112O6	988.845891	1006.879717	0.74			271183258.43	144897193.33	148166362.77	1.87	1.02
62	6	50	22.49	1008.896549	TG	[M+NH4]+	TG(18:1_20:4_24:1)	Bisex_Supercontrol	C65H114O6	990.861541	1008.895367	1.17			291074046.89	155141783.67	134400497.90	1.88	0.87
64	13	38	21.75	1022.818413	TG	[M+NH4]+	TG(20:4_22:4_22:5)	Bisex_Supercontrol	C67H104O6	1004.783291	1022.817117	1.27			24785655.05	0.00	1564763.44	#DIV/0!	#DIV/0!
63	4	55	22.81	1026.944751	TG	[M+NH4]+	TG(18:2_20:2_25:0)	Supercontrol_Bisex	C66H120O6	1008.908492	1026.942317	2.37			14682053.36	23300173.82	13956582.46	0.63	0.60
64	10	44	22.12	1028.865883	TG	[M+NH4]+	TG(20:1_22:4_22:5)	Bisex_Supercontrol	C67H110O6	1010.830241	1028.864067	1.77			57678260.70	4983404.00	10940324.61	11.57	2.20
64	9	46	22.29	1030.879784	TG	[M+NH4]+	TG(20:4_22:1_22:4)	Bisex_Singlesex	C67H112O6	1012.845891	1030.879717	0.06	Bisex_ Supercontrol		97325160.60	30779754.10	35186460.14	3.16	1.14
64	8	48	22.35	1032.897302	TG	[M+NH4]+	TG(20:3_22:1_22:4)	Bisex_Singlesex	C67H114O6	1014.861541	1032.895367	1.87	Bisex_ Supercontrol		149469217.96	45892843.81	49371049.44	3.26	1.08
64	7	50	22.52	1034.912119	TG	[M+NH4]+	TG(18:1_22:5_24:1)	Bisex_Singlesex	C67H116O6	1016.877191	1034.911017	1.06	Bisex_ Supercontrol		139444940.53	60753255.60	50486189.12	2.30	0.83
64	5	54	22.78	1038.943148	TG	[M+NH4]+	TG(18:0_22:4_24:1)	Bisex_Supercontrol	C67H120O6	1020.908492	1038.942866	0.27			90244197.95	41424115.39	38581674.44	2.18	0.93
66	6	54	22.78	1064.958708	TG	[M+NH4]+	TG(20:1_22:4_24:1)	Bisex_Singlesex	C69H122O6	1046.924142	1064.957967	0.70	Bisex_ Supercontrol		29133071.60	7331655.96	8557483.83	3.97	1.17

* only identified by head group fragments

3 Bovine skin containing *Besnoitia besnoiti* tissue cysts

3.1 Mass spectrometry imaging of lipid and metabolite distributions in cysts of *Besnoitia besnoiti*-infected bovine skin

ACS Partner Journal

Journal of the American Society for Mass Spectrometry

pubs.acs.org/jasms

Article

Mass Spectrometry Imaging of Lipid and Metabolite Distributions in Cysts of *Besnoitia besnoiti*-Infected Bovine Skin

Katja R. Wiedemann, Stefanie Gerbig, Parviz Ghezellou, Alejandra Pilgram, Carlos Hermosilla, Anja Taubert, Liliana M. R. Silva,*,▽ and Bernhard Spengler*,▽

Cite This: *J. Am. Soc. Mass Spectrom.* 2025, 36, 1017−1026

Read Online

ACCESS | Metrics & More | Article Recommendations | Supporting Information

ABSTRACT: Bovine besnoitiosis is a disease caused by the obligate intracellular parasite *Besnoitia besnoiti*. During its chronic stage, the parasite forms large, thick-walled cysts of up to 600 μm in diameter in the skin and other tissues. To assess an overview of parasite-induced metabolic changes during chronic infection, *B. besnoiti*-infected skin samples were analyzed by high-resolution atmospheric-pressure scanning microprobe matrix-assisted laser desorption/ionization mass spectrometry imaging (AP-SMALDI MSI). Overall, infection-driven, significant changes of 467 lipids and metabolites were found in comparison to noninfected control samples. Most of them belong to the group of phosphatidic acids (PAs), phosphatidylserines (PSs), phosphatidylcholines (PCs)/phosphatidylethanolamines (PEs), triacylglycerides (TGs), phosphatidylinositols (PIs) and phosphatidylglycerols (PGs). When these quantitative data were combined with analyses on the lateral distribution of respective infection markers, MS images of significantly changed ion signals with specific lateral distributions were generated, matching with typical biological structures as observed in Hematoxylin and eosin (H&E)-stained tissue sections. Ultrahigh-resolution MALDI MSI with a pixel size of 2 μm and 3-dimensional reconstruction gave further insights into cyst construction.

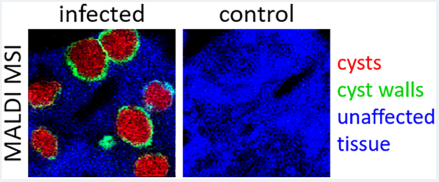

KEYWORDS: *Besnoitiosis, AP-SMALDI, Ultrahigh-resolution mass spectrometry imaging, Host−parasite interaction, Besnoitia besnoiti, Apicomplexa*

INTRODUCTION

For 30 years, matrix-assisted laser desorption/ionization mass spectrometry imaging (MALDI MSI) has been an established method for the (untargeted) analysis of biological tissue while maintaining the topological information on the sample.[1] The matrix-coated sample is analyzed in a rasterized fashion, which allows for the coregistration of MS spectra and the corresponding laser spot coordinates. The matrix is carefully selected based on acidic/basic properties, crystal size, and analyte solubility.

Over the recent years, MALDI MSI instrumentation has significantly improved, now achieving a lateral resolution below 2 μm^2 in dedicated workflows. Furthermore, mass analyzers based on orbital trapping or ion cyclotron resonance (ICR) provide accurate m/z determination with mass errors below ±1 ppm when applying adequate internal calibration measures.[3,4] Therefore, natural compounds in biological specimens can be assigned based on elemental composition and, in the case of sufficient signal intensity, can also be structurally characterized using on-tissue MS/MS.

Using new software approaches, several mass spectrometry data sets being recorded on adjacent tissue sections can be stitched together, resulting in 3-dimensional MS images, reflecting structures of interest.[5]

Besnoitia besnoiti is a cyst-forming and obligate intracellular apicomplexan parasite that causes bovine besnoitiosis, a chronic and debilitating disease manifested by cutaneous and systemic alterations in cattle.[6,7] Bovine besnoitiosis is endemic in Asia and Africa and re-emerging in European countries.[8−13] Besnoitiosis significantly impacts the individual welfare of infected bovine and causes considerable financial losses in the cattle industry,[13,14] especially because it can cause sterility in infected bulls.[14,15]. Besnoitiosis includes subacute, acute, and chronic phases.[16] Outbreaks of cattle besnoitiosis are characterized by nonspecific symptoms such as fever in the acute phase and typical clinical signs such as severe skin alterations or scleroderma in the chronic phase of the disease. As a relevant consequence of the disease, infections of male reproductive tissues (e.g., testicles) may result in bull sterility.[17,18] Acute infection is characterized by the presence of fast-proliferating tachyzoites that mainly replicate in vascular

Received: November 20, 2024
Revised: March 14, 2025
Accepted: March 20, 2025
Published: April 8, 2025

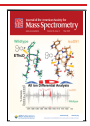

https://doi.org/10.1021/jasms.4c00466
J. Am. Soc. Mass Spectrom. 2025, 36, 1017−1026

endothelial cells, causing vascular lesions. In contrast, in the chronic phases of besnoitiosis, slow-replicating bradyzoites proliferate in mesenchymal cells forming large thick-walled tissue cysts mainly in dermis, sclera, and mucosa.[19] Due to their large size, tissue cysts are macroscopically detectable and, when being localized in the sclera or vaginal mucosa, may even serve for inspective diagnostics in living animals.[19]

B. besnoiti tissue cysts are large and show an average diameter of 200 μm. Cystic tissues often present pericystic inflammatory reactions, depending on the duration of infection and the affected tissue type.[20] Mature cysts can reach 600 μm in diameter.[16,19] Hence, these tissue cysts are easily demonstrated in skin sections of infected cattle experiencing the chronic phase of disease.[16] Tissue cysts consist of a hypertrophied host cell with enlarged nuclei, an intracytoplasmic parasitophorous vacuole (PV) with bradyzoites, a sometimes vacuolated inner cyst wall, and an outer cyst wall (outermost acellular layer) in more developed/mature cysts.[16,21] The outer cyst wall comprises multiple layers of collagen fibrils, arranged in a circular way most probably collagen type I fibers, while the inner cyst wall is made up of elements of the extracellular matrix.[16] Cysts contain only a small rim of host cell cytoplasm, which surrounds the PV, and present a hypertrophic host cell nuclei at their periphery.[16,22]

Bradyzoites typically have a diameter of approximately 2 μm and are 7.5 μm long. Currently, morphological aspects of cysts containing bradyzoites have been described in detail,[19,21,23] and there is also reported data on the proteome of the different life stages of *B. besnoiti*.[24] Moreover, some data on relevant *B. besnoiti* tachyzoite-driven changes of key metabolic pathways and selected metabolites have been reported,[25,26] e.g., transcriptomic data showing altered pathways related to lipid metabolism in bradyzoites.[19]

To date, serological tests for besnoitiosis diagnostics are established,[10,27−29] but major knowledge of parasite-driven host cell alterations or even of major steps of the life cycle (currently unknown definitive hosts) is still lacking.[12] Additionally, neither treatments nor licensed vaccines are currently available in Europe.[12]

MALDI MSI has been used in various cases to study parasites[30−34] and host−parasite interactions.[35−37] Therefore, it was the method of choice to gain further insights into *Besnoitia besnoiti* bradyzoite cysts and their host−parasite interactions, especially in the field of lipidomics.

MATERIALS AND METHODS

Chemicals. A list of all chemicals used can be found in Table S1.

Tissue Samples. Natural *B. besnoiti* infection was confirmed via a polymerase chain reaction investigation of a suspected infected cow from the South of France. The animal was euthanized due to severe clinical conditions. At necropsy, bovine besnoitiosis in the scleroderma phase was confirmed as multiple whitish punctuated cysts were observed in sclera and in mucocutaneous junctions of the mouth and anus. Skin biopsies were collected from the neck, elbow, and shoulder regions. Skin samples were maintained at 4 °C and immediately sent to the Institute of Parasitology at Justus Liebig University Giessen, where they were conserved frozen at −80 °C until further analysis.

For noninfected control samples, neck skin samples were collected from the local abattoir near Giessen, Germany, from cows originating in farms without any history of besnoitiosis and were treated as previously stated.

Sample Preparation. Before sample preparation, hair was removed from skin samples, and sections of 20 μm thickness from different parts of the sample (see Figure 2) were prepared at −25 °C using a Cryostat Microm HM 525 (Thermo Fisher Scientific, Dreieich, Germany). Sections were thaw-mounted onto glass slides. Microscopic images were recorded with a digital microscope (VHX-5000, Keyence, Neu-Isenburg, Germany) before matrix application and after staining.

For 3D-imaging experiments, smaller pieces of the skin samples were embedded in 10% gelatin solution. After the samples were frozen, consecutive sections of 14 μm thickness were prepared as previously stated.

Matrix application was performed with an ultrafine pneumatic sprayer (SMALDIPrep, TransMIT GmbH, Giessen, Germany) as described elsewhere.[38] For positive-ion mode, 100 μL of 2,5-dihydroxybenzoic acid (DHB) solution (30 mg/mL, acetone/H_2O/trifluoroacetic acid (49.95:49.95:0.1, *v*:*v*:*v*)) was applied. Flow rate was set to 10 μL/min, and nitrogen pressure was set to 1 bar. For negative-ion mode, 400 μL of 1,5-diaminonaphthalene (DAN) solution (3.3 mg/mL, H_2O/methanol (0.1:0.9, *v*:*v*)) was applied with a flow rate of 30 μL/min.

Atmospheric-Pressure Scanning Microprobe Matrix-Assisted Laser Desorption/Ionization Mass Spectrometry Imaging (AP-SMALDI MSI) Analysis. For AP-SMALDI MSI analyses, an orbital trapping mass spectrometer (Q Exactive HF, Thermo Fisher Scientific, Bremen, Germany) was used in combination with a high-resolution MS imaging ion source (AP-SMALDI^5 AF, TransMIT GmbH, Giessen, Germany). Instrumental settings are described in Table S2. Pixel size was set to 5 μm. The instrument was freshly calibrated prior to each measurement. Therefore, a blank glass slide spray coated with DHB solution was used. Matrix-cluster ions used for mass calibration are listed in Table S2. Measurements were performed in triplicate for each sample type (infected neck, infected shoulder, infected elbow, control1, control2).

Ultrahigh-Resolution AP-SMALDI MSI Analysis. For ultrahigh-resolution experiments (2 μm pixel size), a prototype ion-source from TransMIT, coupled to a Q Exactive mass spectrometer, was used. The same settings as those for higher pixel sizes were chosen.

On Tissue MS/MS Analysis. On tissue MS/MS experiments were performed with the same instrument settings on an Orbitrap Exploris 480 mass spectrometer (Thermo Fisher Scientific, Bremen, Germany) equipped with an AP-SMALDI^5 AF ion source. To achieve sufficient signal intensity, pixel sizes were increased from 5 to 20 μm and the so-called full-pixel mode was used to ablate the whole pixel area. Ions were chosen after statistical processing (see below) and loaded via an inclusion list into the method. Top 5 ions were fragmentated, and the normalized collision energy was set to 20.

Hematoxylin and Eosin (H&E) Staining. Tissue sections were rinsed with ethanol to wash off the matrix. Afterward, sections were gradually rehydrated in 100%, 70%, and 40% ethanol and deionized water (2 min, each). Then, samples were stained with hematoxylin solution for 12 min, blued for 10 min in tap water, and washed in deionized water for 5 min. After 1 min of incubation in eosin y solution, samples were dehydrated in deionized water, 40%, 70%, and 100% ethanol

https://doi.org/10.1021/jasms.4c00466
J. Am. Soc. Mass Spectrom. 2025, 36, 1017−1026

and xylene for 2 min each. Finally, samples were covered with Eukitt and a glass coverslip. H&E staining was used for infection confirmation.

Data Analysis. For quick visualization and annotation, data were uploaded to Metaspace.[39] All annotated signals (FDR = 10%, found in at least one of these databases: HMDB,[40] Lipid Maps,[41] SwissLipids,[42] Core Metabolome Database) were exported and used to compute summed signal intensity lists with Mirion.[43] Subsequently, summed signal intensities of the three groups (infected, control1, and control2) were compared using MetaboAnalyst.[44] No filtering was applied. Data were normalized row-wise to a constant sum and transformed by log10 normalization. Then, principal component analysis (PCA) was performed. In order to find statistically significant differences, analysis of variance (ANOVA) with $p \leq 0.05$ followed by Tukey's post hoc test was conducted.

MS Image Generation. Infection markers, significantly altered in signal intensities, were selected to create MS images with Mirion. Respective distribution patterns were examined manually, and red-green-blue (RGB) overlay images were created.

3D Reconstruction. For three-dimensional reconstruction, measurements of 28 consecutive tissue sections were performed in positive-ion mode on the same instrument with the same settings as those for the 5 μm pixel size experiments. However, according to a section thickness of 14 μm, a pixel size of 14 μm was chosen, creating cubic voxels. Each measurement consisted of 50 × 50 pixels, leading to an analyzed area of 700 × 700 μm^2 and being large enough to contain several cysts while keeping the measurement time in an affordable scope. All data were loaded into M2aia software.[4] According to previous measurements, the ion signal at m/z 824.56, annotated as either phosphatidylethanolamine (PE) $[PE\ P\text{-}42{:}7 + Na]^+$ or more probably phosphatidylcholine (PC) $[PC\ 36{:}2 + K]^+$, was chosen for cyst visualization because it was found in the whole tissue but with higher intensities inside the cysts. After TIC normalization, all 28 individual ion images were created and stacked as well as aligned in M2aia, leading to a three-dimensional reconstruction.

Parasite Stage Comparison. Lipids and metabolites, significantly altered in signal intensities due to the presence of *B. besnoiti* bradyzoites, were compared with tachyzoite markers derived from an *in vitro* study, described in a previous publication.[34] Measurements from three tachyzoite replicates were stitched using Mirion and uploaded to Metaspace. Since the tachyzoite samples consisted of isolated parasites, all detected signals were regarded as marker signals for tachyzoites. A list containing all annotations (FDR = 10%, HMDB) was generated and compared manually with the bradyzoites markers.

RESULTS AND DISCUSSION

Visualization of Large Intradermal *B. besnoiti*-Tissue Cysts. Based on an average diameter of 200 μm,[20] most intradermal cysts are macroscopically visible without any further visual aids. In the current study, skin cryosections of naturally *B. besnoiti*-infected cattle were H&E stained prior to any further analysis to assess cyst burden and quality. As illustrated in Figure 1, this animal was severely infected with *B. besnoiti* tissue cysts which were highly abundant in the skin sample, remained intact, and did not show any artifactual loss of content due to sample processing or tissue degeneration.

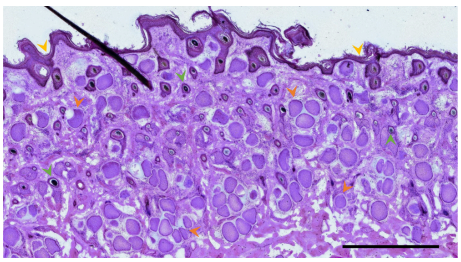

Figure 1. H&E-stained freshly prepared cryosection. *Besnoitia besnoiti* bradyzoite-containing skin cysts of different sizes and shapes are easily recognizable (examples indicated by orange arrowheads). Other relevant structures, used for comparison of optical and corresponding MS images, are hair follicles (examples indicated by green arrowheads) and the epidermis (yellow arrowheads). Scale bar is 1 mm.

H&E staining also verified that the two control animals showed no tissue cysts (see Figure S1) and were noninfected with *B. besnoiti*.

We used skin samples from three different parts of one naturally *B. besnoiti*-infected animal: from the neck, the shoulder, and the elbow (see Figure 2). While the neck and shoulder samples had a high cyst burden, only a few cysts were found in the elbow sections. Results among these three groups were comparable. This is reasonable because they all originated from the same animal, allowing for comparison between high and low cyst-burden areas.

MSI analysis of *B. besnoiti*-infected bovine skin tissue and statistical analysis of signal intensities in comparison to control tissue revealed several infection-induced changes with statistical significance. PCA plot and dendrogram can be found in Figure S2. Since MSI preserves the spatial information, detected ions can be attributed to either host tissue, cyst walls, or cyst content. Overall, 552 ions affected by *B. besnoiti* infection were found, 273 of which were detected in positive-ion mode and 279, in negative-ion mode. However, some species were found in both positive- and negative-ion modes due to adduct formation. For example, LysoPE (18:1) contributed four times to the total number of relevant ions: it was found in positive-ion mode as $+H^+$, $+K^+$ and $+Na^+$ adducts and additionally in negative-ion mode as a deprotonated ion. In total, 36 molecules were detected as several positive adducts, and 23 molecules were detected in positive- as well as negative-ion mode. By correcting this artifact, a total of 467 unique compounds were found that are influenced by parasitic infection, with most of them being lipids. We analyzed all 552 ions without further differentiation of adduct-related duplicates. A list of all annotated analytes can be found in an additional data sheet in the Supporting Information (color coding: green, individual compounds; yellow, adduct- or both-ion-mode-related duplicates); few examples with interesting lateral distributions are in Table 1. There were no statistically significant differences in the lipid level between the infected samples from three different parts of the animal. With on-tissue MS/MS, we were able to identify 18 ions, 9 in positive- and 9 in negative-ion mode, by detecting at least the headgroup of the phospholipid, enabling the differentiation between isomeric phospholipids such as PCs and PEs. An example

https://doi.org/10.1021/jasms.4c00466
J. Am. Soc. Mass Spectrom. 2025, 36, 1017−1026

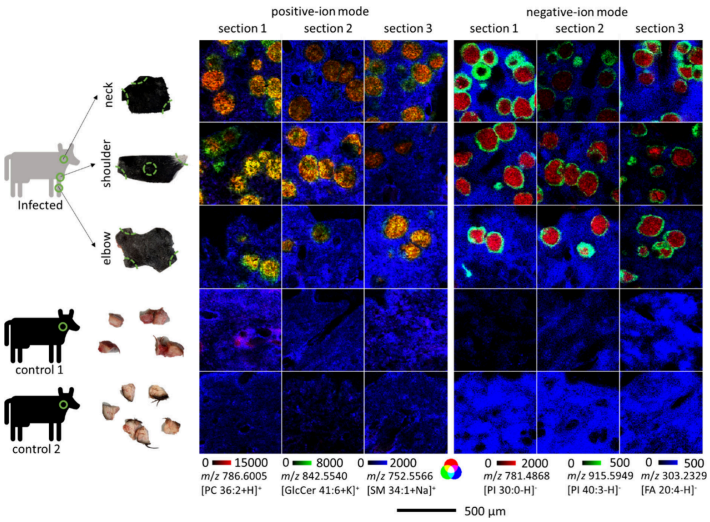

Figure 2. Scheme of the sample origin and resulting ion images of selected markers. *B. besnoiti*-infected samples originated from three different parts of one infected animal: the neck, shoulder, and elbow. Cryosections of 20 μm thickness were prepared from three different sections per skin part, as illustrated with dotted green lines. For comparison, neck samples from two healthy control animals were analyzed in the same manner. MS experiments were performed in positive- and negative-ion mode. For positive-ion mode, m/z 786.6005, annotated as PC 36:2, $[C_{44}H_{84}NO_8P + H]^+$, shown in red, m/z 842.5540, annotated as GlcCer 41:6, $[C_{47}H_{81}NO_9 + K]^+$, shown in green, and m/z 725.5566, annotated as SM 34:1, $[C_{39}H_{79}N_2O_6P + Na]^+$, shown in blue, were overlaid. For negative-ion mode, m/z 781.4868, annotated as PI 30:0, $[C_{39}H_{75}O_{13}P - H]^-$, shown in red, m/z 915.5949, annotated as PI 40:3, $[C_{49}H_{89}O_{13}P - H]^-$, shown in green, and m/z 303.2329, annotated as FA 20:4, $[C_{20}H_{32}O_2 - H]^-$, shown in blue, were overlaid. Intensities were adjusted to the same intensity levels for all of the MS images shown. Scale bar applies to all MS images.

Table 1. Examples of Ions Found with Significantly Different Signal Intensities When Comparing Infected Samples with Control Samples with Characteristic Lateral Distributions

exemp. annotation	mol. class	formula	add.	m/z meas.	structure	MS/MS	found in Tachyzoites?
Glucose phosphate	COH	$C_6H_{13}O_9P$	$[M - H]^-$	259.0224	higher in cysts	phosphate group	
FA(18:1)	FA	$C_{18}H_{34}O_2$	$[M - H]^-$	281.2486	higher in cysts		
Acetylglucosamine sulfate	COH	$C_8H_{15}NO_9S$	$[M - H]^-$	300.0395	walls		
FA(20:4)	FA	$C_{20}H_{32}O_2$	$[M - H]^-$	303.2330	surrounding tissue		
Fructose bisphosphate	COH	$C_6H_{14}O_{12}P_2$	$[M - H]^-$	338.9888	cysts		
Oleoylcarnitine	carnitine	$C_{25}H_{47}NO_4$	$[M + H]^+$	426.3578	higher in walls		
LysoPC(18:1)	LysoPC	$C_{26}H_{52}NO_7P$	$[M + H]^+$	522.3554	higher in cysts		yes
DG(14:0_18:1_0:0)	DG	$C_{35}H_{66}O_5$	$[M + K]^+$	605.4542	cysts		
SM(d18:1_14:0)	SM	$C_{37}H_{75}N_2O_6P$	$[M + H]^+$	675.5436	surrounding tissue		
PC(14:0_18:1)	PC	$C_{40}H_{78}NO_8P$	$[M + H]^+$	732.5538	higher in cysts	PC 32:1	yes
PC(14:0_20:1)	PC	$C_{42}H_{82}NO_8P$	$[M + H]^+$	760.5851	higher in cysts	PC 34:1	yes
PI(16:0_14:0)	PI	$C_{39}H_{75}O_{13}P$	$[M - H]^-$	781.4873	cysts	Kadesch: PI	
PC(18:1_18:1)	PC	$C_{44}H_{84}NO_8P$	$[M + H]^+$	786.6007	higher in cysts	PC 36:2	yes
PC(14:0_20:1)	PC	$C_{42}H_{82}NO_8P$	$[M + K]^+$	798.5410	higher in walls	PC 34:1	
PC(18:1_18:1)	PC	$C_{44}H_{84}NO_8P$	$[M + K]^+$	824.5566	higher in cysts	PC 36:2	
GlcCer(iso-t17:0_24:6)	GlcCer	$C_{47}H_{81}NO_9$	$[M + K]^+$	842.5543	higher in walls		
PI(18:3_22:0)	PI	$C_{49}H_{89}O_{13}P$	$[M - H]^-$	915.5968	walls	Kadesch: PI	

can be seen in Figure S3, identifying m/z 671.4654 as phosphatidic acid (PA) (16:0_18:2). However, potential in-source fragmentation cannot be excluded. Therefore, the headgroup might have also lost an ethanolamine or serine group prior to intentional fragmentation. For corresponding fragment ions, see Table S3.

Interpretation of our data is challenging since little is known about *B. besnoiti* infection and host−parasite interaction on the lipidomic and metabolic level. However, other parasites from the same family Sarcocystidae (e.g., *Toxoplasma gondii* and *Neospora caninum*) and the same subphylum Apicomplexa (e.g., *Plasmodium falciparum*) that have been studied in more detail can serve as a basis for careful speculation. It is well-

https://doi.org/10.1021/jasms.4c00466
J. Am. Soc. Mass Spectrom. 2025, 36, 1017−1026

known that apicomplexan parasites scavenge several molecular classes from their host cells for intracellular development. For example, Apicomplexa are generally considered as defective in cholesterol synthesis and have to scavenge cholesterol from their host cells for successful replication.[45] Consequently, most of the altered lipids identified here likely originated from the host and were not produced by the parasite itself. Due to its obligatory intracellular lifestyle within a PV and enclosed by a cyst wall, the parasite has no direct access to extracellular molecule sources and therefore satisfies its need from the host cell.[46,47] Besides other molecule classes, apicomplexan parasites scavenge host lipids, as reported for phospholipids, fatty acids, and cholesterol in *T. gondii*.[48,49] Likewise, *B. besnoiti* tachyzoites were recently shown to drive host cellular cholesterol biosynthesis and to profit from enhanced availability of exogenous lipid sources.[47] Therefore, we here expected to detect parasite-infection-driven changes in lipid signals. On the other hand, related apicomplexan parasites like *T. gondii* and *P. falciparum* synthesize PCs by themselves during intracellular development,[50,51] which aligns well with our results since several PCs were found inside the parasitic cysts.

Figure 2 nicely reflects that we were able to visualize *B. besnoiti*-formed cysts inside the tissue using AP-SMALDI MSI. By using simple statistics, we also found differences in signal intensities: Except for the sphingomyelin (SM) 34:1 (blue ion channel in positive-ion mode), all ions shown in Figure 2 were found to have significant intensity changes when comparing infected samples to controls. However, results can only be tentative, since only one infected animal was studied ($n = 1$), as it is extremely difficult to access fresh samples from infected animals in Germany. Cyst burden was different in the three regions (higher cyst load in the neck and shoulder samples than in the elbow sample), but there were no significant differences in the lipid level between these three groups.

Additionally, Figure 2 shows that some of the lipids and metabolites varied not only in signal intensities but also in lateral distribution. For example, the red ion channel was chosen to represent an ion mainly found inside the cysts, while the green ion channel was chosen to represent an ion mainly found in the cyst walls or the outer part of the cysts. In contrast, the ion shown in blue was barely found inside the cysts, more reflecting the surrounding tissue. In total, the ion distribution patterns differed based on presence or absence and increase or depletion in the cyst center, the cyst walls, or the surrounding tissue. Some additional examples for positive- and negative-ion modes are shown in Figure 3.

Taking a deeper look into these ion signals reveals interesting findings. For example, the ion shown in Figure 3C was annotated as fructosebisphosphate (or other isomers, like glucosebisphosphate). It was found only inside the cysts and is an intermediate in glycolysis. Taubert et al. showed that *B. besnoiti* tachyzoite infection led to upregulation of glycolysis in host cells to fulfill the high energy needs of the replicating parasite.[52] Even when bradyzoites are the slow-replicating stage of the parasite, it is interesting to see that they seem to perform glycolysis on their own, since the intermediate is not found in the host tissue but only in the parasitic tissue. Also, another intermediate of glycolysis, glucose phosphate, was found in the MS imaging experiments. This metabolite was found to be present in the whole tissue but with higher intensities inside the cysts.

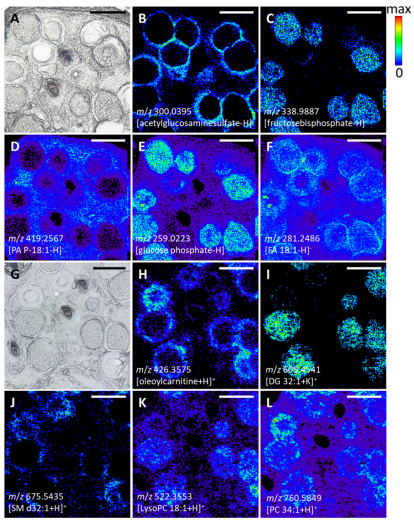

Figure 3. Morphological structures induced by *B. besnoiti* parasite infection, as represented by selected ion signals in the MS images in comparison with the microscopic images. (A, G) Corresponding light microscopic images taken prior to the measurements. (B) m/z 300.0395, annotated as acetylglucosaminesulfate, $[C_8H_{15}NO_9S - H]^-$, representing the walls of the parasite-induced cysts; (C) m/z 338.9887, annotated as fructosebisphosphate, $[C_6H_{14}O_{12}P_2 - H]^-$, representing the contents of the parasite-induced cysts; (D) m/z 419.2567, annotated as PA P-18:1, $[C_{21}H_{41}O_6P - H]^-$, being present in the whole tissue section but depleted inside the cysts; (E) m/z 259.0223, annotated as glucose phosphate, $[C_6H_{13}O_9P - H]^-$, being present in the whole tissue section but enriched inside the cysts; (F) m/z 281.2486, annotated as FA 18:1, $[C_{18}H_{34}O_2 - H]^-$, being present in the whole tissue section but enriched in the cyst walls; (H) m/z 426.3575, annotated as oleoylcarnitine, $[C_{22}H_{44}NO_6P + H]^+$, representing the walls of the parasite-induced cysts; (I) m/z 605.4541, annotated as DG 32:1, $[C_{35}H_{66}O_5 + K]^+$, representing the content of the parasite-induced cysts; (J) m/z 675.5435, annotated as SM d32:1, $[C_{37}H_{75}N_2O_6P + H]^+$, being present in the whole tissue section but depleted inside the cysts; (K) m/z 522.3553, annotated as LysoPC 18:1, $[C_{26}H_{52}NO_7P + H]^+$, being present in the whole tissue section but enriched inside the cysts; (L) m/z 760.5849, annotated as PC 34:1, $[C_{42}H_{82}NO_8P + H]^+$, being present in the whole tissue section but enriched in the cyst walls. Scale bars: 200 μm.

The enrichment of the fatty acid (FA) 18:1 in the cyst walls (Figure 3F) and also FA 16:1 (not shown) can be a hint that these fatty acids are needed by the parasite for proliferation. However, the ions detected there can also be an artifact of the ionization process. We cannot exclude that they are fragmentation products, originating from phospholipids containing these fatty acid chains. Phospholipids in general are the main compounds of cell membranes, and parasitic cysts are mainly composed of one extremely enlarged host cell. Therefore, at least the outer parts of the cyst walls are composed of the former host cell membrane. On the other hand, FA 20:4 was mainly found in the surrounding tissue, but neither inside the cysts nor the cyst walls (see blue ion channel of negative-ion MS images in Figure 2).

https://doi.org/10.1021/jasms.4c00466
J. Am. Soc. Mass Spectrom. 2025, 36, 1017−1026

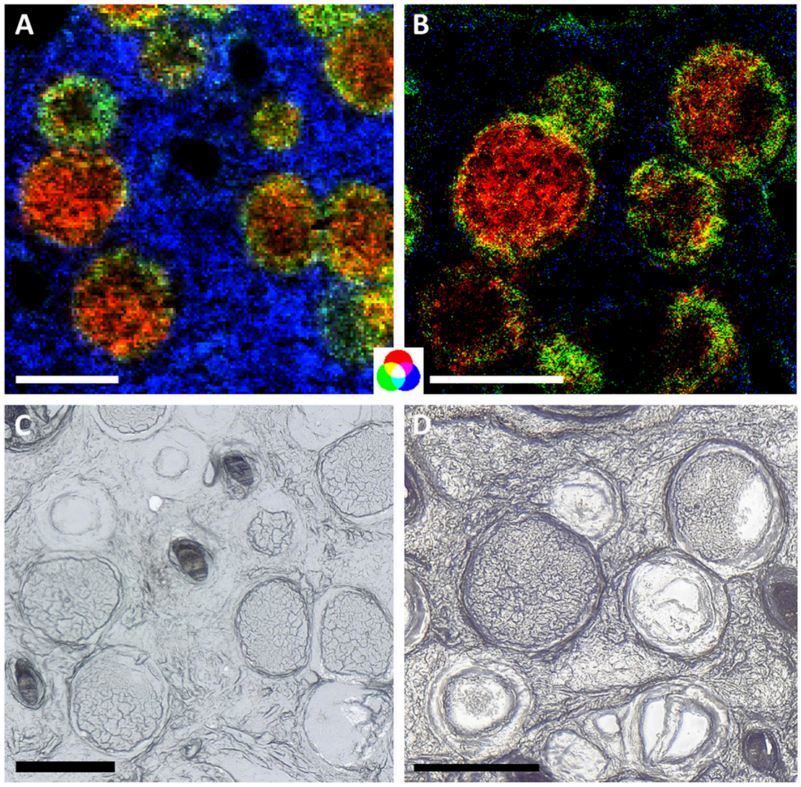

Figure 4. Improvement of the image quality when changing from 5 to 2 μm pixel size. m/z 732.5539, identified as PC 32:1 $[C_{40}H_{78}NO_8P + H]^+$, shown in red; m/z 798.5408, identified as PC 34:1 $[C_{42}H_{82}NO_8P + K]^+$, shown in green; and m/z 725.5566, annotated as SM 34:1 $[C_{39}H_{79}N_2O_6P + Na]^+$, shown in blue. (A) *B. besnoiti*-infected skin tissue, measured with a 5 μm pixel size. (B) *B. besnoiti*-infected skin tissue, measured with 2 μm pixel size. The same ion channels were used to generate both images; however, signals are not adjusted to the same intensity scale. (C, D) Corresponding optical images. Scale bars are 200 μm.

Ultrahigh-Resolution MS Imaging. Given the fact that, especially the cyst walls are thin structures of only a few micrometer thickness, we conducted ultrahigh-resolution MS imaging experiments on infected tissue samples. One example is shown in Figure 4. The left-hand side (A) shows infected tissue measured with 5 μm pixel size, and the right-hand side (B) shows a neighboring section measured with 2 μm pixel size. Both images show the same ions with the same color code. We did not find any additional metabolites specifically located in the cyst walls using a higher lateral resolution. This might be due to the lower signal intensities resulting from the smaller ablation spot size. Observed signal intensities were 20 to 40 times lower when reducing the laser spot area. Additionally, with smaller laser ablation spots, the total number of spots per analyzed area also increased. To visualize an appropriate area, we moved from 150 × 150 pixels (5 μm) to 300 × 300 pixels (2 μm). Therefore, the measurement time increased from 4 h (5 μm) to 15.5 h (2 μm) per sample. Also, we were not able to differentiate further between the different layers of the cyst walls. However, we were still able to detect known signals with sufficient signal intensities. As can be seen, the resulting images have a higher image quality in terms of structural details than the ones with 5 μm pixel size. Additionally, slight differences in ion distributions were found. While the ions of the red channel seem to be distributed nearly uniformly inside the cysts in Figure 4A, the higher resolution reveals slightly different distributions in Figure 4B. They do not seem to be uniformly spread but are more scattered. Looking at the corresponding optical image, the cysts seem to contain some cracks and might have shrunk during storage at −80 °C, resulting in inhomogeneous parasite and ion signal distributions.

The ultrahigh-resolution images better resolved the connecting area between the cyst content and the cyst wall. In Figure 4, the cyst content is mainly represented by the ion shown in red, while the cyst walls are represented by the ion shown in green. If both ions are found in one pixel, the overlap of the red and green ion channels results in a yellow pixel. In

https://doi.org/10.1021/jasms.4c00466
J. Am. Soc. Mass Spectrom. 2025, 36, 1017−1026

the less resolved ion image in Figure 4A (5 μm pixel size), many pixels on the cyst borders are yellow, indicating an overlap of green and red. In contrast, the ultrahigh-resolution ion image in Figure 4B (2 μm pixel size) contains only a few yellow pixels, while most pixels of the borders are clearly dedicated to either green or red.

Both filled and empty cysts are visible in the optical images. The empty cysts are thought to be preparational artifacts created during the cryosection process. We assume that only the outer cyst wall remained in the tissue section in these cases, and imperfect sample preparation leading to artifacts, in fact, gave us the opportunity to further study the composition of the walls. *B. besnoiti*-cyst walls are of high importance when it comes to studying new drug targets, since they are the connection between host and parasite stages (i.e., bradyzoites). One example, also found in the cyst walls of filled cysts but especially in the remainders of empty cysts, is the potassium adduct of PC(34:1), shown in green in Figure 4. Other examples for possible enrichment in the cyst walls can be found in Figure S4. One of these examples is the signal annotated as glucosyl ceramide (GlcCer) 41:6 in Figure S4B. Glucosyl ceramides as well as galactosyl ceramides are known to be present in the outer part of the lipid bilayer of cell walls,[53] so it is reasonable to find them in the leftovers of a cyst.

3D Reconstruction. To gain deeper insights into the three-dimensional structures of the cysts inside the skin, two 3D reconstructions of m/z 798.5 and m/z 824.5 were created (Supporting Information Videos 1 and 2, respectively). This is especially helpful to examine the orientation of the cysts relative to each other. As already seen in the skin sections, the cysts seem to be grouped together. This is confirmed by the 3D view acquired from a set of 28 consecutive section measurements, each of them having a thickness and pixel size of 14 μm. Whether the cysts interact with each other has to be examined in further studies.

Parasite Stage Comparison. The life cycle of *B. besnoitia* includes two different parasite stages in the intermediate host (for example, bovines). As such, during acute besnoitiosis, tachyzoite stages rapidly proliferate intracellularly, while the chronicity of infection is characterized by a slow replication process of bradyzoites within tissue cysts. Overall, it is well documented that apicomplexan tachyzoite and bradyzoite stages differ significantly in their antigenic[54,55] and metabolic repertoire.[56,57] Hence, the differential replication behavior of the parasite stages is also reflected in their metabolic activities. As such, *T. gondii* switches from aerobic respiration to mostly anaerobic metabolic pathways when converting from tachyzoites to bradyzoites.[56,57]

The current study revealed a total of 552 ion signals significantly changed in ion abundance in *B. besnoiti* cyst-infected skin tissue considering a mass range of m/z 250–1000. It is very difficult to isolate a sufficient number of bradyzoites from the cysts for MSI measurements. It relies on separation from the freshest skin samples directly after collection of the samples, which was impossible in this case. However, the conservation protocol used for the samples allowed us to analyze bradyzoites inside their cysts and within the host tissue. This is as close as possible to the *in vivo* situation and opened the opportunity to study host–parasite interactions in addition to the lipid profile of bradyzoites alone.

In a previous study, Kadesch et al. analyzed primary bovine endothelial host cell cultures infected with tachyzoite stages by AP-SMALDI MSI in a mass range from m/z 500 to 2000.[34] They applied a pixel size of 10 μm and DHB as a matrix in positive-ion mode. Referring to these MSI data, we here compared changes driven by tachyzoite (Kadesch et al.) and bradyzoite (current study) infections. Overall, 82 ions that were found to be significantly changed in signal intensity in bradyzoite-containing skin measurements were also detected in tachyzoite-infected cell layers. Overall, there was no distinct lipid group found, being specific either for bradyzoite or tachyzoite infection. Many overlapping markers were found enriched in *B. besnoiti* cysts, suggesting that these compounds may either be needed for parasite development or metabolism and that related pathways may therefore be preserved. Interestingly, in negative-ion mode, there were also seven ions ((phosphatidylinositols (PI) PI(38:2), PI(38:4), PI(38:5), PE(38:4), PE-Cer(d44:1), CerP(d44:2), and PC-(dO-36:4), all deprotonated) found in the tachyzoite measurements, present only outside the cysts or maybe in the cyst walls, but none found in the cyst content in the bradyzoite measurements.

All cyst-content-related markers in the m/z range of 500–1000 were also present in pure tachyzoites, except for the phosphatidylserine (PS) PS44:10. The almost perfect overlap between tachyzoite and bradyzoite infection-derived signals may result from the fact that the tachyzoite stage converts into the bradyzoite stage and vice versa; thus, the chemical composition of lipids and smaller metabolites may grossly be preserved. At least for *T. gondii*, tachyzoites and bradyzoites do not differ much in their structural composition;[58] therefore, for *B. besnoiti* stages, molecular compositions should also be quite similar.

Overall, the most abundant lipid species found in *B. besnoiti* cyst-infected skin were PAs, PSs, PCs/PEs, TGs, PIs, and phopsphatidylglycerols (PGs) (see Figure S5). While little is known about *B. besnoiti*-mediated lipid requirements or compositions, data on *Plasmodium* erythrocyte infection also indicated elevated levels of PC, PE, and PA compared to noninfected cells.[51] In *T. gondii* tachyzoites, PCs, PEs, PSs, and PIs were the most abundant phospholipids.[59] Also, Welti et al. found PCs, PE-Cers, and PAs enriched in *T. gondii* compared to host cells.[60] Additionally, Kadesch et al. mainly found PCs and PIs as infection markers for *T. gondii* and *B. besnoiti* tachyzoites,[34] fitting well to our recent data.

CONCLUSION

We were able to study the cyst-forming parasite *B. besnoiti* and its host in parallel using AP-SMALDI MSI. With database annotation and statistical analysis, we discovered 552 *B. besnoiti* infection-related ion signatures in the skin of cattle. The comparison of deduced MS images with corresponding light microscopic images allowed for the direct assignment of molecules to characteristic biological structures such as cyst compartments. Only minimal sample preparation had to be applied, enabling the analysis of delicate material, such as bradyzoites. In this study, we analyzed *B. besnoiti* cyst-infected skin tissue *ex vivo* and therefore addressed the chronic phase of disease with bradyzoite stages. To the best of our knowledge, this is the first *ex vivo* study of *B. besnoiti* bradyzoites using the MALDI MSI methodology. As expected, a plethora of metabolites matched previous data from *B. besnoiti* tachyzoite stages, which were obtained from *in vitro* cultures. Additionally, we employed ultrahigh-resolution MSI to further differentiate between biological structures. Also, we were able to identify

https://doi.org/10.1021/jasms.4c00466
J. Am. Soc. Mass Spectrom. 2025, 36, 1017–1026

some of the annotated ions by on-tissue MALDI MS/MS. Finally, we created a 3D reconstruction, showing the cysts inside the skin and their spatial orientation to each other.

Expanding the method to other substance classes and metabolites will further broaden our knowledge of the metabolism and composition of this neglected parasite.

In summary, we successfully implemented a novel AP-SMALDI MS-based method and applied it to a host−parasite tissue model. Further analyses are needed to elucidate the stage-specific substance requirements of this understudied parasite species.

Limitations of the Study. Please note that most compounds were only annotated based on their accurate mass and thus might in fact be structural isomers with the same elemental composition. For unambiguous identification, liquid chromatography combined with tandem mass spectrometry from homogenized neighboring tissue sections is needed in future experiments, further supported by comparison to reference standards.

Validation of results from different individuals ($n > 1$) was not yet possible due to unavailability of material. We are convinced, however, that the generated data are nevertheless a useful basis for future research on *B. besnoiti*-infected skin.

■ ASSOCIATED CONTENT

Supporting Information

The Supporting Information is available free of charge at https://pubs.acs.org/doi/10.1021/jasms.4c00466.

Used chemicals, instrument settings, PCA and dendrogram of statistical analysis, additional MS images, and pie chart of found lipid species (PDF)

List of altered ions (XLSX)

Video 1 of 3D reconstruction, m/z 798.5 (MP4)

Video 2 of 3D reconstruction, m/z 824.5 (MP4)

■ AUTHOR INFORMATION

Corresponding Authors

Liliana M. R. Silva − *Institute of Parasitology, Justus Liebig University Giessen, 35392 Giessen, Germany; Egas Moniz Center for Interdisciplinary Research (CiiEM), Egas Moniz School of Health & Science, 2829-511 Caparica, Almada, Portugal; MED − Mediterranean Institute for Agriculture, Environment and Development & CHANGE − Global Change and Sustainability Institute, Universidade de Évora, 7006-554 Évora, Portugal*; Email: liliana.silva@vetmed.uni-giessen.de

Bernhard Spengler − *Institute of Inorganic and Analytical Chemistry, Justus Liebig University Giessen, 35392 Giessen, Germany*; orcid.org/0000-0003-0179-5653; Phone: +49 641 99-34800; Email: bernhard.spengler@anorg.chemie.uni-giessen.de; Fax: +49 641 99-34809

Authors

Katja R. Wiedemann − *Institute of Inorganic and Analytical Chemistry, Justus Liebig University Giessen, 35392 Giessen, Germany*; orcid.org/0000-0003-2145-9868

Stefanie Gerbig − *Institute of Inorganic and Analytical Chemistry, Justus Liebig University Giessen, 35392 Giessen, Germany*

Parviz Ghezellou − *Institute of Inorganic and Analytical Chemistry, Justus Liebig University Giessen, 35392 Giessen, Germany*

Alejandra Pilgram − *Institute of Inorganic and Analytical Chemistry, Justus Liebig University Giessen, 35392 Giessen, Germany*

Carlos Hermosilla − *Institute of Parasitology, Justus Liebig University Giessen, 35392 Giessen, Germany*

Anja Taubert − *Institute of Parasitology, Justus Liebig University Giessen, 35392 Giessen, Germany*

Complete contact information is available at: https://pubs.acs.org/10.1021/jasms.4c00466

Author Contributions

[▽]L.M.R.S. and B.S. contributed equally. Conceptualization, S.G., C.H., A.T., L.M.R.S. and B.S.; Methodology, K.R.W., S.G., P.G., A.P., L.M.R.S.; Investigation, K.R.W.; Formal Analysis, K.R.W., S.G., P.G., and A.P., Writing−Original Draft, K.R.W, S.G., P.G., and A.P.; Writing−Review & Editing, K.R.W., S.G., P.G., A.P., A.T., C.H., L.M.R.S., and B.S.; Funding Acquisition, C.H., A.T., and B.S.; Resources, L.M.R.S. and B.S.; Supervision, C.H., A.T., L.M.R.S., and B.S.

Notes

The authors declare the following competing financial interest(s): B.S. is a consultant and S.G. is a part-time employee of TransMIT GmbH, Giessen, Germany. The other authors declare to have no conflicts of interest.

■ ACKNOWLEDGMENTS

We are grateful to Professor Dr. Philippe Jacquiet, Professor of Parasitology at the National Veterinary School of Toulouse, France, for the supply of infected skin samples. We thank Jonas Cordes from the groups of Prof. Ivo Wolf and Prof. Carsten Hopf (University of Applied Sciences Mannheim) for creating the 3D-reconstructions of our imaging data. Financial support by the Hessian Ministry of Science, Higher Education and Art (HMWK), LOEWE Center DRUID, and Deutsche Forschungsgemeinschaft DFG (Sp314-23-1, INST 162/500-1 FUGG) is gratefully acknowledged.

■ REFERENCES

(1) Spengler, B.; Hubert, M.; Kaufmann, R. MALDI Ion Imaging and Biological Ion Imaging with a new Scanning UV-Laser Microprobe. In *Proceedings of the 42nd ASMS Conference on Mass Spectrometry*, 1994; p 1041.

(2) Kompauer, M.; Heiles, S.; Spengler, B. Atmospheric pressure MALDI mass spectrometry imaging of tissues and cells at 1.4-mu m lateral resolution. *Nat. Methods* **2017**, *14* (1), 90−96.

(3) Hu, Q. Z.; Noll, R. J.; Li, H. Y.; Makarov, A.; Hardman, M.; Cooks, R. G. The Orbitrap: a new mass spectrometer. *Journal of Mass Spectrometry* **2005**, *40* (4), 430−443.

(4) Marshall, A. G.; Hendrickson, C. L.; Jackson, G. S. Fourier transform ion cyclotron resonance mass spectrometry: A primer. *Mass Spectrom. Rev.* **1998**, *17* (1), 1−35.

(5) Cordes, J.; Enzlein, T.; Marsching, C.; Hinze, M.; Engelhardt, S.; Hopf, C.; Wolf, I. M^2 aia-Interactive, fast, and memory-efficient analysis of 2D and 3D multi-modal mass spectrometry imaging data. *Gigascience* **2021**, *10*, giab049.

(6) Diezma-Diaz, C.; Jimenez-Melendez, A.; Fernandez, M.; Gutierrez-Exposito, D.; Garcia-Lunar, P.; Ortega-Mora, L. M.; Perez-Salas, J. A.; Blanco-Murcia, J.; Ferre, I.; Alvarez-Garcia, G. Bovine chronic besnoitiosis in a calf: Characterization of a novel *B. besnoiti* isolate from an unusual case report. *Veterinary Parasitology* **2017**, *247*, 10−18.

(7) Langenmayer, M. C.; Gollnick, N. S.; Scharr, J. C.; Schares, G.; Herrmann, D. C.; Majzoub-Altweck, M.; Hermanns, W. *Besnoitia besnoiti* infection in cattle and mice: ultrastructural pathology in acute

and chronic besnoitiosis. *Parasitology Research* **2015**, *114* (3), 955−963.
(8) Cortes, H.; Leitao, A.; Gottstein, B.; Hemphill, A. A review on bovine besnoitiosis: a disease with economic impact in herd health management, caused by *Besnoitia besnoiti* (Franco and Borges, 1916). *Parasitology* **2014**, *141* (11), 1406−1417.
(9) Chatikobo, P.; Choga, T.; Ncube, C.; Mutambara, J. Participatory diagnosis and prioritization of constraints to cattle production in some smallholder farming areas of Zimbabwe. *Preventive Veterinary Medicine* **2013**, *109* (3−4), 327−333.
(10) Goldman, M.; Pipano, E. Serological Studies on Bovine Besnoitiosis in Israel. *Tropical Animal Health and Production* **1983**, *15* (1), 32−38.
(11) Fernandez-Garcia, A.; Risco-Castillo, V.; Pedraza-Diaz, S.; Aguado-Martinez, A.; Alvarez-Garcia, G.; Gomez-Bautista, M.; Collantes-Fernandez, E.; Ortega-Mora, L. M. First Isolation of *Besnoitia besnoiti* From a Chronically Infected Cow in Spain. *Journal of Parasitology* **2009**, *95* (2), 474−476.
(12) Alvarez-Garcia, G.; Frey, C. F.; Mora, L. M. O.; Schares, G. A century of bovine besnoitiosis: an unknown disease re-emerging in Europe. *Trends in Parasitology* **2013**, *29* (8), 407−415.
(13) European Food Safety Authority. Bovine Besnoitiosis: An emerging disease in Europe. *EFSA Journal* **2010**, *8* (2), 1499.
(14) Cortes, H.; Leitao, A.; Vidal, R.; Vila-Vicosa, M. J.; Ferreira, M. L.; Caeiro, V.; Hjerpe, C. A. Besnoitiosis in bulls in Portugal. *Veterinary Record* **2005**, *157* (9), 262−264.
(15) Sekoni, V.; Sanusi, A.; Abatan, M.; Oyedipe, E.; Rekwot, P.; Eduvie, L. Loss Of Libido And Terminal Sterility In A Friesian Bull Naturally Infected With *Besnoitia besnoiti* In Northern Nigeria - A Case-Report. *Theriogenology* **1992**, *37* (2), 533−549.
(16) Langenmayer, M. C.; Gollnick, N. S.; Majzoub-Altweck, M.; Scharr, J. C.; Schares, G.; Hermanns, W. Naturally Acquired Bovine Besnoitiosis: Histological and Immunohistochemical Findings in Acute, Subacute, and Chronic Disease. *Veterinary Pathology* **2015**, *52* (3), 476−488.
(17) Esteban-Gil, A.; Jacquiet, P.; Florentin, S.; Decaudin, A.; Berthelot, X.; Ronsin, P.; Grisez, C.; Prevot, F.; Alzieu, J. P.; Marois, M.; Corboz, N.; Peglion, M.; Vilardell, C.; Liénard, E.; Bouhsira, E.; Castillo, J. A.; Franc, M.; Picard-Hagen, N. Does bovine besnoitiosis affect the sexual function of chronically infected bulls? *Theriogenology* **2016**, *86* (5), 1325−1332.
(18) Grau-Roma, L.; Martinez, J.; Esteban-Gil, A.; Lopez, J.; Marco, A.; Majo, N.; Castillo, J.; Domingo, M. Pathological findings in genital organs of bulls naturally infected with Besnoitia besnoiti. *Parasitology Research* **2020**, *119* (7), 2257−2262.
(19) Ramakrishnan, C.; Krishnan, A.; Francisco, S.; Schmid, M. W.; Russo, G.; Leitao, A.; Hemphill, A.; Soldati-Favre, D.; Hehl, A. B. Dissection of *Besnoitia besnoiti* intermediate host life cycle stages: From morphology to gene expression. *Plos Pathogens* **2022**, *18* (11), e1010955.
(20) Gonzalez-Barrio, D.; Diezma-Diaz, C.; Gutierrez-Exposito, D.; Tabanera, E.; Jimenez-Melendez, A.; Pizarro, M.; Gonzalez-Huecas, M.; Ferre, I.; Ortega-Mora, L. M.; Alvarez-Garcia, G. Identification of molecular biomarkers associated with disease progression in the testis of bulls infected with *Besnoitia besnoiti*. *Veterinary Research* **2021**, *52* (1), 18.
(21) Mehlhorn, H.; Klimpel, S.; Schein, E.; Heydorn, A.; Al-Quraishy, S.; Selmair, J. Another African disease in Central Europa: Besnoitiosis of cattle. I. Light and electron microscopical study. *Parasitology Research* **2009**, *104* (4), 861−868.
(22) Dubey, J. P.; van Wilpe, E.; Blignaut, D. J. C.; Schares, G.; Williams, J. H. Development of Early Tissue Cysts and Associated Pathology of *Besnoitia besnoiti* in a Naturally Infected Bull (*Bos Taurus*) From South Africa. *Journal of Parasitology* **2013**, *99* (3), 459−466.
(23) Dubey, J. P.; Shkap, V.; Pipano, E.; Fish, L.; Fritz, D. L. Ultrastructure of *Besnoitia besnoiti* tissue cysts and bradyzoites. *Journal of Eukaryotic Microbiology* **2003**, *50* (4), 240−244.
(24) Fernandez-Garcia, A.; Alvarez-Garcia, G.; Marugan-Hernandez, V.; Garcia-Lunar, P.; Aguado-Martinez, A.; Risco-Castillo, V.; Ortega-Mora, L. M. Identification of *Besnoitia besnoiti* proteins that showed differences in abundance between tachyzoite and bradyzoite stages by difference gel electrophoresis. *Parasitology* **2013**, *140* (8), 999−1008.
(25) Zhou, E. S.; Silva, L. M. R.; Conejeros, I.; Velasquez, Z. D.; Hirz, M.; Gartner, U.; Jacquiet, P.; Taubert, A.; Hermosilla, C. *Besnoitia besnoiti* bradyzoite stages induce suicidal- and rapid vital-NETosis. *Parasitology* **2020**, *147* (4), 401−409.
(26) Munoz Caro, T.; Hermosilla, C.; Silva, L. M. R.; Cortes, H.; Taubert, A. Neutrophil Extracellular Traps as Innate Immune Reaction against the Emerging Apicomplexan Parasite *Besnoitia besnoiti*. *PLoS One* **2014**, *9* (3), 9.
(27) Shkap, V.; Ungarwaron, H.; Pipano, E.; Greenblatt, C. Enzyme linked immunosorbent-assay for detection of antibodies against *Besnoitia besnoiti* in cattle. *Tropical Animal Health and Production* **1984**, *16* (4), 233−238.
(28) Janitschke, K.; Devos, A. J.; Bigalke, R. D. Serodiagnosis of bovine besnoitiosis by elisa and immunofluorescence tests. *Onderstepoort Journal of Veterinary Research* **1984**, *51* (4), 239−243.
(29) García-Lunar, P.; Ortega-Mora, L.; Schares, G.; Gollnick, N.; Jacquiet, P.; Grisez, C.; Prevot, F.; Frey, C.; Gottstein, B.; Alvarez-García, G. An Inter-Laboratory Comparative Study of Serological Tools Employed in the Diagnosis of Besnoitia besnoiti Infection in Bovines. *Transboundary and Emerging Diseases* **2013**, *60* (1), 59−68.
(30) Kadesch, P.; Quack, T.; Gerbig, S.; Grevelding, C. G.; Spengler, B. Tissue- and sex-specific lipidomic analysis of *Schistosoma mansoni* using high-resolution atmospheric pressure scanning microprobe matrix-assisted laser desorption/ionization mass spectrometry imaging. *Plos Neglected Tropical Diseases* **2020**, *14* (5), e0008145.
(31) Mokosch, A. S.; Gerbig, S.; Grevelding, C. G.; Haeberlein, S.; Spengler, B. High-resolution AP-SMALDI MSI as a tool for drug imaging in *Schistosoma mansoni*. *Anal. Bioanal. Chem.* **2021**, *413* (10), 2755−2766.
(32) Morawietz, C.; Houhou, H.; Puckelwaldt, O.; Hehr, L.; Dreisbach, D.; Mokosch, A.; Roeb, E.; Roderfeld, M.; Spengler, B.; Haeberlein, S. Targeting Kinases in *Fasciola hepatica*: Anthelminthic Effects and Tissue Distribution of Selected Kinase Inhibitors. *Frontiers in Veterinary Science* **2020**, *7*, 1.
(33) Morawietz, C.; Ventura, A.; Grevelding, C.; Haeberlein, S.; Spengler, B. Spatial visualization of drug uptake and distribution in *Fasciola hepatica* using high-resolution AP-SMALDI mass spectrometry imaging. *Parasitology Research* **2022**, *121*, 1145−1153.
(34) Kadesch, P.; Hollubarsch, T.; Gerbig, S.; Schneider, L.; Silva, L. M. R.; Hermosilla, C.; Taubert, A.; Spengler, B. Intracellular Parasites *Toxoplasma gondii* and *Besnoitia besnoiti*, Unveiled in Single Host Cells Using AP-SMALDI MS Imaging. *J. Am. Soc. Mass Spectrom.* **2020**, *31* (9), 1815−1824.
(35) Luh, D.; Heiles, S.; Roderfeld, M.; Grevelding, C.; Roeb, E.; Spengler, B. Hepatic Topology of Glycosphingolipids in *Schistosoma mansoni*-Infected Hamsters. *Anal. Chem.* **2024**, *96*, 6311−6320.
(36) Wiedemann, K.; Ventura, A.; Gerbig, S.; Roderfeld, M.; Quack, T.; Grevelding, C.; Roeb, E.; Spengler, B. Changes in the lipid profile of hamster liver after *Schistosoma mansoni* infection, characterized by mass spectrometry imaging and LC-MS/MS analysis. *Anal. Bioanal. Chem.* **2022**, *414*, 3653−3665.
(37) Anschütz, N.; Gerbig, S.; Ghezellou, P.; Silva, L.; Vélez, J.; Hermosilla, C.; Taubert, A.; Spengler, B. Mass Spectrometry Imaging of *In Vitro Cryptosporidium parvum*-Infected Cells and Host Tissue. *Biomolecules* **2023**, *13*, 1200.
(38) Bouschen, W.; Schulz, O.; Eikel, D.; Spengler, B. Matrix vapor deposition/recrystallization and dedicated spray preparation for high-resolution scanning microprobe matrix-assisted laser desorption/ionization imaging mass spectrometry (SMALDI-MS) of tissue and single cells. *Rapid Commun. Mass Spectrom.* **2010**, *24* (3), 355−364.
(39) Palmer, A.; Phapale, P.; Chernyavsky, I.; Lavigne, R.; Fay, D.; Tarasov, A.; Kovalev, V.; Fuchser, J.; Nikolenko, S.; Pineau, C.; Becker, M.; Alexandrov, T. FDR-controlled metabolite annotation for

https://doi.org/10.1021/jasms.4c00466
J. Am. Soc. Mass Spectrom. 2025, 36, 1017−1026

high-resolution imaging mass spectrometry. *Nat. Methods* **2017**, *14* (1), 57−60.
(40) Wishart, D. S.; Feunang, Y. D.; Marcu, A.; Guo, A. C.; Liang, K.; Vazquez-Fresno, R.; Sajed, T.; Johnson, D.; Li, C. R.; Karu, N.; Sayeeda, Z.; Lo, E.; Assempour, N.; Berjanskii, M.; Singhal, S.; Arndt, D.; Liang, Y.; Badran, H.; Grant, J.; Serra-Cayuela, A.; Liu, Y.; Mandal, R.; Neveu, V.; Pon, A.; Knox, C.; Wilson, M.; Manach, C.; Scalbert, A. HMDB 4.0: the human metabolome database for 2018. *Nucleic Acids Res.* **2018**, *46* (D1), D608−D617.
(41) Sud, M.; Fahy, E.; Cotter, D.; Brown, A.; Dennis, E.; Glass, C.; Merrill, A.; Murphy, R.; Raetz, C.; Russell, D.; Subramaniam, S. LMSD: LIPID MAPS structure database. *Nucleic Acids Res.* **2007**, *35*, D527−D532.
(42) Aimo, L.; Liechti, R.; Hyka-Nouspikel, N.; Niknejad, A.; Gleizes, A.; Götz, L.; Kuznetsov, D.; David, F.; van der Goot, F.; Riezman, H.; Bougueleret, L.; Xenarios, I.; Bridge, A. The SwissLipids knowledgebase for lipid biology. *Bioinformatics* **2015**, *31*, 2860−2866.
(43) Paschke, C.; Leisner, A.; Hester, A.; Maass, K.; Guenther, S.; Bouschen, W.; Spengler, B. Mirion-A Software Package for Automatic Processing of Mass Spectrometric Images. *J. Am. Soc. Mass Spectrom.* **2013**, *24* (8), 1296−1306.
(44) Chong, J.; Soufan, O.; Li, C.; Caraus, I.; Li, S. Z.; Bourque, G.; Wishart, D. S.; Xia, J. G. MetaboAnalyst 4.0: towards more transparent and integrative metabolomics analysis. *Nucleic Acids Res.* **2018**, *46* (W1), W486−W494.
(45) Bansal, D.; Bhatti, H. S.; Sehgal, R. Role of cholesterol in parasitic infections. *Lipids in Health and Disease* **2005**, *4*, 10.
(46) Zuzarte-Luis, V.; Mota, M. M. Parasite Sensing of Host Nutrients and Environmental Cues. *Cell Host & Microbe* **2018**, *23* (6), 749−758.
(47) Silva, L. M. R.; Lutjohann, D.; Hamid, P.; Velasquez, Z. D.; Kerner, K.; Larrazabal, C.; Failing, K.; Hermosilla, C.; Taubert, A. *Besnoitia besnoiti* infection alters both endogenous cholesterol de novo synthesis and exogenous LDL uptake in host endothelial cells. *Sci. Rep.* **2019**, *9*, 18.
(48) Charron, A. J.; Sibley, L. D. Host cells: mobilizable lipid resources for the intracellular parasite *Toxoplasma gondii*. *Journal of Cell Science* **2002**, *115* (15), 3049−3059.
(49) Coppens, I.; Sinai, A. P.; Joiner, K. A. *Toxoplasma gondii* exploits host low-density lipoprotein receptor-mediated endocytosis for cholesterol acquisition. *J. Cell Biol.* **2000**, *149* (1), 167−180.
(50) Gupta, N.; Zahn, M. M.; Coppens, I.; Joiner, K. A.; Voelker, D. R. Selective disruption of phosphatidylcholine metabolism of the intracellular parasite *Toxoplasma gondii* arrests its growth. *J. Biol. Chem.* **2005**, *280* (16), 16345−16353.
(51) Vial, H. J.; Eldin, P.; Tielens, A. G. M.; van Hellemond, J. J. Phospholipids in parasitic protozoa. *Mol. Biochem. Parasitol.* **2003**, *126* (2), 143−154.
(52) Taubert, A.; Hermosilla, C.; Silva, L. M. R.; Wieck, A.; Failing, K.; Mazurek, S. Metabolic signatures of *Besnoitia besnoiti*-infected endothelial host cells and blockage of key metabolic pathways indicate high glycolytic and glutaminolytic needs of the parasite. *Parasitology Research* **2016**, *115* (5), 2023−2034.
(53) Reza, S.; Ugorski, M.; Suchanski, J. Glucosylceramide and galactosylceramide, small glycosphingolipids with significant impact on health and disease. *Glycobiology* **2021**, *31*, 1416−1434.
(54) Kasper, L. H.; Bradley, M. S.; Pfefferkorn, E. R. Identification of stage-specific sporozoite antigens of *Toxoplasma gondii* by monoclonal-antibodies. *J. Immunol.* **1984**, *132* (1), 443−449.
(55) Fernandez-Garcia, A.; Alvarez-Garcia, G.; Risco-Castillo, V.; Aguado-Martinez, A.; Marugan-Hernandez, V.; Ortega-Mora, L. M. Pattern of recognition of *Besnoitia besnoiti* tachyzoite and bradyzoite antigens by naturally infected cattle. *Veterinary Parasitology* **2009**, *164* (2−4), 104−110.
(56) Denton, H.; Roberts, C. W.; Alexander, J.; Thong, K. W.; Coombs, G. H. Enzymes of energy metabolism in the bradyzoites and tachyzoites of *Toxoplasma gondii*. *Fems Microbiology Letters* **1996**, *137* (1), 103−108.
(57) Wastling, J. M.; Xia, D.; Sohal, A.; Chaussepied, M.; Pain, A.; Langsley, G. Proteomes and transcriptomes of the Apicomplexa - Where's the message? *International Journal for Parasitology* **2009**, *39* (2), 135−143.
(58) Dubey, J. P.; Lindsay, D. S.; Speer, C. A. Structures of *Toxoplasma gondii* tachyzoites, bradyzoites, and sporozoites and biology and development of tissue cysts. *Clin. Microbiol. Rev.* **1998**, *11* (2), 267.
(59) Foussard, F.; Gallois, Y.; Girault, A.; Menez, J. F. Lipids and fatty acids of tachyzoites and purified pellicles of *Toxoplasma gondii*. *Parasitology Research* **1991**, *77* (6), 475−477.
(60) Welti, R.; Mui, E.; Sparks, A.; Wernimont, S.; Isaac, G.; Kirisits, M.; Roth, M.; Roberts, C. W.; Botte, C.; Marechal, E.; McLeod, R. Lipidomic analysis of *Toxoplasma gondii* reveals unusual polar lipids. *Biochemistry* **2007**, *46* (48), 13882−13890.

https://doi.org/10.1021/jasms.4c00466
J. Am. Soc. Mass Spectrom. 2025, 36, 1017−1026

3.2 Supplementary information

Mass spectrometry imaging of lipid and metabolite distributions in cysts of *Besnoitia besnoiti*-infected bovine skin

Katja R. Wiedemann[1], Stefanie Gerbig[1], Parviz Ghezellou[1], Alejandra Pilgram[1], Carlos Hermosilla[2], Anja Taubert[2], Liliana M. R. Silva[2,3,4*], Bernhard Spengler[1*]

[1]*Institute of Inorganic and Analytical Chemistry, Justus Liebig University Giessen, 35392 Giessen, Germany*
[2]*Institute of Parasitology, Justus Liebig University Giessen, 35392 Giessen, Germany*
[3]*Egas Moniz Center for Interdisciplinary Research (CiiEM); Egas Moniz School of Health & Science, 2829-511 Caparica, Almada, Portugal*
[4]*MED – Mediterranean Institute for Agriculture, Environment and Development & CHANGE – Global Change and Sustainability Institute, Universidade de Évora, 7006-554 Évora, Portugal*

* Authors to whom correspondence should be addressed, these authors contributed equally
E-Mail addresses: bernhard.spengler@anorg.chemie.uni-giessen.de; liliana.silva@vetmed.uni-giessen.de

Supporting information

Chemicals

Table S1: Used chemicals and their suppliers.

Chemical name	Quality grade	manufacturer
1,5-diaminonaphthalene	97%	Thermo Fisher, Kandel, Germany
2,5-dihydroxybenzoic acid	for synthesis	Merck, Darmstadt, Germany
acetone	HiPerSolv	VWR International, Fontenay-sous-Bois, France
Eosin Y solution		Sigma-Aldrich, Steinheim, Germany
ethanol	Uvasol	Merck, Darmstadt, Germany
Eukitt quick hardening medium		Sigma-Aldrich, Steinheim, Germany
gelatin		VWR International, Leuven, Berlgium
Mayer's hematoxylin solution		Sigma-Aldrich, Steinheim, Germany
methanol	Rotisolv HPLC gradient grade	Carl Roth, Karlsruhe, Germany
trifluoro acetic acid	Uvasol	Merck, Darmstadt, Germany
water	HiPerSolv	VWR International, Fontenay-sous-Bois, France
xylene	for analysis	Merck, Darmstadt, Germany

Table S2: Settings used for data acquisition with MALDI MSI.

Parameter	Setting
m/z	250-1000
Resolution	240,000 at *m/z* 200
Ion injection time	500 ms
Scan rate	1.6 pixel / s
Spray voltage	3 kV
Capillary temperature	250°C
Lock mass	*m/z* 585.06396 [4 DHB − 3 H_2O + Na]$^+$ in positive-ion mode; *m/z* 313.14587 [2DAN − H − H_2]$^-$ in negative-ion mode
Calibration	Positive-ion mode: *m/z* 273.03936 [2 DHB + H -2 H_2O]$^+$ *m/z* 409.05541 [3 DHB + H – 3 H_2O]$^+$ *m/z* 545.07145 [4 DHB + H – 4 H_2O]$^+$ *m/z* 681.08750 [5 DHB + H – 5 H_2O]$^+$ *m/z* 817.10354 [6 DHB + H – 6 H_20]$^+$ *m/z* 953.11958 [7 DHB + H – 7 H_2O]$^+$ Negative-ion mode: *m/z* 289.03538 [2 DHB – H – H_20]$^-$ *m/z* 329.02789 [2 DHB – 2 H + Na]$^-$ *m/z* 465.04393 [3 DHB – 2 H + Na – H_2O]$^-$ *m/z* 579.07803 [4 DHB – H- 2 H_2O]$^-$ *m/z* 715.09407 [5 DHB – H – 3 H_2O]$^-$
Pixel size	5 µm
Mode	2D pixel mode

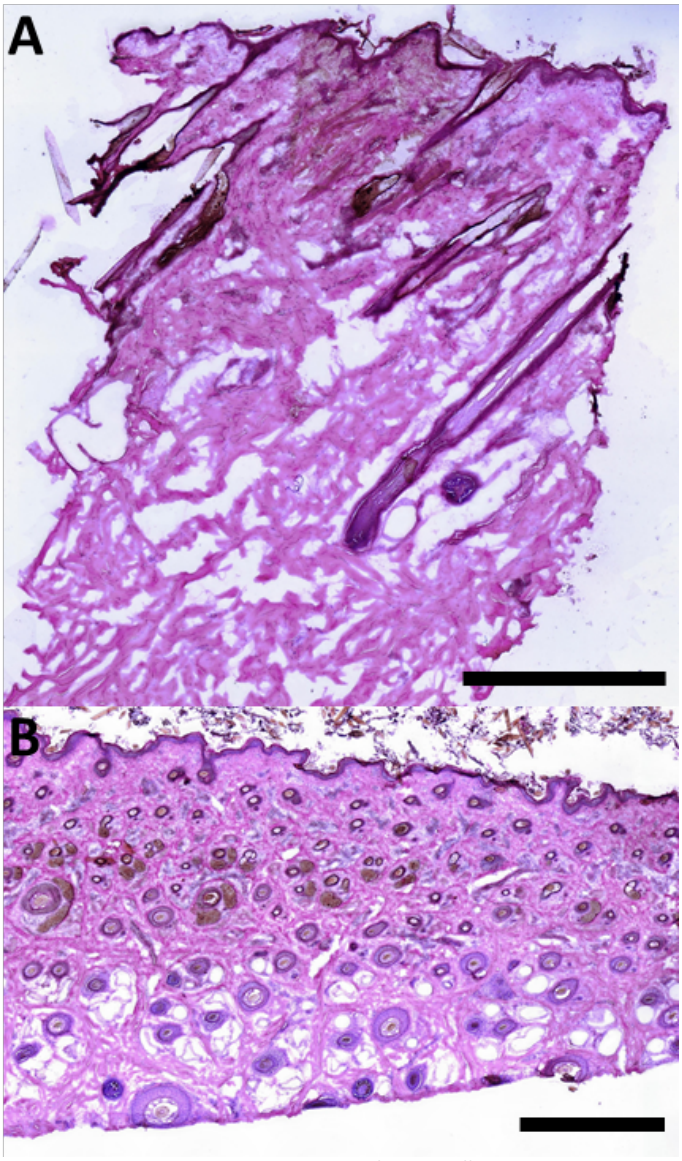

Figure S1: Representative H&E-stained tissue sections of the two different control animals. Both showed neither clinical symptoms nor tissue cysts. Scale bars are 1 mm.

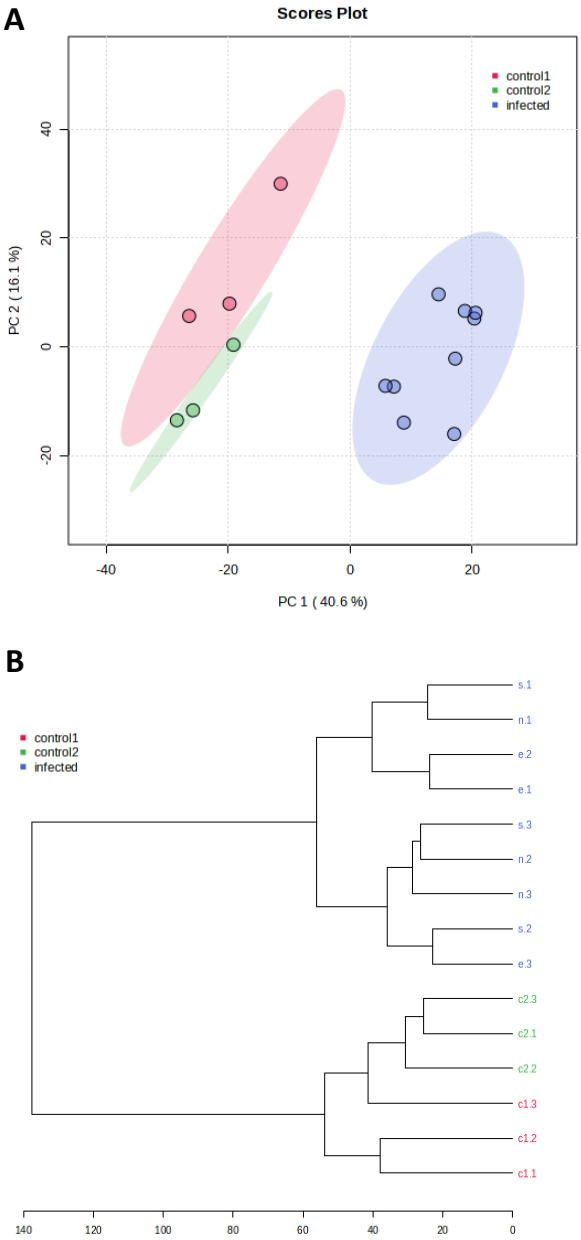

Figure S2: Results of statistical analyses. PCA (A) shows a clear separation of control samples and infected ones. Additionally, control samples cluster together, even when originating from different animals. This is also shown in the dendrogram (B).

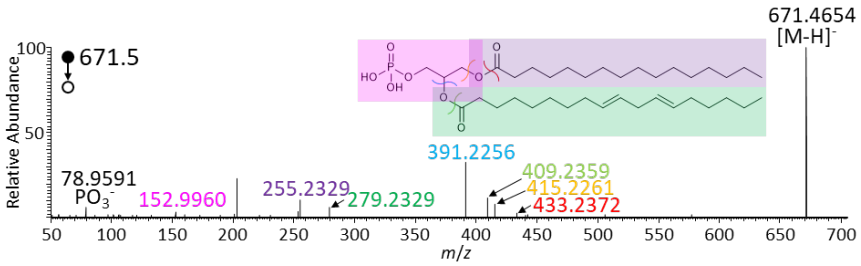

Figure S3: On-tissue tandem mass spectrum of *m/z* 671.4654, fragmented with a normalized collision energy of 20 and identified as [PA(16:0_18:2)-H]$^-$.

Table S3: Annotation of fragment ions in spectrum Figure 4.

Mass detected	Fragment ion	Theoretical mass	Deviation / ppm	Fragment
671.4654	$[C_{37}H_{69}PO_8\text{-}H]^-$	671.4652	+ 0.30	Precursor ion
433.2372	$C_{21}H_{38}PO_7^-$	433.2355	+ 3.92	Loss of FA 16:0 chain as ketene
415.2261	$C_{21}H_{36}PO_6^-$	415.2250	+ 2,65	Loss of FA 16:0
409.2359	$C_{19}H_{38}PO_7^-$	409.2355	+ 0,98	Loss of FA 18:2 chain as ketene
391.2256	$C_{19}H_{36}PO_6^-$	391.2250	+ 1,53	Loss of FA 18:2
279.2329	$[C_{18}H_{32}O_2\text{-}H]^-$	279.2324	+ 1,79	FA 18:2
255.2329	$[C_{16}H_{32}O_2\text{-}H]^-$	255.2324	+ 1,96	FA 16:0
152.9960	$C_3H_6PO_5^-$	152.9953	+ 4,58	PA head group $-H_2O$
78.9591	PO_3^-	78.9585	+ 7,60	PO_3^-

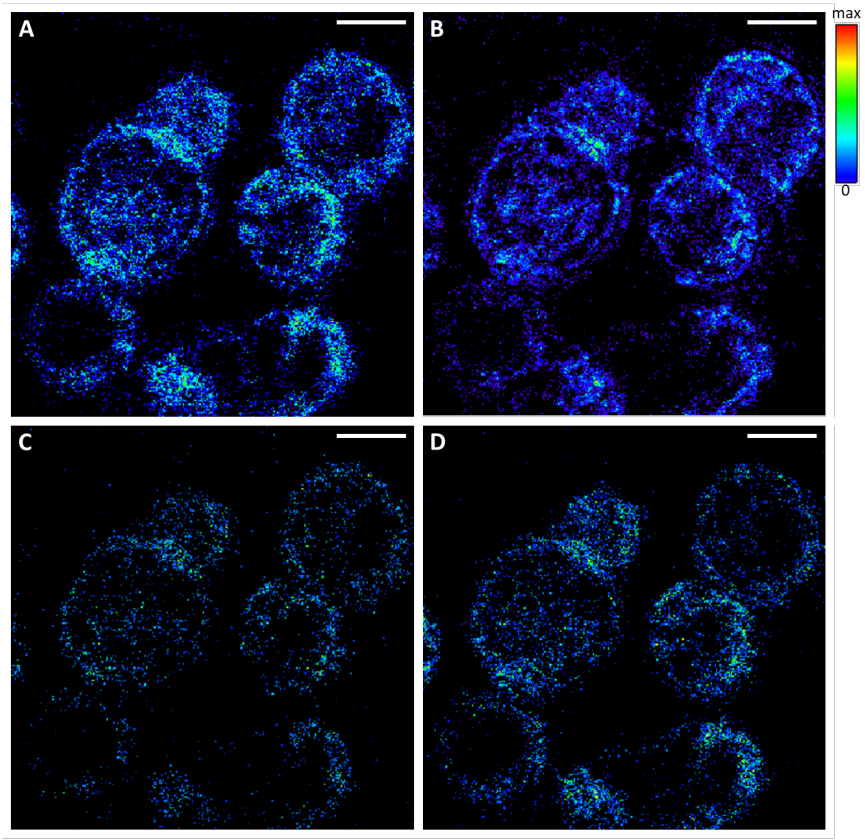

Figure S4: Examples of lipids mainly found inside the skin cysts with possible enrichment in the cyst walls. A) *m/z* 744.4942, identified as PC 30:0 [$C_{38}H_{76}NO_8P$ + K]$^+$. B) *m/z* 842.5543, annotated as GlcCer 41:6 [$C_{47}H_{81}NO_9$ + K]$^+$. C) *m/z* 728.5202, identified as PC 32:3 [$C_{40}H_{74}NO_8P$ + H]$^+$. D) *m/z* 716.4628, annotated as PC 28:0 [$C_{36}H_{72}NO_8P$ + K]$^+$. Imaging experiments were performed with 2 µm pixel size, scale bars are 100 µm. Please note that for clearness only the most probable annotation was mentioned here. All possible annotations can be found in the supplementary excel sheet ("altered ions.xlsx"). However, PC 30:0 and PC 32:3, shown in A and C, respectively, were identified by on-tissue MS/MS.

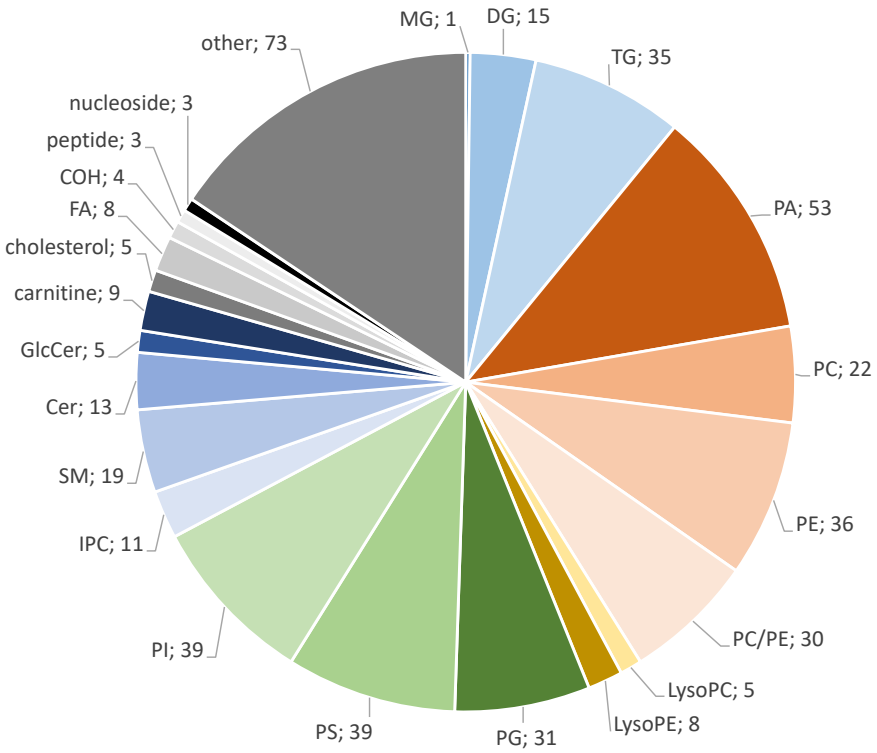

Figure S5: Substance class distribution of signals significantly changed in intensities in *B. besnoiti*-infected skin (substance class; number of species). Only one adduct was considered per species, so that species were not counted multiple times when they occurred as different adducts. MG: monoacylglycerol, DG: diacylglycerol, TG: triacylglycerol, PA: phosphatidic acid, PC: phosphatidylcholine, PE: phosphatidylethanolamine, PG: phosphatidylglycerol, PS: phosphatidylserine, PI: phosphatidylinositol, IPC: ceramide phosphoinositol, SM: sphingomyelin, Cer: ceramide, GlcCer: glucosylceramide, FA: fatty acid, COH: carbohydrate.

3.3 Altered ions

For better readability a condensed version of the supplementary excel table showing all altered ions is shown. The full table can be found here: https://doi.org/10.1021/jasms.4c00466 .

example annotation*	molecule class	sum formula	add.	*m/z* theor.	*m/z* meas.	Δ / ppm	p.value	-LOG10(p)	FDR	Tukey's HSD	structure	MSMS	found in Tachyz.?
Methoxybrassitin	other	C12H14N2O2S	M+H	251,0849	251,0849	0,00	0,0013	2,8828	0,0125	infected-control1; infected-control2	-		
Didesmethyl doxepin	other	C17H17NO	M+H	252,1383	252,1383	0,00	0,0034	2,4683	0,0270	infected-control1; infected-control2	-		
FA 16:1	FA	C16H30O2	M-H	253,2162	253,2173	-4,33	0,0008	3,0811	0,0053	infected-control1; infected-control2	higher in cysts		
Thiamylal	other	C12H18N2O2S	M+H	255,1162	255,1162	0,00	0,0085	2,0692	0,0498	infected-control1	-		
Glucose phosphate	COH	C6H13O9P	M-H	259,0213	259,0224	-4,23	0,0000	5,4330	0,0000	infected-control1; infected-control2	higher in cysts	phosphate group	
Urolithin D	other	C13H8O6	M-H	259,0237	259,0248	-4,24	0,0113	1,9456	0,0372	infected-control2	-		
Fluorouridine	other	C9H11FN2O6	M+H	263,0674	263,0674	0,00	0,0081	2,0940	0,0486	infected-control1	-		
(Tetradecadienyl)-cyclobutanone	other	C18H30O	M+H	263,2369	263,2369	0,00	0,0082	2,0875	0,0486	infected-control1; infected-control2	-		
Glyceric acid biphosphate	other	C3H8O10P2	M+H	266,9665	266,9665	0,01	0,0046	2,3419	0,0327	infected-control1; infected-control2	-		
Inosine	other	C10H12N4O5	M-H	267,0724	267,0735	-4,11	0,0038	2,4240	0,0175	infected-control2	surrounding tissue		
Adenosine	nucleosid	C10H13N5O4	M+H	268,1040	268,1040	0,00	0,0017	2,7725	0,0154	infected-control1; infected-control2	-		
Sotalol	other	C12H20N2O3S	M+H	273,1267	273,1267	0,00	0,0029	2,5442	0,0233	control2-control1; infected-control1	-		
FA 18:3	FA	C18H30O2	M-H	277,2162	277,2173	-3,96	0,0050	2,3038	0,0213	infected-control2	dermis		
Glutaminyl-methionine	peptide	C10H19N3O4S	M+H	278,1169	278,1169	0,00	0,0027	2,5630	0,0229	infected-control1; infected-control2	-		
Murrayacine	other	C18H15NO2	M+H	278,1176	278,1176	0,00	0,0036	2,4402	0,0283	infected-control1; infected-control2	-		
Levosimendan	other	C14H12N6O	M+H	281,1145	281,1145	0,00	0,0036	2,4419	0,0283	infected-control1; infected-control2	-		
FA 18:1	FA	C18H34O2	M-H	281,2475	281,2486	-3,90	0,0000	5,8858	0,0000	infected-control1; infected-control2	higher in cysts		

*for lack of space only one possible annotation is shown

example annotation*	molecule class	sum formula	add.	*m/z* theor.	*m/z* meas.	Δ / ppm	p.value	-LOG10(p)	FDR	Tukey's HSD	structure	MSMS	found in Tachyz.?
Dinoseb acetate	other	C12H14N2O6	M+H	283,0925	283,0925	0,00	0,0019	2,7290	0,0164	infected-control1; infected-control2	-		
Guanosine	nucleosid	C10H13N5O5	M+H	284,0989	284,0989	0,00	0,0002	3,6295	0,0033	infected-control1; infected-control2	-		
Avocadyne	other	C17H32O3	M+H	285,2424	285,2424	0,00	0,0002	3,6334	0,0033	infected-control1; infected-control2	cysts		
Histidinyl-Methionine	peptide	C11H18N4O3S	M+H	287,1172	287,1172	0,00	0,0082	2,0884	0,0486	infected-control1	-		
Mesquitol	other	C15H14O6	M-H	289,0707	289,0718	-3,80	0,0106	1,9735	0,0358	control2-control1; infected-control1	-		
Aminooxo-(trihydroxypropyl)-diquinoid-dihydroxypterin	other	C9H15N5O6	M+H	290,1095	290,1095	0,00	0,0012	2,9172	0,0119	infected-control1; infected-control2	-		
Piscidic acid	other	C11H12O7	M+K	295,0215	295,0215	0,00	0,0068	2,1698	0,0442	infected-control1; infected-control2	-		
Phenylalanyl-Methionine	peptide	C14H20N2O3S	M-H	295,1111	295,1122	-3,72	0,0130	1,8867	0,0402	infected-control1	lower in cysts		
Hydroxyoleate	other	C18H34O3	M-H	297,2424	297,2435	-3,69	0,0130	1,8876	0,0402	infected-control2	tissue		
N-Acetylglu-cosamine sulfate	COH	C8H15NO9S	M-H	300,0384	300,0395	-3,66	0,0000	4,9869	0,0001	infected-control1; infected-control2	walls		
FA 20:4	FA	C20H32O2	M-H	303,2319	303,2330	-3,62	0,0043	2,3684	0,0190	infected-control1; infected-control2	surrounding tissue		
FA 20:3	FA	C20H34O2	M-H	305,2475	305,2486	-3,59	0,0108	1,9678	0,0359	infected-control2	surrounding tissue		
FA 20:2	FA	C20H36O2	M-H	307,2632	307,2643	-3,57	0,0000	5,4577	0,0000	control2-control1; infected-control1; infected-control2	walls		
FA 20:1	FA	C20H38O2	M-H	309,2788	309,2799	-3,55	0,0000	7,4499	0,0000	infected-control1; infected-control2	cysts		

*for lack of space only one possible annotation is shown

example annotation*	molecule class	sum formula	add.	*m/z* theor.	*m/z* meas.	Δ / ppm	p.value	-LOG10(p)	FDR	Tukey's HSD	structure	MSMS	found in Tachyz.?
Hydroxyepoxy-octadecenoate	other	C18H32O4	M-H	311,2217	311,2228	-3,53	0,0155	1,8088	0,0459	infected-control2	-		
Geranyl diphosphate	other	C10H20O7P2	M-H	313,0601	313,0612	-3,50	0,0038	2,4204	0,0176	infected-control1	tissue		
PE(6:0)	PC/PE	C11H24NO7P	M+H	314,1363	314,1363	0,00	0,0056	2,2522	0,0379	infected-control1	-		
Melanin	other	C18H10N2O4	M-H	317,0557	317,0568	-3,46	0,0006	3,2059	0,0042	control2-control1; infected-control1	-		
Phytosphingosine	other	C18H39NO3	M+H	318,3003	318,3003	0,00	0,0056	2,2488	0,0379	infected-control1; infected-control2	-		
Henicosanoate	other	C21H42O2	M-H	325,3101	325,3112	-3,37	0,0065	2,1867	0,0262	infected-control1; infected-control2	-		
O-dimethyl-nonanoyl carnitine	carnitine	C18H35NO4	M-H	328,2482	328,2493	-3,34	0,0025	2,5999	0,0132	control2-control1; infected-control2	-		
Quercetin dimethyl ether	other	C17H14O7	M-H	329,0656	329,0667	-3,33	0,0049	2,3127	0,0211	infected-control1	-		
Trihydroxystearic acid	other	C18H36O5	M-H	331,2479	331,2490	-3,31	0,0171	1,7663	0,0494	infected-control1	tissue		
Glycerophospho-myoinositol	other	C9H19O11P	M-H	333,0581	333,0592	-3,29	0,0008	3,1103	0,0050	infected-control1; infected-control2	tissue		
Docosatrienoic acid	FA	C22H38O2	M-H	333,2788	333,2799	-3,29	0,0000	6,5997	0,0000	infected-control1; infected-control2	walls		
Glucosebis-phosphate	COH	C6H14O12P2	M-H	338,9877	338,9888	-3,23	0,0000	7,7919	0,0000	infected-control1; infected-control2	cysts		
MG(P-18:2)	MG	C21H38O3	M+H	339,2894	339,2894	0,00	0,0001	4,0083	0,0017	infected-control1; infected-control2	higher in cysts		
Hydroxyunde-canoyl carnitine	carnitine	C18H35NO5	M-H	344,2431	344,2442	-3,19	0,0000	5,8701	0,0000	control2-control1; infected-control2	-		
Hydroxydode-cenoyl carnitine	carnitine	C19H35NO5	M-H	356,2431	356,2442	-3,08	0,0000	5,6657	0,0000	control2-control1; infected-control2	-		

*for lack of space only one possible annotation is shown

example annotation*	molecule class	sum formula	add.	*m/z* theor.	*m/z* meas.	Δ / ppm	p.value	-LOG10(p)	FDR	Tukey's HSD	structure	MSMS	found in Tachyz.?
Hydroxydode-canoyl carnitine	carnitine	C19H37NO5	M-H	358,2588	358,2599	-3,06	0,0000	5,0246	0,0001	control2-control1; infected-control2	-		
Dihydroxytetra-norcalciol	other	C23H36O3	M+H	361,2737	361,2737	0,00	0,0030	2,5200	0,0242	infected-control1	tissue		
Hydroxytri-decanoyl carnitine	carnitine	C20H39NO5	M-H	372,2744	372,2755	-2,95	0,0001	3,8631	0,0012	control2-control1; infected-control1; infected-control2	hair follicles		
Tetradecanoyl-glycerophosphate	other	C17H35O7P	M-H	381,2037	381,2048	-2,87	0,0000	5,9140	0,0000	infected-control1; infected-control2	cysts		
Nonyl palmitate	other	C25H50O2	M-H	381,3727	381,3738	-2,88	0,0090	2,0441	0,0321	infected-control1; infected-control2	-		
Farnesyl diphosphate	other	C15H28O7P2	M+H	383,1383	383,1383	0,01	0,0054	2,2692	0,0368	infected-control1	-		
Sphingofungin B	other	C20H39NO6	M-H	388,2694	388,2705	-2,83	0,0000	6,4507	0,0000	control2-control1; infected-control1; infected-control2	tissue		
Ketodeoxycholic acid	other	C24H38O4	M+H	391,2843	391,2843	0,00	0,0024	2,6175	0,0207	infected-control1; infected-control2	-		
Isodeoxycholate	other	C24H40O4	M+H	393,2999	393,2999	0,00	0,0065	2,1898	0,0425	infected-control2	-		
Hydroxymethyltetra-cosanoic acid	other	C25H50O3	M-H	397,3676	397,3687	-2,76	0,0004	3,4501	0,0026	infected-control1; infected-control2	-		
Palmitoylcarnitine	carnitine	C23H45NO4	M+H	400,3421	400,3421	0,00	0,0075	2,1230	0,0467	infected-control1; infected-control2	cysts		
Hydroxy-cholesterol	cholesterol	C27H46O2	M-H	401,3414	401,3425	-2,73	0,0062	2,2061	0,0254	infected-control2	-		
PA(16:1)	PA	C19H37O7P	M-H	407,2193	407,2204	-2,69	0,0000	5,5412	0,0000	infected-control1; infected-control2	cysts		
PA(P-18:2)	PA	C21H39O6P	M-H	417,2401	417,2411	-2,63	0,0000	6,0849	0,0000	infected-control1; infected-control2	higher in cysts		
PA(P-18:1)	PA	C21H41O6P	M-H	419,2557	419,2568	-2,61	0,0169	1,7724	0,0489	infected-control1	surrounding tissue	cPA 18:0?	

*for lack of space only one possible annotation is shown

example annotation*	molecule class	sum formula	add.	*m/z* theor.	*m/z* meas.	Δ / ppm	p.value	-LOG10(p)	FDR	Tukey's HSD	structure	MSMS	found in Tachyz.?
Palmityl laurate	other	C28H56O2	M-H	423,4197	423,4208	-2,59	0,0104	1,9818	0,0352	infected-control1; infected-control2	-		
Oleoylcarnitine	carnitine	C25H47NO4	M+H	426,3578	426,3578	0,00	0,0008	3,1183	0,0082	infected-control1; infected-control2	higher in walls		
Bipindogenin	other	C23H34O6	M+Na	429,2248	429,2248	0,00	0,0081	2,0889	0,0486	infected-control2	-		
Hydroxystigma-stenone	other	C29H48O2	M+H	429,3727	429,3727	0,00	0,0046	2,3396	0,0327	infected-control2	-		
Octadecatrienoyl-glycerophosphate	other	C21H37O7P	M-H	431,2193	431,2204	-2,54	0,0012	2,9355	0,0070	infected-control1; infected-control2	tissue		
CerP(d21:1)	Cer	C21H42NO6P	M-H	434,2666	434,2677	-2,52	0,0003	3,4853	0,0024	control2-control1; infected-control1	higher in cysts		
PA(18:1)	PA	C21H41O7P	M-H	435,2506	435,2517	-2,52	0,0001	4,2895	0,0005	control2-control1; infected-control1; infected-control2	higher in cysts		
PE(P-16:0e)	PE	C21H44NO6P	M-H	436,2823	436,2833	-2,51	0,0024	2,6138	0,0129	infected-control1	surrounding tissue		
Hydroxyocta-cosanoate	other	C28H56O3	M-H	439,4146	439,4157	-2,50	0,0010	2,9842	0,0064	infected-control1; infected-control2	-		
O-geranylgeranyl-glycerol phosphate	other	C23H41O6P	M-H	443,2557	443,2568	-2,47	0,0000	4,6485	0,0002	control2-control1; infected-control1; infected-control2	higher in cysts		
PA(P-20:1)	PA	C23H45O6P	M-H	447,2870	447,2881	-2,45	0,0162	1,7908	0,0474	infected-control2	surrounding tissue		
Teasterone	other	C28H48O4	M-H	447,3469	447,3480	-2,45	0,0030	2,5226	0,0151	infected-control2	-		
LysoPE(16:1)	LysoPE	C21H42NO7P	M-H	450,2615	450,2626	-2,43	0,0003	3,5654	0,0021	infected-control1; infected-control2	walls		
CerP(d22:1)	Cer	C22H44NO6P	M+H	450,2979	450,2979	0,00	0,0005	3,3388	0,0054	infected-control1; infected-control2	cysts		
Myristyl palmitate	other	C30H60O2	M-H	451,4510	451,4521	-2,43	0,0073	2,1374	0,0279	infected-control1; infected-control2	-		

*for lack of space only one possible annotation is shown

example annotation*	molecule class	sum formula	add.	*m/z* theor.	*m/z* meas.	Δ / ppm	p.value	-LOG10(p)	FDR	Tukey's HSD	structure	MSMS	found in Tachyz.?
LysoPE(16:0)	LysoPE	C21H44NO7P	M-H	452,2772	452,2783	-2,42	0,0000	4,4051	0,0004	control2-control1; infected-control1; infected-control2	higher in cysts		
PA(20:4)	PA	C23H39O7P	M-H	457,2350	457,2361	-2,40	0,0026	2,5926	0,0133	infected-control2	tissue		
PE(P-18:2)	PE	C23H44NO6P	M-H	460,2823	460,2833	-2,38	0,0001	3,8282	0,0012	control2-control1; infected-control1; infected-control2	higher in cysts		
PA(20:2)	PA	C23H43O7P	M-H	461,2663	461,2674	-2,38	0,0000	5,1987	0,0001	infected-control1; infected-control2	higher in cysts		
Dehydrocholeste-rolsulfate ester	cholesterol	C27H44O4S	M-H	463,2877	463,2888	-2,37	0,0103	1,9891	0,0350	infected-control1; infected-control2	dermis		
N-Oleoyl tyrosine	other	C27H43NO4	M+Na	468,3084	468,3084	0,00	0,0000	4,5551	0,0007	infected-control1; infected-control2	cysts		
LysoPC(14:0)	lysoPC	C22H46NO7P	M+H	468,3085	468,3085	0,00	0,0000	4,5551	0,0007	infected-control1; infected-control2	cysts		
PE(18:2)	LysoPE	C23H44NO7P	M-H	476,2772	476,2783	-2,30	0,0119	1,9243	0,0379	control2-control1; infected-control2	surrounding tissue		
PE(18:1)	PC/PE	C23H46NO7P	M-H	478,2928	478,2939	-2,29	0,0001	4,0688	0,0008	control2-control1; infected-control1	higher in walls		
Palmityl palmitate	other	C32H64O2	M-H	479,4823	479,4834	-2,29	0,0043	2,3669	0,0190	infected-control1; infected-control2	-		
LysoPE(18:1)	LysoPE	C23H46NO7P	M+H	480,3085	480,3085	0,00	0,0076	2,1216	0,0467	infected-control2	surrounding tissue		
Hydroxyocta-decenoyl carnitine	carnitine	C25H47NO5	M+K	480,3086	480,3086	0,00	0,0075	2,1233	0,0467	infected-control2	surrounding tissue		
CITICOLINE	other	C14H26N4O11P2	M+H	489,1146	489,1146	0,01	0,0001	3,9147	0,0020	infected-control1; infected-control2	tissue	Citicolin	
LysoPC(14:0)	lysoPC	C22H46NO7P	M+Na	490,2904	490,2904	0,00	0,0000	4,7806	0,0005	infected-control1; infected-control2	cysts		

*for lack of space only one possible annotation is shown

example annotation*	molecule class	sum formula	add.	*m/z* theor.	*m/z* meas.	Δ / ppm	p.value	-LOG10(p)	FDR	Tukey's HSD	structure	MSMS	found in Tachyz.?
Hydroxy-leukotriene E4	other	C23H37NO6S	M+K	494,1973	494,1973	0,00	0,0076	2,1183	0,0468	infected-control1	-		
PE(18:0)	PC/PE	C23H46NO8P	M-H	494,2877	494,2888	-2,22	0,0155	1,8088	0,0459	infected-control2	-		
Cervonyl carnitine	carnitine	C29H45NO4	M+Na	494,3241	494,3241	0,00	0,0004	3,4426	0,0044	infected-control1; infected-control2	cysts		
LysoPC(16:1)	lysoPC	C24H48NO7P	M+H	494,3241	494,3241	0,00	0,0004	3,4395	0,0044	infected-control1; infected-control2	cysts		
Yuccaol A	other	C29H20O8	M-H	495,1074	495,1085	-2,22	0,0002	3,8004	0,0013	infected-control1; infected-control2	-		
Methyltetra-hydrofolic acid	other	C20H25N7O6	M+K	498,1498	498,1498	0,00	0,0000	4,9065	0,0004	control2-control1; infected-control1; infected-control2	-		
LysoPE(20:4)	LysoPE	C25H44NO7P	M-H	500,2772	500,2783	-2,19	0,0047	2,3289	0,0205	infected-control2	surrounding tissue		
LysoPE(18:1)	LysoPE	C23H46NO7P	M+Na	502,2904	502,2904	0,00	0,0018	2,7398	0,0163	control2-control1; infected-control1	tissue		
LysoPE(20:4)	LysoPE	C25H44NO7P	M+H	502,2928	502,2928	0,00	0,0009	3,0541	0,0090	control2-control1; infected-control1	tissue		
LysoPE(20:3)	LysoPE	C25H46NO7P	M-H	502,2928	502,2939	-2,18	0,0032	2,4990	0,0155	infected-control2	surrounding tissue		
LysoPE(20:2)	LysoPE	C25H48NO7P	M-H	504,3085	504,3096	-2,17	0,0088	2,0539	0,0318	control2-control1; infected-control2	surrounding tissue		
PC(P-18:2)	lysoPC	C26H50NO6P	M+H	504,3449	504,3449	0,00	0,0008	3,1172	0,0082	infected-control1; infected-control2	cysts		
dCTP	other	C9H16N3O13P3	M+K	505,9528	505,9528	0,01	0,0050	2,3026	0,0353	infected-control1; infected-control2	surrounding tissue		
LysoPC(14:0)	lysoPC	C22H46NO7P	M+K	506,2643	506,2643	0,00	0,0000	6,0202	0,0001	infected-control1; infected-control2	cysts		

*for lack of space only one possible annotation is shown

example annotation*	molecule class	sum formula	add.	*m/z* theor.	*m/z* meas.	Δ / ppm	p.value	-LOG10(p)	FDR	Tukey's HSD	structure	MSMS	found in Tachyz.?
LysoPE(20:1)	LysoPE	C25H50NO7P	M-H	506,3241	506,3252	-2,16	0,0000	4,7863	0,0002	control2-control1; infected-control1; infected-control2	higher in cysts		
CITICOLINE	other	C14H26N4O11P2	M+Na	511,0966	511,0966	0,01	0,0001	4,1895	0,0012	infected-control1; infected-control2	tissue	Citicolin	
Taurocholic acid	other	C26H45NO7S	M-H	514,2833	514,2844	-2,13	0,0000	5,9351	0,0000	control2-control1; infected-control1; infected-control2	surrounding tissue		
PE(20:3)	PE	C25H44NO8P	M-H	516,2721	516,2732	-2,12	0,0017	2,7665	0,0095	infected-control1; infected-control2	tissue		
LysoPC(16:1)	lysoPC	C24H48NO7P	M+Na	516,3061	516,3061	0,00	0,0041	2,3910	0,0310	infected-control1; infected-control2	cysts		
LysoPE(18:1)	LysoPE	C23H46NO7P	M+K	518,2643	518,2643	0,00	0,0020	2,6919	0,0177	infected-control2	surrounding tissue		
DG(P-30:2)	DG	C33H60O4	M+H	521,4564	521,4564	0,00	0,0002	3,7526	0,0027	infected-control1; infected-control2	cysts		
LysoPC(18:1)	LysoPC	C26H52NO7P	M+H	522,3554	522,3554	0,00	0,0000	4,3241	0,0010	infected-control1; infected-control2	higher in cysts		yes
LysoPE(20:4)	LysoPE	C25H44NO7P	M+Na	524,2748	524,2748	0,00	0,0014	2,8686	0,0128	infected-control1	surrounding tissue		
PE(22:6)	PE	C27H44NO7P	M-H	524,2772	524,2783	-2,09	0,0003	3,4868	0,0024	infected-control1; infected-control2	tissue		
CITICOLINE	other	C14H26N4O11P2	M+K	527,0705	527,0705	0,01	0,0000	4,6265	0,0006	infected-control1; infected-control2	tissue		
Raffinose	other	C18H32O16	M+Na	527,1583	527,1583	0,00	0,0000	4,5045	0,0007	infected-control1; infected-control2	tissue		
LysoPC(16:1)	lysoPC	C24H48NO7P	M+K	532,2800	532,2800	0,00	0,0003	3,5982	0,0034	infected-control1; infected-control2	cysts		
Eurysterol B sulfonic acid	other	C27H44O7S	M+Na	535,2700	535,2700	0,00	0,0025	2,5970	0,0214	infected-control1; infected-control2	-		

*for lack of space only one possible annotation is shown

example annotation*	molecule class	sum formula	add.	*m/z* theor.	*m/z* meas.	Δ / ppm	p.value	-LOG10(p)	FDR	Tukey's HSD	structure	MSMS	found in Tachyz.?
LysoPE(20:4)	LysoPE	C25H44NO7P	M+K	540,2487	540,2487	0,00	0,0011	2,9478	0,0114	infected-control1	tissue		
PE(22:4)	PE	C27H46NO8P	M-H	542,2877	542,2888	-2,02	0,0090	2,0463	0,0321	infected-control2	tissue		
Raffinose	other	C18H32O16	M+K	543,1322	543,1322	0,00	0,0003	3,5192	0,0039	infected-control1; infected-control2	tissue		
PS(19:2)	PS	C25H44NO10P	M-H	548,2619	548,2630	-2,00	0,0012	2,9287	0,0071	infected-control1; infected-control2	tissue		
DG(P-32:2)	DG	C35H64O4	M+H	549,4877	549,4877	0,00	0,0002	3,7608	0,0026	infected-control1; infected-control2	cysts		yes
LysoPC(18:1)	LysoPC	C26H52NO7P	M+K	560,3113	560,3113	0,00	0,0004	3,4433	0,0044	infected-control1; infected-control2	higher in cysts		
Protoporphyrin IX	other	C34H34N4O4	M+H	563,2653	563,2653	0,00	0,0001	3,8688	0,0022	infected-control1; infected-control2	-		
PI(16:0)	PI	C25H49O12P	M-H	571,2878	571,2889	-1,92	0,0000	6,7408	0,0000	control2-control1; infected-control1; infected-control2	higher in cysts		yes
Phenolic phthiocerol	other	C37H68O4	M+H	577,5190	577,5190	0,00	0,0018	2,7447	0,0163	infected-control1; infected-control2	higher in cysts		yes
PI(P-18:2)	PI	C27H49O11P	M-H	579,2929	579,2940	-1,89	0,0000	8,3848	0,0000	control2-control1; infected-control1; infected-control2	higher in cysts		
DG(30:0)	DG	C33H64O5	M+K	579,4385	579,4385	0,00	0,0002	3,8115	0,0024	infected-control1; infected-control2	cysts		
DG(32:1)	DG	C35H66O5	M+Na	589,4802	589,4802	0,00	0,0000	4,7922	0,0005	infected-control1; infected-control2	cysts		yes
DG(34:4)	DG	C37H64O5	M+H	589,4827	589,4827	0,00	0,0001	4,2733	0,0011	infected-control1; infected-control2	cysts		
PA(28:0)	PA	C31H61O8P	M-H	591,4020	591,4031	-1,85	0,0000	7,2828	0,0000	infected-control1; infected-control2	cysts		yes

*for lack of space only one possible annotation is shown

example annotation*	molecule class	sum formula	add.	*m/z* theor.	*m/z* meas.	Δ / ppm	p.value	-LOG10(p)	FDR	Tukey's HSD	structure	MSMS	found in Tachyz.?
PI(18:1)	PI	C27H51O12P	M-H	597,3034	597,3045	-1,83	0,0000	9,0882	0,0000	control2-control1; infected-control1; infected-control2	higher in cysts		yes
CerP(d33:1)	Cer	C33H66NO6P	M-H	602,4544	602,4555	-1,82	0,0030	2,5183	0,0151	infected-control1; infected-control2	surrounding tissue		
PS(30:1)	PS	C26H48NO10P	M+K	604,2647	604,2647	0,00	0,0000	4,4741	0,0008	infected-control1; infected-control2	cysts		
PS(23:3)	PS	C29H50NO10P	M+H	604,3245	604,3245	0,00	0,0000	4,5345	0,0007	infected-control1; infected-control2	cysts		
PC(O-24:1)	PC/PE	C32H64NO7P	M-H	604,4337	604,4348	-1,81	0,0092	2,0347	0,0325	infected-control1; infected-control2	-		
PA(29:0)	PA	C32H63O8P	M-H	605,4177	605,4188	-1,81	0,0000	7,9656	0,0000	infected-control1; infected-control2	cysts		yes
DG(32:1)	DG	C35H66O5	M+K	605,4542	605,4542	0,00	0,0000	7,1811	0,0000	infected-control1; infected-control2	cysts		
Pelargonidin sophoroside	other	C28H33O14	M+Na	616,1763	616,1763	0,00	0,0000	4,8946	0,0004	infected-control1; infected-control2	-		
PA(30:1)	PA	C33H63O8P	M-H	617,4177	617,4188	-1,77	0,0000	7,3925	0,0000	infected-control1; infected-control2	cysts		yes
DG(34:1)	DG	C37H70O5	M+Na	617,5115	617,5115	0,00	0,0009	3,0505	0,0090	infected-control1; infected-control2	cysts		yes
DG(36:4)	DG	C39H68O5	M+H	617,5140	617,5140	0,00	0,0018	2,7339	0,0163	infected-control1; infected-control2	cysts		
Diglucopyranosyltri-hydroxyflavanone	other	C27H32O15	M+Na	619,1633	619,1633	0,00	0,0008	3,1199	0,0082	infected-control1; infected-control2	-		
PA(30:0)	PA	C33H65O8P	M-H	619,4333	619,4344	-1,77	0,0000	7,3141	0,0000	infected-control1; infected-control2	higher in cysts		yes
DG(P-38:5)	DG	C41H70O4	M+H	627,5347	627,5347	0,00	0,0068	2,1650	0,0443	infected-control1	tissue		
PC(P-26:1)	PC/PE	C34H66NO7P	M-H	630,4493	630,4504	-1,74	0,0162	1,7904	0,0474	infected-control1	tissue		

*for lack of space only one possible annotation is shown

example annotation*	molecule class	sum formula	add.	*m/z* theor.	*m/z* meas.	Δ / ppm	p.value	-LOG10(p)	FDR	Tukey's HSD	structure	MSMS	found in Tachyz.?
CerP(d35:1)	Cer	C35H70NO6P	M-H	630,4857	630,4868	-1,74	0,0072	2,1453	0,0277	infected-control1	surrounding tissue		
PA(31:1)	PA	C34H65O8P	M-H	631,4333	631,4344	-1,74	0,0000	5,6608	0,0000	infected-control1; infected-control2	cysts		yes
DG(34:2)	DG	C37H68O5	M+K	631,4698	631,4698	0,00	0,0072	2,1450	0,0453	infected-control1	cysts		
PE-Cer(d32:1)	SM	C34H69N2O6P	M-H	631,4810	631,4820	-1,74	0,0051	2,2911	0,0218	infected-control1; infected-control2	walls		
PE(28:2)	PE	C33H62NO8P	M+H	632,4286	632,4286	0,00	0,0000	4,7954	0,0005	infected-control1; infected-control2	cysts		
PC(O-26:1)	PC/PE	C34H68NO7P	M-H	632,4650	632,4661	-1,73	0,0118	1,9283	0,0378	infected-control2	dermis		
PA(31:0)	PA	C34H67O8P	M-H	633,4490	633,4501	-1,73	0,0000	4,5561	0,0003	control2-control1; infected-control1; infected-control2	cysts		yes
DG(34:1)	DG	C37H70O5	M+K	633,4855	633,4855	0,00	0,0000	5,5930	0,0002	infected-control1; infected-control2	cysts		
lysoPC(26:0)	lysoPC	C34H70NO7P	M-H	634,4806	634,4817	-1,73	0,0028	2,5487	0,0144	infected-control2	-		
Oxidized glutathione	other	C20H32N6O12S2	M+Na	635,1412	635,1412	0,00	0,0070	2,1532	0,0447	infected-control1	surrounding tissue		
PA(30:1)	PA	C33H63O8P	M+Na	641,4153	641,4153	0,00	0,0000	5,5286	0,0002	infected-control1; infected-control2	cysts		
PA(32:2)	PA	C35H65O8P	M-H	643,4333	643,4344	-1,70	0,0012	2,9310	0,0071	infected-control1	cysts		yes
DG(36:2)	DG	C39H72O5	M+Na	643,5272	643,5272	0,00	0,0000	4,9349	0,0004	infected-control1; infected-control2	cysts		yes
DG(38:5)	DG	C41H70O5	M+H	643,5296	643,5296	0,00	0,0000	5,1196	0,0003	infected-control1; infected-control2	cysts		
CerP(d36:1)	Cer	C36H72NO6P	M-H	644,5014	644,5024	-1,70	0,0038	2,4246	0,0175	infected-control2	surrounding tissue		
Cer(d40:1)	Cer	C40H79NO3	M+Na	644,5952	644,5952	0,00	0,0070	2,1524	0,0447	control2-control1; infected-control1	-		

*for lack of space only one possible annotation is shown

example annotation*	molecule class	sum formula	add.	*m/z* theor.	*m/z* meas.	Δ / ppm	p.value	-LOG10(p)	FDR	Tukey's HSD	structure	MSMS	found in Tachyz.?
PA(32:1)	PA	C35H67O8P	M-H	645,4490	645,4501	-1,70	0,0000	7,4149	0,0000	infected-control1; infected-control2	higher in cysts		yes
Rhizochalinin D	other	C35H70N2O8	M-H	645,5048	645,5059	-1,70	0,0115	1,9393	0,0374	infected-control2	surrounding tissue		
Heme	other	C34H32FeN4O4	M+K	655,1405	653,1451	#####	0,0015	2,8283	0,0138	infected-control1; infected-control2	-		
PE(28:2)	PE	C33H62NO8P	M+Na	654,4105	654,4105	0,00	0,0006	3,2352	0,0067	infected-control1; infected-control2	cysts		yes
PA(30:1)	PA	C33H63O8P	M+K	657,3892	657,3892	0,00	0,0000	6,6056	0,0000	infected-control1; infected-control2	cysts		
PS(27:4)	PS	C33H56NO10P	M+H	658,3715	658,3715	0,00	0,0001	3,9156	0,0020	infected-control1; infected-control2	higher in cysts		
PC(P-28:1)	PC/PE	C36H70NO7P	M-H	658,4806	658,4817	-1,66	0,0122	1,9124	0,0385	infected-control2	surrounding tissue		
Cer(d41:1)	Cer	C41H81NO3	M+Na	658,6109	658,6109	0,00	0,0067	2,1747	0,0438	infected-control1	-		
PA(33:1)	PA	C36H69O8P	M-H	659,4646	659,4657	-1,66	0,0002	3,7818	0,0013	control2-control1;	higher in		yes
PA(P-34:1)	PA	C37H71O7P	M+H	659,5010	659,5010	0,00	0,0000	5,3474	0,0002	infected-control1; infected-control2	cysts		
DG(36:2)	DG	C39H72O5	M+K	659,5011	659,5011	0,00	0,0000	5,3474	0,0002	infected-control1; infected-control2	cysts		
PE(30:1)	PE	C35H68NO8P	M-H	660,4599	660,4610	-1,66	0,0005	3,3155	0,0034	infected-control1; infected-control2	cysts		
PE(P-31:0)	PC/PE	C36H72NO7P	M-H	660,4963	660,4974	-1,66	0,0121	1,9189	0,0382	infected-control2	surrounding tissue		
PE(30:0)	PC/PE	C35H70NO8P	M-H	662,4755	662,4766	-1,65	0,0000	6,8027	0,0000	infected-control1; infected-control2	cysts		yes
PE(30:0)	PE	C35H70NO8P	M+H	664,4912	664,4912	0,00	0,0000	4,7408	0,0005	infected-control1; infected-control2	-		
Glycogen	COH	C24H42O21	M-H	665,2135	665,2146	-1,65	0,0034	2,4739	0,0161	infected-control2	-		

*for lack of space only one possible annotation is shown

example annotation*	molecule class	sum formula	add.	*m/z* theor.	*m/z* meas.	Δ / ppm	p.value	-LOG10(p)	FDR	Tukey's HSD	structure	MSMS	found in Tachyz.?
PA(32:2)	PA	C35H65O8P	M+Na	667,4309	667,4309	0,00	0,0001	3,9803	0,0018	infected-control1; infected-control2	cysts		
PA(32:1)	PA	C35H67O8P	M+Na	669,4466	669,4466	0,00	0,0000	6,5887	0,0000	infected-control1; infected-control2	cysts		yes
PA(34:4)	PA	C37H65O8P	M+H	669,4490	669,4490	0,00	0,0000	7,0634	0,0000	infected-control1; infected-control2	cysts		
PE(28:2)	PE	C33H62NO8P	M+K	670,3845	670,3845	0,00	0,0000	4,3745	0,0009	infected-control1; infected-control2	cysts		
CerP(d38:2)	Cer	C38H74NO6P	M-H	670,5170	670,5181	-1,63	0,0101	1,9937	0,0348	infected-control2	surrounding tissue		
Trihydroxy-({hydroxymethyl [(tetrahydroxy-oxanyl)methoxy]-[(trihydroxymethyl-oxanyl)oxy]oxanyl}oxy)oxanecarboxylic acid	other	C24H40O20	M+Na	671,2005	671,2005	0,00	0,0000	4,7632	0,0005	infected-control1; infected-control2	walls		
PA(34:2)	PA	C37H69O8P	M-H	671,4646	671,4657	-1,63	0,0063	2,2024	0,0255	control2-control1; infected-control1	higher in cysts	PA 16:0_18:2	yes
PE(O-32:2)	PC/PE	C37H72NO7P	M-H	672,4963	672,4974	-1,63	0,0000	4,4236	0,0004	infected-control1; infected-control2	walls		
PA(34:1)	PA	C37H71O8P	M-H	673,4803	673,4814	-1,63	0,0008	3,1109	0,0050	infected-control1	higher in walls	PA 16:0_18:1	yes
SM(d32:1)	SM	C37H75N2O6P	M-H	673,5279	673,5290	-1,63	0,0016	2,8011	0,0089	infected-control1; infected-control2	surrounding tissue		
CE(18:1)	cholesterol	C45H78O2	M+Na	673,5894	673,5894	0,00	0,0002	3,6405	0,0033	infected-control1; infected-control2	cysts		yes
SM(iso-t31:1)	SM	C36H73N2O7P	M-H	675,5072	675,5083	-1,62	0,0005	3,3108	0,0034	infected-control1; infected-control2	tissue		

*for lack of space only one possible annotation is shown

example annotation*	molecule class	sum formula	add.	*m/z* theor.	*m/z* meas.	Δ / ppm	p.value	-LOG10(p)	FDR	Tukey's HSD	structure	MSMS	found in Tachyz.?
SM(d32:1)	SM	C37H75N2O6P	M+H	675,5436	675,5436	0,00	0,0036	2,4394	0,0283	control2-control1; infected-control2	surrounding tissue		
SM(d32:0)	SM	C37H77N2O6P	M-H	675,5436	675,5446	-1,62	0,0010	2,9935	0,0063	infected-control2	-		
PS(P-29:1)	PS	C35H66NO9P	M+H	676,4548	676,4548	0,00	0,0000	5,4094	0,0002	infected-control1; infected-control2	cysts		
PC(28:0)	PC/PE	C36H72NO8P	M+H	678,5068	678,5068	0,00	0,0000	6,0016	0,0001	infected-control1; infected-control2	cysts		yes
PA(35:4)	PA	C38H67O8P	M-H	681,4490	681,4501	-1,61	0,0028	2,5501	0,0144	infected-control2	-		
PA(32:2)	PA	C35H65O8P	M+K	683,4049	683,4049	0,00	0,0000	4,6724	0,0006	infected-control1; infected-control2	cysts		
PA(35:3)	PA	C38H69O8P	M-H	683,4646	683,4657	-1,60	0,0020	2,6896	0,0110	control2-control1; infected-control2	tissue		
PA(P-35:6)	PA	C38H63O7P	M+Na	685,4204	685,4204	0,00	0,0000	8,1375	0,0000	infected-control1; infected-control2	cysts		
PA(32:1)	PA	C35H67O8P	M+K	685,4205	685,4205	0,00	0,0000	8,1302	0,0000	infected-control1; infected-control2	cysts		yes
PG(P-31:3)	PG	C37H67O9P	M-H	685,4439	685,4450	-1,60	0,0030	2,5276	0,0150	infected-control2	-		
PA(35:2)	PA	C38H71O8P	M-H	685,4803	685,4814	-1,60	0,0119	1,9251	0,0379	control2-control1; infected-control2	tissue		yes
DG(42:11)	DG	C45H66O5	M-H	685,4827	685,4837	-1,60	0,0117	1,9332	0,0377	control2-control1; infected-control2	tissue		
Cer(d32:2)	Cer	C42H81NO3	M+K	686,5848	686,5848	0,00	0,0075	2,1242	0,0467	infected-control1; infected-control2	-		
PG(P-31:2)	PG	C37H69O9P	M-H	687,4595	687,4606	-1,59	0,0137	1,8631	0,0418	control2-control1; infected-control2	tissue		
PA(35:1)	PA	C38H73O8P	M-H	687,4959	687,4970	-1,59	0,0007	3,1680	0,0045	control2-control1; infected-control1	higher in walls		
DG(42:10)	DG	C45H68O5	M-H	687,4983	687,4994	-1,60	0,0007	3,1605	0,0045	control2-control1; infected-control1	higher in walls		

*for lack of space only one possible annotation is shown

example annotation*	molecule class	sum formula	add.	*m/z* theor.	*m/z* meas.	Δ / ppm	p.value	-LOG10(p)	FDR	Tukey's HSD	structure	MSMS	found in Tachyz.?
PE(32:1)	PC/PE	C37H72NO8P	M-H	688,4912	688,4923	-1,59	0,0000	4,4352	0,0004	infected-control1; infected-control2	cysts		yes
CE(18:1)	cholesterol	C45H78O2	M+K	689,5633	689,5633	0,00	0,0015	2,8295	0,0138	infected-control1; infected-control2	cysts		
PE(32:1)	PC/PE	C37H72NO8P	M+H	690,5068	690,5068	0,00	0,0044	2,3580	0,0326	infected-control1; infected-control2	cysts		
PE(32:0)	PC/PE	C37H74NO8P	M-H	690,5068	690,5079	-1,59	0,0000	6,3353	0,0000	infected-control1; infected-control2	higher in walls		yes
PS(29:1)	PS	C35H66NO10P	M+H	692,4497	692,4497	0,00	0,0000	4,9739	0,0004	infected-control1; infected-control2	cysts		
PE(32:0)	PC/PE	C37H74NO8P	M+H	692,5225	692,5225	0,00	0,0000	4,9137	0,0004	infected-control1; infected-control2	cysts		yes
PA(34:2)	PA	C37H69O8P	M+Na	695,4622	695,4622	0,00	0,0004	3,4043	0,0047	infected-control1; infected-control2	cysts		yes
PA(36:5)	PA	C39H67O8P	M+H	695,4646	695,4646	0,00	0,0004	3,4350	0,0044	infected-control1; infected-control2	cysts		
PA(36:4)	PA	C39H69O8P	M-H	695,4646	695,4657	-1,58	0,0078	2,1089	0,0289	infected-control2	surrounding tissue		
PS(30:4)	PS	C36H62NO10P	M-H	698,4028	698,4039	-1,57	0,0068	2,1683	0,0268	infected-control1; infected-control2	cysts		
PS(P-29:1)	PS	C35H66NO9P	M+Na	698,4367	698,4367	0,00	0,0008	3,0861	0,0086	infected-control1; infected-control2	higher in cysts		
PE(P-34:2)	PC/PE	C39H74NO7P	M-H	698,5119	698,5130	-1,57	0,0013	2,9023	0,0074	control2-control1; infected-control1	surrounding tissue		
PIP3(7:0)	PIP	C16H32O22P4	M-H	699,0252	699,0263	-1,56	0,0074	2,1306	0,0281	control2-control1; infected-control2	-		
DG(40:10)	DG	C43H64O5	M+K	699,4385	699,4385	0,00	0,0006	3,2140	0,0069	infected-control1; infected-control2	cysts		
PC(28:0)	PC/PE	C36H72NO8P	M+Na	700,4888	700,4888	0,00	0,0000	5,5689	0,0002	infected-control1; infected-control2	cysts		yes

*for lack of space only one possible annotation is shown

example annotation*	molecule class	sum formula	add.	*m/z* theor.	*m/z* meas.	Δ / ppm	p.value	-LOG10(p)	FDR	Tukey's HSD	structure	MSMS	found in Tachyz.?
PE(33:3)	PE	C38H70NO8P	M+H	700,4912	700,4912	0,00	0,0000	5,5647	0,0002	infected-control1; infected-control2	cysts		
PC(30:2)	PC/PE	C38H72NO8P	M-H	700,4912	700,4923	-1,56	0,0074	2,1293	0,0281	control2-control1; infected-control1	tissue		
PE(P-34:1)	PC/PE	C39H76NO7P	M-H	700,5276	700,5287	-1,56	0,0001	3,9763	0,0009	control2-control1; infected-control1	surrounding tissue		
PG(31:4)	PG	C37H65O10P	M+H	701,4388	701,4388	0,00	0,0041	2,3924	0,0310	infected-control1; infected-control2	-		
Demethyl-menaquinone	other	C50H70O2	M-H	701,5292	701,5303	-1,56	0,0001	4,0457	0,0008	control2-control1; infected-control1	surrounding tissue		
SM(d34:1)	SM	C39H79N2O6P	M-H	701,5592	701,5603	-1,56	0,0004	3,4169	0,0028	infected-control1; infected-control2	surrounding tissue		
PE(30:0)	PE	C35H70NO8P	M+K	702,4471	702,4471	0,00	0,0000	4,6632	0,0006	infected-control1; infected-control2	cysts		
Cer(d44:0)	Cer	C44H89NO3	M+Na	702,6735	702,6735	0,00	0,0000	4,8973	0,0004	infected-control1; infected-control2	cysts		
PIP(19:2)	PIP	C28H50O16P2	M-H	703,2490	703,2501	-1,56	0,0103	1,9863	0,0350	control2-control1; infected-control1	-		
PG(31:2)	PG	C37H69O10P	M-H	703,4545	703,4556	-1,56	0,0013	2,8795	0,0076	control2-control1; infected-control2	-		
SM(iso-t33:1)	SM	C38H77N2O7P	M-H	703,5385	703,5396	-1,56	0,0081	2,0920	0,0299	infected-control2	surrounding tissue		
PC(30:1)	PC/PE	C38H74NO8P	M+H	704,5225	704,5225	0,00	0,0001	4,2560	0,0011	infected-control1; infected-control2	cysts		yes
SM(t33:0)	SM	C38H79N2O7P	M-H	705,5541	705,5552	-1,55	0,0058	2,2342	0,0243	infected-control2	tissue		
PC(30:0)	PC/PE	C38H76NO8P	M+H	706,5381	706,5381	0,00	0,0000	8,5979	0,0000	infected-control1; infected-control2	higher in cysts		yes
PC(32:5)	PC/PE	C40H72NO7P	M-H	708,4963	708,4974	-1,55	0,0013	2,8908	0,0076	control2-control1; infected-control2	surrounding tissue		
PE(34:4)	PE	C39H70NO8P	M-H	710,4755	710,4766	-1,54	0,0117	1,9315	0,0377	infected-control2	tissue		

*for lack of space only one possible annotation is shown

example annotation*	molecule class	sum formula	add.	*m/z* theor.	*m/z* meas.	Δ / ppm	p.value	-LOG10(p)	FDR	Tukey's HSD	structure	MSMS	found in Tachyz.?
PA(34:2)	PA	C37H69O8P	M+K	711,4362	711,4362	0,00	0,0000	4,3043	0,0010	infected-control1; infected-control2	cysts		
PG(O-33:4)	PG	C39H71O9P	M-H	713,4752	713,4763	-1,54	0,0027	2,5749	0,0138	infected-control2	tissue		
PA(37:2)	PA	C40H75O8P	M-H	713,5116	713,5127	-1,54	0,0040	2,3962	0,0183	infected-control1	higher in cysts		
DG(44:11)	DG	C47H70O5	M-H	713,5140	713,5150	-1,54	0,0040	2,4000	0,0183	infected-control1	higher in cysts		
PS(P-29:1)	PS	C35H66NO9P	M+K	714,4107	714,4107	0,00	0,0003	3,5633	0,0036	infected-control1; infected-control2	higher in cysts		
PS(29:1)	PS	C35H66NO10P	M+Na	714,4317	714,4317	0,00	0,0014	2,8652	0,0129	infected-control1; infected-control2	cysts		
PC(28:1)	PC/PE	C36H70NO8P	M+K	714,4471	714,4471	0,00	0,0007	3,1260	0,0082	infected-control1; infected-control2	cysts		
SM(d35:1)	SM	C40H81N2O6P	M-H	715,5749	715,5759	-1,53	0,0022	2,6508	0,0119	infected-control2	surrounding tissue		
PE(34:6)	PE	C39H68NO7P	M+Na	716,4626	716,4626	0,00	0,0000	6,4285	0,0000	infected-control1; infected-control2	higher in cysts		
PC(28:0)	PC/PE	C36H72NO8P	M+K	716,4627	716,4627	0,00	0,0000	6,4281	0,0000	infected-control1; infected-control2	higher in walls		
PE(34:1)	PE	C39H76NO8P	M-H	716,5225	716,5236	-1,53	0,0000	4,5933	0,0003	infected-control1; infected-control2	higher in cysts	PE 18:1_16:0	yes
PG(i-30:0)	PG	C36H71O10P	M+Na	717,4677	717,4677	0,00	0,0000	6,0948	0,0001	infected-control1; infected-control2	cysts		
PE(34:1)	PC/PE	C39H76NO8P	M+H	718,5381	718,5381	0,00	0,0070	2,1574	0,0445	infected-control1; infected-control2	cysts		yes
PC(O-32:0)	PC/PE	C40H82NO7P	M-H	718,5745	718,5756	-1,52	0,0111	1,9547	0,0366	infected-control2	-		
PG(32:1)	PG	C38H73O10P	M-H	719,4858	719,4869	-1,52	0,0001	3,8830	0,0011	infected-control1; infected-control2	walls		
PA(38:4)	PA	C41H73O8P	M-H	723,4959	723,4970	-1,51	0,0005	3,2692	0,0036	infected-control1; infected-control2	surrounding tissue		yes

*for lack of space only one possible annotation is shown

example annotation*	molecule class	sum formula	add.	*m/z* theor.	*m/z* meas.	Δ / ppm	p.value	-LOG10(p)	FDR	Tukey's HSD	structure	MSMS	found in Tachyz.?
PC(32:4)	PC/PE	C40H72NO8P	M-H	724,4912	724,4923	-1,51	0,0031	2,5099	0,0153	infected-control2	tissue		
Tetradecanyl-(ladderaneoctanyl)glycerophospho-choline	other	C42H80NO6P	M-H	724,5640	724,5650	-1,51	0,0109	1,9641	0,0361	control2-control1; infected-control1	surrounding tissue		
PC(30:1)	PC/PE	C38H74NO8P	M+Na	726,5044	726,5044	0,00	0,0001	4,1131	0,0014	infected-control1; infected-control2	cysts	Kadesch: PC	yes
PC(32:4)	PC/PE	C40H72NO8P	M+H	726,5068	726,5068	0,00	0,0001	4,0767	0,0015	infected-control1; infected-control2	cysts		
PC(32:3)	PC/PE	C40H74NO8P	M-H	726,5068	726,5079	-1,51	0,0070	2,1553	0,0274	control2-control1; infected-control2	tissue		
PE(O-36:3)	PC/PE	C41H78NO7P	M-H	726,5432	726,5443	-1,51	0,0002	3,6497	0,0018	control2-control1; infected-control1	surrounding tissue		
PG(33:4)	PG	C39H69O10P	M-H	727,4545	727,4556	-1,51	0,0089	2,0521	0,0318	infected-control2	-		
PE(P-35:6)	PE	C40H68NO7P	M+Na	728,4626	728,4626	0,00	0,0054	2,2696	0,0368	infected-control1; infected-control2	cysts		
PE(32:1)	PC/PE	C37H72NO8P	M+K	728,4627	728,4627	0,00	0,0053	2,2728	0,0368	infected-control1; infected-control2	cysts		
PC(30:0)	PC/PE	C38H76NO8P	M+Na	728,5201	728,5201	0,00	0,0000	5,0568	0,0003	infected-control1; infected-control2	higher in cysts	Kadesch: PC + PE	yes
PC(32:3)	PC	C40H74NO8P	M+H	728,5225	728,5225	0,00	0,0000	5,6972	0,0002	infected-control1; infected-control2	higher in walls	PC 32:3	
PE(O-36:2)	PC/PE	C41H80NO7P	M-H	728,5589	728,5600	-1,50	0,0059	2,2271	0,0245	control2-control1; infected-control1	surrounding tissue		
CerP(d42:1)	Cer	C42H84NO6P	M-H	728,5953	728,5963	-1,50	0,0066	2,1782	0,0265	infected-control1; infected-control2	surrounding tissue		
PG(33:3)	PG	C39H71O10P	M-H	729,4701	729,4712	-1,50	0,0013	2,8831	0,0076	infected-control1; infected-control2	-		
SM(d36:1)	SM	C41H83N2O6P	M-H	729,5905	729,5916	-1,50	0,0084	2,0782	0,0302	infected-control2	surrounding tissue		

*for lack of space only one possible annotation is shown

example annotation*	molecule class	sum formula	add.	*m/z* theor.	*m/z* meas.	Δ / ppm	p.value	-LOG10(p)	FDR	Tukey's HSD	structure	MSMS	found in Tachyz.?
PS(29:1)	PS	C35H66NO10P	M+K	730,4056	730,4056	0,00	0,0003	3,5619	0,0036	infected-control1; infected-control2	cysts		
PE(32:0)	PC/PE	C37H74NO8P	M+K	730,4784	730,4784	0,00	0,0000	5,5027	0,0002	infected-control1; infected-control2	cysts		
PG(33:2)	PG	C39H73O10P	M-H	731,4858	731,4869	-1,50	0,0049	2,3088	0,0212	infected-control2	tissue		
PC(32:1)	PC	C40H78NO8P	M+H	732,5538	732,5538	0,00	0,0000	4,6487	0,0006	infected-control1; infected-control2	higher in cysts	PC 32:1	yes
PE(O-36:0)	PC/PE	C41H84NO7P	M-H	732,5902	732,5913	-1,50	0,0123	1,9094	0,0386	infected-control2	-		
PE(36:6)	PE	C41H70NO8P	M-H	734,4755	734,4766	-1,49	0,0015	2,8148	0,0087	infected-control1; infected-control2	-		
PC(34:5)	PC/PE	C42H76NO7P	M-H	736,5276	736,5287	-1,49	0,0075	2,1275	0,0281	infected-control2	surrounding tissue		
PG(P-35:5)	PG	C41H71O9P	M-H	737,4752	737,4763	-1,49	0,0043	2,3639	0,0190	infected-control1; infected-control2	tissue		
PA(39:4)	PA	C42H75O8P	M-H	737,5116	737,5127	-1,49	0,0137	1,8630	0,0418	infected-control2	tissue		
Di-O-myristoyl-O-(sulfoquinovo-pyranosyl)glycerol	other	C37H70O12S	M+H	739,4661	739,4661	0,00	0,0082	2,0838	0,0487	infected-control2	higher in cysts		yes
PA(36:2)	PA	C39H73O8P	M+K	739,4675	739,4675	0,00	0,0083	2,0834	0,0487	infected-control2	higher in cysts		
PG(O-35:5)	PG	C41H73O9P	M-H	739,4908	739,4919	-1,48	0,0011	2,9413	0,0070	infected-control1; infected-control2	tissue		
PE(P-36:6)	PE	C41H70NO7P	M+Na	742,4782	742,4782	0,00	0,0000	4,5383	0,0007	infected-control1; infected-control2	cysts		
PC(30:1)	PC/PE	C38H74NO8P	M+K	742,4784	742,4784	0,00	0,0000	4,5339	0,0007	infected-control1; infected-control2	cysts	Kadesch: PC	
PS(33:2)	PS	C39H72NO10P	M-H	744,4810	744,4821	-1,47	0,0122	1,9151	0,0384	infected-control2	tissue		
PE(P-36:5)	PC/PE	C41H72NO7P	M+Na	744,4939	744,4939	0,00	0,0000	7,2384	0,0000	infected-control1; infected-control2	higher in cysts		yes

*for lack of space only one possible annotation is shown

example annotation*	molecule class	sum formula	add.	*m/z* theor.	*m/z* meas.	Δ / ppm	p.value	-LOG10(p)	FDR	Tukey's HSD	structure	MSMS	found in Tachyz.?
PC(30:0)	PC	C38H76NO8P	M+K	744,4940	744,4940	0,00	0,0000	7,2386	0,0000	infected-control1; infected-control2	higher in walls	PC 30:0	
PC(dO-36:4)	PC	C43H70NO7P	M+H	744,4963	744,4963	0,00	0,0000	7,2841	0,0000	infected-control1; infected-control2	higher in cysts		
PE(36:1)	PE	C41H80NO8P	M-H	744,5538	744,5549	-1,47	0,0075	2,1239	0,0282	infected-control1	higher in walls	PE 18:1_18:0	
PG(32:0)	PG	C38H75O10P	M+Na	745,4990	745,4990	0,00	0,0000	7,9590	0,0000	infected-control1; infected-control2	higher in cysts		
PE(P-38:4)	PE	C43H78NO7P	M-H	750,5432	750,5443	-1,46	0,0003	3,4809	0,0024	infected-control1; infected-control2	surrounding tissue	PE P-18:0_20:4	
PA(40:4)	PA	C43H77O8P	M-H	751,5272	751,5283	-1,46	0,0144	1,8418	0,0434	infected-control2	surrounding tissue		
PC(34:4)	PC/PE	C42H76NO8P	M-H	752,5225	752,5236	-1,46	0,0155	1,8100	0,0459	infected-control2	surrounding tissue		
Hexadecanyl-(ladderaneoctanyl)glycerophospho-choline	other	C44H84NO6P	M-H	752,5953	752,5963	-1,46	0,0153	1,8167	0,0456	infected-control1	surrounding tissue		yes
GlcCer(d36:0)	GlcCer	C42H83NO8	M+Na	752,6011	752,6011	0,00	0,0077	2,1137	0,0472	control2-control1; infected-control1	-		
PI(28:0)	PI	C37H71O13P	M-H	753,4549	753,4560	-1,45	0,0000	8,5683	0,0000	infected-control1; infected-control2	cysts		
PC(32:1)	PC/PE	C40H78NO8P	M+Na	754,5357	754,5357	0,00	0,0002	3,8154	0,0024	infected-control1; infected-control2	higher in cysts		yes
PC(34:4)	PC/PE	C42H76NO8P	M+H	754,5381	754,5381	0,00	0,0001	3,8447	0,0023	infected-control1; infected-control2	higher in cysts		
PE(P-38:2)	PE	C43H82NO7P	M-H	754,5745	754,5756	-1,45	0,0000	5,6125	0,0000	control2-control1; infected-control1; infected-control2	walls		

*for lack of space only one possible annotation is shown

example annotation*	molecule class	sum formula	add.	*m/z* theor.	*m/z* meas.	Δ / ppm	p.value	-LOG10(p)	FDR	Tukey's HSD	structure	MSMS	found in Tachyz.?
CerP(d44:2)	Cer	C44H86NO6P	M-H	754,6109	754,6120	-1,45	0,0129	1,8910	0,0401	infected-control1	surrounding tissue		yes
Diadenosine triphosphate	nucleosid	C20H27N10O16P3	M-H	755,0736	755,0747	-1,45	0,0020	2,7089	0,0106	control2-control1; infected-control2	-		
PG(35:4)	PG	C41H73O10P	M-H	755,4858	755,4869	-1,45	0,0005	3,3233	0,0034	infected-control1; infected-control2	-		
PE(P-37:6)	PE	C42H72NO7P	M+Na	756,4939	756,4939	0,00	0,0051	2,2898	0,0359	infected-control1; infected-control2	cysts		
PE(34:1)	PC/PE	C39H76NO8P	M+K	756,4940	756,4940	0,00	0,0051	2,2900	0,0359	infected-control1; infected-control2	cysts		
PS(P-35:2)	PS	C41H76NO9P	M-H	756,5174	756,5185	-1,45	0,0107	1,9715	0,0358	infected-control2	tissue		
PC(34:2)	PC	C42H80NO8P	M-H	756,5538	756,5549	-1,45	0,0101	1,9946	0,0348	control2-control1; infected-control2	tissue		yes
PG(35:3)	PG	C41H75O10P	M-H	757,5014	757,5025	-1,45	0,0015	2,8163	0,0087	infected-control1; infected-control2	-		
SM(d38:1)	SM	C43H87N2O6P	M-H	757,6218	757,6229	-1,45	0,0032	2,4953	0,0155	infected-control2	surrounding tissue		
PS(34:2)	PS	C40H74NO10P	M-H	758,4967	758,4978	-1,44	0,0004	3,3686	0,0031	infected-control1; infected-control2	tissue		
PC(34:1)	PC	C42H82NO8P	M+H	760,5851	760,5851	0,00	0,0017	2,7715	0,0154	infected-control2	higher in cysts	PC 34:1	yes
PC(34:0)	PC/PE	C42H84NO8P	M-H	760,5851	760,5862	-1,44	0,0138	1,8590	0,0420	infected-control1	cysts		yes
PC(P-36:4)	PC	C44H80NO7P	M-H	764,5589	764,5600	-1,43	0,0164	1,7853	0,0477	infected-control2	surrounding tissue		
PA(38:3)	PA	C41H75O8P	M+K	765,4831	765,4831	0,00	0,0074	2,1297	0,0467	infected-control2	higher in cysts		
PG(P-37:5)	PG	C43H75O9P	M-H	765,5065	765,5076	-1,43	0,0103	1,9861	0,0350	infected-control1; infected-control2	tissue		
PE(38:4)	PE	C43H78NO8P	M-H	766,5381	766,5392	-1,43	0,0002	3,7962	0,0013	infected-control1; infected-control2	surrounding tissue	PE 20:4_18:0	yes

*for lack of space only one possible annotation is shown

example annotation*	molecule class	sum formula	add.	*m/z* theor.	*m/z* meas.	Δ / ppm	p.value	-LOG10(p)	FDR	Tukey's HSD	structure	MSMS	found in Tachyz.?
PE(38:3)	PE	C43H80NO8P	M-H	768,5538	768,5549	-1,43	0,0076	2,1173	0,0285	infected-control2	surrounding tissue	PE 20:3_18:0	yes
PIP2(16:0)	PIP	C25H49O19P3	M+Na	769,1973	769,1973	0,01	0,0005	3,2878	0,0060	infected-control1; infected-control2	-		
SM(iso-d39:2)	SM	C44H87N2O6P	M-H	769,6218	769,6229	-1,42	0,0056	2,2538	0,0235	infected-control1	surrounding tissue		
PE(O-38:7)	PE	C43H74NO7P	M+Na	770,5095	770,5095	0,00	0,0000	4,4656	0,0008	infected-control1; infected-control2	higher in cysts		yes
PC(32:1)	PC	C40H78NO8P	M+K	770,5097	770,5097	0,00	0,0000	4,4656	0,0008	infected-control1; infected-control2	higher in cysts	PC 32:1	
PG(34:1)	PG	C40H77O10P	M+Na	771,5147	771,5147	0,00	0,0000	4,4924	0,0008	infected-control1; infected-control2	higher in cysts		
SM(d39:1)	SM	C44H89N2O6P	M-H	771,6375	771,6385	-1,42	0,0063	2,1975	0,0257	infected-control1; infected-control2	surrounding tissue		
PS(33:0)	PS	C39H76NO10P	M+Na	772,5099	772,5099	0,00	0,0000	4,3106	0,0010	infected-control1; infected-control2	cysts		
PS(35:2)	PS	C41H76NO10P	M-H	772,5123	772,5134	-1,42	0,0066	2,1837	0,0263	infected-control2	-		
PE(P-40:7)	PE	C45H76NO7P	M-H	772,5276	772,5287	-1,42	0,0053	2,2730	0,0226	infected-control2	tissue		
PA(40:5)	PA	C43H75O8P	M+Na	773,5092	773,5092	0,00	0,0043	2,3619	0,0325	infected-control2	cysts		
PA(42:8)	PA	C45H73O8P	M+H	773,5116	773,5116	0,00	0,0033	2,4789	0,0264	infected-control2	cysts		
PS(35:1)	PS	C41H78NO10P	M-H	774,5280	774,5291	-1,41	0,0067	2,1750	0,0265	control2-control1; infected-control2	surrounding tissue		
PG(36:1)	PG	C42H81O10P	M-H	775,5484	775,5495	-1,41	0,0084	2,0781	0,0302	infected-control1	surrounding tissue		
PPA(36:2)	PA	C39H74O11P2	M-H	779,4623	779,4634	-1,40	0,0007	3,1715	0,0045	infected-control1; infected-control2	cysts		
PI(30:1)	PI	C39H73O13P	M-H	779,4705	779,4716	-1,41	0,0000	8,7813	0,0000	infected-control1; infected-control2	cysts		

*for lack of space only one possible annotation is shown

example annotation*	molecule class	sum formula	add.	*m/z* theor.	*m/z* meas.	Δ / ppm	p.value	-LOG10(p)	FDR	Tukey's HSD	structure	MSMS	found in Tachyz.?
PS(36:5)	PS	C42H72NO10P	M-H	780,4810	780,4821	-1,40	0,0000	4,6512	0,0002	control2-control1; infected-control1; infected-control2	-		
PS(O-37:5)	PS	C43H76NO9P	M-H	780,5174	780,5185	-1,40	0,0091	2,0403	0,0323	infected-control2	tissue		
PC(36:4)	PC	C44H80NO8P	M-H	780,5538	780,5549	-1,40	0,0097	2,0148	0,0338	infected-control2	surrounding tissue		
PE(O-40:4)	PE	C45H84NO7P	M-H	780,5902	780,5913	-1,40	0,0109	1,9615	0,0362	control2-control1; infected-control1	walls		
PI(30:0)	PI	C39H75O13P	M-H	781,4862	781,4873	-1,40	0,0000	11,4130	0,0000	infected-control1; infected-control2	cysts	Kadesch: PI	
PS(P-37:3)	PS	C43H78NO9P	M-H	782,5330	782,5341	-1,40	0,0037	2,4333	0,0173	infected-control2	tissue		
PE(P-40:2)	PE	C45H86NO7P	M-H	782,6058	782,6069	-1,40	0,0000	5,0417	0,0001	infected-control1; infected-control2	walls		
SM(iso-t39:2)	SM	C44H87N2O7P	M-H	785,6167	785,6178	-1,39	0,0000	6,3491	0,0000	infected-control1; infected-control2	cysts		
SM(d40:2)	SM	C45H89N2O6P	M+H	785,6531	785,6531	0,00	0,0000	5,1547	0,0003	control2-control1; infected-control2	surrounding tissue		
SM(d40:1)	SM	C45H91N2O6P	M-H	785,6531	785,6542	-1,39	0,0048	2,3199	0,0208	infected-control1; infected-control2	surrounding tissue		
PC(36:2)	PC	C44H84NO8P	M+H	786,6007	786,6007	0,00	0,0016	2,7999	0,0146	infected-control1; infected-control2	higher in cysts	PC 36:2	yes
PS(36:1)	PS	C42H80NO10P	M-H	788,5436	788,5447	-1,39	0,0083	2,0789	0,0302	control2-control1; infected-control2	surrounding tissue	PS 18:1_18:0	
SM(t39:0)	SM	C44H91N2O7P	M-H	789,6480	789,6491	-1,39	0,0082	2,0851	0,0302	infected-control2	-		
(3'-sulfo)-GalCer(d35:1)	other	C41H79NO11S	M-H	792,5290	792,5301	-1,38	0,0040	2,3971	0,0183	control2-control1; infected-control2	tissue		
PE(40:4)	PC/PE	C45H82NO8P	M-H	794,5694	794,5705	-1,38	0,0032	2,5007	0,0155	infected-control2	surrounding tissue		
PS(P-36:1)	PS	C42H80NO9P	M+Na	796,5463	796,5463	0,00	0,0028	2,5476	0,0233	infected-control2	-		

*for lack of space only one possible annotation is shown

example annotation*	molecule class	sum formula	add.	*m/z* theor.	*m/z* meas.	Δ / ppm	p.value	-LOG10(p)	FDR	Tukey's HSD	structure	MSMS	found in Tachyz.?
PE(40:3)	PC/PE	C45H84NO8P	M-H	796,5851	796,5862	-1,38	0,0009	3,0225	0,0060	infected-control2	surrounding tissue		
PC(P-36:0)	PC	C44H88NO7P	M+Na	796,6191	796,6191	0,00	0,0018	2,7384	0,0163	infected-control1	-		
PC(P-38:3)	PC	C46H86NO7P	M+H	796,6215	796,6215	0,00	0,0018	2,7430	0,0163	infected-control1	-		
PE(P-40:6)	PE	C45H78NO7P	M+Na	798,5408	798,5408	0,00	0,0078	2,1093	0,0473	infected-control1; infected-control2	higher in cysts		yes
PC(34:1)	PC	C42H82NO8P	M+K	798,5410	798,5410	0,00	0,0078	2,1093	0,0473	infected-control1; infected-control2	higher in walls	PC 34:1	
PS(O-36:1)	PS	C42H82NO9P	M+Na	798,5619	798,5619	0,00	0,0055	2,2612	0,0373	infected-control2	-		
PC(P-38:1)	PC/PE	C46H90NO7P	M-H	798,6371	798,6382	-1,37	0,0000	5,2125	0,0001	infected-control1; infected-control2	cysts		
PI(P-33:4)	PI	C42H73O12P	M-H	799,4756	799,4767	-1,37	0,0019	2,7261	0,0103	infected-control1; infected-control2	cysts		
PG(36:1)	PG	C42H81O10P	M+Na	799,5460	799,5460	0,00	0,0069	2,1636	0,0443	infected-control2	higher in cysts		
SM(d41:1)	SM	C46H93N2O6P	M-H	799,6688	799,6698	-1,37	0,0032	2,4936	0,0155	infected-control1; infected-control2	surrounding tissue		yes
(3'-sulfo)-GalCer(d36:4)	other	C42H75NO11S	M-H	800,4977	800,4988	-1,37	0,0013	2,8809	0,0076	infected-control1	tissue		
PS(35:0)	PS	C41H80NO10P	M+Na	800,5412	800,5412	0,00	0,0012	2,9103	0,0120	infected-control1; infected-control2	higher in cysts		
PE(40:2)	PC/PE	C45H86NO8P	M+H	800,6164	800,6164	0,00	0,0039	2,4035	0,0304	infected-control2	cysts		yes
PC(P-38:0)	PC	C46H92NO7P	M-H	800,6528	800,6539	-1,37	0,0003	3,4954	0,0024	infected-control1; infected-control2	-		
PA(42:5)	PA	C45H79O8P	M+Na	801,5405	801,5405	0,00	0,0012	2,9253	0,0118	infected-control1; infected-control2	higher in cysts		
PA(44:8)	PA	C47H77O8P	M+H	801,5429	801,5429	0,00	0,0012	2,9252	0,0118	infected-control1; infected-control2	higher in cysts		
PS(37:1)	PS	C43H82NO10P	M-H	802,5593	802,5604	-1,37	0,0073	2,1378	0,0279	control2-control1; infected-control2	tissue		yes

*for lack of space only one possible annotation is shown

example annotation*	molecule class	sum formula	add.	*m/z* theor.	*m/z* meas.	Δ / ppm	p.value	-LOG10(p)	FDR	Tukey's HSD	structure	MSMS	found in Tachyz.?
PI(32:2)	PI	C41H75O13P	M-H	805,4862	805,4873	-1,36	0,0156	1,8082	0,0459	infected-control1	cysts		
PI(32:1)	PI	C41H77O13P	M-H	807,5018	807,5029	-1,36	0,0000	9,1447	0,0000	infected-control1; infected-control2	higher in cysts	Kadesch: PI	yes
SM(d40:2)	SM	C45H89N2O6P	M+Na	807,6350	807,6350	0,00	0,0035	2,4582	0,0275	infected-control2	surrounding tissue		
PI(32:0)	PI	C41H79O13P	M-H	809,5175	809,5186	-1,35	0,0057	2,2461	0,0238	infected-control1	dermis		
PS(O-39:4)	PS	C45H82NO9P	M-H	810,5643	810,5654	-1,35	0,0021	2,6819	0,0111	infected-control1; infected-control2	tissue		
PS(38:3)	PS	C44H80NO10P	M-H	812,5436	812,5447	-1,35	0,0000	4,3670	0,0004	infected-control1; infected-control2	surrounding tissue		
PC(36:0)	PC	C44H88NO8P	M+Na	812,6140	812,6140	0,00	0,0008	3,0754	0,0086	control2-control1; infected-control1	tissue		
PC(38:3)	PC	C46H86NO8P	M+H	812,6164	812,6164	0,00	0,0008	3,0758	0,0086	control2-control1; infected-control1	tissue		
SM(d42:1)	SM	C47H95N2O6P	M-H	813,6844	813,6855	-1,35	0,0143	1,8448	0,0433	infected-control2	surrounding tissue		
GlcCer(iso-t39:6)	GlcCer	C45H77NO9	M+K	814,5230	814,5230	0,00	0,0000	6,4140	0,0000	infected-control1; infected-control2	cysts		
Thyroxine	other	C15H11I4NO4	M+K	815,6498	815,6498	-0,01	0,0001	4,2377	0,0011	infected-control1; infected-control2	cysts		
TG(O-49:7)	TG	C52H88O5	M+Na	815,6524	815,6524	0,00	0,0001	4,2559	0,0011	infected-control1; infected-control2	cysts		
PA(44:1)	PA	C47H91O8P	M+H	815,6524	815,6524	0,00	0,0001	4,2559	0,0011	infected-control1; infected-control2	cysts		
TG(46:1)	TG	C49H92O6	M+K	815,6525	815,6525	0,00	0,0001	4,2587	0,0011	infected-control1; infected-control2	cysts		
PE(P-40:5)	PE	C45H80NO7P	M+K	816,5304	816,5304	0,00	0,0001	3,8739	0,0022	infected-control1; infected-control2	cysts		
PS(38:1)	PS	C44H84NO10P	M-H	816,5749	816,5760	-1,34	0,0042	2,3778	0,0188	control2-control1; infected-control2	surrounding tissue		

*for lack of space only one possible annotation is shown

example annotation*	molecule class	sum formula	add.	*m/z* theor.	*m/z* meas.	Δ / ppm	p.value	-LOG10(p)	FDR	Tukey's HSD	structure	MSMS	found in Tachyz.?
PC(38:0)	PC	C46H92NO8P	M-H	816,6477	816,6488	-1,34	0,0000	7,3093	0,0000	infected-control1; infected-control2	cysts		
PC(P-38:3)	PC	C46H86NO7P	M+Na	818,6034	818,6034	0,00	0,0030	2,5245	0,0242	infected-control1	-		
PC(P-40:6)	PC	C48H84NO7P	M+H	818,6058	818,6058	0,00	0,0037	2,4360	0,0283	infected-control1	-		
(3'-sulfo)-GalCer(d37:1)	other	C43H83NO11S	M-H	820,5603	820,5614	-1,34	0,0043	2,3638	0,0190	control2-control1; infected-control1	cysts		
PI(33:1)	PI	C42H79O13P	M-H	821,5175	821,5186	-1,33	0,0000	6,1747	0,0000	infected-control1; infected-control2	cysts		
PS(39:5)	PS	C45H78NO10P	M-H	822,5280	822,5291	-1,33	0,0000	5,2280	0,0001	infected-control1; infected-control2	cysts		yes
SM(d40:2)	SM	C45H89N2O6P	M+K	823,6090	823,6090	0,00	0,0002	3,6522	0,0033	infected-control1; infected-control2	surrounding tissue		
PS(39:4)	PS	C45H80NO10P	M-H	824,5436	824,5447	-1,33	0,0005	3,3197	0,0034	infected-control1; infected-control2	cysts		
(3'-sulfo)Galbeta-Cer(d36:1(2OH))	other	C42H81NO12S	M+H	824,5552	824,5552	0,00	0,0028	2,5484	0,0233	infected-control1; infected-control2	higher in cysts		
PE(P-42:7)	PE	C47H80NO7P	M+Na	824,5565	824,5565	0,00	0,0028	2,5484	0,0233	infected-control1; infected-control2	higher in cysts		
PC(36:2)	PC	C44H84NO8P	M+K	824,5566	824,5566	0,00	0,0028	2,5484	0,0233	infected-control1; infected-control2	higher in cysts	PC 36:2	
PS(P-38:1)	PS	C44H84NO9P	M+Na	824,5776	824,5776	0,00	0,0015	2,8235	0,0139	infected-control2	-		
PE(40:1)	PE	C45H88NO8P	M+Na	824,6140	824,6140	0,00	0,0022	2,6588	0,0189	infected-control2	surrounding tissue		
PG(38:2)	PG	C44H83O10P	M+Na	825,5616	825,5616	0,00	0,0029	2,5384	0,0235	infected-control1; infected-control2	higher in cysts		
SM(iso-d43:2)	SM	C48H95N2O6P	M-H	825,6844	825,6855	-1,33	0,0163	1,7887	0,0475	infected-control1	dermis		
PS(39:3)	PS	C45H82NO10P	M-H	826,5593	826,5604	-1,33	0,0010	3,0011	0,0062	infected-control1; infected-control2	cysts		
PA(44:6)	PA	C47H81O8P	M+Na	827,5561	827,5561	0,00	0,0002	3,6213	0,0033	infected-control1; infected-control2	cysts		

*for lack of space only one possible annotation is shown

example annotation*	molecule class	sum formula	add.	*m/z* theor.	*m/z* meas.	Δ / ppm	p.value	-LOG10(p)	FDR	Tukey's HSD	structure	MSMS	found in Tachyz.?
TG(48:1)	TG	C51H96O6	M+Na	827,7099	827,7099	0,00	0,0064	2,1957	0,0423	infected-control1; infected-control2	cysts		yes
TG(50:4)	TG	C53H94O6	M+H	827,7123	827,7123	0,00	0,0062	2,2059	0,0415	infected-control1; infected-control2	cysts		
PS(39:2)	PS	C45H84NO10P	M-H	828,5749	828,5760	-1,32	0,0114	1,9440	0,0372	infected-control1	cysts		
PE(42:1)	PE	C47H92NO8P	M-H	828,6477	828,6488	-1,32	0,0145	1,8379	0,0436	infected-control2	dermis		
PC(P-38:3)	PC	C46H86NO7P	M+K	834,5774	834,5773	0,00	0,0060	2,2234	0,0400	infected-control1	-		
PI(34:1)	PI	C43H81O13P	M-H	835,5331	835,5342	-1,31	0,0000	9,0790	0,0000	infected-control1; infected-control2	higher in cysts		yes
18:0-Glc-Cholesterol	cholesterol	C51H90O7	M+Na	837,6579	837,6579	0,00	0,0085	2,0717	0,0497	infected-control1	-		
PE(44:10)	PE	C49H78NO8P	M-H	838,5381	838,5392	-1,31	0,0000	9,6280	0,0000	infected-control1; infected-control2	cysts		yes
PE(42:7)	PE	C47H80NO8P	M+Na	840,5514	840,5514	0,00	0,0002	3,6093	0,0033	infected-control1; infected-control2	cysts		
PE(44:10)	PE	C49H78NO8P	M+H	840,5538	840,5538	0,00	0,0004	3,4543	0,0044	infected-control1; infected-control2	cysts		
Cer(iso-t55:4)	Cer	C55H103NO4	M-H	840,7803	840,7814	-1,30	0,0115	1,9376	0,0374	control2-control1; infected-control2	-		
GlcCer(iso-t41:6)	GlcCer	C47H81NO9	M+K	842,5543	842,5543	0,00	0,0000	7,3915	0,0000	infected-control1; infected-control2	higher in walls		
TG(O-51:7)	TG	C54H92O5	M+Na	843,6837	843,6837	0,00	0,0001	4,2249	0,0011	infected-control1; infected-control2	cysts		
PA(46:1)	PA	C49H95O8P	M+H	843,6837	843,6837	0,00	0,0001	4,2249	0,0011	infected-control1; infected-control2	cysts		yes
TG(48:1)	TG	C51H96O6	M+K	843,6838	843,6838	0,00	0,0001	4,2250	0,0011	infected-control1; infected-control2	cysts		
PI(32:1)	PI	C41H77O13P	M+K	847,4733	847,4733	0,00	0,0000	4,6320	0,0006	infected-control1; infected-control2	cysts		

*for lack of space only one possible annotation is shown

example annotation*	molecule class	sum formula	add.	*m/z* theor.	*m/z* meas.	Δ / ppm	p.value	-LOG10(p)	FDR	Tukey's HSD	structure	MSMS	found in Tachyz.?
PI(35:1)	PI	C44H83O13P	M-H	849,5488	849,5499	-1,29	0,0000	4,4199	0,0004	infected-control1; infected-control2	tissue		
PE(42:6(2OH))	PE	C47H82NO10P	M-H	850,5593	850,5604	-1,29	0,0000	9,8605	0,0000	infected-control1; infected-control2	cysts		yes
PS(41:4)	PS	C47H84NO10P	M-H	852,5749	852,5760	-1,29	0,0000	6,6311	0,0000	infected-control1; infected-control2	cysts		
TG(50:2)	TG	C53H98O6	M+Na	853,7256	853,7256	0,00	0,0045	2,3453	0,0327	infected-control1	cysts		yes
TG(52:5)	TG	C55H96O6	M+H	853,7280	853,7280	0,00	0,0046	2,3403	0,0327	infected-control1	cysts		
PS(38:1)	PS	C44H84NO10P	M+K	856,5464	856,5464	0,00	0,0005	3,2658	0,0063	infected-control1; infected-control2	cysts		
PI(36:4)	PI	C45H79O13P	M-H	857,5175	857,5186	-1,28	0,0019	2,7265	0,0103	infected-control1	surrounding tissue	Kadesch: PI	yes
PI(34:1)	PI	C43H81O13P	M+Na	859,5307	859,5307	0,00	0,0000	5,1505	0,0003	infected-control1; infected-control2	cysts		yes
PI(36:3)	PI	C45H81O13P	M-H	859,5331	859,5342	-1,27	0,0041	2,3902	0,0184	infected-control1	surrounding tissue	Kadesch: PI	
PS(42:6)	PS	C48H82NO10P	M-H	862,5593	862,5604	-1,27	0,0037	2,4376	0,0173	control2-control1; infected-control1	-		
IPC(d40:1)	IPC	C46H90NO11P	M-H	862,6168	862,6179	-1,27	0,0000	7,3112	0,0000	infected-control1; infected-control2	cysts		
PC(40:3)	PC	C48H90NO8P	M+Na	862,6296	862,6296	0,00	0,0043	2,3657	0,0325	control2-control1; infected-control2	-		
GlcCer(iso-t45:4)	GlcCer	C51H93NO9	M-H	862,6767	862,6778	-1,27	0,0133	1,8777	0,0409	control2-control1; infected-control2	-		
PI(36:1)	PI	C45H85O13P	M-H	863,5644	863,5655	-1,27	0,0000	5,3385	0,0001	infected-control1; infected-control2	surrounding tissue	PI 36:1	
PI(36:0)	PI	C45H87O13P	M-H	865,5801	865,5812	-1,27	0,0000	6,7687	0,0000	infected-control1; infected-control2	surrounding tissue		
PA(46:0)	PA	C49H97O8P	M+Na	867,6813	867,6813	0,00	0,0002	3,6223	0,0033	infected-control1; infected-control2	cysts		

*for lack of space only one possible annotation is shown

example annotation*	molecule class	sum formula	add.	*m/z* theor.	*m/z* meas.	Δ / ppm	p.value	-LOG10(p)	FDR	Tukey's HSD	structure	MSMS	found in Tachyz.?
TG(O-53:9)	TG	C56H92O5	M+Na	867,6837	867,6837	0,00	0,0002	3,6324	0,0033	infected-control1; infected-control2	cysts		
PA(48:3)	PA	C51H95O8P	M+H	867,6837	867,6837	0,00	0,0002	3,6324	0,0033	infected-control1; infected-control2	cysts		
TG(50:3)	TG	C53H96O6	M+K	867,6838	867,6838	0,00	0,0002	3,6324	0,0033	infected-control1; infected-control2	cysts		
TG(O-53:8)	TG	C56H94O5	M+Na	869,6993	869,6993	0,00	0,0007	3,1388	0,0080	infected-control1; infected-control2	higher in cysts		
PA(48:2)	PA	C51H97O8P	M+H	869,6994	869,6994	0,00	0,0007	3,1388	0,0080	infected-control1; infected-control2	higher in cysts		yes
TG(50:2)	TG	C53H98O6	M+K	869,6995	869,6995	0,00	0,0007	3,1383	0,0080	infected-control1; infected-control2	higher in cysts		
TG(O-55:11)	TG	C58H92O5	M+H	869,7018	869,7018	0,00	0,0007	3,1486	0,0080	infected-control1; infected-control2	higher in cysts		
PI(O-38:4)	PI	C47H85O12P	M-H	871,5695	871,5706	-1,26	0,0009	3,0405	0,0058	infected-control1; infected-control2	-		
PC(40:6)	PC	C48H84NO8P	M+K	872,5566	872,5566	0,00	0,0084	2,0748	0,0495	infected-control2	tissue		
PI(34:1)	PI	C43H81O13P	M+K	875,5046	875,5046	0,00	0,0000	6,0549	0,0001	infected-control1; infected-control2	cysts		
PI(37:2)	PI	C46H85O13P	M-H	875,5644	875,5655	-1,25	0,0004	3,3990	0,0029	infected-control1; infected-control2	higher in walls		
(3'-sulfo)Galbeta-Cer(d40:1(2OH))	other	C46H89NO12S	M-H	878,6022	878,6033	-1,25	0,0018	2,7334	0,0102	infected-control1	-		
PC(40:3)	PC	C48H90NO8P	M+K	878,6036	878,6036	0,00	0,0006	3,2145	0,0069	control2-control1; infected-control2	-		
IPC(t40:1)	IPC	C46H90NO12P	M-H	878,6117	878,6128	-1,25	0,0000	8,3252	0,0000	infected-control1; infected-control2	cysts		
TG(52:3)	TG	C55H100O6	M+Na	879,7412	879,7412	0,00	0,0003	3,4872	0,0041	infected-control1; infected-control2	cysts		yes

*for lack of space only one possible annotation is shown

example annotation*	molecule class	sum formula	add.	*m/z* theor.	*m/z* meas.	Δ / ppm	p.value	-LOG10(p)	FDR	Tukey's HSD	structure	MSMS	found in Tachyz.?
TG(54:6)	TG	C57H98O6	M+H	879,7436	879,7436	0,00	0,0003	3,4893	0,0041	infected-control1; infected-control2	cysts		
PS(42:9)	PS	C48H76NO10P	M+Na	880,5099	880,5099	0,00	0,0003	3,5146	0,0039	infected-control1; infected-control2	cysts		
PI(36:4)	PI	C45H79O13P	M+Na	881,5151	881,5151	0,00	0,0002	3,6826	0,0031	infected-control1; infected-control2	cysts		yes
PI(38:6)	PI	C47H79O13P	M-H	881,5175	881,5186	-1,24	0,0000	4,7167	0,0002	infected-control1; infected-control2	surrounding tissue		
PC(40:1)	PC	C48H94NO8P	M+K	882,6349	882,6349	0,00	0,0076	2,1214	0,0467	infected-control2	-		
PI(38:6)	PI	C47H81O13P	M-H	883,5331	883,5342	-1,24	0,0002	3,8081	0,0013	control2-control1; infected-control1; infected-control2	surrounding tissue		yes
PI(38:4)	PI	C47H83O13P	M-H	885,5488	885,5499	-1,24	0,0016	2,8088	0,0088	infected-control2	surrounding tissue		yes
PS(42:5)	PS	C48H84NO10P	M+Na	888,5725	888,5725	0,00	0,0001	4,0129	0,0017	infected-control1; infected-control2	-		
PS(44:8)	PS	C50H82NO10P	M+H	888,5749	888,5749	0,00	0,0002	3,8121	0,0024	infected-control1; infected-control2	-		
(3'-sulfo)-GalCer(d42:2)	other	C48H91NO11S	M-H	888,6229	888,6240	-1,23	0,0035	2,4560	0,0167	control2-control1; infected-control2	-		
PI(36:0)	PI	C45H87O13P	M+Na	889,5777	889,5777	0,00	0,0001	3,9052	0,0021	infected-control1; infected-control2	-		
PI(38:3)	PI	C47H85O13P	M+H	889,5801	889,5801	0,00	0,0001	3,8466	0,0023	infected-control1; infected-control2	-		
PC(DiMe(11,3)/ DiMe(11,3))	PC	C48H85NO10P	M+Na	889,5803	889,5803	0,00	0,0001	3,8303	0,0023	infected-control1; infected-control2	-		
PI(38:2)	PI	C47H87O13P	M-H	889,5801	889,5812	-1,23	0,0000	4,4986	0,0003	infected-control1; infected-control2	higher in walls		yes
(3'-sulfo)-GalCer(d42:1)	other	C48H93NO11S	M-H	890,6386	890,6397	-1,23	0,0002	3,7846	0,0013	infected-control1; infected-control2	cysts		

*for lack of space only one possible annotation is shown

example annotation*	molecule class	sum formula	add.	*m/z* theor.	*m/z* meas.	Δ / ppm	p.value	-LOG10(p)	FDR	Tukey's HSD	structure	MSMS	found in Tachyz.?
IPC(d42:1)	IPC	C48H94NO11P	M-H	890,6481	890,6492	-1,23	0,0000	10,4340	0,0000	infected-control1; infected-control2	cysts		
GlcCer(iso-t47:4)	GlcCer	C53H97NO9	M-H	890,7080	890,7091	-1,23	0,0072	2,1439	0,0277	control2-control1; infected-control2	-		
PG(P-46:5)	PG	C52H93O9P	M-H	891,6473	891,6484	-1,23	0,0000	10,3060	0,0000	infected-control1; infected-control2	cysts		
TG(56:13)	TG	C59H88O6	M-H	891,6497	891,6508	-1,23	0,0000	10,6460	0,0000	infected-control1; infected-control2	cysts		
PA(48:2)	PA	C51H97O8P	M+Na	891,6813	891,6813	0,00	0,0026	2,5824	0,0220	infected-control1; infected-control2	cysts		
TG(O-55:11)	TG	C58H92O5	M+Na	891,6837	891,6837	0,00	0,0053	2,2721	0,0368	infected-control1	cysts		
TG(52:5)	TG	C55H96O6	M+K	891,6838	891,6838	0,00	0,0051	2,2890	0,0359	infected-control1	cysts		
22:1-Glc-cholesterol	cholesterol	C55H96O7	M+Na	891,7048	891,7048	0,00	0,0003	3,5256	0,0039	infected-control1; infected-control2	-		
PA(48:1)	PA	C51H99O8P	M+Na	893,6970	893,6970	0,00	0,0008	3,0812	0,0086	infected-control1; infected-control2	cysts		
TG(O-55:10)	TG	C58H94O5	M+Na	893,6993	893,6993	0,00	0,0008	3,1107	0,0082	infected-control1; infected-control2	cysts		
TG(42:4)	TG	C55H98O6	M+K	893,6995	893,6995	0,00	0,0008	3,1107	0,0082	infected-control1; infected-control2	cysts		
PA(48:0)	PA	C51H101O8P	M+Na	895,7126	895,7126	0,00	0,0000	4,8064	0,0005	infected-control1; infected-control2	cysts		
TG(O-55:9)	TG	C58H96O5	M+Na	895,7150	895,7150	0,00	0,0000	4,7834	0,0005	infected-control1; infected-control2	cysts		
PA(50:3)	PA	C53H99O8P	M+H	895,7150	895,7150	0,00	0,0000	4,7834	0,0005	infected-control1; infected-control2	cysts		
TG(52:3)	TG	C55H100O6	M+K	895,7151	895,7151	0,00	0,0000	4,7834	0,0005	infected-control1; infected-control2	cysts		
PI(36:4)	PI	C45H79O13P	M+K	897,4890	897,4890	0,00	0,0000	4,3859	0,0009	infected-control1; infected-control2	cysts		

*for lack of space only one possible annotation is shown

example annotation*	molecule class	sum formula	add.	*m/z* theor.	*m/z* meas.	Δ / ppm	p.value	-LOG10(p)	FDR	Tukey's HSD	structure	MSMS	found in Tachyz.?
PI(O-40:5)	PI	C49H87O12P	M-H	897,5851	897,5862	-1,22	0,0060	2,2210	0,0247	control2-control1; infected-control2	-		
TG(O-55:8)	TG	C58H98O5	M+Na	897,7306	897,7306	0,00	0,0045	2,3455	0,0327	infected-control1	cysts		
PA(50:2)	PA	C53H101O8P	M+H	897,7307	897,7307	0,00	0,0045	2,3455	0,0327	infected-control1	cysts		
TG(52:2)	TG	C55H102O6	M+K	897,7308	897,7308	0,00	0,0045	2,3455	0,0327	infected-control1	cysts		yes
TG(O-57:11)	TG	C60H96O5	M+H	897,7331	897,7331	0,00	0,0044	2,3535	0,0327	infected-control1	cysts		
PI(39:4)	PI	C48H85O13P	M-H	899,5644	899,5655	-1,22	0,0032	2,4997	0,0155	infected-control1	walls		
PI(39:3)	PI	C48H87O13P	M-H	901,5801	901,5812	-1,22	0,0000	4,5160	0,0003	infected-control1; infected-control2	walls		
TG(54:5)	TG	C57H100O6	M+Na	903,7412	903,7412	0,00	0,0081	2,0907	0,0486	infected-control1; infected-control2	cysts		
TG(56:8)	TG	C59H98O6	M+H	903,7436	903,7436	0,00	0,0046	2,3338	0,0330	infected-control1; infected-control2	cysts		
PG(46:6)	PG	C52H91O10P	M-H	905,6266	905,6277	-1,21	0,0000	11,7240	0,0000	infected-control1; infected-control2	cysts		
TG(54:4)	TG	C57H102O6	M+Na	905,7569	905,7569	0,00	0,0013	2,8879	0,0124	infected-control1; infected-control2	cysts		yes
PS(44:10)	PS	C50H78NO10P	M+Na	906,5256	906,5256	0,00	0,0025	2,6047	0,0212	infected-control1; infected-control2	cysts		
PC(46:11)	PC	C54H86NO8P	M-H	906,6007	906,6018	-1,21	0,0069	2,1580	0,0273	infected-control1; infected-control2	-		
(3'-sulfo)Galbeta-Cer(d42:1(2OH))	other	C48H93NO12S	M-H	906,6335	906,6346	-1,21	0,0000	5,6073	0,0000	infected-control1; infected-control2	cysts		
IPC(t42:1)	IPC	C48H94NO12P	M-H	906,6430	906,6441	-1,21	0,0000	12,1070	0,0000	infected-control1; infected-control2	cysts		
PG(46:5)	PG	C52H93O10P	M-H	907,6423	907,6434	-1,21	0,0000	9,6370	0,0000	infected-control1; infected-control2	cysts		
TG(54:3)	TG	C57H104O6	M+Na	907,7725	907,7725	0,00	0,0001	4,2360	0,0011	infected-control1; infected-control2	cysts		yes

*for lack of space only one possible annotation is shown

example annotation*	molecule class	sum formula	add.	*m/z* theor.	*m/z* meas.	Δ / ppm	p.value	-LOG10(p)	FDR	Tukey's HSD	structure	MSMS	found in Tachyz.?
TG(56:6)	TG	C59H102O6	M+H	907,7749	907,7749	0,00	0,0001	4,2465	0,0011	infected-control1; infected-control2	cysts		yes
PI(40:6)	PI	C49H83O13P	M-H	909,5488	909,5499	-1,20	0,0001	4,2352	0,0005	control2-control1; infected-control1	surrounding tissue	Kadesch: PI	
PI(40:5)	PI	C49H85O13P	M-H	911,5644	911,5655	-1,20	0,0005	3,2738	0,0036	control2-control1; infected-control1	surrounding tissue		
PS(P-46:1)	PS	C52H100NO9P	M-H	912,7052	912,7063	-1,20	0,0027	2,5720	0,0138	infected-control2	-		
PI(40:4)	PI	C49H87O13P	M-H	913,5801	913,5812	-1,20	0,0003	3,5457	0,0022	control2-control1; infected-control1	surrounding tissue	Kadesch: PI	
PG(O-45:0)	PG	C51H103O9P	M+Na	913,7232	913,7232	0,00	0,0064	2,1919	0,0425	infected-control2	-		
TG(45:7)	TG	C58H98O6	M+Na	913,7256	913,7256	0,00	0,0068	2,1655	0,0443	infected-control2	-		
TG(57:10)	TG	C60H96O6	M+H	913,7280	913,7280	0,00	0,0081	2,0889	0,0486	infected-control2	-		
PIP(34:1)	PIP	C43H82O16P2	M-H	915,4994	915,5005	-1,20	0,0000	7,0825	0,0000	infected-control1; infected-control2	cysts		yes
PI(40:3)	PI	C49H89O13P	M-H	915,5957	915,5968	-1,20	0,0000	10,7290	0,0000	infected-control1; infected-control2	walls	Kadesch: PI	
PI(38:0)	PI	C47H91O13P	M+Na	917,6090	917,6090	0,00	0,0022	2,6671	0,0186	control2-control1; infected-control1	-		
PI(40:2)	PI	C49H91O13P	M-H	917,6114	917,6125	-1,19	0,0001	3,8472	0,0012	infected-control1; infected-control2	walls		
PG(O-38:7)	PG	C54H95O9P	M-H	917,6630	917,6641	-1,19	0,0000	10,0880	0,0000	infected-control1; infected-control2	cysts		
PA(50:3)	PA	C53H99O8P	M+Na	917,6970	917,6970	0,00	0,0030	2,5198	0,0242	infected-control1; infected-control2	cysts		
IPC(d44:1)	IPC	C50H98NO11P	M-H	918,6794	918,6805	-1,19	0,0000	8,7278	0,0000	infected-control1; infected-control2	cysts		
PG(O-48:6)	PG	C54H97O9P	M-H	919,6786	919,6797	-1,19	0,0000	10,6670	0,0000	infected-control1; infected-control2	cysts		
TG(58:13)	TG	C61H92O6	M-H	919,6810	919,6821	-1,19	0,0000	10,2250	0,0000	infected-control1; infected-control2	cysts		

*for lack of space only one possible annotation is shown

example annotation*	molecule class	sum formula	add.	*m/z* theor.	*m/z* meas.	Δ / ppm	p.value	-LOG10(p)	FDR	Tukey's HSD	structure	MSMS	found in Tachyz.?
PA(50:2)	PA	C53H101O8P	M+Na	919,7126	919,7126	0,00	0,0052	2,2876	0,0359	infected-control1	cysts		
TG(O-57:11)	TG	C60H96O5	M+Na	919,7150	919,7150	0,00	0,0045	2,3444	0,0327	infected-control1	cysts		
TG(54:5)	TG	C57H100O6	M+K	919,7151	919,7151	0,00	0,0043	2,3641	0,0325	infected-control1	cysts		
PA(40:1)	PA	C53H103O8P	M+Na	921,7283	921,7283	0,00	0,0000	5,4344	0,0002	infected-control1; infected-control2	cysts		
TG(O-57:10)	TG	C60H98O5	M+Na	921,7306	921,7306	0,00	0,0000	5,3662	0,0002	infected-control1; infected-control2	cysts		
TG(54:4)	TG	C57H102O6	M+K	921,7308	921,7308	0,00	0,0000	5,3663	0,0002	infected-control1; infected-control2	cysts		
PS(44:10)	PS	C50H78NO10P	M+K	922,4995	922,4995	0,00	0,0070	2,1578	0,0445	infected-control1; infected-control2	-		
PA(50:0)	PA	C53H105O8P	M+Na	923,7439	923,7439	0,00	0,0000	5,2359	0,0003	infected-control1; infected-control2	cysts		yes
TG(O-57:9)	TG	C60H100O5	M+Na	923,7463	923,7463	0,00	0,0000	5,2301	0,0003	infected-control1; infected-control2	cysts		
PA(52:3)	PA	C55H103O8P	M+H	923,7463	923,7463	0,00	0,0000	5,2301	0,0003	infected-control1; infected-control2	cysts		
TG(54:3)	TG	C57H104O6	M+K	923,7464	923,7464	0,00	0,0000	5,2301	0,0003	infected-control1; infected-control2	cysts		
TG(O-59:12)	TG	C62H98O5	M+H	923,7487	923,7487	0,00	0,0000	5,2524	0,0003	infected-control1; infected-control2	cysts		
PE(P-38:7)	PE	C53H92NO7P	M+K	924,6243	924,6243	0,00	0,0012	2,9165	0,0119	infected-control1; infected-control2	higher in cysts		
IPC(t42:0(2OH))	IPC	C48H96NO13P	M-H	924,6536	924,6547	-1,19	0,0000	9,8460	0,0000	control2-control1; infected-control1; infected-control2	cysts		
PS(DiMe(11,3)/ MonoMe(13,5))	PS	C49H82NO12P	M+Na	930,5467	930,5467	0,00	0,0004	3,3550	0,0052	infected-control1; infected-control2	cysts		
PG(48:6)	PG	C54H95O10P	M-H	933,6579	933,6590	-1,17	0,0000	10,7570	0,0000	infected-control1; infected-control2	cysts		

*for lack of space only one possible annotation is shown

example annotation*	molecule class	sum formula	add.	*m/z* theor.	*m/z* meas.	Δ / ppm	p.value	-LOG10(p)	FDR	Tukey's HSD	structure	MSMS	found in Tachyz.?
IPC(t44:1)	IPC	C50H98NO12P	M-H	934,6743	934,6754	-1,17	0,0000	9,7946	0,0000	infected-control1; infected-control2	cysts		
PG(48:5)	PG	C54H97O10P	M-H	935,6736	935,6747	-1,17	0,0000	6,2794	0,0000	infected-control1; infected-control2	cysts		
TG(56:3)	TG	C59H108O6	M+Na	935,8038	935,8038	0,00	0,0043	2,3667	0,0325	infected-control1	-		yes
AzI	other	C48H74O18	M-H	937,4791	937,4802	-1,17	0,0000	8,4316	0,0000	infected-control1; infected-control2	cysts		yes
PIP(34:2)	PIP	C43H80O16P2	M+Na	937,4814	937,4814	0,00	0,0000	4,6453	0,0006	infected-control1; infected-control2	cysts		
PA(52:4)	PA	C55H101O8P	M+Na	943,7126	943,7126	0,00	0,0020	2,7005	0,0174	infected-control1; infected-control2	cysts		
PG(P-50:6)	PG	C56H99O9P	M-H	945,6943	945,6954	-1,16	0,0000	9,3493	0,0000	infected-control1; infected-control2	cysts		
PA(52:3)	PA	C55H103O8P	M+Na	945,7283	945,7283	0,00	0,0005	3,2637	0,0063	infected-control1; infected-control2	cysts		
IPC(t42:1)	IPC	C48H94NO12P	M+K	946,6145	946,6145	0,00	0,0013	2,8920	0,0124	infected-control1	tissue		
IPC(d46:1)	IPC	C52H102NO11P	M-H	946,7107	946,7118	-1,16	0,0000	6,0929	0,0000	infected-control1; infected-control2	cysts		
PG(O-50:6)	PG	C56H101O9P	M-H	947,7099	947,7110	-1,16	0,0000	8,9221	0,0000	infected-control1; infected-control2	cysts		
TG(50:13)	TG	C63H96O6	M-H	947,7123	947,7134	-1,16	0,0000	8,0313	0,0000	infected-control1; infected-control2	cysts		
PS(O-49:5)	PS	C55H100NO9P	M-H	948,7052	948,7063	-1,16	0,0083	2,0790	0,0302	infected-control2	-		
PI(40:6)	PI	C49H83O13P	M+K	949,5203	949,5203	0,00	0,0056	2,2483	0,0379	infected-control2	walls		
PE(52:10)	PE	C57H94NO8P	M-H	950,6633	950,6644	-1,15	0,0000	11,2870	0,0000	infected-control1; infected-control2	cysts		
PA(52:0)	PA	C55H109O8P	M+Na	951,7752	951,7752	0,00	0,0013	2,8967	0,0123	infected-control1	cysts		
TG(O-59:9)	TG	C62H104O5	M+Na	951,7776	951,7776	0,00	0,0003	3,5707	0,0036	infected-control1; infected-control2	cysts		

*for lack of space only one possible annotation is shown

example annotation*	molecule class	sum formula	add.	*m/z* theor.	*m/z* meas.	Δ / ppm	p.value	-LOG10(p)	FDR	Tukey's HSD	structure	MSMS	found in Tachyz.?
TG(56:3)	TG	C59H108O6	M+K	951,7777	951,7777	0,00	0,0003	3,5712	0,0036	infected-control1; infected-control2	cysts		
IPC(t44:0(2OH))	IPC	C50H100NO13P	M-H	952,6849	952,6860	-1,15	0,0000	7,8125	0,0000	control2-control1; infected-control1; infected-control2	cysts		
PG(50:6)	PG	C56H99O10P	M-H	961,6892	961,6903	-1,14	0,0000	11,8900	0,0000	infected-control1; infected-control2	cysts		
IPC(t46:1)	IPC	C52H102NO12P	M-H	962,7056	962,7067	-1,14	0,0000	9,5152	0,0000	infected-control1; infected-control2	cysts		
PIP(38:5)	PIP	C47H82O16P2	M-H	963,4994	963,5005	-1,14	0,0071	2,1500	0,0276	infected-control1; infected-control2	tissue		yes
PG(50:5)	PG	C56H101O10P	M-H	963,7049	963,7060	-1,14	0,0000	7,2561	0,0000	infected-control1; infected-control2	cysts		
PS(O-50:4)	PS	C56H104NO9P	M-H	964,7365	964,7376	-1,14	0,0059	2,2327	0,0243	control2-control1; infected-control2	-		
PC(P-50:2)	PC	C58H112NO7P	M-H	964,8093	964,8104	-1,14	0,0101	1,9964	0,0348	infected-control2	-		
TG(62:14)	TG	C65H98O6	M-H	973,7280	973,7291	-1,13	0,0000	7,1634	0,0000	infected-control1; infected-control2	cysts		
PE(54:10)	PE	C59H98NO8P	M-H	978,6946	978,6957	-1,12	0,0000	10,0570	0,0000	infected-control1; infected-control2	cysts		
IPC(t46:0(2OH))	IPC	C52H104NO13P	M-H	980,7162	980,7173	-1,12	0,0000	8,1621	0,0000	infected-control1; infected-control2	cysts		

*for lack of space only one possible annotation is shown

Curriculum vitae

The curriculum vitae was removed from the electronic version of this thesis.

The curriculum vitae was removed from the electronic version of this thesis.

The curriculum vitae was removed from the electronic version of this thesis.

The curriculum vitae was removed from the electronic version of this thesis.

Acknowledgments

First of all I would like to thank **Prof. Dr. Bernhard Spengler** for giving me the opportunity to work in his research group during the last eight years, starting with my bachelor thesis in 2017, followed by internships and my master thesis in 2019 and finally my doctoral research. Also, he gave me the chance to participate at national and international MS and interdisciplinary conferences where I learned a lot and got a different view about the research we do.

Also, I would like to thank **PD Dr. Simone Häberlein** for volunteering as a second referee as well as **Prof. Dr. Richard Göttlich** and **Prof. Dr. Martin Rühl** for accepting being auditors.

I would also like to thank **Prof. Dr. Liliana M. R. Silva** for introducing me into the world of *Apicomplexa* and all her advices. Additionally, I am grateful for all the fruitful discussions with **Prof. Dr. Anja Taubert** and **Prof. Dr. Carlos Hermosilla**. The same applies for **Prof. Dr. Christoph G. Grevelding** in the context of *Schistosomiasis*.

For the same period of time as Prof. Spengler, also **Dr. Stefanie Gerbig** guided me through my academic career. She taught me most of the things I know and was always there to help me out. Without you, I would not have made it to the finish line.

Another great mentor was **Dr. Parviz Ghezellou**. I learned a lot from the discussions with you and your effort improved my work a lot.

Additionally I would like to thank the whole **AG Spengler** for the always nice and respectful working environment. Everyone helps everyone, that's definitely something not to take for granted. Especially I would like to name **Annika S. Mokosch** and **Carolin M. Morawietz** who often gave me the push I needed or just had an open ear for my complaints.

Dr. Svenja-K. Otto, **Dennis S. Pietruschka** and **Julian A. Schneider** also have to be named without whom I would not have even finished my bachelor studies. We were a great team and I still enjoy our memories we made together.

Special thanks go to **Dr. Torben Wiedemann**, who solved all my LaTeXproblems and stood beside me, when noone else ourstood our academic pathes at family parties.

All this would not have been possible without a proper balance, but **Hera**, **Hades** and especially **Zeus** did a great job clearing my mind or supporting me while writing by simply lying next or onto me, being pur(r)ely present. Also, I would like to thank **Jan Werner** for having my back and reminding me that there is also life beyond academia.

Last but not least, I had endless support by my parents, **Erika Fuchs-Wiedemann** and **Andreas Wiedemann**, and I am grateful for all they did.